

# Diffraction in Deep Inelastic Scattering

A. Hebecker

*Institut für Theoretische Physik der Universität Heidelberg  
Philosophenweg 16, 69120 Heidelberg, Germany*

## Abstract

Different theoretical methods used for the description of diffractive processes in small- $x$  deep inelastic scattering are reviewed. The semiclassical approach, where a partonic fluctuation of the incoming virtual photon scatters off a superposition of target colour fields, is used to explain the basic physical effects. In this approach, diffraction occurs if the emerging partonic state is in a colour singlet, thus fragmenting independently of the target. Other approaches, such as the idea of the pomeron structure function and two gluon exchange calculations, are also discussed in some detail. Particular attention is paid to the close relation between the semiclassical approach and the method of diffractive parton distributions, which is linked to the relation between the target rest frame and the Breit frame point of view. While the main focus is on diffractive structure functions, basic issues in the diffractive production of mesons and of other less inclusive final states are also discussed. Models of the proton colour field, which can be converted into predictions for diffractive cross sections using the semiclassical approach, are presented. The concluding overview of recent experimental results is very brief and mainly serves to illustrate implications of the theoretical methods presented.



# Contents

<b>1</b>	<b>Introduction</b>	<b>5</b>
1.1	Preface . . . . .	5
1.2	Models for diffraction . . . . .	6
1.3	The semiclassical method and its relation to other approaches . . . . .	10
<b>2</b>	<b>Basic Concepts and Phenomena</b>	<b>14</b>
2.1	Kinematics . . . . .	14
2.2	Fundamental observations . . . . .	18
2.3	Diffractive structure function . . . . .	20
<b>3</b>	<b>Semiclassical Approach</b>	<b>23</b>
3.1	Eikonal formulae for high-energy scattering . . . . .	23
3.2	Production of $q\bar{q}$ pairs . . . . .	26
3.3	Higher Fock states . . . . .	30
3.4	Field averaging . . . . .	35
<b>4</b>	<b>From Soft Pomeron to Diffractive Parton Distributions</b>	<b>39</b>
4.1	Soft pomeron . . . . .	39
4.2	Pomeron structure function . . . . .	43
4.3	Diffractive parton distributions . . . . .	45
4.4	Target rest frame point of view . . . . .	51
<b>5</b>	<b>Two Gluon Exchange</b>	<b>58</b>
5.1	Elastic meson production . . . . .	58
5.2	Factorization . . . . .	64
5.3	Charm and high- $p_{\perp}$ jets . . . . .	69

5.4	Inclusive diffraction . . . . .	74
<b>6</b>	<b>Models for the Colour Field of the Proton</b>	<b>78</b>
6.1	Small colour dipole . . . . .	78
6.2	Large hadron . . . . .	80
6.3	Stochastic vacuum . . . . .	86
<b>7</b>	<b>Recent Experimental Results</b>	<b>91</b>
7.1	Diffractive structure function . . . . .	91
7.2	Final states . . . . .	102
7.3	Meson production . . . . .	105
<b>8</b>	<b>Conclusions</b>	<b>109</b>
<b>A</b>	<b>Derivation of Eikonal Formulae</b>	<b>112</b>
<b>B</b>	<b>Spinor Matrix Elements</b>	<b>115</b>
<b>C</b>	<b>Derivation of Diffractive Quark and Gluon Distribution</b>	<b>117</b>
<b>D</b>	<b>Inclusive Parton Distributions</b>	<b>123</b>

# 1 Introduction

## 1.1 Preface

The term diffraction is derived from optics, where it describes the deflection of a beam of light and its decomposition into components with different frequencies. In high energy physics it was originally used for small-angle elastic scattering of hadrons. If one of the hadrons, say the projectile, is transformed into a set of two or more final state particles, the process is called diffractive dissociation or inelastic diffraction. Good and Walker have pointed out that a particularly intuitive physical picture of such processes emerges if the projectile is described as a superposition of different components which scatter elastically off the target [1]. Since the corresponding elastic amplitude is different for each component, the outgoing beam will contain a new superposition of these components and therefore, in general, new physical states. These are the dissociation products of the projectile.

Even at very high energy, the above processes are generically soft, i.e., the momentum transfer is small and the dissociation products have small  $p_{\perp}$ . Therefore, no immediate relation to perturbative QCD is apparent.

By contrast, diffractive jet production, observed at the CERN  $Spp\bar{p}S$  collider in proton-antiproton collisions [2], involves a hard scale. Although one of the hadrons escapes essentially unscathed, a high- $p_{\perp}$  jet pair, which is necessarily associated with a high virtuality in the intermediate states, is produced in the central rapidity range. The cross section of the process is parametrically unsuppressed relative to non-diffractive jet production. This seems to contradict a naïve partonic picture since the colour neutrality of the projectile is destroyed if one parton is removed to participate in the hard scattering. The interplay of soft and hard physics necessary to explain the effect provides one of the main motivations for the study of these ‘hard diffractive’ processes.

The present review is focussed on diffraction in deep inelastic scattering (DIS), which is another example of a hard diffractive process. This process became experimentally viable with the advent of the electron-proton collider HERA, where DIS at very small values of the Bjorken variable  $x$  can be studied. In the small- $x$  or high-energy region, a significant fraction of the observed DIS events have a large rapidity gap between the photon and the proton fragmentation region [3,4]. In contrast to the standard DIS process  $\gamma^*p \rightarrow X$ , the relevant reaction reads  $\gamma^*p \rightarrow XY$ , where  $X$  is a high-mass hadronic state and  $Y$  is the elastically scattered proton or a low-mass excitation of it. Again, these events are incompatible with the naïve picture of a partonic target and corresponding simple ideas about the colour flow. Naïvely, the parton struck by the virtual photon destroys the

colour neutrality of the proton, a colour string forms between struck quark and proton remnant, and hadronic activity is expected throughout the detector. Nevertheless, the observed diffractive cross section is not power suppressed at high virtualities  $Q^2$  with respect to standard DIS.

The main theoretical interest is centered around the interplay of soft and hard physics represented by the elastic or almost elastic scattering of the proton and the scattering of the highly virtual photon respectively. Diffractive DIS is much simpler than hard diffraction in hadronic reactions since only one non-perturbative object is involved. In a large fraction of the events, the momentum transfer to the proton is very small. Therefore, one can hope to gain a better understanding of the bound state dynamics of the proton by studying diffractive DIS. Inclusive reactions of the virtual photon with hadronic targets are well-studied theoretically and constrained by a large amount of DIS data. It is a challenge to utilize this knowledge for the investigation of the non-perturbative dynamics of diffraction and, thereby, of the proton structure.

The paper is organized as follows. In the remainder of the Introduction, different approaches to diffractive DIS are put into historical and physical perspective. The semiclassical model, which is particularly close to the interests of the author, is emphasized. Chapter 2 is concerned with the fundamental observations, the basic concepts required for their understanding, and the necessary kinematic considerations. The semiclassical approach, which is used as the starting point for the discussion of other models, is introduced in Chapter 3. In Chapter 4, the concepts of soft pomeron, triple pomeron vertex and pomeron structure function are discussed. Diffractive parton distributions, which are the more fundamental objects from the point of view of perturbative QCD, are introduced. The semiclassical approach is put in relation to the method of diffractive parton distributions, and explicit formulae for these quantities are derived. In Chapter 5, two gluon exchange calculations are discussed. The emphasis is on their rigorous validity in specific kinematic situations and on their partial correspondence to the semiclassical approach. Chapter 6 introduces three models for the colour field of the proton, which can be converted into predictions for diffractive cross sections using the methods of Chapters 3 and 4. A discussion of recent experimental results and their description by theoretical models is given in Chapter 7, followed by the Conclusions.

## 1.2 Models for diffraction

The claim that diffraction in DIS should be a leading twist effect, and the understanding of the fundamental mechanism underlying such processes can be traced back to the famous paper of Bjorken and Kogut [5]. Their argument is based on a qualitative picture of DIS in the target rest frame, where the incoming virtual photon can be considered as a superposition of partonic states. The large virtuality  $Q^2$  sets the scale, so that states with low- $p_\perp$  partons, i.e., aligned configurations, are suppressed in the photon wave function. However, in contrast to high- $p_\perp$  configurations, these aligned states have a large hadronic interaction cross section with the proton. Therefore, their contribution to the DIS cross section is expected to be of leading twist. Naturally, part of this leading twist

contribution is diffractive since the above low- $p_{\perp}$  configurations represent transversely extended, hadron-like objects, which have a large elastic cross section with the proton.

Note that the basic technical methods date back even further, namely, to the calculation of  $\mu^+\mu^-$  pair electroproduction off an external electromagnetic field by Bjorken, Kogut and Soper [6]. They derive the transition amplitude of the incoming virtual photon into a  $\mu^+\mu^-$  pair, which corresponds to the  $q\bar{q}$  wave function of the virtual photon employed by Nikolaev and Zakharov in their seminal work on diffraction at HERA [7].

The above physical picture, commonly known as the aligned jet model of diffractive and non-diffractive DIS, can naturally be extended to account for a soft energy growth of both processes. (Note that we are dealing with the underlying energy dependence of the soft scattering process, not with the additional  $x$ -dependence induced by Altarelli-Parisi evolution, that is added on top of it.) Since a large sample of hadronic cross sections can be consistently parametrized using the concept of the Donnachie-Landshoff or soft pomeron [8], it is only natural to assume that this concept can also be used to describe the energy dependence of the interaction of the aligned jet component of the small- $x$  virtual photon and the target. This gives rise to the desired non-trivial energy dependence although, as will be discussed in more detail later on, this energy dependence is not sufficiently steep in the diffractive case. Note, however, that the above soft energy dependence may also be logarithmic, which has the advantage of explicit consistency with unitarity at arbitrarily high energies.

A more direct way of applying the concept of the soft pomeron to the phenomenon of hard diffraction was suggested by Ingelman and Schlein in the context of diffractive jet production in hadronic collisions [9]. Their idea of a partonic structure of the pomeron, which can be tested in hard processes, applies to the case of diffractive DIS as well [10]. Essentially, one assumes that the pomeron can, like a real hadron, be characterized by a parton distribution. This distribution factorizes from the pomeron trajectory and the pomeron-proton vertex, which are both obtained from the analysis of purely soft hadronic reactions. The above non-trivial assumptions are often referred to as ‘Regge hypothesis’ or ‘Regge factorization’.

The Ingelman-Schlein approach described above is based on the intuitive picture of a pomeron flux associated with the proton beam and on the conventional partonic description of the pomeron photon collision. In the limit where not only the total proton-photon center-of-mass energy but also the energy of the pomeron-photon collision becomes large, the concept of the triple pomeron vertex can be applied [11]. At HERA, this limit corresponds to rapidity gap events with very large diffractive masses.

The concept of fracture functions of Veneziano and Trentadue [12] or, more specifically, the diffractive parton distributions of Berera and Soper [13] provide a framework for the study of diffractive DIS that is firmly rooted in perturbative QCD. Loosely speaking, diffractive parton distributions describe the probability of finding, in a fast moving proton, a parton with a certain momentum fraction  $x$ , under the additional requirement that the proton remains intact losing only a certain fraction of its momentum. This idea is closely related to the concept of a partonic pomeron described above, but it gives up the Regge hypothesis, thus being less predictive. This weaker factorization assumption

is sometimes referred to as ‘diffractive factorization’, as opposed to the stronger Regge factorization assumption.

An essential feature of diffractive DIS is the colour singlet exchange in the  $t$  channel, necessary to preserve the colour neutrality of the target. None of the above approaches address this requirement explicitly within the framework of QCD. Instead, the colour singlet exchange is postulated by assuming elastic scattering in the aligned jet model, by using the concept of the pomeron, or by defining diffractive parton distributions. If one insists on using the fundamental degrees of freedom of QCD, the simplest possibility of realizing colour singlet exchange at high energy is the exchange of two gluons [14]. One could say that two gluons form the simplest model for the pomeron.

The fundamental problem with this approach is the applicability of perturbative QCD to the description of diffractive DIS. As will be discussed in more detail below, the hard scale  $Q^2$  of the photon does not necessarily justify a perturbative description of the  $t$  channel exchange with the target.

Diffractive processes where the  $t$  channel colour singlet exchange is governed by a hard scale include the electroproduction of heavy vector mesons [15], electroproduction of light vector mesons in the case of longitudinal polarization [16] or at large  $t$  [17], and virtual Compton scattering [18–20]. In the leading logarithmic approximation, the relevant two-gluon form factor of the proton can be related to the inclusive gluon distribution [15]. Accordingly, a very steep energy dependence of the cross section, which is now proportional to the square of the gluon distribution, is expected from the known steep behaviour of small- $x$  structure functions. The origin of this steep rise itself may be attributed to a combination of the  $x$ -dependence of the input distributions and their Altarelli-Parisi evolution, or to the BFKL resummation of large logarithms of  $x$ .

To go beyond leading logarithmic accuracy, the non-zero momentum transferred to the proton has to be taken into account. This requires the use of ‘non-forward’ or ‘off-diagonal’ parton distributions (see [18, 21] and refs. therein), which were discussed in [19, 20] within the present context. Although their scale dependence is predicted by well-known evolution equations, only limited information about the relevant input distributions is available. In particular, the simple proportionality to the square of the conventional gluon distribution is lost.

The perturbative calculations of meson electroproduction discussed above were put on a firmer theoretical basis by the factorization proof of [22], where the conditions required for the applicability of perturbation theory are discussed in detail. As shown explicitly in the simple model calculation of [23], QCD gauge invariance ensures that the non-perturbative meson formation process takes place *after* the scattering off the hadronic target.

The situation becomes even more complicated if two gluon exchange calculations are applied to more general diffractive final states. Examples are the exclusive electroproduction of heavy quark pairs [24–27] or high- $p_\perp$  jets [28–31]. A straightforward perturbative analysis shows that the virtual photon side of the process is dominated by small transverse distances, establishing two gluon exchange as the dominant mechanism. However, it is not obvious whether the very definition ‘exclusive’, meaning exclusive on a partonic



level, can be extended to all orders in perturbation theory. As will become clear later on, additional soft partons in the final state may destroy the hardness provided by the large  $p_{\perp}$  or the heavy quark mass.

From the point of view of the full diffractive cross section, perturbative two gluon exchange corresponds to a higher twist effect. However, it can be argued that it dominates the kinematic region where the mass  $M$  of the diffractively produced final state  $X$  is relatively small,  $M \ll Q$  [32]. More generally, higher twist effects in diffraction, their calculability and possibilities for their experimental observation are discussed in [32–34].

Eventually it is possible to attempt the description of the full cross section of diffractive DIS within the framework of two gluon exchange. In such a general setting, perturbation theory can not be rigorously justified and two gluons are basically used as a model for the soft colour singlet exchange in the  $t$  channel. Nevertheless, it is interesting to see to what extent concepts and formulae emerging from perturbation theory can describe a wider range of phenomena. In particular, much attention has been devoted to the energy dependence of diffractive cross sections both in the framework of conventional BFKL summation of gluon ladders [35, 36] and within the colour dipole approach to small- $x$  resummation [28, 37].

An apparently quite different approach emerged with the idea that soft colour interactions might be responsible for the large diffractive cross section at HERA. The starting point is Buchmüller’s observation of the striking similarity between  $x$  and  $Q^2$  dependence of diffractive and inclusive DIS at small  $x$  [38]. It is then natural to assume that the same hard partonic processes underlie both cross sections and that differences in the final states are the result of non-perturbative soft colour exchange [39, 40].

In Ref. [39], boson-gluon fusion was proposed as the dominant partonic process, and diffraction was claimed to be the result of soft colour neutralization of the produced  $q\bar{q}$  pair. A simple statistical assumption about the occurrence of this colour neutralization lead to a surprisingly good fit to the data. Note that similar ideas concerning the rotation of quarks in colour space had previously been discussed by Nachtmann and Reiter [41] in connection with QCD vacuum effects on hadron-hadron scattering.

A closely related approach was introduced in [40], where the assumption of soft colour neutralization was implemented in a Monte Carlo event generator based on perturbation theory. Normally, the partonic cascades underlying the Monte Carlo determine the colour of all partons produced and, with a certain model dependence, the hadronic final state. The introduction of an ad-hoc probability for partons within the cascade to exchange colour in a non-perturbative way leads to a significant increase of final states with rapidity gaps, resulting in a good description of the observed diffractive events.

Both of the above models share a fundamental theoretical problem: the soft colour exchange is introduced in an ad-hoc manner, independently of kinematic configuration or space-time distances of the partons involved. If all relevant distances are large, our ignorance of the true mechanism of non-perturbative interactions justifies the naïve assumption of random colour exchange. However, in many other situations, e.g., if a small colour dipole is involved, colour exchange is suppressed in a perturbatively calculable way. This is known as colour transparency. The above simple soft colour models do not

properly account for this effect. One possibility of incorporating the knowledge of the perturbative aspects of QCD while keeping the essential idea of soft colour exchange as the source of leading twist diffraction is the semiclassical treatment.

### 1.3 The semiclassical method and its relation to other approaches

The semiclassical approach to diffractive electroproduction evolved from the attempt to justify the phenomenologically successful idea of soft colour exchange [39, 40] within the framework of QCD. The starting point is the proton rest frame picture of DIS advocated long ago in [5] and developed since by many authors (see in particular [7]). To describe diffraction within this framework, the scattering of energetic partons in the photon wave function off the hadronic target needs to be understood. While the scattering of small transverse size configurations is calculable perturbatively, i.e., via two gluon exchange, different models may be employed for larger size configurations. A rather general framework is provided by the concept of the dipole cross section  $\sigma(\rho)$  utilized in the analysis of [7].

It is helpful to begin by recalling the discussion of high-energy electroproduction of  $\mu^+\mu^-$  pairs off atomic targets given by Bjorken, Kogut and Soper in [6]. There, the closely related QED problem was solved by treating the high-energy scattering of  $\mu^+\mu^-$  pairs off a given electromagnetic field in the eikonal approximation. An analogous QCD process was considered by Collins, Soper and Sterman in [42], where the production of heavy quark pairs in an external colour field was calculated. In Ref. [43], Nachtmann developed the idea of eikonalized interactions with soft colour field configurations as a method for the treatment of elastic high-energy scattering of hadrons.

The semiclassical approach to diffraction, introduced in [44], combines the concepts and methods outlined above. The proton is modelled by a soft colour field, and the interactions of the fast partons in the photon wave function with this field are treated in the eikonal approximation. As a result, the non-perturbative proton structure is encoded in a combination of non-Abelian phase factors associated with the partons. In the simplest case of a  $q\bar{q}$  fluctuation, two such phase factors are combined in a Wegner-Wilson loop, which carries all the information about the target. Since the outgoing  $q\bar{q}$  pair can be either in a colour singlet or in a colour octet state, both diffractive and non-diffractive events are naturally expected in this approach. Thus, both types of events are described within the same framework. The colour state of the produced pair is the result of the fundamentally non-perturbative interaction with the proton colour field, very much in the spirit of the soft colour neutralization of [39].

The essential difference between the semiclassical calculation and the soft colour proposal is the recognition that the possibility of soft colour exchange is intimately related to parton level kinematics. The semiclassical approach allows for a consistent treatment of the scattering of both small and large transverse size configurations. The requirement of colour neutrality in the final state of diffractive events is explicitly shown

to suppress the former ones. This confirms the familiar qualitative arguments on which the aligned jet model is based [5].

A further essential step is the inclusion of higher Fock states in the photon wave function. In the framework of two gluon exchange, corresponding calculations for the  $q\bar{q}g$  state were performed in [28]. The semiclassical analysis of the  $q\bar{q}g$  state [45] demonstrates that, to obtain leading twist diffraction, at least one of the three partons has to have small  $p_\perp$  and has to carry a small fraction of the photon's longitudinal momentum. This is a natural generalization of the aligned jet model, which was previously discussed on a qualitative level in [46].

A fundamental prediction derived from the semiclassical treatment of the  $q\bar{q}g$  state is the leading twist nature of diffractive electroproduction of heavy quark pairs [47] and of high- $p_\perp$  jets [48]. These large cross sections arise from  $q\bar{q}g$  configurations where the gluon is relatively soft and has small  $p_\perp$ , so that the  $t$  channel colour singlet exchange remains soft in spite of the additional hard scale provided by the  $q\bar{q}$  pair.

As mentioned previously, considerable work has been done attempting to employ the additional hardness provided by final states with jets or heavy quarks in order to probe mechanisms of perturbative colour singlet exchange [24–31]. In fact, the semiclassical approach is also well suited to follow this line of thinking. As demonstrated in [48], the features of diffractive jet production from  $q\bar{q}$  and  $q\bar{q}g$  fluctuations of the photon, both treated consistently in the semiclassical framework, are very different. In the  $q\bar{q}$  case, a small-size colour dipole tests the small distance structure of the proton colour field. It can be shown within the semiclassical framework that the relevant operator is the same as in inclusive DIS, thus reproducing the well-known relation with the square of the gluon distribution [15]. In the  $q\bar{q}g$  case, the additional soft gluon allows for a non-perturbative colour neutralization mechanism even though the final state contains two high- $p_\perp$  jets.

The semiclassical treatment of leading twist diffraction is equivalent to a treatment based on diffractive parton distributions [49]. To be more precise, the results of [45] lead to the conclusion that a leading twist contribution to diffraction can arise only from virtual photon fluctuations that include at least one soft parton. Starting from this premise, the diffractive production of final states with one soft parton and a number of high- $p_\perp$  partons was considered in [49]. It was shown that the cross section can be written as a convolution of a hard partonic cross section and a diffractive parton distribution. The latter is given explicitly in terms of an average over the target colour field configurations underlying the semiclassical calculation.

From this point of view, the semiclassical prediction of the dominance of  $q\bar{q}g$  final states and soft colour neutralization in high- $p_\perp$  jet and heavy quark production appears natural. It corresponds simply to the dominant partonic process, boson-gluon fusion, with the gluon taken from the diffractive gluon distribution. The additional gluon in the final state is, from the point of view of parton distributions, merely a consequence of the preserved colour neutrality of the target. From the point of view of the semiclassical calculation, it is the scattering product of the original gluon from the photon wave function that is necessary for the softness of the colour singlet exchange.

Even without an explicit model for the proton colour field, the semiclassical approach

provides an intuitive overall picture of inclusive and diffractive small- $x$  DIS and predicts a number of qualitative features of the final state. However, the ultimate goal is to develop the understanding of non-perturbative colour dynamics that is needed to calculate the required field averages.

A very successful description of a number of hadronic reactions was obtained in the framework of the stochastic vacuum. Different effects of the non-trivial structure of the QCD vacuum in high-energy hadron-hadron scattering were considered in [41]. Field strength correlators in a theory with vacuum condensate were employed in [50, 51] to describe the pomeron. The model of the stochastic vacuum was introduced by Dosch and Simonov [52] in the context of gluon field correlators in the Euclidean theory. Based on ideas of [50, 51] and, in particular, on Nachtmann's suggestion to describe high-energy hadron-hadron scattering in an eikonal approach [43], the stochastic vacuum model was adapted to Minkowski space and applied to high-energy processes by Dosch and Krämer [53]. In the present context of diffractive and non-diffractive electroproduction, the work on inclusive DIS [54],  $C$ - and  $P$ -odd contributions to diffraction [55], and exclusive vector meson production [56–58] is particularly relevant. Results on diffractive structure functions have recently been reported [59].

In the special case of a very large hadronic target, the colour field averages required in the semiclassical approach can be calculated without specifying the details of the non-perturbative colour dynamics involved. McLerran and Venugopalan observed that the large target size, realized, e.g., in an extremely heavy nucleus, introduces a new hard scale into the process of DIS [60]. From the target rest frame point of view, this means that the typical transverse size of the partonic fluctuations of the virtual photon remains perturbative [61]. Thus, the perturbative treatment of the photon wave function in the semiclassical calculation is justified. Note that the small size of the partonic fluctuations of the photon does not imply a complete reduction to perturbation theory. The long distance which the partonic fluctuation travels in the target compensates for its small transverse size, thus requiring the eikonalization of gluon exchange.

For a large target it is natural to introduce the additional assumption that the gluonic fields encountered by the partonic probe in distant regions of the target are not correlated. In this situation, inclusive and diffractive DIS cross sections become completely calculable. A corresponding analysis of inclusive and diffractive parton distributions was performed in [62]. Starting from the above large target model, expressions for the inclusive quark distribution, which had previously been discussed in a similar framework in [63], and for the inclusive gluon distribution were obtained. Diffractive quark and gluon distributions were calculated, within the same model for the colour field averaging, on the basis of formulae from [49]. The resulting structure functions, obtained from the above input distributions by Altarelli-Parisi evolution, provide a satisfactory description of the experimental data [62].

A number of further approaches to diffractive DIS were proposed by several authors. For example, it was argued in [64] that a super-critical pomeron with colour-charge parity  $C_c = -1$  plays an essential role. As a result, the main features of the naïve boson-gluon fusion model of [39] are reproduced while its problems, which were outlined above, are avoided. In a different approach, a geometric picture of diffraction, based on the idea

of colourless gluon clusters, was advertised (see, e.g., [65]). There can be no doubt that far more material relevant to the present subject exists which, because of the author's bias or unawareness, is not appropriately reflected in this introduction or the following chapters.

## 2 Basic Concepts and Phenomena

In this chapter, the kinematics of diffractive electroproduction at small  $x$  is explained in some detail, and the notation conventionally used for the description of this phenomenon is introduced. The main experimental observations are discussed, and the concept of the diffractive structure function, which is widely used in analyses of inclusive diffraction, is explained. This standard material may be skipped by readers familiar with the main HERA results on diffractive DIS.

### 2.1 Kinematics

To begin, recall the conventional variables for the description of DIS. An electron with momentum  $k$  collides with a proton with momentum  $P$ . In neutral current processes, a photon with momentum  $q$  and virtuality  $q^2 = -Q^2$  is exchanged, and the outgoing electron has momentum  $k' = k - q$ . In inclusive DIS, no questions are asked about the hadronic final state  $X_W$ , which is only known to have an invariant mass square  $W^2 = (P + q)^2$ . The Bjorken variable  $x = Q^2/(Q^2 + W^2)$  characterizes, in the naïve parton model, the momentum fraction of the incoming proton carried by the quark that is struck by the virtual photon. If  $x \ll 1$ , which is the relevant region in the present context,  $Q$  is much smaller than the photon energy in the target rest frame. In this sense, the photon is almost real even though  $Q^2 \gg \Lambda^2$  (where  $\Lambda$  is some soft hadronic scale). It is then convenient to think in terms of a high-energy  $\gamma^*p$  collision with centre-of-mass energy  $W$ .

The small- $x$  limit of DIS became experimentally viable only a few years ago, with the advent of the HERA accelerator (Hadron-Elektron-Ring-Anlage) at the DESY accelerator centre in Hamburg. In this machine, 27 GeV electrons (or positrons) are collided with 920 GeV protons at interaction points inside the H1 and ZEUS detectors. The large centre-of-mass energy of the  $ep$  collision,  $\sqrt{s} \simeq 300$  GeV, allows for a very high hadronic energy  $W$  and thus for the observation of events with both very small  $x$  and high  $Q^2$ . For values of  $Q^2$  well in the perturbative domain, a statistically usable number of events with  $x$  as small as  $10^{-4}$  is observed.

Loosely speaking, diffraction is the subset of DIS characterized by a quasi-elastic interaction between virtual photon and proton. A particularly simple definition of diffraction is obtained by demanding that, in the  $\gamma^*p$  collision, the proton is scattered elastically. Thus, in diffractive events, the final state contains the scattered proton with momentum  $P'$  and a diffractive hadronic state  $X_M$  with mass  $M$  (see Fig. 2.1). Since diffractive events form a subset of DIS events, the total invariant mass of the outgoing proton and

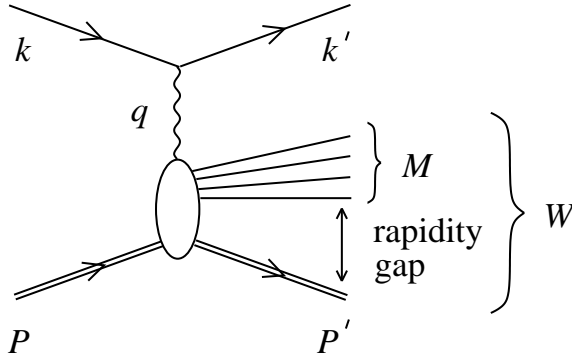


**Figure 2.1:** Diffractive electroproduction. The full hadronic final state with invariant mass  $W$  contains the elastically scattered proton and the diffractive state with invariant mass  $M$ .

the diffractive state  $X_M$  is given by the standard DIS variable  $W$ .

The following parallel description of inclusive and diffractive DIS suggests itself.

In the former, virtual photon and proton collide to form a hadronic state  $X_W$  with mass  $W$ . The process can be characterized by the virtuality  $Q^2$  and the scaling variable  $x = Q^2/(Q^2 + W^2)$ , the momentum fraction of the struck quark in the naïve parton model.

In the latter, a colour neutral cluster of partons is stripped off the proton. The virtual photon forms, together with this cluster, a hadronic state  $X_M$  with mass  $M$ . The process can be characterized by  $Q^2$ , as above, and by a new scaling variable  $\beta = Q^2/(Q^2 + M^2)$ , the momentum fraction of this cluster carried by the struck quark.

Since diffraction is a subprocess of inclusive DIS, the struck quark from the colour neutral cluster also carries a fraction  $x$  of the proton momentum. Therefore, the ratio  $\xi = x/\beta$  characterizes the momentum fraction that the proton loses to the colour neutral exchange typical of an elastic reaction. This exchanged colour neutral cluster loses a momentum fraction  $\beta$  to the struck quark that absorbs the virtual photon. As expected, the product  $x = \beta\xi$  is the fraction of the original proton's momentum carried by this struck quark. Since the name pomeron is frequently applied to whichever exchange with vacuum quantum numbers dominates the high-energy limit, many authors use the notation  $x_P = \xi$ , thus implying that the proton loses a momentum fraction  $\xi$  to the exchanged pomeron.

Therefore,  $x$ ,  $Q^2$  and  $\beta$  or, alternatively,  $x$ ,  $Q^2$  and  $\xi$  are the main kinematic variables characterizing diffractive DIS. A further variable,  $t = (P - P')^2$ , is necessary if the transverse momenta of the outgoing proton and the state  $X_M$  relative to the  $\gamma^*P$  axis are measured. Since the proton is a soft hadronic state, the value of  $|t|$  is small in most events. The small momentum transferred by the proton also implies that  $M \ll W$ .

To see this in more detail, introduce light-cone co-ordinates  $q_{\pm} = q_0 \pm q_3$  and  $q_{\perp} = (q_1, q_2)$ . It is convenient to work in a frame where the transverse momenta of the incoming particles vanish,  $q_{\perp} = P_{\perp} = 0$ . Let  $\Delta$  be the momentum transferred by the proton,

$\Delta = P - P'$ , and  $m_p^2 = P^2 = P'^2$  the proton mass squared. For forward scattering,  $P'_\perp = 0$ , the relation

$$t = \Delta^2 = \Delta_+ \Delta_- = -\xi^2 m_p^2 \quad (2.1)$$

holds. Since  $\xi = (Q^2 + M^2)/(Q^2 + W^2)$ , this means that small  $M$  implies small  $|t|$  and vice versa. Note, however, that the value of  $|t|$  is larger for non-forward processes, where  $t = \Delta_+ \Delta_- - \Delta_\perp^2$ .

So far, diffractive events have been characterized as those DIS events which contain an elastically scattered proton in their hadronic final state. An even more striking feature is the large gap of hadronic activity seen in the detector between the scattered proton and the diffractive state  $X_M$ . It will now be demonstrated that this feature, responsible for the alternative name ‘rapidity gap events’, is a direct consequence of the relevant kinematics.

Recall the definition of the rapidity  $y$  of a particle with momentum  $k$ ,

$$y = \frac{1}{2} \ln \frac{k_+}{k_-} = \frac{1}{2} \ln \frac{k_0 + k_3}{k_0 - k_3}. \quad (2.2)$$

This is a convenient quantity for the description of high-energy collisions along the  $z$ -axis. Massless particles moving along this axis have rapidity  $-\infty$  or  $+\infty$ , while all other particles are characterized by some finite intermediate value of  $y$  (for a detailed discussion of the role of rapidity in the description of diffractive kinematics see, e.g., [66].)

In the centre-of-mass frame of the  $\gamma^*p$  collision, with the  $z$ -axis pointing in the proton beam direction, the rapidity of the incoming proton is given by  $y_p = \ln(P_+/m_p)$ . At small  $\xi$ , the rapidity of the scattered proton is approximately the same. This is to be compared with the highest rapidity  $y_{\max}$  of any of the particles in the diffractive state  $X_M$ . Since the total plus component of the 4-momentum of  $X_M$  is given by  $(\xi - x)P_+$ , and the pion, with mass  $m_\pi$ , is the lightest hadron, none of the particles in  $X_M$  can have a rapidity above  $y_{\max} = \ln((\xi - x)P_+/m_\pi)$ . Thus, a rapidity gap of size  $\Delta y = \ln(m_\pi/(\xi - x)m_p)$  exists between the outgoing proton and the state  $X_M$ . For typical values of  $\xi \sim 10^{-3}$  (cf. the more detailed discussion of the experimental setting below) the size of this gap can be considerable.

Note, however, that the term ‘rapidity gap events’ was coined to describe the appearance of diffractive events in the HERA frame, i.e., a frame defined by the electron-proton collision axis. The rapidity in this frame is, in general, different from the photon-proton frame rapidity discussed above. Nevertheless, the existence of a gap surrounding the outgoing proton in the  $\gamma^*p$  frame clearly implies the existence of a similar gap in the  $ep$  frame. The exact size of the  $ep$ -frame rapidity gap follows from the specific event kinematics. The main conclusion so far is the kinematic separation of outgoing proton and diffractive state  $X_M$  in diffractive events with small  $\xi$ .

The appearance of a typical event in the ZEUS detector is shown in Fig. 2.2, where FCAL, BCAL, and RCAL are the forward, central (barrel) and rear calorimeters. The absence of a significant energy deposit in the forward region is the most striking feature of this DIS event. In the naïve parton model of DIS, a large forward energy deposit is expected due to the fragmentation of the proton remnant, which is left after a quark has



been knocked out by the virtual photon. In addition, the whole rapidity range between proton remnant and current jet is expected to fill with the hadronization products of the colour string that develops because of the colour charge carried by the struck quark. Thus, the event in Fig. 2.2 shows a clear deviation from typical DIS, even though the outgoing proton left through the beam pipe and remains undetected. Hence, the name rapidity gap events is also common for what was called diffractive electroproduction in the previous paragraphs.

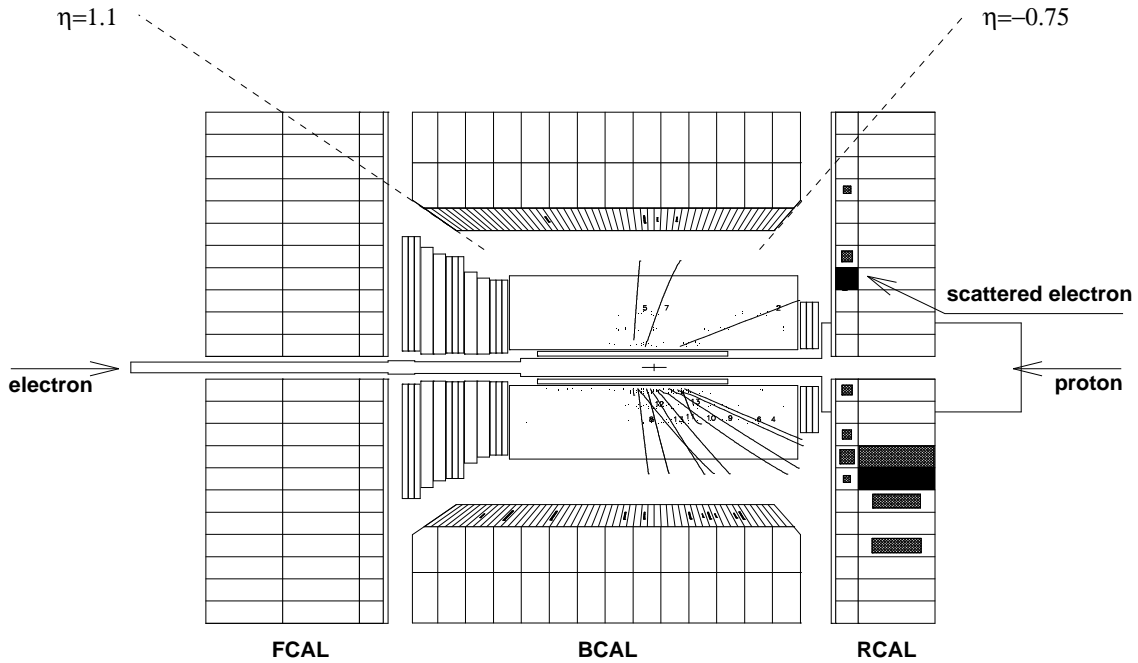


**Figure 2.2:** Diffractive event in the ZEUS detector (figure from [3]).

The definition of diffraction used above is narrower than necessary. Without losing any of the qualitative results, the requirement of a final state proton  $P'$  can be replaced by the requirement of a low-mass hadronic state  $Y$ , well separated from the diffractive state  $X_M$ . In this case, the argument connecting elastically scattered proton and rapidity gap has to be reversed: the existence of a gap between  $X_M$  and  $Y$  becomes the distinctive feature of diffraction and, under certain kinematic conditions, the interpretation of  $Y$  as an excitation of the incoming proton, which is now *almost* elastically scattered, follows.

However, this wider definition of diffraction has the disadvantage of introducing a further degree of freedom, namely, the mass of the proton excitation. If one insists on using only the previous three parameters,  $x$ ,  $Q^2$  and  $\xi$ , the definition of a diffractive event becomes ambiguous. More details are found in the discussion of the experimental results below and in the relevant experimental papers.

## 2.2 Fundamental observations

Rapidity gaps are expected even if in all DIS events a quark is knocked out of the proton leaving a coloured remnant. The reason for this is the statistical distribution of the produced hadrons, which results in a small yet finite probability for final states with little activity in any specified detector region. However, the observations described below are clearly inconsistent with this explanation of rapidity gap events.

The first analysis of rapidity gap events at HERA was performed by the ZEUS collaboration [3]. More than 5% of DIS events were found to possess a rapidity gap. The large excess of the event numbers compared to naïve parton model expectations was soon confirmed by an H1 measurement [4]. The analyses are based on the pseudo-rapidity  $\eta = -\ln \tan(\theta/2)$ , where  $\theta$  is the angle of an outgoing particle relative to the beam axis. Pseudo-rapidity and rapidity are identical for massless particles; the difference between these two quantities is immaterial for the qualitative discussion below.

In the ZEUS analysis, a rapidity  $\eta_{\max}$  was defined as the maximum rapidity of a calorimeter cluster in an event. A cluster was defined as an isolated set of adjacent cells with summed energy higher than 400 MeV. The measured  $\eta_{\max}$  distribution is shown in Fig. 2.3. (Note that the smallest detector angle corresponds to  $\eta_{\max} = 4.3$ ; larger values are an artifact of the clustering algorithm.)

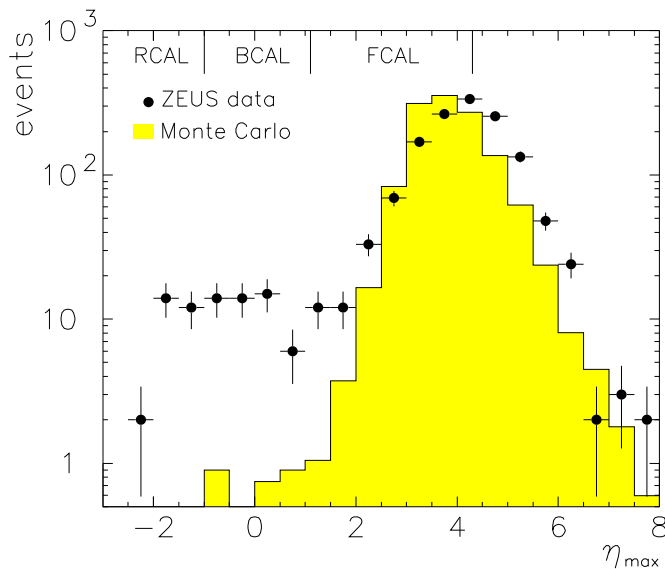


**Figure 2.3:** Distribution of  $\eta_{\max}$ , the maximum rapidity of a calorimeter cluster in an event, measured at HERA (figure from [3]).

To appreciate the striking qualitative signal of diffraction at HERA, the measured  $\eta_{\max}$  distribution has to be compared with naïve expectations based on a purely partonic picture of the proton. This is best done using a parton-model-based Monte Carlo event generator. The corresponding  $\eta_{\max}$  distribution, which is also shown in Fig. 2.3, is strongly suppressed at small  $\eta_{\max}$ . This qualitative behaviour is expected since the Monte Carlo (for more details see [3] and refs. therein) starts from a partonic proton, calculates the

hard process and the perturbative evolution of the QCD cascade, and finally models the hadronization using the Lund string model (see, e.g., [67]). According to the Lund model, the colour string, which connects all final state partons and the coloured proton remnant, breaks up via  $q\bar{q}$  pair creation, thus producing the observed mesons. The rapidities of these particles follow a Poisson distribution, resulting in an exponential suppression of large gaps.

It should be clear from the above discussion that this result is rather general and does not depend on the details of the Monte Carlo. QCD radiation tends to fill the rapidity range between the initially struck quark and the coloured proton remnant with partons. A colour string connecting these partons is formed, and it is highly unlikely that a large gap emerges in the final state after the break-up of this string.

However, the data shows a very different behaviour. The expected exponential decrease of the event number with  $\eta_{\max}$  is observed only above  $\eta_{\max} \simeq 1.5$ ; below this value a large plateau is seen. Thus, the naïve partonic description of DIS misses an essential qualitative feature of the data, namely, the existence of non-suppressed large rapidity gap events.

To give a more specific discussion of the diffractive event sample, it is necessary to define which events are to be called diffractive or rapidity gap events. It is clear from Fig. 2.3 that, on a qualitative level, this can be achieved by an  $\eta_{\max}$  cut separating the events of the plateau. The resulting qualitative features, observed both by the ZEUS [3] and H1 collaborations [4], are the following.

There exists a large rapidity interval where the  $\eta_{\max}$  distribution is flat. For high  $\gamma^*p$  energies  $W$ , the ratio of diffractive events to all DIS events is approximately independent of  $W$ . The  $Q^2$  dependence of this ratio is also weak, suggesting a leading-twist contribution of diffraction to DIS. Furthermore, the diffractive mass spectrum is consistent with a  $1/M^2$  distribution.

A number of additional remarks are in order. Note first that the observation of a flat  $\eta_{\max}$  distribution and of a  $1/M^2$  spectrum are interdependent as long as masses and transverse momenta of final state particles are much smaller than  $M^2$ . To see this, observe that the plus component of the most forward particle momentum and the minus component of the most backward particle momentum are largely responsible for the total invariant mass of the diffractive final state. This gives rise to the relation  $dM^2/M^2 = d\ln M^2 \sim d\eta_{\max}$ , which is equivalent to the desired result.

Furthermore, it has already been noted in [4] that a significant contribution from exclusive vector meson production, e.g., the process  $\gamma^*p \rightarrow \rho p$ , is present in the rapidity gap event sample. A more detailed discussion of corresponding cross sections, which have by now been measured, and of relevant theoretical considerations is given in Chapters 5 and 7. The discussion of other, more specific features of the diffractive final state, such as the presence of charmed mesons or high- $p_{\perp}$  jets, is also postponed.

## 2.3 Diffractive structure function

The diffractive structure function, introduced in [68] and first measured by the H1 collaboration [69], is a powerful concept for the analysis of data on diffractive DIS, which is now widely used by experimentalists and theoreticians.

Recall the relevant formulae for inclusive DIS (see, e.g., [70]). The cross section for the process  $ep \rightarrow eX$  can be calculated if the hadronic tensor,

$$W_{\mu\nu}(P, q) = \frac{1}{4\pi} \sum_X \langle P | j_\nu^\dagger(0) | X \rangle \langle X | j_\mu(0) | P \rangle (2\pi)^4 \delta^4(q + P - p_X), \quad (2.3)$$

is known. Here  $j$  is the electromagnetic current, and the sum is over all hadronic final states  $X$ . Because of current conservation,  $q \cdot W = W \cdot q = 0$ , the tensor can be decomposed according to

$$W_{\mu\nu}(P, q) = \left( g_{\mu\nu} - \frac{q_\mu q_\nu}{q^2} \right) W_1(x, Q^2) + \left( P_\mu + \frac{1}{2x} q_\mu \right) \left( P_\nu + \frac{1}{2x} q_\nu \right) W_2(x, Q^2). \quad (2.4)$$

The data is conveniently analysed in terms of the two structure functions

$$F_2(x, Q^2) = (P \cdot q) W_2(x, Q^2) \quad (2.5)$$

$$F_L(x, Q^2) = (P \cdot q) W_2(x, Q^2) - 2x W_1(x, Q^2). \quad (2.6)$$

Introducing the ratio  $R = F_L/(F_2 - F_L)$ , the electron-proton cross section can be written as

$$\frac{d^2 \sigma_{ep \rightarrow eX}}{dx dQ^2} = \frac{4\pi \alpha_{\text{em}}^2}{x Q^4} \left\{ 1 - y + \frac{y^2}{2[1 + R(x, Q^2)]} \right\} F_2(x, Q^2), \quad (2.7)$$

where  $y = Q^2/sx$ , and  $s$  is the electron-proton centre-of-mass energy squared. In the naïve parton model or at leading order in  $\alpha_s$  in QCD, the longitudinal structure function  $F_L(x, Q^2)$  vanishes, and  $R = 0$ . Since  $R$  corresponds to the ratio of longitudinal and transverse virtual photon cross sections,  $\sigma_L/\sigma_T$ , it is always positive, and the corrections associated with a non-zero  $R$  are small at low values of  $y$ .

In the simplest definition of diffraction, the inclusive final state  $X$  is replaced by the state  $X_M P'$ , which consists of a diffractively produced hadronic state with mass  $M$  and the scattered proton. This introduces the two additional kinematic variables  $\xi$  and  $t$ . However, no additional independent 4-vector is introduced as long as the measurement is inclusive with respect to the azimuthal angle of the scattered proton. Therefore, the decomposition in Eq. (2.4) remains valid, and the two diffractive structure functions  $F_{2,L}^{D(4)}(x, Q^2, \xi, t)$  can be defined. The diffractive cross section reads

$$\frac{d^2 \sigma_{ep \rightarrow ep X_M}}{dx dQ^2 d\xi dt} = \frac{4\pi \alpha_{\text{em}}^2}{x Q^4} \left\{ 1 - y + \frac{y^2}{2[1 + R^{D(4)}(x, Q^2, \xi, t)]} \right\} F_2^{D(4)}(x, Q^2, \xi, t), \quad (2.8)$$

where  $R^D = F_L^D/(F_2^D - F_L^D)$ . In view of the limited precision of the data, the dominance of the small- $y$  region, and the theoretical expectation of the smallness of  $F_L^D$ , the corrections associated with a non-zero value of  $R^D$  are neglected in the following.

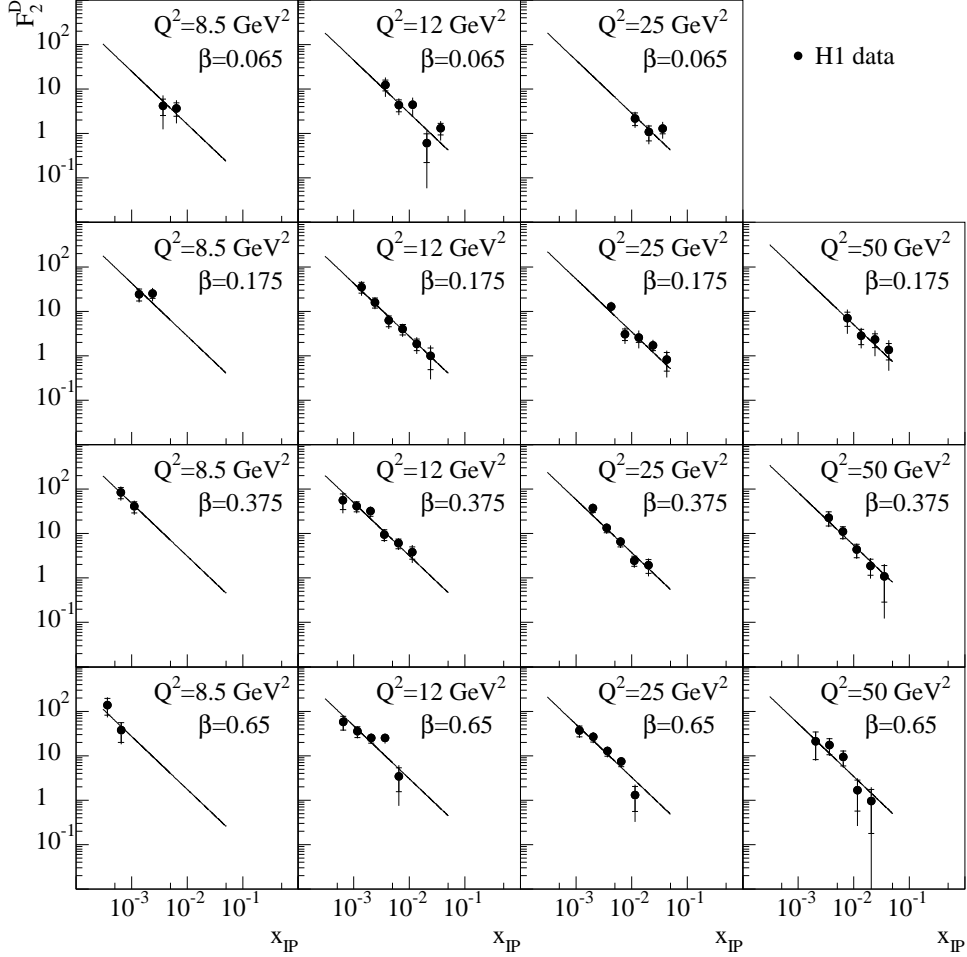


**Figure 2.4:** First measurement of the diffractive structure function  $F_2^{D(3)}(x, Q^2, \xi)$ . The fit is based on a factorizable  $\xi$  dependence of the form  $\xi^{-1.19}$  (figure from [69]).

A more inclusive and experimentally more easily accessible quantity can be defined by performing the  $t$  integration,

$$F_2^{D(3)}(x, Q^2, \xi) = \int dt F_2^{D(4)}(x, Q^2, \xi, t). \quad (2.9)$$

The results of the first measurement of this structure function, performed by the H1 collaboration, are shown in Fig. 2.4. (The underlying cross section includes events with small-mass excitations of the proton in the final state.) Far more precise measurements, since performed by both the H1 and ZEUS collaborations, are discussed in Chapter 7 together with different theoretical predictions.

The main qualitative features of diffractive electroproduction, already discussed in the previous section, become particularly apparent if the functional form of  $F_2^{D(3)}$  is considered. The  $\beta$  and  $Q^2$  dependence of  $F_2^{D(3)}$  is relatively flat. This corresponds to the observations discussed earlier that diffraction is a leading twist effect and that the mass distribution is consistent with a  $1/M_X^2$  spectrum. The success of a  $1/\xi^n$  fit, with  $n$  a

number close to 1, reflects the approximate energy independence of the diffractive cross section. More specifically, however, and in view of more precise recent measurements, it can be stated that the fitted exponent is above 1, so that a slight energy growth of the diffractive cross section is observed. This will be discussed in more detail later on.

Note finally that the formal definition of  $F_2^{D(3)}$  as an integral of  $F_2^{D(4)}$  [69] is not easy to implement since the outgoing proton or proton excitation is usually not tagged. Therefore, most measurements rely on different kinematic cuts, in particular an  $\eta_{\max}$  cut, and on models of the non-diffractive DIS background. A somewhat different definition of  $F_2^{D(3)}$ , based on the subtraction of ‘conventional DIS’ in the  $M_X^2$  distribution, was introduced in the ZEUS analysis of [71]. From a theoretical perspective, the direct measurement of  $F_2^{D(4)}$  by tagging the outgoing proton appears most desirable. Recently, such a measurement has been presented by the ZEUS collaboration [72] although the statistics are, at present, far worse than in the best available direct analyses of  $F_2^{D(3)}$  [73, 74].

# 3 Semiclassical Approach

In this chapter, the main physical idea and the technical methods of the semiclassical approach to diffraction are introduced. Although historically the semiclassical approach is not the first relevant model, it is, in the author's opinion, well suited as a starting point for the present review. On the one hand, it is sufficiently simple to be explained on a technical level within the limited space available. On the other hand, it allows for a clear demonstration of the interplay between the relevant kinematics and the fundamental QCD degrees of freedom.

The underlying idea is very simple. From the proton rest frame point of view, the very energetic virtual photon develops a partonic fluctuation long before the target. The interaction with the target is modelled as the scattering off a superposition of soft target colour fields, which, in the high-energy limit, can be calculated in the eikonal approximation. Diffraction occurs if this partonic system is quasi-elastically scattered off the proton. This means, in particular, that both the target and the partonic fluctuation remain in a colour singlet state.

## 3.1 Eikonal formulae for high-energy scattering

The amplitude for an energetic parton to scatter off a given colour field configuration is a fundamental building block in the semiclassical approach. This amplitude is the subject of the present section. The two other basic ingredients for the diffractive cross section, i.e., the amplitudes for the photon to fluctuate into different partonic states and the integration procedure over all colour field configurations of the target proton are discussed in the remainder of this chapter.

The essential assumptions are the softness and localization of the colour field and the very large energy of the scattered parton. Localization means that, in a suitable gauge, the colour field potential  $A_\mu(x)$  vanishes outside a region of size  $\sim 1/\Lambda$ , where  $\Lambda$  is a typical hadronic scale. Later on, it will be assumed that typical colour field configurations of the proton fulfil this condition. Softness means that the Fourier decomposition of  $A_\mu(x)$  is dominated by frequencies much smaller than the energy of the scattered parton. The assumption that this holds for all fields contributing to the proton state is a non-trivial one. It will be discussed in more detail at the end of this chapter.

The relevant physical situation is depicted in Fig. 3.1, where the blob symbolizes the target colour field configuration. Consider first the case of a scalar quark that is

minimally coupled to the gauge field via the Lagrangian

$$\mathcal{L}_{\text{scalar}} = (D_\mu \Phi)^* (D^\mu \Phi) \quad (3.1)$$

with the covariant derivative

$$D_\mu = \partial_\mu + igA_\mu. \quad (3.2)$$

In the high-energy limit, where the plus component of the quark momentum becomes large, the amplitude of Fig. 3.1 then reads

$$i2\pi\delta(k'_0 - k_0)T = 2\pi\delta(k'_0 - k_0)2k_0 \left[ \tilde{U}(k'_\perp - k_\perp) - (2\pi)^2\delta^2(k'_\perp - k_\perp) \right]. \quad (3.3)$$

It is normalized as is conventional for scattering processes off a fixed target (see, e.g., [75]). The expression in square brackets is the Fourier transform of the impact parameter space amplitude,  $U(x_\perp) - 1$ , where

$$U(x_\perp) = P \exp \left( -\frac{ig}{2} \int_{-\infty}^{\infty} A_-(x_+, x_\perp) dx_+ \right) \quad (3.4)$$

is the non-Abelian eikonal factor. The unit matrix  $1 \in SU(N_c)$ , with  $N_c$  the number of colours, subtracts the field independent part, and the path ordering operator  $P$  sets the field at smallest  $x_+$  to the rightmost position.

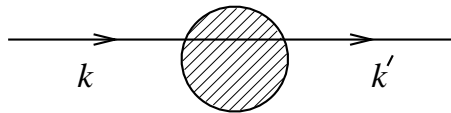


**Figure 3.1:** Scattering of a quark off the target colour field.

This formula or, more precisely, its analogue in the more realistic case of a spinor quark was derived by many authors. In the Abelian case, the high-energy amplitude was calculated in [6] in the framework of light-cone quantization. This result was taken over to QCD in [42]. A derivation in covariant gauge, based on the solution of the equation of motion for a particle in the colour background field, was given in [43]. In [45], the amplitude for the scattering of a fast gluon off a soft colour field was derived by similar methods.

For completeness, a derivation of the amplitude in Eq. (3.3), based on the summation of diagrams of the type shown in Fig. 3.2, is given in Appendix A of the present review. For the purpose of this section, it is sufficient to explain the main elements of Eq. (3.3) in a physical way, without giving the technical details of the derivation.

To begin with, it is intuitively clear that the eikonal factor  $U(x_\perp)$  appears since the fast parton, travelling in  $x_+$  direction and passing through the target at transverse position  $x_\perp$ , is rotated in colour space by the field  $A_\mu(x)$  that it encounters on its way.

Furthermore, the above amplitude is given for the situation in which the parton is localized at  $x_- \simeq 0$ . This co-ordinate of the fast parton does not change during the scattering process. Thus,  $A_\mu$  is always evaluated at  $x_- \simeq 0$ , and the  $x_-$  dependence is not shown explicitly.



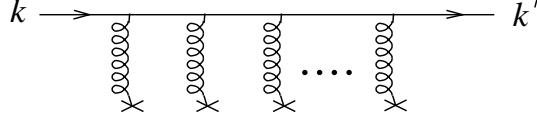


**Figure 3.2:** Typical diagrammatic contribution to the eikonal amplitude, Eq. (3.3). Attachments of gluon lines with crosses correspond to vertices at which the classical external field appears.

The energy  $\delta$ -function in Eq. (3.3) is an approximate one. It appears because the energy of the parton can not be significantly changed by the soft colour field.

Finally, due to the explicit factor  $k_0$ , the amplitude grows linearly with the parton energy, as is expected for a high-energy process with  $t$ -channel exchange of vector particles, in this case, of gluons.

The amplitude of Eq. (3.3) is easily generalized to the case of a spinor quark, where the new spin degrees of freedom are characterized by the indices  $s$  and  $s'$  (conventions of Appendix B). In the eikonal approximation, which is valid in the high-energy limit, helicity flip contributions are suppressed by a power of the quark energy (see Appendix A for more details). Thus, the generalization of Eq. (3.3) reads

$$i2\pi\delta(k'_0 - k_0)T_{ss'} = 2\pi\delta(k'_0 - k_0)2k_0 \left[ \tilde{U}(k'_\perp - k_\perp) - (2\pi)^2\delta^2(k'_\perp - k_\perp) \right] \delta_{ss'}. \quad (3.5)$$

Similarly, the amplitude for the scattering of a very energetic gluon off a soft colour field is readily obtained from the basic formula, Eq. (3.3). Note that, although the fast gluon and the gluons of the target colour field are the same fundamental degrees of freedom of QCD, the semiclassical approximation is still meaningful since an energy cut can be used to define the two different types of fields. The polarization of the fast gluon is conserved in the scattering process. The main difference to the quark case arises from the adjoint representation of the gluon, which determines the representation of the eikonal factor. Thus, the amplitude corresponding to Fig. 3.3 reads

$$i2\pi\delta(k'_0 - k_0)T_{\lambda\lambda'} = 2\pi\delta(k'_0 - k_0)2k_0 \left[ \tilde{U}^A(k'_\perp - k_\perp) - (2\pi)^2\delta^2(k'_\perp - k_\perp) \right] \delta_{\lambda\lambda'}, \quad (3.6)$$

where  $\lambda, \lambda'$  are the polarization indices and  $\tilde{U}^A$  is the Fourier transform of  $U^A(x_\perp)$ , the adjoint representation of the matrix  $U(x_\perp)$  defined in Eq. (3.4).

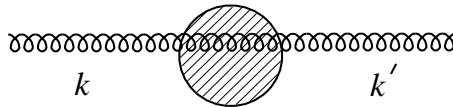


**Figure 3.3:** Scattering of a gluon off the target colour field.

Clearly, the above eikonal amplitudes have no physical meaning on their own since free incoming quarks or gluons cannot be realized. However, they serve as the basic building blocks for the high-energy scattering of colour neutral objects discussed in the next section.

## 3.2 Production of $q\bar{q}$ pairs

In this section, the eikonal approximation is used for the calculation of the amplitude for  $q\bar{q}$  pair production off a given target colour field [45]. Both diffractive and inclusive cross sections are obtained from the same calculation, diffraction being defined by the requirement of colour neutrality of the produced pair. The qualitative results of this section are unaffected by the procedure of integrating over all proton colour field configurations, which is discussed in Sect. 3.4.

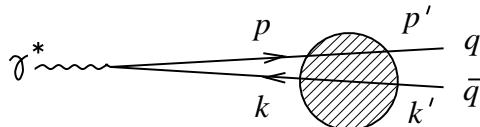


**Figure 3.4:** Electroproduction of a  $q\bar{q}$  pair off the target colour field.

The process is illustrated in Fig. 3.4. The corresponding  $T$  matrix element has three contributions,

$$T = T_{q\bar{q}} + T_q + T_{\bar{q}}, \quad (3.7)$$

where  $T_{q\bar{q}}$  corresponds to both the quark and antiquark interacting with the field, while  $T_q$  and  $T_{\bar{q}}$  correspond to only one of the partons interacting with the field.

Let  $V_q(p', p)$  and  $V_{\bar{q}}(k', k)$  be the effective vertices for an energetic quark and antiquark interacting with a soft gluonic field. For quarks with charge  $e$ , the first contribution to the amplitude of Eq. (3.7) reads

$$i2\pi\delta(k'_0 + k_0 - q_0)T_{q\bar{q}} = ie \int \frac{d^4k}{(2\pi)^4} \bar{u}_{s'}(p')V_q(p', p) \frac{i}{\not{p}' - m} \not{\epsilon}(q) \frac{i}{-\not{k} - m} V_{\bar{q}}(k, k')v_{r'}(k'), \quad (3.8)$$

where  $q = p + k$  by momentum conservation,  $\epsilon(q)$  is the polarization vector of the incoming photon, and  $r', s'$  label the spins of the outgoing quarks.

At small  $x$ , the quark and antiquark have large momenta in the proton rest frame. Hence, the propagators in Eq. (3.8) can be treated in a high-energy approximation. In a co-ordinate system where the photon momentum is directed along the  $z$ -axis, the large components are  $p_+$  and  $k_+$ . It is convenient to introduce, for each vector  $k$ , a vector  $\bar{k}$  whose minus component satisfies the mass shell condition,

$$\bar{k}_- = \frac{k_{\perp}^2 + m^2}{k_+}, \quad (3.9)$$

while the other components are identical to those of  $k$ . The propagators in Eq. (3.8) can be rewritten according to the identities

$$\frac{1}{\not{k} + m} = \frac{\sum_r v_r(\bar{k})\bar{v}_r(\bar{k})}{k^2 - m^2} + \frac{\gamma_+}{2k_+}, \quad (3.10)$$

$$\frac{1}{\not{p}' - m} = \frac{\sum_s u_s(\bar{p})\bar{u}_s(\bar{p})}{p'^2 - m^2} + \frac{\gamma_+}{2p_+}. \quad (3.11)$$

To obtain the first term in a high-energy expansion of the scattering amplitude  $T_{q\bar{q}}$ , the terms proportional to  $\gamma_+$  in Eqs. (3.10) and (3.11) can be dropped.

After inserting Eqs. (3.10) and (3.11) into Eq. (3.8), the relations

$$\bar{u}_{s'}(p')V_q(p',p)u_s(p) = 2\pi\delta(p'_0 - p_0)2p_0 \left[ \tilde{U}(p'_\perp - p_\perp) - (2\pi)^2\delta^2(p'_\perp - p_\perp) \right] \delta_{ss'}, \quad (3.12)$$

$$\bar{v}_r(k)V_{\bar{q}}(k,k')v_{r'}(k') = 2\pi\delta(k'_0 - k_0)2k_0 \left[ \tilde{U}^\dagger(k_\perp - k'_\perp) - (2\pi)^2\delta^2(k'_\perp - k_\perp) \right] \delta_{rr'}, \quad (3.13)$$

which correspond to Eq. (3.5) and its antiquark analogue, can be applied. Writing the loop integration as  $d^4k = (1/2)dk_+dk_-d^2k_\perp$  and using the approximation  $\delta(l_0) \simeq 2\delta(l_+)$  for the energy  $\delta$ -functions, the  $k_+$  integration becomes trivial. The  $k_-$  integral is done by closing the integration contour in the upper or lower half of the complex  $k_-$  plane. The result reads

$$T_{q\bar{q}} = -\frac{ie}{4\pi^2} q_+ \int d^2k_\perp \frac{\alpha(1-\alpha)}{N^2 + k_\perp^2} \bar{u}_{s'}(\bar{p})\not{e}(q)v_{r'}(\bar{k}) \times \left[ \tilde{U}(p'_\perp - p_\perp) - (2\pi)^2\delta^2(p'_\perp - p_\perp) \right] \left[ \tilde{U}^\dagger(k_\perp - k'_\perp) - (2\pi)^2\delta^2(k'_\perp - k_\perp) \right] \quad (3.14)$$

where

$$p'_+ = (1-\alpha)q_+, \quad k'_+ = \alpha q_+, \quad N^2 = \alpha(1-\alpha)Q^2 + m^2. \quad (3.15)$$

Thus,  $\alpha$  and  $1-\alpha$  characterize the fractions of the photon momentum carried by the two quarks, while  $(N^2 + k_\perp^2)$  measures the off-shellness of the partonic fluctuation before it hits the target. In the following, the quark mass is set to  $m = 0$ .

The above expression for  $T_{q\bar{q}}$  contains terms proportional to  $UU^\dagger$ ,  $U$ , and  $U^\dagger$ , as well as a constant term. The amplitudes  $T_q$  and  $T_{\bar{q}}$ , which contain terms proportional to  $U$  and  $U^\dagger$  and a constant term, are derived by the same methods. Calculating the full amplitude according to Eq. (3.7), the terms proportional to  $U$  and  $U^\dagger$  cancel. Thus, the colour field dependence of  $T$  is given by the expression

$$\left[ \tilde{U}(p'_\perp - p_\perp)\tilde{U}^\dagger(k_\perp - k'_\perp) - (2\pi)^4\delta^2(p'_\perp - p_\perp)\delta^2(k'_\perp - k_\perp) \right]. \quad (3.16)$$

Introducing the fundamental function

$$W_{x_\perp}(y_\perp) = U(x_\perp)U^\dagger(x_\perp + y_\perp) - 1, \quad (3.17)$$

which encodes all the information about the external field, the complete amplitude can eventually be given in the form

$$T = -\frac{ie}{4\pi^2} q_+ \int d^2k_\perp \frac{\alpha(1-\alpha)}{N^2 + k_\perp^2} \bar{u}_{s'}(\bar{p})\not{e}(q)v_{r'}(\bar{k}) \int_{x_\perp} e^{-i\Delta_\perp x_\perp} \tilde{W}_{x_\perp}(k'_\perp - k_\perp), \quad (3.18)$$

where  $\tilde{W}_{x_\perp}$  is the Fourier transform of  $W_{x_\perp}(y_\perp)$  with respect to  $y_\perp$ , and  $\Delta_\perp = k'_\perp + p'_\perp$  is the total transverse momentum of the final  $q\bar{q}$  state.

From the above amplitude, the transverse and longitudinal virtual photon cross sections are calculated in a straightforward manner using the explicit formulae for

$\bar{u}_{s'}(\bar{p})\not{e}(q)v_{r'}(\bar{k})$  given in Appendix B. Summing over all  $q\bar{q}$  colour combinations, as appropriate for the inclusive DIS cross section, the following result is obtained,

$$\frac{d\sigma_L}{d\alpha dk_{\perp}^{\prime 2}} = \frac{2e^2 Q^2}{(2\pi)^6} (\alpha(1-\alpha))^2 \int_{x_{\perp}} \left| \int d^2 k_{\perp} \frac{\tilde{W}_{x_{\perp}}(k'_{\perp} - k_{\perp})}{N^2 + k_{\perp}^2} \right|^2, \quad (3.19)$$

$$\frac{d\sigma_T}{d\alpha dk_{\perp}^{\prime 2}} = \frac{e^2}{2(2\pi)^6} (\alpha^2 + (1-\alpha)^2) \int_{x_{\perp}} \left| \int d^2 k_{\perp} \frac{k_{\perp} \tilde{W}_{x_{\perp}}(k'_{\perp} - k_{\perp})}{N^2 + k_{\perp}^2} \right|^2. \quad (3.20)$$

Note that only a single integration over transverse coordinates appears. This is a consequence of the  $\delta$ -function induced by the phase space integration over  $\Delta_{\perp}$ , applied to  $\exp[-i\Delta_{\perp}x_{\perp}]$  from Eq. (3.18) and to the corresponding exponential from the complex conjugate amplitude. The contraction of the colour indices of the two  $W$  matrices is implicit.

Consider the longitudinal cross section in more detail. The integrand can be expanded around  $k_{\perp} = k'_{\perp}$ . Shifting the integration variable  $k_{\perp}$  to  $l_{\perp} = k_{\perp} - k'_{\perp}$ , the Taylor expansion of the denominator in powers of  $l_{\perp}$  yields

$$\frac{1}{N^2 + (k'_{\perp} + l_{\perp})^2} = \frac{1}{N^2 + k_{\perp}^{\prime 2}} - \frac{2l_{\perp}k'_{\perp}}{(N^2 + k_{\perp}^{\prime 2})^2} + \dots \quad (3.21)$$

From the definition of the colour matrix  $W_{x_{\perp}}(y_{\perp})$  in Eq. (3.17), it is clear that

$$\int d^2 l_{\perp} \tilde{W}_{x_{\perp}}(-l_{\perp}) = (2\pi)^2 W_{x_{\perp}}(0) = 0, \quad (3.22)$$

$$\int d^2 l_{\perp} l_{\perp} \tilde{W}_{x_{\perp}}(-l_{\perp}) = i(2\pi)^2 \partial_{\perp} W_{x_{\perp}}(0). \quad (3.23)$$

Using rotational invariance, i.e.,  $k'_i k'_j \rightarrow \frac{1}{2} \delta_{ij} k_{\perp}^{\prime 2}$ , the result

$$\frac{d\sigma_L}{d\alpha dk_{\perp}^{\prime 2}} = \frac{4e^2 \alpha(1-\alpha) N^2 k_{\perp}^{\prime 2}}{(2\pi)^2 (N^2 + k_{\perp}^{\prime 2})^4} \int_{x_{\perp}} |\partial_{\perp} W_{x_{\perp}}(0)|^2 \quad (3.24)$$

is obtained. It evaluates to the total longitudinal cross section

$$\sigma_L = \frac{e^2}{6\pi^2 Q^2} \int_{x_{\perp}} |\partial_{\perp} W_{x_{\perp}}(0)|^2. \quad (3.25)$$

The transverse contribution can be evaluated in a similar way. In the perturbative region, where  $\alpha(1-\alpha) \gg \Lambda^2/Q^2$  and  $k_{\perp}^{\prime 2} \gg \Lambda^2$ , the integrand can again be expanded around  $k_{\perp} = k'_{\perp}$ . The analogue of Eq. (3.24) reads

$$\frac{d\sigma_T}{d\alpha dk_{\perp}^{\prime 2}} = \frac{e^2 [\alpha^2 + (1-\alpha)^2] [N^4 + k_{\perp}^{\prime 4}]}{2(2\pi)^2 (N^2 + k_{\perp}^{\prime 2})^4} \int_{x_{\perp}} |\partial_{\perp} W_{x_{\perp}}(0)|^2. \quad (3.26)$$

While, in the longitudinal case, the  $\alpha$  and  $k'_{\perp}$  integrations were readily performed, a divergence is encountered in the transverse case, Eq. (3.26). The  $k'_{\perp}$  integration gives rise to a factor  $1/\alpha(1-\alpha)$ , so that the  $\alpha$  integral diverges logarithmically at  $\alpha \rightarrow 0$  and

at  $\alpha \rightarrow 1$ . Thus, the region of small  $\alpha(1-\alpha)$ , where the expansion around  $k_\perp = k'_\perp$  does not work, is important for the total cross section  $\sigma_T$ , which therefore can not be obtained by integrating Eq. (3.26). Instead, the endpoint region, where the large distance structure of  $W_{x_\perp}(y_\perp)$  is important, can be separated by a cutoff  $\mu^2$  ( $\Lambda^2 \ll \mu^2 \ll Q^2$ ). The complete leading twist result for the transverse cross section, where contributions suppressed by powers of  $\Lambda^2/\mu^2$  or  $\mu^2/Q^2$  have been dropped, reads

$$\begin{aligned} \sigma_T &= \frac{e^2}{6\pi^2 Q^2} \left( \ln \frac{Q^2}{\mu^2} - 1 \right) \int_{x_\perp} |\partial_\perp W_{x_\perp}(0)|^2 \\ &+ \frac{e^2}{(2\pi)^6} \int_0^{\mu^2/Q^2} d\alpha \int dk'_\perp{}^2 \int_{x_\perp} \left| \int d^2 k_\perp \frac{k_\perp \tilde{W}_{x_\perp}(k'_\perp - k_\perp)}{N^2 + k_\perp^2} \right|^2. \end{aligned} \quad (3.27)$$

The resulting physical picture can be summarized as follows. For longitudinal photon polarization, the produced  $q\bar{q}$  pair has small transverse size and shares the photon momentum approximately equally. Only the small distance structure of the target colour field, characterized by the quantity  $|\partial_\perp W_{x_\perp}(0)|^2$ , is tested. For transverse photon polarization, an additional leading twist contribution comes from the region where  $\alpha$  or  $1-\alpha$  is small and  $k'_\perp{}^2 \sim \Lambda^2$ . In this region, the  $q\bar{q}$  pair penetrating the target has large transverse size, and the large distance structure of the target colour field, characterized by the function  $W_{x_\perp}(y_\perp)$  at large  $y_\perp$ , is tested. This physical picture, known as the aligned jet model, was introduced in [5] on a qualitative level and was used more recently for a quantitative discussion of small- $x$  DIS in [7].

It is now straightforward to derive the cross sections for the production of colour singlet  $q\bar{q}$  pairs corresponding, within the present approach, to diffractive processes. Note that the cross sections in Eqs. (3.19) and (3.20) can be interpreted as linear functionals of  $\text{tr}(W_{x_\perp}(y_\perp)W_{x_\perp}^\dagger(y'_\perp))$ , where the trace appears because of the summation over all colours of the produced  $q\bar{q}$  pair in the final state. Introducing a colour singlet projector into the underlying amplitude corresponds to the substitution

$$\text{tr} \left( W_{x_\perp}(y_\perp) W_{x_\perp}^\dagger(y'_\perp) \right) \rightarrow \frac{1}{N_c} \text{tr} W_{x_\perp}(y_\perp) \text{tr} W_{x_\perp}^\dagger(y'_\perp) \quad (3.28)$$

in Eqs. (3.19) and (3.20). This change of the colour structure has crucial consequences for the subsequent calculations.

Firstly, the longitudinal cross section, given by Eqs. (3.24) and (3.25), vanishes at leading twist since the derivative  $\partial_\perp W_{x_\perp}(0)$  is in the Lie-algebra of  $SU(N_c)$ , and therefore  $\text{tr} \partial_\perp W_{x_\perp}(0) = 0$ .

Secondly, for the same reason the  $\ln Q^2$  term in the transverse cross section, given by Eq. (3.27), disappears. The whole cross section is dominated by the endpoints of the  $\alpha$  integration, i.e., the aligned jet region, and therefore determined by the large distance structure of the target colour field. At leading order in  $1/Q^2$ , the diffractive cross sections read

$$\sigma_L^D = 0 \quad (3.29)$$

$$\sigma_T^D = \frac{e^2}{(2\pi)^6 N_c} \int_0^\infty d\alpha \int dk'_\perp{}^2 \int_{x_\perp} \left| \int d^2 k_\perp \frac{k_\perp \text{tr} \tilde{W}_{x_\perp}(k'_\perp - k_\perp)}{N^2 + k_\perp^2} \right|^2. \quad (3.30)$$

The cutoff of the  $\alpha$  integration,  $\mu^2/Q^2$ , has been dropped since, due to the colour singlet projection, the integration is automatically dominated by the soft endpoint.

In summary, the leading-twist cross section for small- $x$  DIS receives contributions from both small- and large-size  $q\bar{q}$  pairs, the latter corresponding to aligned jet configurations. The requirement of colour neutrality in the final state suppresses the small-size contributions. Thus, leading twist diffraction is dominated by the production of pairs with large transverse size testing the non-perturbative large-distance structure of the target colour field.

### 3.3 Higher Fock states

Given the leading order results for  $q\bar{q}$  pair production of the last section, it is natural to ask about the importance of radiative corrections. A systematic procedure for calculating to all orders in perturbation theory does not yet exist in the semiclassical framework. However, as will be seen in the following chapters, the summation of leading logarithms in  $Q^2$  is understood. Here, the particularly important case of the diffractive production of a quark-antiquark-gluon system (see Fig. 3.5) is discussed in some detail [45]. The purpose of this discussion is to establish, as one of the essential features of diffractive DIS, the necessary presence of a wee parton in the wave function of the incoming virtual photon.

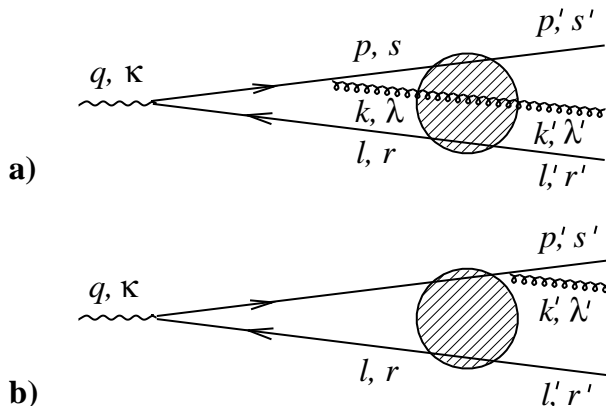


**Figure 3.5:** Diagrams for the process  $\gamma^* \rightarrow q\bar{q}g$ . Two similar diagrams with the gluon radiated from the produced antiquark have to be added.

Consider the sum of diagram Fig. 3.5a and its analogue with the gluon radiated from the antiquark. If the quark propagators with momenta  $p$  and  $l$  are rewritten according to Eqs. (3.10) and (3.11) and the  $\gamma_+$  terms are dropped, the corresponding amplitude can be given in the form

$$i2\pi\delta(p'_0 + k'_0 + l'_0 - q_0)T_{(a)} = \int \frac{d^4k}{(2\pi)^4} \int \frac{d^4l}{(2\pi)^4} \sum_{sr\lambda} T_{s's, r'r, \lambda'\lambda}^{(1)} T_{sr\lambda}^{(2)}. \quad (3.31)$$

Here  $T^{(1)}$  is the amplitude for the scattering of the  $q\bar{q}g$  system off the target colour field,

and  $T^{(2)}$  is the remainder of the diagram, describing the fluctuation of the virtual photon into the partonic state. In the following calculation, the  $k_{\perp}$  integration will be performed in such a way that the gluon propagator goes on shell. Anticipating this procedure, the sum over the intermediate gluon polarizations  $\lambda$  is restricted to the two physical polarizations, defined with respect to the on-shell vector  $\bar{k}$ . According to Eqs. (3.5) and (3.6), the contribution to  $T^{(1)}$  where quark, antiquark and gluon interact with the field reads

$$\left(T_{qqg}^{(1)}\right)_{s's, r'r, \lambda'\lambda} = i2\pi\delta(p'_0 - p_0)2p_0 \left[\tilde{U}(p'_{\perp} - p_{\perp}) - (2\pi)^2\delta^2(p'_{\perp} - p_{\perp})\right] \delta_{s's} \quad (3.32)$$

$$\times i2\pi\delta(l'_0 - l_0)2l_0 \left[\tilde{U}^{\dagger}(l_{\perp} - l'_{\perp}) - (2\pi)^2\delta^2(l'_{\perp} - l_{\perp})\right] \delta_{r'r} \quad (3.33)$$

$$\times i2\pi\delta(k'_0 - k_0)2k_0 \left[\tilde{U}^{\mathcal{A}}(k'_{\perp} - k_{\perp}) - (2\pi)^2\delta^2(k'_{\perp} - k_{\perp})\right] \delta_{\lambda'\lambda}. \quad (3.34)$$

As explained at the beginning of Sect. 3.2, contributions where not all of the partons interact with the field have to be added.

The photon- $q\bar{q}g$  transition amplitude  $T^{(2)}$ , with all colour indices suppressed, reads

$$T_{sr\lambda}^{(2)} = \frac{ieg_s}{p^2 k^2 l^2} \bar{u}_s(\bar{p}) \left[ \not{\epsilon}_{\lambda}(\bar{k}) \frac{i}{\not{p} + \not{k} - m} \not{\epsilon}(q) + \not{\epsilon}(q) \frac{i}{-\not{l} - \not{k} - m} \not{\epsilon}_{\lambda}(\bar{k}) \right] v_r(\bar{l}). \quad (3.35)$$

The colour structure of  $T_{(a)}$  is given by the combination of the  $U$  matrices in  $T^{(1)}$ , the indices of which are partially contracted according to the perturbative amplitude  $T^{(2)}$ . This colour structure is characterized by the colour tensor

$$(\tilde{W}^{(3)})_{\alpha\beta}^a = \int_{x_{\perp}, y_{\perp}, z_{\perp}} e^{i[x_{\perp}(p_{\perp} - p'_{\perp}) + y_{\perp}(k_{\perp} - k'_{\perp}) + z_{\perp}(l_{\perp} - l'_{\perp})]} (W^{(3)}(x_{\perp}, y_{\perp}, z_{\perp}))_{\alpha\beta}^a, \quad (3.36)$$

where

$$(W^{(3)}(x_{\perp}, y_{\perp}, z_{\perp}))_{\alpha\beta}^a = (U^{\mathcal{A}}(y_{\perp}))^{ab} (U(x_{\perp})T^b U^{\dagger}(z_{\perp}))_{\alpha\beta} - T_{\alpha\beta}^a, \quad (3.37)$$

and  $T_{\alpha\beta}^a$  are the conventional  $SU(N_c)$  generators with adjoint ( $a = 1 \cdots N_c^2 - 1$ ) and fundamental ( $\alpha, \beta = 1 \cdots N_c$ ) indices. The notation  $W^{(3)}$  is chosen to stress the similarity with the  $q\bar{q}$  case, where the external field is tested by the function  $W \equiv W^{(2)}$ , defined in Eq. (3.17). In analogy to this equation, the last term in Eq. (3.37) subtracts the unphysical contribution where none of the partons is scattered by the external field. One can think of  $x_{\perp}$ ,  $y_{\perp}$  and  $z_{\perp}$  as the transverse positions at which quark, gluon and antiquark penetrate the proton field, picking up corresponding non-Abelian eikonal factors. The indices  $\alpha, \beta$  and  $a$  correspond to the colours of the produced quark, antiquark and gluon.

To obtain the complete result, the amplitude  $T_{(b)}$ , which is the sum of the diagram in Fig. 3.5b and its analogue with the gluon radiated from the antiquark, has to be added. The calculation is similar to the case of the amplitude  $T_{(a)}$ . Since the gluon is radiated after the quark pair passes the target field, the colour structure is determined by the same function  $W$  that appeared in the  $q\bar{q}$  production amplitude of the last section.

The diagrams in Fig. 3.5, with summation over all possible colours of the  $q\bar{q}g$  final state, represent an  $\alpha_s$  correction to inclusive  $q\bar{q}$  pair production according to Fig. 3.4. The factor  $\alpha_s$  is accompanied by a factor  $\ln Q^2$ . Higher Fock states lead to additional factors

$\alpha_s \ln Q^2$ , and an all-orders summation can be performed using standard renormalization group techniques, i.e., Altarelli-Parisi evolution. The implementation of this summation in the semiclassical framework is explained in more detail at the end of Sect. 4.4 and in Appendix D. Hence, the inclusive case is not further discussed in this section.

For the diffractive case, the following situation can be anticipated on the basis of the experience of the last section. There are three qualitatively different kinematic configurations. First, if all three transverse momenta,  $p'_\perp$ ,  $k'_\perp$  and  $l'_\perp$  are soft, the large distance structure of the target field is tested, and a leading twist contribution to the DIS cross section results. Second, if all three momenta are large,  $p'^2_\perp, k'^2_\perp, l'^2_\perp \gg \Lambda^2$ , all three positions  $x_\perp, y_\perp$  and  $z_\perp$  in Eq. (3.37) are close together, and an expansion in powers of the target colour field can be performed. The leading term corresponds to colour octet exchange, so that no leading twist contribution to diffractive DIS results. Third, if two of the produced partons have high transverse momenta and the remaining parton is soft, a leading twist diffractive contribution arises. The two possible situations, depicted in Figs. 3.6 and 3.7, are discussed quantitatively below. The results of this calculation justify the physical picture outlined above.

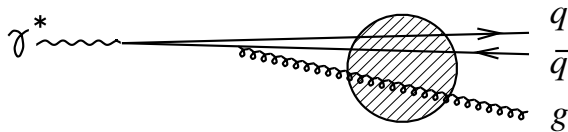


**Figure 3.6:** Space-time picture in the case of fast, high- $p_\perp$  quark and antiquark, passing the proton at small transverse separation, with a relatively soft gluon further away.

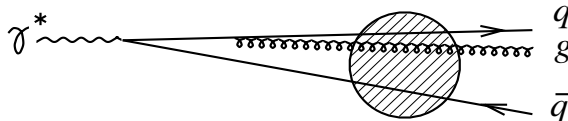


**Figure 3.7:** Space-time picture in the case of fast, high- $p_\perp$  quark and gluon, passing the proton at small transverse separation, with a relatively soft antiquark further away.

Consider first the case of high- $p_\perp$  quark and antiquark, i.e.,  $p'^2_\perp, l'^2_\perp \gg \Lambda^2$ , and relatively soft gluon, i.e.,  $k'^2_\perp \sim \Lambda^2$  and  $\alpha' \ll 1$ . Here  $\alpha' = k'_0/q_0$  is the analogue of the variable  $\alpha$  of the last section.

The assumption of a smooth external field implies small transverse momentum transfer from the proton, i.e.,  $|l''_\perp| \sim \Lambda$ , where  $l''_\perp = l'_\perp - l_\perp$ . The  $l_\perp$  integration in Eq. (3.31) can be replaced by an  $l''_\perp$  integration, substituting at the same time

$$l_\perp = l'_\perp - l''_\perp \quad \text{and} \quad p_\perp = -l'_\perp + l''_\perp - k_\perp. \quad (3.38)$$

Neglecting  $l''_\perp$  in  $T^{(2)}$ , which is justified since  $|l''^2_\perp| \ll |p'^2_\perp|, |l'^2_\perp|$ , the only remaining  $l''_\perp$  dependence is located in the colour factor  $\tilde{W}^{(3)}$ . This simplifies the  $l''_\perp$  integration to

$$\int \frac{d^2 l''_\perp}{(2\pi)^2} (\tilde{W}^{(3)})^a_{\alpha\beta}. \quad (3.39)$$



Defining  $\Delta \equiv p' + k' + l' - p - k - l$  to be the total momentum transferred from the proton,  $\tilde{W}^{(3)}$  can be given in the form

$$(\tilde{W}^{(3)})_{\alpha\beta}^a = \int_{x_\perp} e^{-ix_\perp \Delta_\perp} \int_{y_\perp, z_\perp} e^{iy_\perp(k_\perp - k'_\perp) + z_\perp(l_\perp - l'_\perp)} W^{(3)}(x_\perp, x_\perp + y_\perp, x_\perp + z_\perp)_{\alpha\beta}^a, \quad (3.40)$$

where  $l_\perp$  is given by Eq. (3.38). The  $l'_\perp$  integration gives a  $\delta$ -function of the variable  $z_\perp$ , thus resulting in the final formula

$$\int \frac{d^2 l'_\perp}{(2\pi)^2} (\tilde{W}^{(3)})_{\alpha\beta}^a = \int_{x_\perp} e^{-ix_\perp \Delta_\perp} \int_{y_\perp} e^{iy_\perp(k_\perp - k'_\perp)} W^{(3)}(x_\perp, x_\perp + y_\perp, x_\perp)_{\alpha\beta}^a. \quad (3.41)$$

This expression shows that in the kinematic situation with two high- $p_\perp$  quark jets and a relatively soft gluon the leading twist contribution is not affected by the transverse separation of the quarks. It is the transverse separation between quark-pair and gluon which tests large distances in the proton field and which can lead to non-perturbative effects.

The colour singlet projection of the colour tensor  $W^{(3)}$  reads

$$S(W^{(3)}) = \sqrt{\frac{2}{N_c^2 - 1}} (W^{(3)})_{\alpha\beta}^a T_{\beta\alpha}^a. \quad (3.42)$$

Using the identity

$$(U^{\mathcal{A}})^{ab} = 2 \operatorname{tr}[U^{-1} T^a U T^b], \quad (3.43)$$

where  $U \in SU(N_c)$ , the contribution relevant for diffraction, i.e., the production of a colour singlet  $q\bar{q}g$ -system, takes the form

$$\int \frac{d^2 l'_\perp}{(2\pi)^2} S(W^{(3)}) = \int_{x_\perp} e^{-ix_\perp \Delta_\perp} \frac{1}{\sqrt{2(N_c^2 - 1)}} \operatorname{tr}[\tilde{W}_{x_\perp}^{\mathcal{A}}(k_\perp - k'_\perp)], \quad (3.44)$$

where

$$W_{x_\perp}^{\mathcal{A}}(y_\perp) = U^{\mathcal{A}}(x_\perp) U^{\mathcal{A}\dagger}(x_\perp + y_\perp) - 1. \quad (3.45)$$

This is analogous to the quark pair production of the previous section (cf. Eq. (3.17)). However, now the two lines probing the field at positions  $x_\perp$  and  $x_\perp + y_\perp$  correspond to matrices in the adjoint representation. An intuitive explanation of this result is that the two high- $p_\perp$  quarks are close together and are rotated in colour space like a vector in the octet representation (cf. Fig. 3.6).

To make this last statement more precise, recall that an upper bound for the Ioffe-time of the fluctuation with two high- $p_\perp$  quarks is given by  $q_0/p_\perp^2$ . This means that the distance between the point where the virtual photon splits into the  $q\bar{q}$ -pair and the proton can not be larger than  $q_0/p_\perp^2$ . As long as the pair shares the longitudinal momentum of the photon approximately equally, i.e.,  $\alpha(1-\alpha) = \mathcal{O}(1)$ , the opening angle is  $\sim p_\perp/q_0$ . Hence, when quark and antiquark hit the proton, their transverse distance is  $\sim 1/|p_\perp| \ll 1/\Lambda$ .

The diagram in Fig. 3.5b and its analogue with the gluon radiated from the antiquark do not contribute to the diffractive cross section for high- $p_\perp$   $q\bar{q}$  pair production. This

is obvious since the colour field is probed only by the  $q\bar{q}$  system, the small transverse size of which prevents colour singlet exchange. Thus, the full cross section follows from Eq. (3.31), the simplified colour tensor of Eq. (3.44), and the formulae of Appendix B, which are used for the evaluation of the  $q\bar{q}\gamma$  and  $q\bar{q}g$  vertices in Eq. (3.35).

The results for longitudinal and transverse photon polarization read

$$\frac{d\sigma_L}{d\alpha dp_\perp^2 d\alpha' dk_\perp'^2} = \frac{\alpha_{\text{em}}\alpha_s}{2\pi^2(N_c^2 - 1)} \frac{\alpha' Q^2 p_\perp'^2}{[\alpha(1-\alpha)]^2 \hat{Q}^4} f_1(\alpha' \hat{Q}^2, k'_\perp), \quad (3.46)$$

$$\frac{d\sigma_T}{d\alpha dp_\perp'^2 d\alpha' dk_\perp'^2} = \frac{\alpha_{\text{em}}\alpha_s}{16\pi^2(N_c^2 - 1)} \frac{\alpha'[\alpha^2 + (1-\alpha)^2][p_\perp'^4 + N^4]}{[\alpha(1-\alpha)]^4 \hat{Q}^4} f_1(\alpha' \hat{Q}^2, k'_\perp), \quad (3.47)$$

with

$$f_1(\alpha' \hat{Q}^2, k'_\perp) = \int_{x_\perp} \left| \int \frac{d^2 k_\perp}{(2\pi)^2} \left( \delta^{ij} + \frac{2k_\perp^i k_\perp^j}{\alpha' \hat{Q}^2} \right) \frac{\text{tr} \tilde{W}_{x_\perp}^A(k'_\perp - k_\perp)}{\alpha' \hat{Q}^2 + k_\perp^2} \right|^2, \quad (3.48)$$

and

$$\hat{Q}^2 = Q^2 + \frac{p_\perp'^2}{\alpha(1-\alpha)}, \quad N^2 = \alpha(1-\alpha)Q^2. \quad (3.49)$$

At this point, the fundamental assumption of the softness of the gluon can be quantitatively justified. To achieve this, fix  $\alpha$  and  $p'_\perp$  and perform the integration over  $\alpha'$  and  $k'_\perp$ . As in Eq. (3.30), these two integrations are dominated by the region  $\alpha' \ll 1$  and  $k'_\perp \sim \Lambda^2$ . Thus, the diffractive production of a  $q\bar{q}g$  system with high- $p_\perp$  quark and antiquark occurs predominantly in a generalized aligned jet configuration, where the gluon is the wee parton in the photon wave function. It is this soft gluon that is responsible for the resulting leading twist cross section with colour singlet exchange.

As already pointed out above, another leading twist contribution to diffraction arises from the kinematic region where the quark or the antiquark is the soft particle and, accordingly, the outgoing antiquark-gluon or quark-gluon system has large transverse momentum. The calculation proceeds along the same lines as in the soft gluon case. The main qualitative difference is in the colour structure. In analogy to the discussion leading to Eq. (3.41), the large  $p_\perp$  of quark and gluon results in a small transverse separation (cf. Fig. 3.7), so that effectively the high- $p_\perp$  quark-gluon system is colour rotated like a single quark. Accordingly, the field is tested by the same function  $W$ , built from  $U$  matrices in the fundamental representation, that appeared in the  $q\bar{q}$  production cross section. Notice also that, in contrast to the soft gluon case, the diagram in Fig. 3.5b has to be taken into account.

The final results for the transverse and longitudinal cross sections read

$$\frac{d\sigma_L}{d\alpha dp_\perp'^2 d\alpha' dk_\perp'^2} = \frac{\alpha_{\text{em}}\alpha_s(N_c^2 - 1)}{2\pi^2 N_c^2} \frac{Q^2}{\alpha(1-\alpha)\hat{Q}^4} f_2(\alpha' \hat{Q}^2, k'_\perp), \quad (3.50)$$

$$\frac{d\sigma_T}{d\alpha dp_\perp'^2 d\alpha' dk_\perp'^2} = \frac{\alpha_{\text{em}}\alpha_s(N_c^2 - 1)}{8\pi^2 N_c^2 p_\perp'^2 \hat{Q}^4} \left[ \hat{Q}^4 - 2Q^2(\hat{Q}^2 + Q^2) + \frac{\hat{Q}^4 + Q^4}{\alpha(1-\alpha)} \right] f_2(\alpha' \hat{Q}^2, k'_\perp), \quad (3.51)$$

with

$$f_2(\alpha' \hat{Q}^2, k'_\perp) = \int_{x_\perp} \left| \int \frac{d^2 k_\perp}{(2\pi)^2} \frac{k_\perp \text{tr} \tilde{W}_{x_\perp}(k'_\perp - k_\perp)}{\alpha' \hat{Q}^2 + k_\perp^2} \right|^2. \quad (3.52)$$

These cross sections include both the soft quark and the soft antiquark regions. The kinematic variables do not correspond to Fig. 3.5. They are generic in the sense that  $p'_\perp$  and  $-p'_\perp$  are the transverse momenta of the two hard jets,  $\alpha$  and  $1-\alpha$  are the corresponding momentum fractions, and the soft parton, in this case the quark or the antiquark, is characterized by the transverse momentum  $k'_\perp$  and the longitudinal momentum fraction  $\alpha'$ . These conventions are chosen to emphasize the similarity with the soft gluon result of Eqs. (3.46)–(3.49). Again, the  $\alpha'$  and  $k'_\perp$  integrations are dominated by the region  $\alpha' \ll 1$  and  $k'^2_\perp \sim \Lambda^2$ .

### 3.4 Field averaging

So far, electroproduction off a fixed ‘soft’ colour field has been considered. As a consequence, electroproduction cross sections approach constant values as  $x \rightarrow 0$ . However, a proper treatment of the target requires the integration over all relevant colour field configurations.

Following the discussion of [45], consider first the elastic scattering of a quark off a proton. Although this process is unphysical since quarks are confined, it can serve to illustrate the method of calculation. Therefore in the following, confinement is ignored, and quarks are treated as asymptotic states. The generalization to the physical case of electroproduction is straightforward and will be discussed subsequently.

A point-like quark with initial momentum  $q$  scatters off the proton, which is a relativistic bound state with initial momentum  $p$ . Let  $m_p$  be the proton mass, and  $s$  and  $t$  the usual Mandelstam variables for a  $2 \rightarrow 2$  process. In the high-energy limit,  $s \gg t, m_p^2$ , the contribution from the annihilation of the incoming quark with an antiquark of the proton is negligible. The amplitude is dominated by diagrams with a fermion line going directly from the initial to the final quark state. Therefore, the proton can be described by a Schrödinger wave functional  $\Phi_P[A]$  (cf. [76]) depending on the gluon field only. Quarks are integrated out, yielding a modification of the gluonic action.

For a scattering process, the amplitude can be written in the proton rest frame as

$$\langle q'P' | qP \rangle = \lim_{T \rightarrow \infty} \int DA_T DA_{-T} \Phi_{P'}^*[A_T] \Phi_P[A_{-T}] \int_{A_{-T}}^{A_T} DA e^{iS[A]} \langle q' | q \rangle_A . \quad (3.53)$$

Here the fields  $A_{-T}$  and  $A_T$  are defined on three-dimensional surfaces at constant times  $-T$  and  $T$ , and  $A$  is defined in the four-dimensional region bounded by these surfaces. The field  $A$  has to coincide with  $A_{-T}$  and  $A_T$  at the boundaries, and the action  $S$  is defined by an integration over the domain of  $A$ . The amplitude  $\langle q' | q \rangle_A$  describes the scattering of a quark by the given external field  $A$ .

The initial state proton, having well defined momentum  $\vec{P}$ , is not well localized in space. However, the dominant field configurations in the proton wave functional are localized on a scale  $\Lambda \sim \Lambda_{QCD}$ . The field configurations  $A(\vec{x}, t)$ , which interpolate between initial and final proton state, are also localized in space at each time  $t$ . Assume that the incoming quark wave packet is localized such that it passes the origin  $\vec{x} = 0$  at time

$t = 0$ . At this instant the field configuration  $A(\vec{x}, t)$  is centered at

$$\vec{x}[A] \equiv \int d^3\vec{x} E_A(\vec{x}) \cdot \vec{x} \Big/ \int d^3\vec{x} E_A(\vec{x}), \quad (3.54)$$

where  $E_A(\vec{x})$  is the energy density of the field  $A(\vec{x}, t)$  at  $t = 0$ . The amplitude (3.53) can now be written as

$$\langle q'P'|qP \rangle = \lim_{T \rightarrow \infty} \int d^3\vec{x} \int DA_T DA_{-T} \Phi_{P'}^* \Phi_P \int_{A-T}^{A_T} DA e^{iS} \delta^3(\vec{x}[A] - \vec{x}) \langle q'|q \rangle_A. \quad (3.55)$$

Using the transformation properties under translations,

$$\langle q'|q \rangle_{L_{\vec{x}}A} = e^{i(\vec{q}-\vec{q}')\vec{x}} \langle q'|q \rangle_A, \quad \Phi_{P'}^*[L_{\vec{x}}A] \Phi_P[L_{\vec{x}}A] = e^{i(\vec{P}-\vec{P}')\vec{x}} \Phi_{P'}^*[A] \Phi_P[A], \quad (3.56)$$

where

$$L_{\vec{x}}A(\vec{y}) \equiv A(\vec{y} - \vec{x}), \quad (3.57)$$

one obtains,

$$\langle q'P'|qP \rangle = 2m_p (2\pi)^3 \delta^3(\vec{P}' + \vec{q}' - \vec{P} - \vec{q}) \int_{\{A\}} \langle q'|q \rangle_A. \quad (3.58)$$

Here  $\int_{\{A\}}$  denotes the operation of averaging over all field configurations contributing to the proton state which are localized at  $\vec{x} = 0$  at time  $t = 0$ . It is defined by

$$\int_{\{A\}} \Psi[A] \equiv \frac{1}{2m_p} \lim_{T \rightarrow \infty} \int DA_T DA_{-T} \Phi_{P'}^* \Phi_P \int_{A-T}^{A_T} DA e^{iS} \delta^3(\vec{x}[A]) \Psi[A] \quad (3.59)$$

for any functional  $\Psi$ . The normalization  $\int_{\{A\}} 1 = 1$  follows from

$$\langle P'|P \rangle = 2P_0 (2\pi)^3 \delta^3(\vec{P}' - \vec{P}). \quad (3.60)$$

More complicated processes can be treated in complete analogy as long as the proton scatters elastically. In particular, the above arguments apply to the creation of colour singlet quark-antiquark pairs,

$$\langle q\bar{q}P'|\gamma^*P \rangle = 2m_p (2\pi)^3 \delta^3(\vec{k}_f - \vec{k}_i) \int_{\{A\}} \langle q\bar{q}|\gamma^* \rangle_A, \quad (3.61)$$

where  $\vec{k}_i$  and  $\vec{k}_f$  are the sums of the momenta in the initial and final states respectively. The generalization of this simplest diffractive process to a process with an additional fast final state gluon,  $\gamma^* \rightarrow q\bar{q}g$  (cf. Sect. 3.3), is straightforward. In contrast to the quark-proton scattering discussed above, here a colour neutral state is scattered off the proton. Therefore no immediate contradiction with colour confinement arises. However, it has to be assumed that the hadronization of the produced partonic state takes place after the interaction with the proton, which is described in terms of fast moving partons.

The amplitude for the scattering off a soft external field contains an approximate energy  $\delta$ -function, giving rise to the definition of a functional  $F$ ,

$$\langle q\bar{q}|\gamma^* \rangle_A = 2\pi \delta(k_q^0 + k_{\bar{q}}^0 - q^0) F[A], \quad (3.62)$$

where  $q$ ,  $k_q$ ,  $k_{\bar{q}}$  are the momenta of the incoming photon and the outgoing quark and antiquark respectively. Since the energy transferred to the proton is small, Eq. (3.61) can now be written as

$$\langle q\bar{q}P' | \gamma^* P \rangle = 2m_p (2\pi)^4 \delta^4(k_f - k_i) \int_{\{A\}} F[A]. \quad (3.63)$$

When calculating the cross section from Eq. (3.63), the square of the 4-momentum-conserving  $\delta$ -function translates into one 4-momentum-conserving  $\delta$ -function using Fermi's trick. The spatial part of this  $\delta$ -function disappears after the momentum integration for the final state proton. The squared amplitude, integrated over the phase space  $\Phi^{(1)}$  of the outgoing proton and normalized to the total space-time volume, reads

$$\frac{1}{VT} \int d\Phi^{(1)} |\langle q\bar{q}P' | \gamma^* P \rangle|^2 = 4\pi m_p \delta(k_q^0 + k_{\bar{q}}^0 - q^0) \left| \int_{\{A\}} F[A] \right|^2, \quad (3.64)$$

as it should for the scattering off a superposition of external fields.

From the above discussion, a simple recipe for the calculation of diffractive processes at high energy follows:

The partonic process is calculated in a given external colour field, localized at  $\vec{x} = 0$  at time  $t = 0$ . The weighted average over all colour fields contributing to the proton state is taken on the amplitude level. It is assumed that the typical contributing field is smooth on a scale  $\Lambda$  and is localized in space on the same scale  $\Lambda$ . Finally, the cross section is calculated using standard formulae for the scattering off an external field.

The above discussion was limited to the case of diffraction and did not address the important question of how inclusive and diffractive electroproduction processes are interrelated. To arrive at a combined treatment of both processes, additional assumptions concerning the treatment of the target colour field have to be introduced. A corresponding discussion, following the analysis of [62], is outlined below.

As explained previously, in the semiclassical framework it is natural to expect diffraction to occur whenever the produced  $q\bar{q}$  pair emerges in a colour singlet state. Non-diffractive events are expected in the colour octet case. A combined treatment clearly forbids the use of the proton wave functional for the description of the final state. Thus, instead of the amplitude in Eq. (3.61), one has to consider the corresponding amplitude in a 'mixed' representation,  $\langle q\bar{q}A | \gamma^* P \rangle$ , where the final state consists of the outgoing  $q\bar{q}$  pair and a colour field configuration  $A$ . This formalism allows for both the creation of colour singlet and non-singlet partonic states.

For simplicity, time evolution of the field between the actual scattering process and the moment at which the final state field configuration  $A$  is defined is neglected. The squared amplitude, summed over all fields  $A$  and normalized to the total space-time volume, reads

$$\frac{1}{VT} \int DA |\langle q\bar{q}A | \gamma^* P \rangle|^2 = 4\pi m_p \delta(k_q^0 + k_{\bar{q}}^0 - q^0) \int DA_{\text{loc}} \left| \Phi_p[A_{\text{loc}}] F[A_{\text{loc}}] \right|^2. \quad (3.65)$$

Here the integral over  $A$  on the l.h. side replaces the phase space integral for the outgoing proton in Eq. (3.64). The index 'loc' symbolizes that, on the r.h. side of Eq. (3.65),

the integration is restricted to fields localized at, say,  $\vec{x} = 0$ . This can be achieved using translation covariance of the proton wave functional and of the matrix element  $\langle q\bar{q} | \gamma^* \rangle_A$ , in an argument similar to the one leading to Eqs. (3.59) and (3.64).

When writing  $W_{x_\perp}(y_\perp)$ , it has so far always been assumed that the functional dependence on the classical colour field configuration  $A_{\text{cl}}$  is implicit, so that one should really read  $W_{x_\perp}(y_\perp)[A_{\text{cl}}]$ . As can be seen from Eq. (3.65), the full inclusive cross sections are obtained from the previous formulae by the substitution

$$\text{tr}\left(W_{x_\perp}(y_\perp)[A_{\text{cl}}] W_{x_\perp}^\dagger(y_\perp)[A_{\text{cl}}]\right) \rightarrow \int DA_{\text{loc}} \left| \Phi_P[A_{\text{loc}}] \right|^2 \text{tr}\left(W_{x_\perp}(y_\perp)[A_{\text{loc}}] W_{x_\perp}^\dagger(y_\perp)[A_{\text{loc}}]\right). \quad (3.66)$$

The same applies to the diffractive cross sections, which are obtained by introducing a colour singlet projector on the amplitude level (cf. Eq. (3.28)).

Decomposing the field  $A_{\text{loc}}$  in Eq. (3.65) into its Fourier modes  $\tilde{A}_{\text{loc}}(\vec{k})$ , the path integral can be written as

$$\int_{A_{\text{loc}}} = \prod_{|\vec{k}| \ll |\vec{q}|} \int d\tilde{A}_{\text{loc}}(\vec{k}), \quad (3.67)$$

where the cutoff  $|\vec{q}|$  is required to ensure that the basic precondition for the semiclassical treatment, the softness of the target colour field with respect to the momenta of the fast particles, is respected. This cutoff induces a non-trivial energy dependence of the squared amplitude in Eq. (3.65) and therefore of both the inclusive and diffractive cross sections.

At present, no complete derivation of the explicit form of that energy dependence from first principles exists. However, a number of interesting related developments, approaching the high-energy limit of QCD from the perspective of colour fields and eikonized interactions, can be found, e.g., in [77, 78].

On the basis of the above qualitative picture, a soft, non-perturbative energy growth was ascribed to the input parton distributions used in the phenomenological analysis of [62] (see Sects. 6.2 and 7.1 for more details).

The discussion of the present section is closely related to Nachtmann's original proposal to treat high-energy hadron-hadron scattering in the eikonal approximation [43]. The above viewpoint corresponds to the rest frame of the proton, where the colour field encountered by the fast partons of the projectile is naturally considered to be part of the proton state. The viewpoint of [43] corresponds to the centre-of-mass frame of high-energy processes. In hadron-hadron scattering, both incoming particles are characterized by their parton content. These partons then interact via gluon fields which belong to neither of the two hadrons. So far, this is completely general. However, once the eikonal approximation is used to treat the parton propagators in the colour field background, one is forced to rely on modelling the light-cone wave function of the proton. In this case, the method becomes more predictive but less general than the wave functional treatment of the proton target discussed above.

# 4 From Soft Pomeron to Diffractive Parton Distributions

In the previous chapter, small- $x$  DIS was described as the eikonalized interaction of a partonic fluctuation of the virtual photon with a superposition of colour field configurations of the proton. Diffraction occurs whenever the partonic fluctuation preserves its overall colour neutrality. An essential feature of this approach is its formulation exclusively in terms of the fundamental degrees of freedom of QCD.

It is now appropriate to step back and take a look at diffraction from the historical perspective of soft hadronic physics (see [79] for a recent review of hadronic diffraction). It will soon become clear how partonic ideas arise in this framework and in which way they are related to the results of the last chapter.

## 4.1 Soft pomeron

Before introducing the pomeron, a concept from soft hadronic physics, it is appropriate to give a simple argument why, even at very high photon virtualities, diffractive DIS is largely a soft process. Such an argument was presented by Bjorken and Kogut in the framework of their aligned jet model [5] (see also [80]).

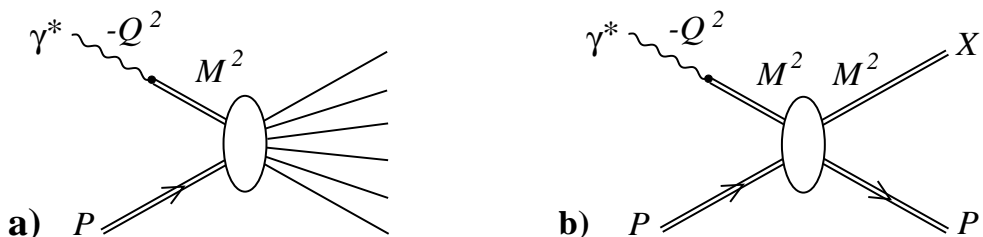


**Figure 4.1:** Vector meson dominance inspired picture of inclusive (a) and diffractive (b) electroproduction.

The underlying physical picture is based on vector meson dominance ideas. At high energy or small  $x$ , the incoming photon with virtuality  $q^2 = -Q^2$  fluctuates into a hadronic state with mass  $M$ , which then collides with the target (see Fig. 4.1a). The corresponding cross section for transverse photon polarization is estimated by

$$\frac{d\sigma_T}{dM^2} \sim \frac{dP(M^2)}{dM^2} \cdot \sigma(M^2), \quad (4.1)$$

where the probability for the photon to develop a fluctuation with mass  $M$  is given by

$$dP(M^2) \sim \frac{M^2 dM^2}{(M^2 + Q^2)^2}, \quad (4.2)$$

and  $\sigma(M^2)$  is the cross section for this fluctuation to scatter off the target. The above expression for  $dP(M^2)$  is most easily motivated in the framework of old-fashioned perturbation theory, where the energy denominator of the amplitude is proportional to the off-shellness of the hadronic fluctuation,  $Q^2 + M^2$ . If this is the only source for a  $Q^2$  dependence, the numerator factor  $M^2$  is necessary to obtain a dimensionless expression. (See the original derivation of Gribov [81] for more details.)

Bjorken and Kogut assume that, for large  $M^2$ , the intermediate hadronic state typically contains two jets and that  $\sigma(M^2)$  is suppressed for configurations with high  $p_\perp$  (the latter effect being now known under the name of colour transparency). Consider hadronic fluctuations with a certain  $M^2$ , which, in their respective rest frames, are realized by two back-to-back jets. Under the assumption that the probability distribution of the direction of the jet axis is isotropic, simple geometry implies that aligned configurations, defined by  $p_\perp^2 < \Lambda^2$  (where  $\Lambda^2$  is a soft hadronic scale), are suppressed by  $\Lambda^2/M^2$ . If only such configurations are absorbed with a large, hadronic cross section, the relations  $\sigma(M^2) \sim 1/M^2$  and

$$\frac{d\sigma_T}{dM^2} \sim \frac{1}{(M^2 + Q^2)^2} \quad (4.3)$$

follow. Thus, the above cross section can be interpreted as the total high-energy cross section of target proton and aligned jet fluctuation of the photon, i.e., of two soft hadronic objects. Therefore, a similar elastic cross section is expected,  $\sigma_T^D \sim \sigma_T$  (cf. Fig. 4.1b). The resulting diffractive structure function, as defined in the previous chapter, reads

$$F_2^{D(3)}(\xi, \beta, Q^2) \sim \frac{\beta}{\xi}. \quad (4.4)$$

It is interesting that the very simple arguments outlined above result in an expression for  $F_2^{D(3)}$  that captures two important features of the HERA data: the leading-twist nature of diffraction and the approximate  $1/\xi$  behaviour. The main problems of the model are the precise energy dependence, which is measured to be somewhat steeper than  $1/\xi$ , and the limit  $\beta \rightarrow 0$ , where a constant or even rising behaviour of  $F_2^{D(3)}$  is observed.

The above discussion shows, in very simple terms, what was also one of the main qualitative results of the more technical treatment of the last chapter: diffractive electroproduction is based on a soft hadronic high-energy cross section. Such cross sections are very successfully described within the framework of pomeron exchange [8]. Let us recall the basic underlying concepts (see [82] for a detailed discussion or [83] for a brief introduction).

Using analyticity and crossing symmetry, the amplitude  $T_{12 \rightarrow 34}(s, t)$ , depicted in Fig. 4.2, can be related to the amplitude  $T_{1\bar{3} \rightarrow 2\bar{4}}(s', t')$ , where  $s' = t$ ,  $t' = s$ , and bared



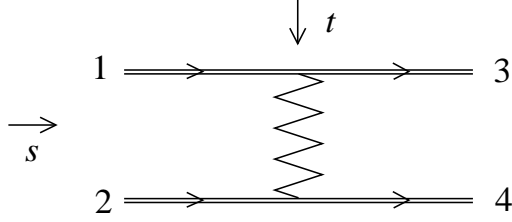


**Figure 4.2:** Scattering process  $12 \rightarrow 34$  via reggeon exchange.

numbers denote antiparticles. The partial wave expansion for this crossed amplitude reads

$$T_{1\bar{3} \rightarrow \bar{2}4}(s', t') = \sum_{l=0}^{\infty} (2l+1) a_l(s') P_l(\cos \theta), \quad (4.5)$$

where  $\theta$  is the centre-of-mass frame scattering angle, which is a function of  $s', t'$  and the particle masses, and  $P_l$  are Legendre polynomials. Let the two functions  $a_\eta(l, t)$  with  $\eta = +1$  and  $\eta = -1$  be the analytic continuations to complex  $l$  of the two sequences  $\{a_l(t), l = 0, 2, 4, \dots\}$  and  $\{a_l(t), l = 1, 3, 5, \dots\}$ . In the simplest non-trivial case, the only singularity of  $a_\eta(l, t)$  is a single  $t$ -dependent pole at  $l = \alpha(t)$ . It can then be shown that, in the limit  $s \rightarrow \infty$ ,

$$T_{12 \rightarrow 34}(s, t) = \beta_{13}(t) \beta_{24}(t) \zeta_\eta(\alpha(t)) \left( \frac{s}{s_0} \right)^{\alpha(t)}, \quad (4.6)$$

where  $s_0$  is an arbitrary scale factor,  $\beta_{13}$  and  $\beta_{24}$  are two unknown functions of  $t$ , and

$$\zeta_\eta(\alpha(t)) = \frac{1 + \eta e^{-i\pi\alpha(t)}}{\sin \pi\alpha(t)} \quad (4.7)$$

is the signature factor, depending on the signature  $\eta$  of the relevant Regge trajectory  $\alpha(t)$ . If  $a_\eta(l, t)$  has a more complicated analytic structure, the rightmost singularity in the  $l$  plane dominates the behaviour at large  $s$ .

Within the present context, the essential predictions of the asymptotic expression Eq. (4.6) are the power-like energy dependence  $s^{\alpha(t)}$  and the factorization of the unknown  $t$  dependence into the two vertex factors  $\beta_{13}$  and  $\beta_{24}$ . This last feature, which underlies the graphic representation of reggeon exchange in Fig. 4.2, is relevant if the same Regge trajectory governs different scattering processes. Note also that, for positive  $t = s'$  and integer  $l$ ,  $\alpha(t)$  describes the positions of poles of the physical amplitude  $T_{1\bar{3} \rightarrow \bar{2}4}(s', t')$ . Such poles are expected whenever an on-shell particle with appropriate mass  $m^2 = s'$  and angular momentum  $l$  can be created in the collision of 1 and  $\bar{3}$ . Indeed, most Regge trajectories pass through known physical states with mass  $m^2 = t$  and angular momentum  $\alpha(t)$ .

The Froissart bound [84] on the high-energy growth of total cross sections,

$$\sigma_{tot} \leq \frac{\pi}{m_\pi^2} \ln^2(s/s_0), \quad (4.8)$$

where  $m_\pi$  is the pion mass and  $s_0$  is an unknown scale factor, implies that  $\alpha(0) \leq 1$  for all Regge trajectories. However, it was observed early on that a very good fit to  $pp$  and  $p\bar{p}$  cross sections, which were measured to rise at high energy, could be obtained by assuming the dominance of a single pole with  $\alpha(0) > 1$  [85]. The corresponding trajectory, originally introduced with  $\alpha(0) = 1$  [86], is known as the pomeron trajectory (cf. the Pomeranchuk condition of [87]).

Donnachie and Landshoff demonstrated that a large set of different hadronic cross sections can be fitted with an intercept  $\alpha_P(0) = 1.08$  [8]. In spite of the power-like growth of Eq. (4.6), the predicted cross sections are so small that the Froissart bound is not violated below the Planck scale. It is then argued that unitarity is not a serious problem at all realistic energies. However, one should keep in mind that all following analyses based on a pomeron trajectory with  $\alpha(0) > 1$  are, strictly speaking, not self-consistent in the framework of Regge theory. In fact, it is likely that the rightmost singularity in the complex  $l$  plane is not a single pole but a cut, in which case many of the following results would have to be reconsidered.

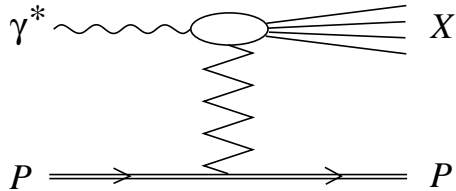


**Figure 4.3:** Diffractive electroproduction via pomeron exchange.

Given the universal success of the Donnachie-Landshoff pomeron, it is natural to apply the same trajectory to the quasi-elastic amplitude of diffractive electroproduction. Thus, the diagram in Fig. 4.1b is interpreted in terms of pomeron exchange (cf. Fig. 4.3). In this situation, the soft energy dependence of the pomeron and the measured  $t$  dependence of the proton-proton-pomeron vertex are naturally combined with the aligned jet model prediction of Eq. (4.3). Ignoring the vertex factor from the upper part of Fig. 4.3, one can write

$$\frac{d\sigma_T}{dt dM^2} \sim \frac{\beta_{pp}^2(t) s^{2(\alpha_P(t)-1)}}{(M^2 + Q^2)^2}. \quad (4.9)$$

The non-trivial energy dependence represents a clear improvement compared to Eqs. (4.3) and (4.4). However, our ignorance of the upper vertex prevents an unambiguous prediction of the  $M^2$  distribution. In fact, the obtained suppression at large  $M^2$ , which corresponds to the region of small  $\beta$ , appears to be the main qualitative problem of the presented model. Furthermore, the treatment of the hard scale  $Q^2$  is rather naïve in view of the impressive successes of QCD perturbation theory in the description of inclusive structure functions.

As is shown in the next section, a better understanding of the  $M^2$  dependence is possible in the framework of Regge theory. The obtained results allow for an interpretation of the upper vertex in Fig. 4.3 in terms of a  $\gamma^*$ -pomeron collision and thus for the application of QCD perturbation theory.

## 4.2 Pomeron structure function

It is the purpose of this section to explain the interpretation of Fig. 4.3 in terms of a  $\gamma^*$ -pomeron collision, thereby providing the background for the ensuing partonic treatment of the pomeron. Before doing so, it is helpful to recall Mueller's generalization of the optical theorem and the resulting triple-pomeron interpretation of single diffractive dissociation.

The optical theorem relates the two-particle total cross section to the imaginary part of the forward amplitude. This is illustrated by the first equality in Fig. 4.4. Here  $\sqrt{s}$  is the centre-of-mass energy of particles 1, 2, i.e., the mass of the system  $X$ , and the discontinuity across the real axis is defined by

$$\text{disc}_s A(s) = A(s + i\epsilon) - A(s - i\epsilon). \quad (4.10)$$

The last equality in Fig. 4.4 illustrates the high-energy limit, which is dominated by pomeron exchange.

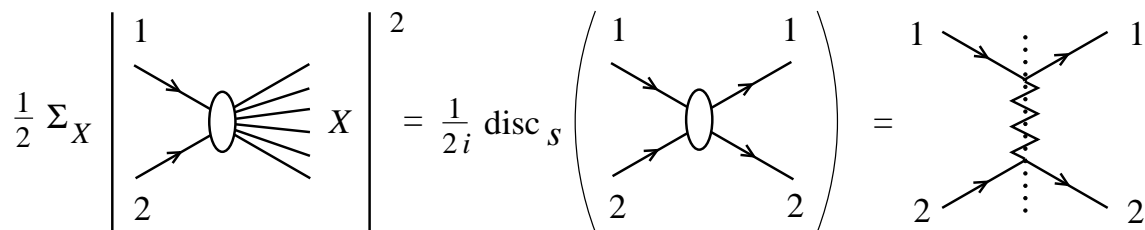


**Figure 4.4:** Graphic representation of the optical theorem for a two-particle total cross section. In the rightmost diagram, which is relevant in the pomeron-dominated high-energy limit, the cut is represented by a dotted line.

Mueller's generalization [88] (see also [82]), which is illustrated by the first equality in Fig. 4.5, relates a one-particle inclusive cross section to a six-particle amplitude. The derivation uses crossing symmetry to reinterpret the outgoing particle 3 as the incoming antiparticle  $\bar{3}$ . In very much the same way as for the usual optical theorem, completeness of the sum over  $X$  and unitarity are employed to relate the inclusive cross section to the discontinuity of the amplitude. Note, however, that in Fig. 4.5 the discontinuity is taken in  $M^2$ , which is the squared mass of the system  $X$  and different from the variable  $s$  characterizing the original process with incoming particles 1 and 2.

The rightmost diagram in Fig. 4.5 is obtained in the double limit  $s/M^2 \rightarrow \infty$  and  $M^2 \rightarrow \infty$  [89] (see also [82]). If  $s \gg M^2$  and  $M^2$  is much larger than any of the other variables, the process  $12 \rightarrow 3X$  is dominated by pomeron exchange, and the amplitude receives a factor  $\zeta_\eta(\alpha(t)) (s/M^2)^{\alpha_P(t)}$ . The appearance of the ratio  $s/M^2$  is a non-trivial result of the relevant kinematics. The remaining  $M^2$  dependence of the amplitude is given by the cut that is left after the two pomerons coupled to particles 2 and 3 are factorized. If the high-energy limit of this amplitude, which corresponds to  $M^2 \rightarrow \infty$ , is again dominated by pomeron exchange, a factor  $\zeta_\eta(\alpha(0)) (M^2)^{\alpha_P(0)}$  results. The appearance of these three 'pomeron propagators' is illustrated by the three zigzag lines on the r.h. side

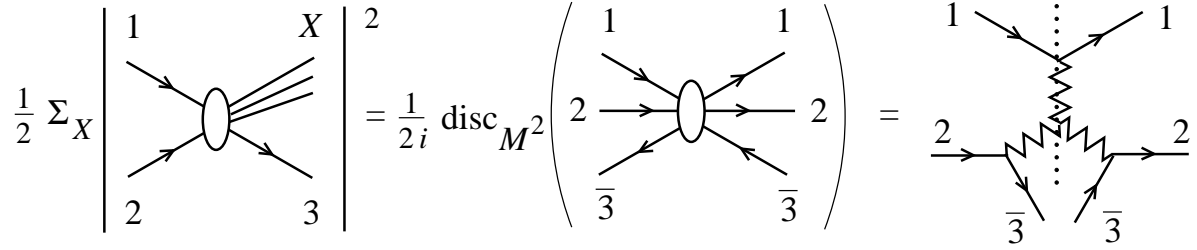


**Figure 4.5:** Graphic representation of Mueller's generalization of the optical theorem. In the rightmost diagram, relevant for  $s/M^2 \rightarrow \infty$  and  $M^2 \rightarrow \infty$ , the cut is only through the pomeron coupled to particle 1.

of Fig. 4.5. The corresponding cut amplitude reads

$$\text{disc } T = \left| \beta_{23}(t) \zeta_\eta(\alpha(t)) \left( \frac{s}{M^2} \right)^{\alpha_{\mathcal{P}}(t)} \right|^2 \text{disc} \left( G(t) \zeta_\eta(\alpha(0)) \left( \frac{M^2}{s_0} \right)^{\alpha_{\mathcal{P}}(0)} \beta_{11}(0) \right), \quad (4.11)$$

where  $G(t)$  is the unknown triple-pomeron vertex. Since the  $t$  dependence of  $G(t)$  is measured to be weak and since, for the pomeron,  $\eta = +1$ , the approximations  $G(t) \simeq G(0)$  and  $|\zeta_\eta| \simeq 1$  can be used at small  $|t|$ . The resulting cross section for the process  $12 \rightarrow 3X$  is given by

$$\frac{d\sigma}{dt dM^2} = \frac{1}{16\pi^2 M^2 s_0} |\beta_{23}(t)|^2 \left( \frac{s}{M^2} \right)^{2(\alpha_{\mathcal{P}}(t)-1)} |G(0)\beta_{11}(0)| \left( \frac{M^2}{s_0} \right)^{\alpha_{\mathcal{P}}(0)-1}. \quad (4.12)$$

This expression for the cross section suggests the following interpretation [90]. Incoming particle 2 radiates a pomeron carrying a fraction  $\xi = M^2/s$  of its momentum. Then, this pomeron collides with particle 1 producing the diffractive state  $X$  with mass  $M$ . According to this interpretation, Eq. (4.12) can be rewritten as

$$\frac{d\sigma}{dt d\xi} = f_{\mathcal{P}}(\xi, t) \sigma_{1\mathcal{P}}(M^2), \quad (4.13)$$

where

$$f_{\mathcal{P}}(\xi, t) = \frac{1}{16\pi^2 s_0} |\beta_{23}(t)|^2 \xi^{1-2\alpha_{\mathcal{P}}(t)} \quad (4.14)$$

is the pomeron flux factor, characterizing the probability for the transition  $2 \rightarrow 3\mathcal{P}$ , and

$$\sigma_{1\mathcal{P}}(M^2) = |G(0)\beta_{11}(0)| \left( \frac{M^2}{s_0} \right)^{\alpha_{\mathcal{P}}(0)-1} \quad (4.15)$$

is the total cross section for the collision of the pomeron and particle 1. Since the pomeron is not a real particle, the decomposition of Eq. (4.12) into pomeron flux and total cross section is ambiguous. The definitions given here correspond to interpreting  $\beta_{23}(t)$  and  $\zeta_\eta(\alpha(t)) (s/M^2)^{\alpha_{\mathcal{P}}}$  in Eq. (4.11) as pomeron-particle-particle vertex and pomeron propagator respectively. The rest of the diagram corresponds to the pomeron-particle scattering amplitude, which is used to define the pomeron-particle cross section.

In their seminal paper on diffractive jet production in hadron-hadron scattering, Ingelman and Schlein exploited this picture to predict the rate of high- $p_{\perp}$  jets within the diffractive final state  $X$  [9]. They suggested that, according to the parton model, hard processes in the collision of particle 1 and pomeron can be described in terms of a convolution of two parton distributions and a hard partonic cross section. The idea of introducing a parton distribution for the pomeron proved to be very successful phenomenologically and was widely used in subsequent analyses of hard diffractive processes.

Donnachie and Landshoff applied this idea to the case of diffractive DIS [10, 11], where particle 1 is a highly virtual photon and can therefore be treated in perturbation theory. In this approach, HERA diffraction at the level of a few per cent of the total DIS cross section was predicted as early as 1987 [10]. In contrast to Ingelman and Schlein, who focussed on the gluon distribution of the pomeron, Donnachie and Landshoff introduced a quark distribution, which can be directly probed by the virtual photon. The resulting physical picture of diffraction is shown in Fig. 4.6.

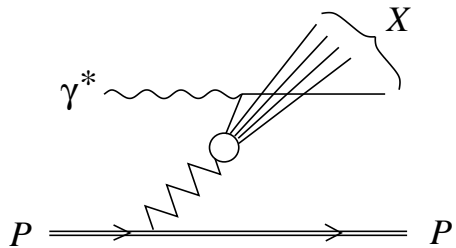


**Figure 4.6:** Diffractive DIS via the pomeron structure function.

In complete analogy to Eq. (4.13), the diffractive cross section can be written as

$$\frac{d\sigma_T}{dt d\xi} = f_P(\xi, t) \sigma_T^{\gamma^* P}, \quad (4.16)$$

where, according to the conventional parton model, the photon-pomeron cross section is given in terms of the quark distribution  $q_P(\beta, Q^2)$  of the pomeron,  $\sigma_T^{\gamma^* P} = (\pi e^2/Q^2) 2\beta q_P(\beta, Q^2)$ . Here  $\beta = x/\xi$  is the fraction of the pomeron momentum carried by the struck quark, and the factor 2 is introduced to account for the antiquark contribution. The resulting diffractive structure function reads

$$F_2^{D(4)}(x, Q^2, \xi, t) = f_P(\xi, t) 2\beta q_P(\beta, Q^2), \quad (4.17)$$

and a non-trivial  $Q^2$  dependence is naturally expected on the basis of the Altarelli-Parisi evolution of the quark distribution.

The above normalization of pomeron flux and pomeron-particle cross section is consistent with [82]. However, other normalizations are also frequently used (compare the conventions of [9–11, 90, 91]).

### 4.3 Diffractive parton distributions

Loosely speaking, the analysis of diffraction in terms of diffractive parton distributions is equivalent to the analysis in terms of the partonic pomeron of Ingelman and Schlein, ‘mi-

nus its Regge content' [92]. Diffractive parton distributions provide a direct, perturbative-QCD-based approach to the hard part of the process, without introducing any less well established non-perturbative concepts.

The basic theoretical ideas are due to Trentadue and Veneziano, who proposed to parametrize semi-inclusive hard processes in terms of 'fracture functions' [12], and to Berera and Soper, who defined similar quantities for the case of hard diffraction [13] and coined the term 'diffractive parton distributions'. The following discussion is limited to the latter, more specialized framework.

In short, diffractive parton distributions are conditional probabilities. A diffractive parton distribution  $df_i^D(y, \xi, t)/d\xi dt$  describes the probability of finding, in a fast moving proton, a parton  $i$  with momentum fraction  $y$ , under the additional requirement that the proton remains intact while being scattered with invariant momentum transfer  $t$  and losing a small fraction  $\xi$  of its longitudinal momentum. Thus, the corresponding  $\gamma^*p$  cross section can be written as [93]

$$\frac{d\sigma(x, Q^2, \xi, t)^{\gamma^*p \rightarrow p'X}}{d\xi dt} = \sum_i \int_x^\xi dy \hat{\sigma}(x, Q^2, y)^{\gamma^*i} \left( \frac{df_i^D(y, \xi, t)}{d\xi dt} \right), \quad (4.18)$$

where  $\hat{\sigma}(x, Q^2, y)^{\gamma^*i}$  is the total cross section for the scattering of a virtual photon characterized by  $x$  and  $Q^2$  and a parton of type  $i$  carrying a fraction  $y$  of the proton momentum. The above factorization formula holds in the limit  $Q^2 \rightarrow \infty$  with  $x$ ,  $\xi$  and  $t$  fixed.

At leading order and in the case of transverse photon polarization, only the quark distribution contributes. For one quark flavour with one unit of electric charge, the well-known partonic cross section reads

$$\hat{\sigma}_T(x, Q^2, y)^{\gamma^*q} = \frac{\pi e^2}{Q^2} \delta(1 - y/x), \quad (4.19)$$

giving rise to the diffractive cross section

$$\frac{d\sigma(x, Q^2, \xi, t)^{\gamma^*p \rightarrow p'X}}{d\xi dt} = \frac{2\pi e^2}{Q^2} \frac{x df_q^D(x, \xi, t)}{d\xi dt}, \quad (4.20)$$

where the factor 2 is introduced to account for the antiquark contribution.

The main difference to fracture functions is the requirement of a specific  $t$  transferred to the final state hadron. Since fracture functions are defined to include the  $t$  integration, a non-negligible contribution to the relevant cross section arises from processes where the outgoing hadron, in this case the proton, belongs to the current fragmentation region. This contribution complicates the  $Q^2$  dependence of fracture functions, but not of diffractive parton distributions. Even if the  $t$  integration is performed, the above problem does not arise in diffractive kinematics, where  $\xi$  is small and the production of a very energetic forward proton in the fragmentation of the current is strongly suppressed.

It is now obvious that Eqs. (4.16) and (4.17) of the last section form a special case of the present more general framework. There, Regge phenomenology and the assumption of a partonic pomeron lead to the specific form

$$x \frac{df_q^D(x, \xi, t)}{d\xi dt} = f_{\mathbb{P}}(\xi, t) \beta_{q\mathbb{P}}(\beta) \quad (4.21)$$

for the diffractive quark distribution. However, the factorizing dependence on  $\beta = x/\xi$  and the expression for the pomeron flux factor  $f_{\mathcal{P}}(\xi, t)$  given in the last section have not been derived in the framework of QCD.

The operator definition of diffractive parton distributions can be obtained as follows [93]. Consider first a complex scalar field  $\phi(x)$ , which can be written as

$$\phi(x) = \int d\tilde{k} \left[ \hat{a}(k) e^{-ikx} + \hat{b}^\dagger(k) e^{ikx} \right] \quad , \quad d\tilde{k} = \frac{d^3\vec{k}}{(2\pi)^3 2k_0} \quad , \quad (4.22)$$

where  $\hat{a}$  and  $\hat{b}$  are the annihilation operators of particles and antiparticles respectively. In this field theory, the number of particles with momentum in the interval  $d^3\vec{k}$  is measured by the operator

$$d\hat{N} = d\tilde{k} \hat{a}^\dagger(k) \hat{a}(k) \quad . \quad (4.23)$$

The conventional inclusive distribution  $f(y)$  of partons of the field  $\phi$  is given by the number of particles in a momentum interval  $dk_+ = P_+ dy$ , normalized to the size of the interval  $dy$ . Note that, in this section, the co-ordinate system is such that the proton and photon momenta have large plus and minus components respectively. This is customary for the discussion of DIS in the Breit frame and contrasts with the remainder of this review, where the proton rest frame is emphasized and, correspondingly, the photon momentum is defined to have a large plus component.

The particle number is measured in the state of a hadron with momentum  $P$ , and integration over all transverse momenta  $k_\perp$  is assumed. Thus, the explicit formula reads

$$(2\pi)^3 2P_0 \delta^3(\vec{P}' - \vec{P}) f(y) dy = \int d^2k_\perp \langle P' | \frac{d\hat{N}}{d^2k_\perp} | P \rangle \quad , \quad (4.24)$$

where the prefactor  $(2\pi)^3 2P_0 \delta^3(\vec{P}' - \vec{P})$  is a result of the normalization of the hadronic state  $|P\rangle$ ,

$$\langle P' | P \rangle = (2\pi)^3 2P_0 \delta^3(\vec{P}' - \vec{P}) \quad . \quad (4.25)$$

It can then be shown that, in terms of the fundamental field  $\phi$ , the distribution of scalar partons reads

$$f(y) = \frac{yP_+}{4\pi} \int dx_- e^{-iyP_+x_-/2} \langle P | \phi^\dagger(0, x_-, 0_\perp) \phi(0, 0, 0_\perp) | P \rangle \quad . \quad (4.26)$$

In the case of a gauge theory, this definition has to be supplemented with a link operator

$$U_{x_-, 0} = P \exp \left( -\frac{i}{2} \int_0^{x_-} A_+(0, y_-, 0_\perp) dy_- \right) \quad , \quad (4.27)$$

connecting the two scalar field operators.

Before generalizing this definition of the parton distribution to the diffractive case, it is convenient to rewrite it in the form

$$f(y) = \frac{yP_+}{4\pi} \int dx_- e^{-iyP_+x_-/2} \sum_X \langle P | \phi^\dagger(0, x_-, 0_\perp) U_{x_-, \infty} | X \rangle \langle X | U_{\infty, 0} \phi(0, 0, 0_\perp) | P \rangle \quad . \quad (4.28)$$

In the diffractive case, the operators describing the creation and annihilation of the parton are the same. However, the proton is required to appear in the final state carrying momentum  $P'$ . Thus, the above definition is changed to

$$\frac{df_q^D(y, \xi, t)}{d\xi dt} = \frac{yP_+}{64\pi^3} \int dx_- e^{-iyP_+x_-/2} \quad (4.29)$$

$$\times \sum_X \langle P | \phi^\dagger(0, x_-, 0_\perp) U_{x_-, \infty} | P', X \rangle \langle P', X | U_{\infty, 0} \phi(0, 0, 0_\perp) | P \rangle,$$

where  $\langle P', X |$  denotes the outgoing state, the only restriction on which is the presence of a scattered proton with momentum  $P'$ .

The above formulae for inclusive and diffractive distributions of scalar partons are generalized to the case of spinor quarks by the substitution

$$\phi^\dagger(0, x_-, 0_\perp) \phi(0, 0, 0_\perp) \longrightarrow \frac{1}{2yP_+} \bar{\psi}(0, x_-, 0_\perp) \gamma_+ \psi(0, 0, 0_\perp), \quad (4.30)$$

and to the case of gluons by the substitution

$$\phi^\dagger(0, x_-, 0_\perp) \phi(0, 0, 0_\perp) \longrightarrow \frac{1}{(yP_+)^2} F^\dagger(0, x_-, 0_\perp)^{+\mu} F(0, 0, 0_\perp)_\mu^+. \quad (4.31)$$

The operator expressions appearing in the definitions of both the inclusive and diffractive parton distributions are ultraviolet divergent. They are conveniently renormalized with the  $\overline{\text{MS}}$  prescription, which introduces the scale  $\mu$  as a further argument. The distribution functions then read  $f(x, \mu^2)$  and  $df^D(x, \xi, t, \mu^2)/d\xi dt$ .

Accordingly, Eq. (4.18) has to be read in the  $\overline{\text{MS}}$  scheme, with a  $\mu$  dependence appearing both in the parton distributions and in the partonic cross sections. The claim that Eq. (4.18) holds to all orders implies that these  $\mu$  dependences cancel, as is well known in the case of conventional parton distributions. Since the partonic cross sections are the same in both cases, the diffractive distributions obey the usual Altarelli-Parisi evolution equations,

$$\frac{d}{d(\ln \mu^2)} \frac{df_i^D(x, \xi, t, \mu^2)}{d\xi dt} = \sum_j \int_x^\xi \frac{dy}{y} P_{ij}(x/y) \frac{df_j^D(y, \xi, t, \mu^2)}{d\xi dt}. \quad (4.32)$$

with the ordinary splitting functions  $P_{ij}(x/y)$ .

Clearly, this is equivalent to the assertion that, in the operator definition of Eq. (4.29), the ultraviolet divergences are independent of the final state proton  $P'$ . If this is the case, the Altarelli-Parisi evolution of the distribution functions follows from the operator definitions exactly as in the inclusive case of Eq. (4.28).

Thus, for the analysis of diffractive DIS, it is essential to gain confidence in the validity of the factorization formula Eq. (4.18). Berera and Soper first pointed out [93] that such a factorization proof could be designed along the lines of related results for other QCD processes [94] (see [95] for a review).



Using Mueller’s method of cut vertices [96], Grazzini, Trentadue and Veneziano [97] proved, in the framework of a simple scalar model, that the above factorization property holds for ‘extended fracture functions’. These objects differ from fracture functions in that they are differential in the momentum transfer  $t$ . They are thus equivalent to the diffractive parton distributions discussed here.

Collins [98] showed that factorization holds in full QCD by generalizing the essential step of dealing with soft gluon interactions, which lies at the heart of many previous factorization proofs [95], to the case of diffractive DIS. A brief summary of the essential arguments is presented below.

To begin with, recall the main ideas of the factorization proof for inclusive DIS. It is based on the dominance of contributions from so-called leading regions, shown in Fig. 4.7a. Here the hard subgraph is denoted by H, the subgraphs with momenta collinear to  $P$  and to the produced jets are denoted by A and  $J_1 \cdots J_n$  respectively, and the soft subgraph is denoted by S. The analysis is performed in the Breit frame, where lines in H have typical virtuality  $Q^2$ , lines in A and  $J_1 \cdots J_n$  have small virtualities but may have large longitudinal momentum components of order  $Q$ , and all components of momenta in S are small compared to  $Q$ .

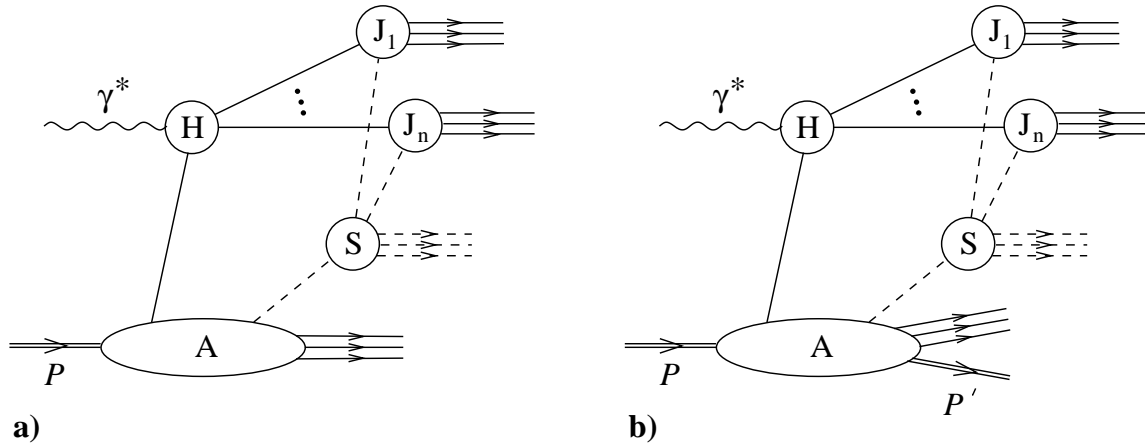


**Figure 4.7:** Leading regions in inclusive (a) and diffractive (b) DIS (cf. [98]).

The rationale behind the discussion in terms of leading regions is the realization that the momentum integrations are dominated by pinch singularities, i.e., poles of the propagators that can not be avoided by deforming the integration contours. In the limit of large  $Q^2$ , such singularities are associated with the leading regions shown in Fig. 4.7. By power counting, only one hard line may connect the A and H subgraphs, while arbitrarily many soft (dashed) lines may connect the soft subgraph with other parts of the diagram.

An essential part of the factorization proof is the demonstration that the soft subgraph can be factored out. More specifically, it has to be shown that the soft lines are not important for the subgraphs H and  $J_1 \cdots J_n$ , so that a perturbative hard cross section with free partons in the final state can be used. This is achieved using Ward identities, which, however, can only be applied in the region where all components of the soft momenta are small and of comparable size. Difficulties arising in the region where one

component of a soft momentum is much smaller than the other components can be solved by appropriately deforming the integration contour.

To see this in more detail, consider the particularly simple diagram of Fig. 4.8, where there is only one current jet, and a single soft gluon connects the corresponding jet subgraph with subgraph A. Let the soft gluon with momentum  $l$  couple to outgoing particles with momenta  $k_J$  and  $k_A$  in the subgraphs J and A respectively. The particle propagators

$$\frac{i}{(k_J - l)^2 - m^2 + i\epsilon} \quad \text{and} \quad \frac{i}{(k_A + l)^2 - m^2 + i\epsilon} \quad (4.33)$$

attached to the gluon vertices produce poles in the complex  $l_+$  and  $l_-$  planes that lie above and below the real axis respectively. This is also true for further  $l$  dependent propagators in J and A since, due to completeness, final state interactions can be disregarded in both subgraphs. Thus, regions where either  $l_+$  or  $l_-$  are too small can always be avoided by deforming the integration contour. This takes us back to the genuinely soft region where all components of  $l$  are small and of comparable size, and where Ward identities can be used to factor out the soft subgraph.

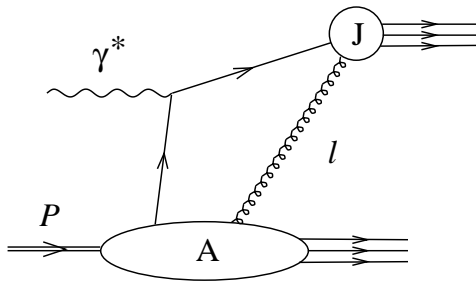


**Figure 4.8:** Leading order process in DIS with additional exchange of a soft gluon between the target and current jet subgraphs (cf. [98]).

It is precisely this part of the factorization proof that is affected in the case of diffraction. The requirement of a final state proton leads to the presence of final state interactions in subgraph A of Fig. 4.8 (as shown in Fig. 4.7b) that can not be neglected. Since both initial and final state interactions appear in A, poles on both sides of the  $l_-$  plane exist, and the contour can no longer be deformed to avoid the dangerous region of too small  $l_-$ . However, Collins was able to demonstrate [98] that deformations of the  $l_+$  contour can instead be used to show that this dangerous region does not produce a non-factorizing contribution. The argument is based on a detailed analysis of the pole structure in subgraphs  $J_1 \cdots J_n$  (or the single jet subgraph J in the simple example above). It leads to the conclusion that, exactly as in the inclusive case, the soft subgraph can be factored out. The result is a convolution of the calculable hard part with diffractive parton distributions.

Note that diffractive factorization does not hold in the case of hadron-hadron collisions. A general argument for this was given in [99], and the effect was also found in the model calculation of [13]. The reason is that, in contrast to the DIS case, the use of completeness in the final state can not be avoided in the factorization proof for hadron-

hadron collisions. This completeness is lost if a final state proton with a given momentum is required, and a breakdown of the factorization theorem results.

## 4.4 Target rest frame point of view

In this section, the connection between the target rest frame point of view, used in the semiclassical approach, and the Breit frame point of view, relevant for the two previous sections, is established. In particular, the consistency of the semiclassical approach with the concept of diffractive parton distributions and with the factorization formulae of the last section are demonstrated.

Even before the all-orders factorization proofs of [97] and [98], it was suggested that diffractive factorization could be understood in the semiclassical picture in the proton rest frame [100]. This was then explicitly shown in the leading order analysis of [49], on which the present section is largely based. Calculating the cross section with the methods of Chapter 3, a result is obtained that can be written as a convolution of a partonic cross section and a diffractive parton distribution. Within the semiclassical model, this diffractive parton distribution is explicitly given in terms of integrals of non-Abelian eikonal factors in the background field.

To be more specific, it is explicitly shown that the amplitude contains two fundamental parts: the usual hard scattering amplitude of a partonic process, and the amplitude for soft eikonal interactions with the external colour field. The latter part is determined by the scattering of one of the partons from the photon wave function. This parton has to have small transverse momentum and has to carry a relatively small fraction of the longitudinal photon momentum. In a frame where the proton is fast, this parton can be interpreted as a parton from the diffractive structure function.

The special role played by the soft parton in the photon wave function was also discussed in [28, 31, 101, 102] in the framework of two gluon exchange. However, the present approach has the two following advantages: firstly, by identifying the hard part as a standard photon-parton scattering cross section, the necessity for non-covariant photon wave function calculations is removed. Secondly, once it is established that the main contribution comes from the soft region, non-perturbative effects are expected to become important. The eikonal approximation provides a simple, self-consistent model for this non-perturbative region.

The explicit calculation closely follows the calculation of Chapter 3. It is convenient to start with the particularly simple case of scalar partons. The kinematic situation is shown symbolically in Fig. 4.9. The process is split into two parts, the hard amplitude for the transition of the photon into a virtual partonic state and the scattering of this state off the external field.

To keep the amplitude for the first part (denoted by H) hard, the transverse momenta  $p'_{(j)\perp}$  ( $j = 1\dots n$ ) are required to be large, i.e.,  $\sim Q$ . The momentum  $k_{\perp}$  is small, i.e.,  $\sim \Lambda$ , and the corresponding parton carries only a small fraction ( $\sim \Lambda^2/Q^2$ ) of the longitudinal photon momentum in the proton rest frame. While the hardness condition for particles 1

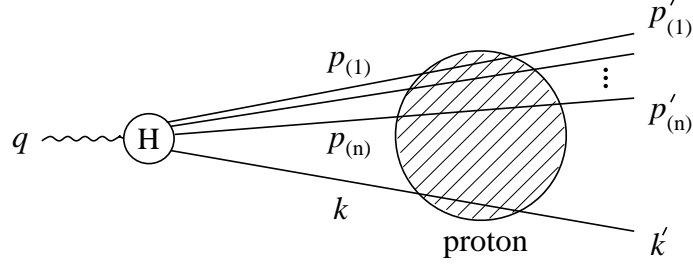


**Figure 4.9:** Hard diffractive process in the proton rest frame. The soft parton with momentum  $k$  is responsible for the leading twist behaviour of the cross section.

through  $n$  is introduced “by hand”, simply to make the process tractable, the softness of the last particle follows automatically from the requirement of leading twist diffraction.

The cross section for the scattering off a soft external field reads

$$d\sigma = \frac{1}{2q_0} |T|^2 2\pi \delta(q_0 - q'_0) dX^{(n+1)}, \quad \text{where } q' = k' + \sum p'_{(j)}. \quad (4.34)$$

All momenta are given in the proton rest frame,  $T$  is the amplitude corresponding to Fig. 4.9, and  $dX^{(n+1)}$  is the usual phase space element for  $n + 1$  particles.

According to Eq. (3.3), each of the particles interacts with the external field via the effective vertex

$$V(p', p) = 2\pi \delta(p'_0 - p_0) 2p_0 \left[ \tilde{U}(p'_\perp - p_\perp) - (2\pi)^2 \delta^2(p'_\perp - p_\perp) \right]. \quad (4.35)$$

The amplitude  $T$  can now be built from the hard amplitude  $T_H$  (symbolized by H in Fig. 4.9) together with the effective vertices defined by Eq. (4.35) and the appropriate propagators. It is convenient to consider first the amplitude  $T'$ , which is defined like  $T$  but without the transverse-space  $\delta$ -function terms of Eq. (4.35),

$$i 2\pi \delta(q_0 - q'_0) T' = \int T_H \prod_j \left( \frac{i}{p_{(j)}^2} 2\pi \delta(p'_{(j)0} - p_{(j)0}) 2p_{(j)0} \tilde{U}(p'_{(j)\perp} - p_{(j)\perp}) \frac{d^4 p_{(j)}}{(2\pi)^4} \right) \\ \times \left( \frac{i}{k^2} 2\pi \delta(k'_0 - k_0) 2k_0 \tilde{U}(k'_\perp - k_\perp) \right). \quad (4.36)$$

In this equation, colour indices have been suppressed. Notice also that some of the produced partons are antiparticles. The corresponding matrices  $U$  have to be replaced by  $U^\dagger$ . To keep the notation simple, this is not shown explicitly.

The integrations over the light-cone components  $p_{(j)+}$  can be performed using the appropriate energy  $\delta$ -functions. After that, the  $p_{(j)-}$  integrations are performed by picking up the poles of the propagators  $1/p_{(j)}^2$ . The result is

$$T' = \int T_H \prod_j \left( \tilde{U}(p'_{(j)\perp} - p_{(j)\perp}) \frac{d^2 p_{(j)\perp}}{(2\pi)^2} \right) \frac{2k_0}{k^2} \tilde{U}(k'_\perp - k_\perp). \quad (4.37)$$

Here poles associated with the  $p_{(j)\perp}$  dependence of  $T_H$  have been disregarded since their contribution is cancelled by diagrams where part of the hard interaction occurs after the scattering off the external field.

Next, a change of integration variables is performed,

$$d^2 p_{(n)\perp} \rightarrow d^2 k_{\perp}. \quad (4.38)$$

Since the external field is assumed to be soft, it can only transfer transverse momenta of order  $\Lambda$ , i.e.,  $p_{(j)\perp} \simeq p'_{(j)\perp}$  for all  $j$ . In general, the amplitude  $T_H$  will be dominated by the hard momenta of order  $Q$ . Therefore, it can be assumed that  $T_H$  is constant if the momenta  $p_{(j)\perp}$  vary on a scale  $\Lambda$ . In this approximation, the integrations over  $p_{(j)\perp}$  ( $j = 1 \dots n - 1$ ) can be performed in Eq. (4.37), resulting in  $\delta$ -functions in impact parameter space. These manipulations give the result

$$T' = \int \frac{d^2 k_{\perp}}{(2\pi)^2} \frac{2k_0}{k^2} T_H \int_{x_{\perp}, y_{\perp}} \left( \prod_j U(x_{\perp}) \right) U(x_{\perp} + y_{\perp}) e^{-ix_{\perp} \Delta_{\perp} - iy_{\perp} (k'_{\perp} - k_{\perp})}, \quad (4.39)$$

where  $\Delta$  is the total momentum transferred from the proton to the diffractive system and, in particular,  $\Delta_{\perp} = k'_{\perp} + \sum p'_{(j)\perp}$ . It is intuitively clear that the relative proximity of the high- $p_{\perp}$  partons in impact parameter space leads to the corresponding eikonal factors being evaluated at the same position  $x_{\perp}$ .

Now, the colour structure of the amplitude will be considered in more detail. Spelling out all the colour indices and introducing explicitly the colour singlet projector  $P$ , the relevant part of the amplitude reads:

$$T'_{colour} = T_H^{a_1 \dots a_n b} \left( \prod_j U(x_{\perp}) \right)_{a_1 \dots a_n}^{a'_1 \dots a'_n} U(x_{\perp} + y_{\perp})_b^{b'} P_{a'_1 \dots a'_n b'}. \quad (4.40)$$

Using the fact that  $T_H$  is an invariant tensor in colour space, and introducing the function  $W$  defined in Eq. (3.17), the following formula is obtained:

$$T_{colour} = T'_{colour} - T_H^{a_1 \dots a_n b} P_{a_1 \dots a_n b} = T_H^{a_1 \dots a_n b} W_b^{b'} P_{a_1 \dots a_n b'}. \quad (4.41)$$

Here the first equality states the explicit relation between  $T'$  and the true amplitude  $T$ , where the trivial contribution of zeroth order in  $A$  has been subtracted. This subtraction corresponds to the unit matrix on the r.h. side of Eq. (3.17).

For colour covariance reasons

$$T_H^{a_1 \dots a_n b} P_{a_1 \dots a_n b'} = \text{const.} \times \delta_{b'}^b. \quad (4.42)$$

Since the photon is colour neutral, the following equality holds:

$$T_H^{a_1 \dots a_n b} T_H^*_{a_1 \dots a_n b} = |T_H^{a_1 \dots a_n b} P_{a_1 \dots a_n b}|^2 = |\text{const.}|^2 N_c^2. \quad (4.43)$$

Here the partons are assumed to be in the fundamental representation of the colour group  $SU(N_c)$ . Combining Eq. (4.41) with Eqs. (4.42) and (4.43), it becomes clear that the colour structure of the hard part decouples from the eikonal factors,

$$|T_{colour}|^2 = \frac{1}{N_c} |\text{tr}[W]|^2 |T_H|^2. \quad (4.44)$$

The hard part will be interpreted in terms of an incoming small- $k_\perp$  parton that collides with the virtual photon to produce the outgoing partons 1 through  $n$ . Therefore, a factor  $1/N_c$  for initial state colour averaging is included in the definition of  $|T_H|^2$ .

In the expression for the cross section, the two functions  $W$  appear in the combination

$$\left(\text{tr}[W_{x_\perp}(y_\perp)]\right)\left(\text{tr}[W_{x'_\perp}(y'_\perp)]\right)^* e^{-i(x_\perp-x'_\perp)\Delta_\perp}, \quad (4.45)$$

with independent integrations over  $x_\perp, x'_\perp, y_\perp$  and  $y'_\perp$ . If the external field is sufficiently smooth, the functions  $W$  vary only slowly with  $x_\perp$  and  $x'_\perp$ . Therefore, after integration over  $x_\perp$  and  $x'_\perp$ , the expression in Eq. (4.45) produces an approximate  $\delta$ -function in  $\Delta_\perp$ . Furthermore, it is assumed that the measurement is sufficiently inclusive, i.e., the hard momenta  $p'_{(j)\perp}$  are not resolved on a soft scale  $\Lambda$ . This corresponds to a  $\Delta_\perp$ -integration, which gives an approximate  $\delta$ -function in  $x_\perp - x'_\perp$ . Since the expression in Eq. (4.45) will always appear under  $x_\perp, x'_\perp$  and  $\Delta_\perp$  integration, the above considerations justify the substitution

$$e^{-i(x_\perp-x'_\perp)\Delta_\perp} \rightarrow (2\pi)^2 \delta^2(x_\perp - x'_\perp) \delta^2(\Delta_\perp). \quad (4.46)$$

Combining Eqs. (4.34), (4.39) and (4.44), the following formula for the cross section results,

$$d\sigma = \frac{1}{2q_0} \int |T_H|^2 \int_{x_\perp} \left| \int \frac{d^2k_\perp}{(2\pi)^2} \frac{\text{tr}[\tilde{W}_{x_\perp}(k'_\perp - k_\perp)]}{\sqrt{N_c} k^2} \right|^2 (2k_0)^2 (2\pi)^3 \delta^2(\sum p_{(j)\perp}) \delta(q_0 - q'_0) dX^{(n+1)}. \quad (4.47)$$

Note that the soft momentum  $k'_\perp$  has been neglected in the transverse  $\delta$ -function.

To finally establish the parton model interpretation of diffraction, the hard partonic cross section based on  $|T_H|^2$  has to be identified in Eq. (4.47). Consider the process

$$\gamma^*(q) + q(yP) \rightarrow q(p'_{(1)}) + \dots + q(p'_{(n)}), \quad (4.48)$$

where the photon collides with a parton carrying a fraction  $y$  of the proton momentum and produces  $n$  high- $p_\perp$  final state partons. The cross section is approximately given by

$$d\hat{\sigma}(y) = \frac{1}{2(\hat{s} + Q^2)} |T_H|^2 (2\pi)^4 \delta^4(q - k - \sum p'_{(j)}) dX^{(n)}, \quad (4.49)$$

where  $\hat{s} = (\sum p'_{(j)})^2$  and the quantities  $|T_H|^2$  and  $k$  are the same as in the previous discussion. Equation (4.49) is not exact for several reasons. On the one hand,  $|T_H|^2$  is defined in terms of the unprimed momenta  $p_{(j)}$ , which differ slightly from  $p'_{(j)}$ . On the other hand, the vector  $k$  is slightly off shell and has, in general, a non-zero transverse component. However, both effects correspond to  $\Lambda/Q$  corrections, where  $Q$  stands generically for the hard scales that dominate  $T_H$ .

Using Eq. (4.49), the cross section of Eq. (4.47) can now be rewritten as

$$d\sigma = \int dk_- \int \frac{\hat{s} + Q^2}{2\pi q_0} (2k_0)^2 d\hat{\sigma}(y) \int_{x_\perp} \left| \int \frac{d^2k_\perp}{(2\pi)^2} \frac{\text{tr}[\tilde{W}_{x_\perp}(k'_\perp - k_\perp)]}{\sqrt{N_c} k^2} \right|^2 \frac{d^3k'}{(2\pi)^3 2k'_0}. \quad (4.50)$$

The light-cone component  $k_-$  is given by  $-k_- = yP_- = ym_p$ . Note that the minus sign in this formula comes from the interpretation of the parton with momentum  $k$

as an incoming particle in Eq. (4.49). This is, in fact, the crucial point of the whole calculation: due to the off-shellness of  $k$ , the corresponding parton can be interpreted as an incoming particle in both the process of Eq. (4.48) and in the soft scattering process off the external field. The latter process, where an almost on-shell parton with momentum  $k$  scatters softly off the external field changing its momentum to the on-shell vector  $k'$ , is most easily described in the proton rest frame. By contrast, the natural frame for the hard part of the diagram is the Breit frame or a similar frame. In such a frame, the  $k_-$  component is large and negative, so that the above parton can be interpreted as an almost on-shell particle with momentum  $-k$ , colliding head-on with the virtual photon.

Substituting the variables  $y$  and  $\xi$  for  $k_-$  and  $k'_3$ , the cross section, Eq. (4.50), takes the form

$$\frac{d\sigma}{d\xi} = \int_x^\xi dy \hat{\sigma}(y) \left( \frac{df_s^D(y, \xi)}{d\xi} \right), \quad (4.51)$$

where the diffractive parton distribution for scalars is

$$\frac{df_s^D(y, \xi)}{d\xi} = \frac{1}{\xi^2} \left( \frac{\beta}{1-\beta} \right) \int \frac{d^2 k'_\perp (k'^2_\perp)^2}{(2\pi)^4 N_c} \int_{x_\perp} \left| \int \frac{d^2 k_\perp}{(2\pi)^2} \frac{\text{tr}[\tilde{W}_{x_\perp}(k'_\perp - k_\perp)]}{k'^2_\perp \beta + k^2_\perp (1-\beta)} \right|^2. \quad (4.52)$$

This result is in complete agreement with the concepts described in the last section. In contrast to the formulae presented there, the above parton distribution is inclusive in  $t$ . However, as will be seen in an example calculation in Sect. 6.1, parton distributions differential in  $t$  can also be obtained in this formalism.

For an external colour field that is smooth on a soft scale  $\Lambda$  and confined to a region of approximate size  $1/\Lambda$ , the function  $\text{tr}[W_{x_\perp}(y_\perp)]$  is also smooth and vanishes at  $y_\perp = 0$  together with its first derivative. From this it can be derived that the  $k_\perp$  and  $k'_\perp$  integrations in Eq. (4.52) are dominated by the soft scale. This justifies, a posteriori, the softness assumption for one of the partons used in the derivation.

The qualitative result is that the eikonal scattering of this soft parton off the proton field determines the diffractive parton distribution. The hard part of the photon evolution can be explicitly separated and expressed in terms of a standard cross section for photon-parton collisions.

Having worked out the kinematics in the simple scalar case, it is straightforward to extend the calculation to realistic quarks and gluons. The introduction of spinor or vector partons does not affect the calculations leading to the generic expression in Eq. (4.51). However, those parts of the calculation responsible for the specific form of Eq. (4.52) have to be changed if the soft parton is a spinor or vector particle.

Referring the reader to Appendix C for details, only the final formulae for diffractive quark and gluon distributions in the semiclassical approach are presented below. They read

$$\frac{df_q^D(y, \xi)}{d\xi} = \frac{2}{\xi^2} \int \frac{d^2 k'_\perp (k'^2_\perp)}{(2\pi)^4 N_c} \int_{x_\perp} \left| \int \frac{d^2 k_\perp}{(2\pi)^2} \frac{k_\perp \text{tr}[\tilde{W}_{x_\perp}(k'_\perp - k_\perp)]}{k'^2_\perp \beta + k^2_\perp (1-\beta)} \right|^2, \quad (4.53)$$

for the case of a realistic spinor quark, and

$$\frac{df_g^D(y, \xi)}{d\xi} = \frac{1}{\xi^2} \left( \frac{\beta}{1-\beta} \right) \int \frac{d^2 k'_\perp (k'^2_\perp)^2}{(2\pi)^4 (N_c^2 - 1)} \int_{x_\perp} \left| \int \frac{d^2 k_\perp}{(2\pi)^2} \frac{\text{tr}[\tilde{W}_{x_\perp}^A(k'_\perp - k_\perp)] t^{ij}}{k'^2_\perp \beta + k^2_\perp (1-\beta)} \right|^2, \quad (4.54)$$

with

$$t^{ij} = \delta^{ij} + \frac{2k^i_\perp k^j_\perp}{k'^2_\perp} \left( \frac{1-\beta}{\beta} \right), \quad (4.55)$$

for the case of a gluon. It was checked explicitly that these distribution functions together with the appropriate partonic cross sections reproduce the results of Sects. 3.2 and 3.3. Henceforth, the simplified notation  $dq(y, \xi)/d\xi$  and  $dg(y, \xi)/d\xi$  will be used for the diffractive quark and gluon distribution calculated above.

The application of these diffractive quark and gluon distributions to diffractive DIS is summarized in an intuitive way in Fig. 4.10. On the l.h. side, the two lowest-order processes,  $q\bar{q}$  and  $q\bar{q}g$  state production, are shown from the target rest frame point of view. On the r.h. side, the same two processes are shown from the Breit frame point of view, which is conventionally used to discuss the partonic interpretation of DIS. The essence of the calculations presented in the present section is the identification of these two viewpoints, as a result of which explicit formulae for the diffractive parton distributions, expressed in terms of the target colour field, are obtained.

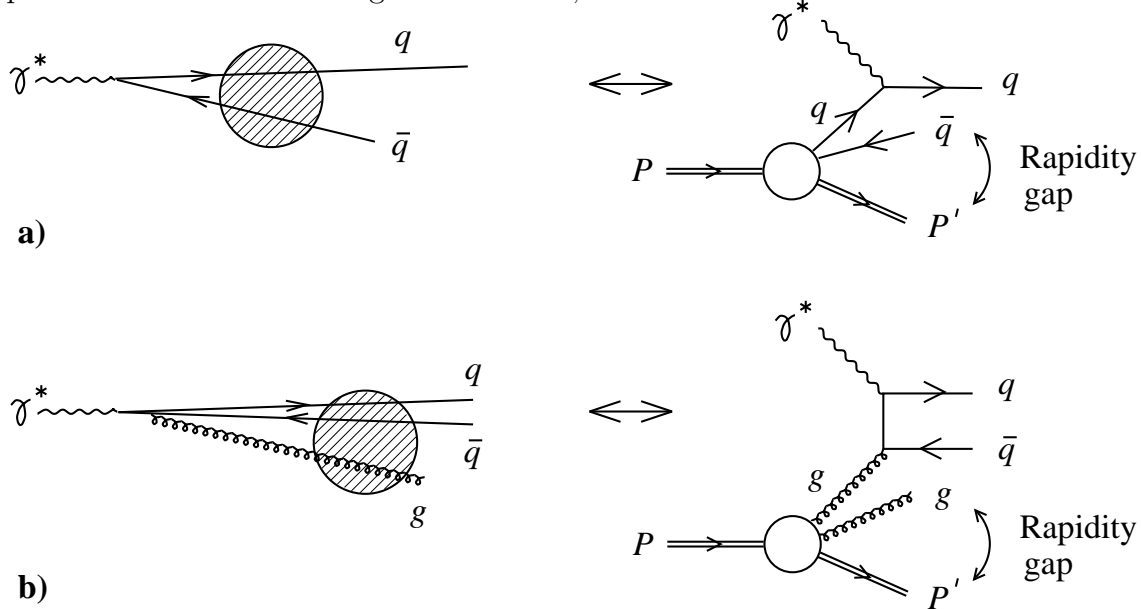


**Figure 4.10:** Diffractive DIS in the proton rest frame (left) and the Breit frame (right); asymmetric quark fluctuations correspond to diffractive quark scattering, asymmetric gluon fluctuations to diffractive boson-gluon fusion.

Note that it is incorrect to interpret the r.h. side of Fig. 4.10 as a two-step process, where a colour-neutral cluster is first emitted by the proton and then probed by the virtual photon. If this was the case, the two-gluon or two-quark cluster relevant in this calculation would necessarily lead to parton distributions symmetric in  $\beta$  and  $1-\beta$ . A counter example to this is provided by the model distributions derived in Sect. 6.2.



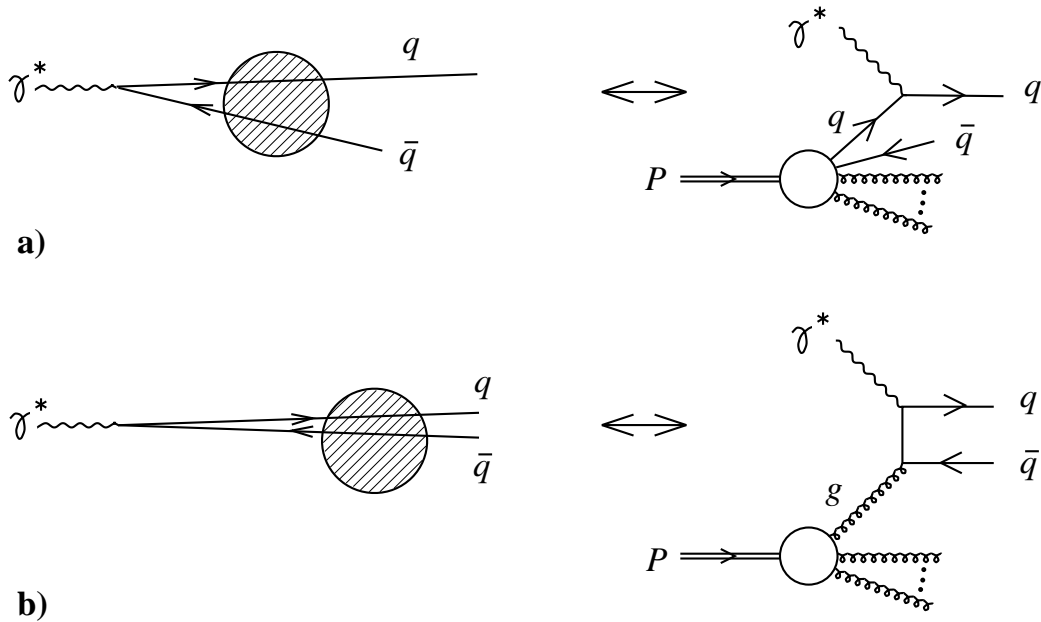


**Figure 4.11:** Inclusive DIS in the proton rest frame (left) and the Breit frame (right); asymmetric fluctuations correspond to quark scattering (a), symmetric fluctuations to boson-gluon fusion (b).

Thus, the idea of a ‘pre-formed’ colour neutral cluster, as it is usually associated with the pomeron structure function, is not supported by the present calculation.

At this point, it is appropriate to add a brief discussion of the target rest frame vs Breit frame interpretations of inclusive DIS [62]. The leading order semiclassical calculation of inclusive DIS, which amounts essentially to inclusive  $q\bar{q}$  pair production off an external field, was given in Sect. 3.2. It was shown that, in contrast to the diffractive case, both asymmetric and symmetric  $q\bar{q}$  configurations contribute to the leading twist cross section. As explained in more detail in Appendix D, these configurations correspond, in the parton model, to leading order quark scattering, testing the inclusive quark distribution, and boson-gluon fusion, testing the inclusive gluon distribution (cf. Fig 4.11). The symmetric configurations have a small transverse size and test directly the one-gluon component of the target colour field. This is the reason why, in the semiclassical framework, the leading order calculation is already sensitive to the gluon distribution of the target.

The inclusive gluon distribution plays a very special role. In contrast to both the inclusive quark distribution and the diffractive quark and gluon distributions, it is only sensitive to the short distance structure of the proton field, and it is enhanced by an explicit factor  $1/\alpha_s$  (see Appendix D). As a result, the dominance of the inclusive over the diffractive DIS cross section, which is of fundamental importance for the successful phenomenological analysis of [62] (cf. Sect. 7.1), emerges.

# 5 Two Gluon Exchange

So far, inclusive diffraction, as parametrized, e.g., by the diffractive structure function  $F_2^D$ , was at the centre of interest of this review. It was argued that, for inclusive processes, the underlying colour singlet exchange is soft, and two corresponding approaches, the semiclassical framework and the pomeron picture, were described in some detail.

In perturbative QCD, the simplest possibility of realizing colour singlet exchange is via two  $t$  channel gluons. In fact, the colour singlet exchange in certain more exclusive diffractive processes is, with varying degree of rigour, argued to be governed by a hard scale. In such cases, two gluon exchange dominates. Some of these processes are discussed in the present chapter. Finally, attempts to approach the whole diffractive cross section in two-gluon models are described.

## 5.1 Elastic meson production

Elastic meson electroproduction is the first diffractive process that was claimed to be calculable in perturbative QCD [15, 16]. It has since been considered by many authors, and a fair degree of understanding has been achieved as far as the perturbative calculability and the factorization of the relevant non-perturbative parton distributions and meson wave functions are concerned.

To begin with, consider the electroproduction of a heavy  $q\bar{q}$  bound state off a given classical colour field. This calculation represents an alternative derivation Ryskin's celebrated result [15] for elastic  $J/\psi$  production.

The relevant amplitude is shown in Fig. 5.1. In the non-relativistic limit, the two outgoing quarks are on-shell, and each carries half of the  $J/\psi$  momentum. Thus, the two quark propagators with momenta  $p' = k' = q'/2$  and the  $J/\psi$  vertex are replaced with the projection operator  $g_J \not{\epsilon}_J (\not{k}' + m)$ . Here

$$g_J^2 = \frac{3\Gamma_{ee}^J m_J}{64\pi\alpha_{\text{em}}^2}, \quad (5.1)$$

$\Gamma_{ee}^J$  is the electronic decay width of the  $J/\psi$  particle,  $m_J = 2m$  is its mass, and  $\epsilon_J$  its polarization vector [103].

Using the notation and calculational technique of Sect. 3.2, the amplitude of Fig. 5.1

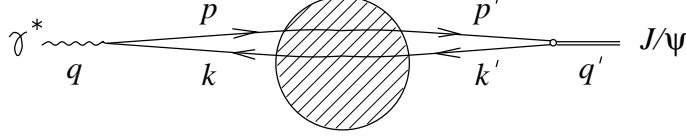


**Figure 5.1:** Leading order amplitude for the elastic production of a  $J/\Psi$  particle off an external colour field.

can now be written as

$$i2\pi\delta(q'_0 - q_0)T_{q\bar{q}} = ie_c g_J \int \frac{d^4 k}{(2\pi)^4} \text{tr} \left[ \not{\epsilon}_J(\not{k}' + m) V_q(p', p) \frac{i}{\not{p}' - m} \not{\epsilon}_\gamma(q) \frac{i}{-\not{k} - m} V_{\bar{q}}(k, k') \right], \quad (5.2)$$

where  $e_c = (2/3)e$  is the electric charge of the charm quark. The Dirac structure is simplified employing the identities

$$-g_J \not{\epsilon}_J(\not{k}' + m) = \frac{g_J}{2m} (\not{k}' - m) \not{\epsilon}_J(\not{k}' + m) = \frac{g_J}{2m} \sum_r v_r(k') \bar{v}_r(k') \not{\epsilon}_J \sum_s u_s(p') \bar{u}_s(p') \quad (5.3)$$

as well as Eqs. (3.10) and (3.11). The further calculation proceeds along the lines of Sect. 3.2 using, in particular, the quark scattering vertices Eqs. (3.12) and (3.13). Adding the two contributions where only the quark or only the antiquark is scattered to Eq. (5.2), the full amplitude  $T = T_{q\bar{q}} + T_q + T_{\bar{q}}$  takes the form

$$T = -\frac{ie_c g_J}{8\pi^2 m} q_+ \int d^2 k_\perp \frac{\alpha(1-\alpha)}{N^2 + k_\perp^2} \sum_{r's'} [\bar{u}_{s'}(\bar{p}) \not{\epsilon}_\gamma(q) v_{r'}(\bar{k})] [\bar{v}_{r'}(\bar{k}') \not{\epsilon}_J(q) u_{s'}(\bar{p}')] \quad (5.4)$$

$$\times \left[ \tilde{U}(p'_\perp - p_\perp) \tilde{U}^\dagger(k_\perp - k'_\perp) - (2\pi)^4 \delta^2(p'_\perp - p_\perp) \delta^2(k'_\perp - k_\perp) \right].$$

Note that this is very similar to Eq. (3.14) with the  $U$  matrix structure replaced according to Eq. (3.16). The main difference is that the produced quarks are projected onto the  $J/\psi$  state.

Since both  $Q$  and  $m$  are considered to be hard scales while  $U$  and  $U^\dagger$  are governed by the soft hadronic scale  $\Lambda$ , the integrand in Eq. (5.4) can be expanded in powers of the soft momentum  $k_\perp$ . The leading power of the amplitude is given by the first non-vanishing term. In the case of forward production,  $p'_\perp = k'_\perp = 0$ , the dependence on the external colour field takes the form

$$\begin{aligned} & \int d^2 k_\perp k_\perp^2 \text{tr} \left[ \tilde{U}(p'_\perp - p_\perp) \tilde{U}^\dagger(k_\perp - k'_\perp) - (2\pi)^4 \delta^2(p'_\perp - p_\perp) \delta^2(k'_\perp - k_\perp) \right] \\ &= \int d^2 k_\perp k_\perp^2 \int_{x_\perp} \int_{y_\perp} \text{tr} \left[ U(x_\perp) U^\dagger(y_\perp) - 1 \right] e^{ik_\perp(y_\perp - x_\perp)} \\ &= -(2\pi)^2 \partial_{y_\perp}^2 \int_{x_\perp} \text{tr} W_{x_\perp}(y_\perp) \Big|_{y_\perp=0}. \end{aligned} \quad (5.5)$$

Now, the crucial observation is that precisely the same dependence on the external field is present in the amplitude for forward Compton scattering shown in Fig. 5.2. In the case of longitudinal photon polarization, the transverse size of the  $q\bar{q}$  pair is always

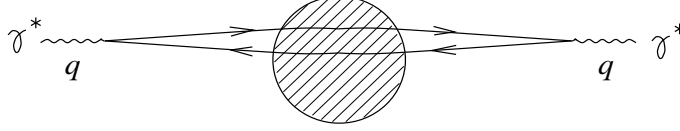


**Figure 5.2:** The Compton scattering amplitude within the semiclassical approach.

small, and the target field enters only via the second derivative of  $W$  that appears in Eq. (5.5).

Thus, comparing with the parton model result for longitudinal photon scattering, this derivative can be identified in terms of the gluon distribution of the target proton [48],

$$-\partial_{y_\perp}^2 \int_{x_\perp} \text{tr} W_{x_\perp}(y_\perp) \Big|_{y_\perp=0} = 2\pi^2 \alpha_s x g(x). \quad (5.6)$$

Using this relation<sup>1</sup> and Eq. (5.4), the amplitudes for the forward production of transversely and longitudinally polarized  $J/\psi$  mesons by transversely and longitudinally polarized virtual photons are obtained. To go from amplitudes for scattering off an external field to usual covariant amplitudes, a factor  $2m_p$  has to be introduced. Under the additional assumption  $Q^2 \gg m_J^2$ , the covariant amplitudes for longitudinal and transverse polarization read

$$T_L = -i64\pi^2 \alpha_s g_J e (xg(x)) \frac{s}{3Q^3}, \quad T_T = \frac{m_J}{Q} T_L, \quad (5.8)$$

where  $\sqrt{s}$  is the centre-of-mass energy of the  $\gamma^*p$  collision.

It is not surprising that the gluon distribution of Eq. (5.6), calculated according to Fig. 5.2, shows no scaling violations and only the trivial Bremsstrahlungs energy dependence  $\sim 1/x$ . The reason for this is the softness assumptions of the semiclassical calculation. Firstly, the eikonal approximation implies that all longitudinal modes of the external field are much softer than the photon energy. Secondly, the reduction of the field dependence to a transverse derivative is only justified if the scales governing the quark loop, i.e.,  $Q^2$  in the case of Fig. 5.2 and  $Q^2$  and  $m^2$  in the case of Fig. 5.1, are harder than the transverse structure of  $W$ . These two approximations, evidently valid for a given soft field, are also justified for a dynamical target governed by QCD as long as only leading logarithmic accuracy in both  $1/x$  and  $Q^2$  is required. Thus, a non-trivial dependence on  $1/x$  and  $Q^2$  can be reintroduced into Eq. (5.8) via the measured gluon distribution, keeping in mind that the result is only valid at double-leading-log accuracy.

Note that this is precisely what was claimed in the original two-gluon exchange calculation of [15]. Note also that, in distinction from this presentation, the calculation of [15] obtains the gluon distribution by coupling the  $t$  channel gluons to the quarks of

<sup>1</sup>Note that this is also consistent with the result for longitudinal photon scattering given in Eq. (3.25) since

$$-\partial_{y_\perp}^2 \int_{x_\perp} \text{tr} W_{x_\perp}(y_\perp) \Big|_{y_\perp=0} = \int_{x_\perp} \text{tr} [\partial_{y_\perp} W_{x_\perp}(0) \partial_{y_\perp} W_{x_\perp}^\dagger(0)], \quad (5.7)$$

which follows from unitarity of the  $U$  matrices.

the target and identifying the logarithmic integral over the transverse gluon momentum as the logarithm accompanying the usual quark-to-gluon splitting function.

The first essential extension of the above fundamental result is related to the treatment of the bound state produced. Brodsky et al. [16] showed that, at least for longitudinal photon polarization, a perturbative calculation is still possible in the case of light, non-perturbative bound states like the  $\rho$  meson. The calculation is based on the concept of the light-cone wave function of this meson. Referring the reader to [104] for a detailed review, a brief description of the main ideas involved is given below (cf. [105]). For this purpose, consider the generic diagram for the production of a light meson in a hard QCD process given in Fig. 5.3.

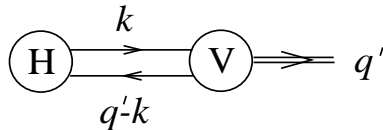


**Figure 5.3:** Generic diagram for meson production in a hard process.

Assume that, as shown in this figure, all diagrams can be cut across two quark-lines, the constituent quarks of the meson, in such a way as to separate the hard process H from the soft meson formation vertex V, which is defined to include the propagators. The amplitude can be written as

$$T = \int d^4k T_H(k) V(k) = \int_0^1 dz T_H(z) \frac{q'_+}{2} \int dk_- d^2k_\perp V(k) = \int_0^1 dz T_H(z) \phi(z), \quad (5.9)$$

where  $z = k_+/q'_+$ , and the last equality is simply the definition of the light-cone wave function  $\phi$  of the meson. The two crucial observations leading to the first of these equalities are the approximate  $k_-$  and  $k_\perp$  independence of  $T_H$  and the restriction of the  $z$  integration to the interval from 0 to 1. The first is the result of the hard scale that dominates  $T_H$ , the second follows from the analytic structure of  $V$ . In QCD, the  $k_\perp$  integration implicit in  $\varphi$  usually has an UV divergence due to gluon exchange between the quarks. Therefore, one should really read  $\phi = \phi(z, \mu^2)$ , where the cutoff  $\mu^2$  is of the order of the hard scale that governs  $T_H$ . At higher orders in  $\alpha_s$ , the hard amplitude  $T_H$  develops a matching IR cutoff dependence.

A more rigorous definition of the light-cone wave function, required, in particular, for the discussion of higher order corrections, can be given in the operator language. Without going into further detail, note that the above wave function  $\phi$  satisfies the relation

$$\langle \text{meson}(q') | \varphi^\dagger(y) \varphi(-y) | 0 \rangle = \int_0^1 dz e^{i(1-2z)(q'y)} \phi(z), \quad (5.10)$$

where  $y^2 = 0$  and  $\varphi$  is the field operator, for simplicity a scalar, corresponding to the particle content of the meson.

The case of the  $\rho$  meson is more complicated because it is a vector particle built from spin-(1/2) constituents. The matrix element relevant for the exclusive electroproduction

of a longitudinally polarized vector meson reads

$$\langle \rho(q') | \bar{\psi}(y) \gamma^\mu \psi(-y) | 0 \rangle = \int_0^1 dz e^{i(1-2z)(q'y)} [q'^\mu (\epsilon \cdot y) f_a(z) + \epsilon^\mu f_b(z) + y^\mu (\epsilon \cdot y) f_c(z)], \quad (5.11)$$

where  $\epsilon$  is the polarization vector of the meson and  $f_{a,b,c}$  are leading twist  $q\bar{q}$  distribution functions (see [106] for more details on these quantities and related issues). After the convolution with the appropriate hard production amplitude, only the combination

$$\phi_\rho(z) = f_b(z) + \frac{i}{2} \frac{\partial}{\partial z} f_a(z) \quad (5.12)$$

survives. Under the simplifying assumption that the  $\rho$  is built from one flavour of quarks with one unit of electric charge (which does not affect the final result if normalized by the decay width) the longitudinal amplitude reads [16, 107]

$$T_L = -i4\pi^2 \alpha_s e (xg(x)) \frac{s}{3Q^3 m_\rho} \int_0^1 dz \frac{\phi_\rho(z)}{z(1-z)}. \quad (5.13)$$

The underlying calculation of the hard scattering process is analogous to the case of the  $J/\psi$  discussed above. Although the shape of the light-cone wave function  $\phi_\rho$  is not known, its normalization can be related to the electronic width  $\Gamma_{ee}^\rho$  of the  $\rho$  via the relations

$$\int_0^1 dz \phi_\rho(z) = \sqrt{2} m_\rho f_\rho \quad , \quad \Gamma_{ee}^\rho = \frac{8\pi \alpha_{\text{em}}^2 f_\rho^2}{3m_\rho}. \quad (5.14)$$

If the non-relativistic approximation used in the  $J/\psi$  case was to be applied here, a wave function  $\phi_\rho$  proportional to  $\delta(z - 1/2)$  would result. In this case, Eqs. (5.13) and (5.14) would give an unambiguous prediction for the  $\rho$  production amplitude in terms of its electronic width, precisely as for the  $J/\psi$  amplitude.

Note that, in the transverse case, the hard amplitude generates a  $z$  dependence which is even more singular at the endpoints than the factor  $1/z(1-z)$  of Eq. (5.13). While the expected fall-off of the wave function at the endpoints is sufficient to render Eq. (5.13) finite, this is probably not true in the transverse case. Thus, perturbative calculability in the sense of the  $J/\psi$  and the longitudinal  $\rho$  amplitudes can not be claimed.

Since the gluon distribution is defined by the imaginary part of the forward Compton scattering amplitude, the above result for longitudinal vector meson production,  $T_L \sim ixg(x)$ , is, strictly speaking, only the imaginary part of the full amplitude. Assuming that the energy dependence is given by  $xg(x) \sim (1/x)^\alpha$ , where the intercept  $\alpha$  belongs to an even signature trajectory, the real part follows from the signature factor of Eq. (4.7). If  $\alpha - 1$  is small, the ratio of real and imaginary part is approximately  $(\pi/2)(\alpha - 1)$ , and the real part correction can be introduced into Eq. (5.13) via the substitution [16, 108]

$$ixg(x) \quad \rightarrow \quad ixg(x) + \frac{\pi}{2} \frac{\partial(xg(x))}{\partial \ln(1/x)}. \quad (5.15)$$

The discussion of vector meson production given above was limited to the double-leading-log approximation as far as the colour singlet exchange in the  $t$  channel is concerned. To go beyond this approximation, the concept of ‘non-forward’ or ‘off-diagonal’

parton distributions, introduced some time ago (see [18, 21] and refs. therein) and discussed by Ji [19] and Radyushkin [20] in the present context, has to be used. Recent reviews of these quantities and their evolution, which interpolates between the Altarelli-Parisi and the Brodsky-Lepage evolution equations, can be found in [109].

Recall first that the semiclassical viewpoint of Figs. 5.1 and 5.2 is equivalent to two gluon exchange as long as the transverse size of the energetic  $q\bar{q}$  state is small. So far, the recoil of the target in longitudinal direction has been neglected. However, such a recoil is evidently required by the kinematics. For what follows, it is convenient to use a frame where  $q_-$  is the large component of the photon momentum. In Fig. 5.4, the exchanged gluons and the incoming and outgoing proton with momenta  $P$  and  $P'$  are labelled by their respective fractions of the plus component of  $\bar{P} \equiv (P + P')/2$ . If  $\Delta$  is the momentum transferred by the proton,  $\xi \bar{P}_+ = \Delta_+/2$ . The variable  $y$  is an integration variable in the gluon loop.

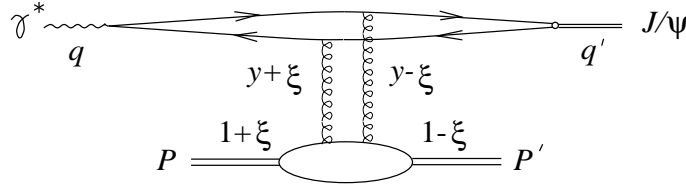


**Figure 5.4:** Elastic  $J/\psi$  production (three further diagrams with the gluons connected in different ways have to be added). The two gluon lines and the incoming and outgoing proton are labelled by their respective fractions of the plus component of  $\bar{P} \equiv (P + P')/2$ .

The lower part of the diagram in Fig. 5.4 is a generalization of the conventional gluon distribution (cf. Eqs. (4.26) and (4.31)). It can be described by the non-forward gluon distribution

$$H_g(y, \xi, t) = \frac{1}{4\pi y P_+} \int dx_- e^{-iy\bar{P}_+ x_-/2} \langle P' | F^\dagger(0, x_-, 0_\perp)^{+\mu} F(0, 0, 0_\perp)_\mu^+ | P \rangle. \quad (5.16)$$

Recently, it has been shown [110] that, as in the case of conventional parton distributions [111], no time ordering of the operators in Eq. (5.16) is required.

The description of elastic meson production in terms of non-forward parton distributions is superior to the double-leading-log approach of [15, 16] since  $\alpha_s$  corrections to the hard amplitude, meson wave function and parton distribution function can, at least in principle, be systematically calculated. However, the direct relation to the measured conventional gluon distribution is lost. A new non-perturbative quantity, the non-forward gluon distribution, is introduced, which has to be measured and the evolution of which has to be tested – a very complicated problem given the uncertainties of the experiment and of the meson wave functions involved.

Over the recent years, the theory of non-forward parton distributions has developed into an active research field in its own rights, a detailed account of which is beyond the scope of this paper (see, however, [109] for recent reviews). Important issues include the investigation of different models for non-forward distribution functions [112], helicity-flip distributions [113], the further study of non-forward evolution equations [114], and

possibilities of predicting the non-forward from the forward distribution functions [115]. The latter suggestion relies on the observation that, at sufficiently high  $Q^2$ , the non-trivial  $\xi$  dependence (cf. Fig. 5.4 and Eq. (5.16)) is largely determined by the  $Q^2$  evolution.

Furthermore, following the basic results of [15, 16], a number of interesting phenomenological analyses of meson production have appeared. The analyses of [116] and [117] focus, among other issues, on the effects of the meson wave functions. More details of these approaches will be given in Sect. 7.3, when experimental results are discussed. The effects of Fermi motion and quark off-shellness have recently also been discussed in [118]. Other interesting topics discussed in the literature include the form of the energy dependence [119], shadowing effects [120], Sudakov suppression [121], effects of polarization [122], the  $t$  slope [117, 123], and the intrinsic transverse momentum of the hadron [124]. Vector meson production at large momentum transfer ( $|t| \gg \Lambda^2$ ) is discussed in [17, 125].

Note especially the proposal of [126] to approach both transversely and longitudinally polarized diffractive  $\rho$  production on the basis of open  $q\bar{q}$  production combined with the idea of parton-hadron duality.

Vector meson electroproduction was also investigated in the framework of the model of the stochastic vacuum, which emphasizes the non-perturbative aspects of the process [56–58]. The crucial observation is that, at realistic  $Q^2$ , the asymptotic hard regime has not yet set in, and the typical transverse size of the  $q\bar{q}$  fluctuation scattering off the target is not small. More details on this approach are found in Sect. 6.3, as well as in Sects. 7.1 and 7.3.

It should be emphasized that the above list of interesting subjects and related papers is in no way complete.

## 5.2 Factorization

Having discussed the leading order results for the cases of heavy vector meson production and light vector meson production with longitudinal polarization, the next logical step is to ask whether the systematic calculation of higher order corrections is feasible. For this, it is necessary to understand the factorization properties of the hard amplitude and the two non-perturbative objects involved, i.e., the meson wave function and the non-forward gluon distribution. In this section, a brief discussion of the general proof by Collins, Frankfurt and Strikman [22] is given. In addition, the essential role played by gauge invariance is explained in the framework of a simple model [23]. This illustrates, in a particularly intuitive target rest frame approach, the physical mechanism underlying factorization properties in the small- $x$  limit.

The analysis of [22] is based on the method of leading regions discussed previously in Sect. 4.3. The leading regions relevant for elastic meson production are shown in Fig. 5.5. The main line of reasoning is analogous to the factorization proofs for inclusive hard scattering. As before, H is the hard subgraph, A is the subgraph with momenta collinear with the incoming and outgoing proton, and S is the soft subgraph. Subgraph



B contains only lines which are collinear with the produced meson.

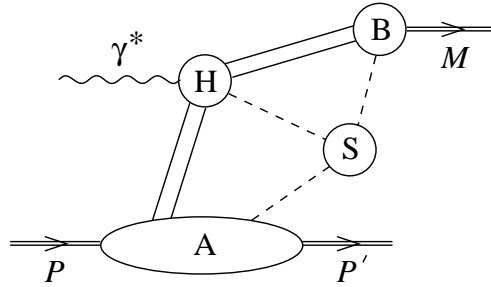


**Figure 5.5:** Leading regions in elastic meson production (cf. [22]).

Factorization means that, to leading order in  $1/Q$ , the amplitude corresponding to the process in Fig. 5.5 can be written as

$$T = \int_0^1 dz \int dy H(y, x/2) T_H(Q^2, y/x, z, \mu^2) \phi_V(z, \mu^2), \quad (5.17)$$

where  $T_H$  is the hard scattering amplitude,  $\phi$  is the light-cone wave function of the vector meson produced, and  $H$  is the non-forward parton distribution of the proton. It could, for example, be the non-forward gluon distribution  $H_g$  of the last section. The variable  $x = x_{Bj}$  is the usual DIS Bjorken variable. Equation (5.17) implies that the soft subgraph in Fig. 5.5 is irrelevant, and only two parton lines, i.e., the minimal number required by the exchanged quantum numbers, connect the hard subgraph H with both A and B.

According to [22], the essential steps of the prove include the demonstration that the leading regions are indeed given by Fig. 5.5, the derivation of a power counting formula showing that H is connected to A and B by the minimal number of lines, and the demonstration of factorization of the soft subgraph using Ward identities.

An important complication compared to conventional factorization proofs results from the fact that final state interactions are important for both the outgoing proton and the produced meson. Thus, the soft gluons of S have to be factorized from both of these subgraphs at the same time.

Furthermore, the so-called endpoint regions for the two quark lines connecting H and B have to be analyzed in detail. Endpoint regions are those kinematic domains where one of the two quarks carries almost all of the meson's longitudinal momentum. They are thus endpoints of the  $z$  integration in Eq. (5.17). An essential result of [22] is the suppression of these endpoint regions to all orders of perturbation theory in the case of longitudinal photon polarization.

In the case of transverse polarization, it was shown that the amplitude is suppressed by a power of  $Q$  relative to the longitudinal case. However, the endpoints are not suppressed relative to the intermediate  $z$  region, and therefore the factorization formula Eq. (5.17) can not be established in the transverse case.

A discussion of helicity and transversity parton distributions, measurable via the polarization of the produced meson, is also contained in [22]. This will not be reproduced

here. More recently, factorization proofs similar to [22] have been given for the process of deeply virtual Compton scattering [127], where the situation is simpler since no soft meson wave function has to be factorized. Note also that the factorization proofs of [22, 127], which use Breit frame kinematics, do not rely on the limit of small  $x$ .

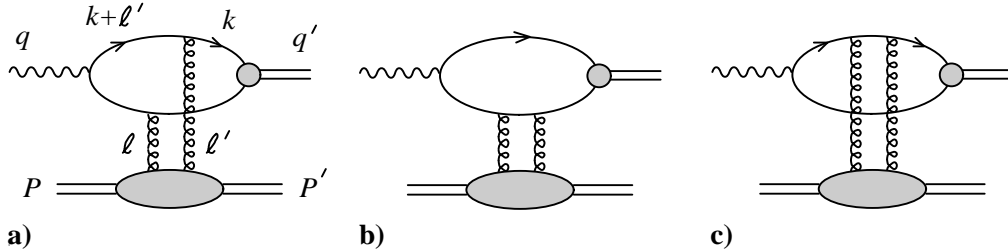


**Figure 5.6:** The leading amplitude for a point-like meson vertex.

However, it is instructive to see in a particularly simple situation how factorization works specifically at small  $x$ , from the point of view of the target rest frame commonly used for the description of small- $x$  processes [23]. For this purpose, consider a very energetic scalar photon that scatters off a hadronic target producing a scalar meson built from two scalar quarks (see Fig. 5.6). The quarks are coupled to the photon and the meson by point-like scalar vertices  $ie$  and  $i\lambda$ , where  $e$  and  $\lambda$  have dimension of mass. The coupling of the gluons to the scalar quarks is given by  $-ig(r_\mu + r'_\mu)$ , where  $r$  and  $r'$  are the momenta of the directed quark lines, and  $g$  is the strong gauge coupling.

Under quite general conditions [23], the gluon momenta satisfy the relations  $\ell_+, \ell'_+ \ll q_+$ ,  $\ell_-, \ell'_- \ll P_-$  and  $\ell^2 \sim \ell'^2 \sim -\ell_\perp^2$ . Then the lower bubble in Fig. 5.6 effectively has the structure

$$F^{\mu\nu}(\ell, \ell', P) \simeq \delta(P_- \ell_+) F(\ell_\perp^2) P^\mu P^\nu, \quad (5.18)$$

which is defined to include both gluon propagators and all colour factors. A similar expression was found by Cheng and Wu [128] in a tree model for the lower bubble.

Assume that  $F$  restricts the gluon momentum to be soft,  $\ell_\perp^2 \ll Q^2$ . In the high-energy limit, it suffices to calculate

$$M = \int \frac{d^4\ell}{(2\pi)^4} T^{\mu\nu} F_{\mu\nu} \simeq \int \frac{d^4\ell}{4(2\pi)^4} T_{++} F_{--}, \quad (5.19)$$

where

$$T^{\mu\nu} = T^{\mu\nu}(\ell, \ell', q) = T_a^{\mu\nu} + T_b^{\mu\nu} + T_c^{\mu\nu} \quad (5.20)$$

is the sum of the upper parts of the diagrams in Fig. 5.6.

Note that, because of the symmetry of  $F_{\mu\nu}$  with respect to the two gluon lines, the amplitude  $T^{\mu\nu}$  of Eq. (5.20) is used instead of the properly-symmetrized upper amplitude

$$T_{\text{sym}}^{\mu\nu}(\ell, \ell', q) = \frac{1}{2}[T^{\mu\nu}(\ell, \ell', q) + T^{\nu\mu}(-\ell', -\ell, q)]. \quad (5.21)$$

The two exchanged gluons together form a colour singlet and so the symmetrized amplitude  $T_{\text{sym}}^{\mu\nu}$  satisfies the same Ward identity as for two photons,

$$T_{\text{sym}}^{\mu\nu}(\ell, \ell', q)\ell_\mu\ell'_\nu = 0. \quad (5.22)$$

Writing this equation in light-cone components and setting  $\ell_\perp = \ell'_\perp$ , as appropriate for forward production, it follows that, for the relevant small values of  $\ell_-$ ,  $\ell'_-$ ,  $\ell_+$  and  $\ell'_+$ ,

$$T_{\text{sym},++} \sim \ell_\perp^2 \quad (5.23)$$

in the limit  $\ell_\perp^2 \rightarrow 0$ . Here the fact that the tensor  $T_{\text{sym}}^{\mu\nu}$ , which is built from  $\ell'$ ,  $\ell$  and  $q$ , has no large minus components has been used. The  $\ell_-$  integration makes this equation hold also for the original, unsymmetrized amplitude,

$$\int d\ell_- T_{++} \sim \ell_\perp^2. \quad (5.24)$$

This is the crucial feature of the two-gluon amplitude that will simplify the calculation and lead to the factorizing result below.

Consider first the contribution from diagram a) of Fig. 5.6 to the  $\ell_-$  integral of  $T_{++}$ , which is required in Eq. (5.19),

$$\int d\ell_- T_{a,++} = -4eg^2q_+ \int \frac{d^4k}{(2\pi)^3} \frac{z(1-z)}{N^2 + (k_\perp + \ell_\perp)^2} \frac{i\lambda}{k^2(q' - k)^2}. \quad (5.25)$$

Here  $N^2 = z(1-z)Q^2$ ,  $z = k_+/q_+$  and the condition  $\ell_+ = 0$ , enforced by the  $\delta$ -function in Eq. (5.18), has been anticipated.

Now  $\int d\ell_- T_{b,++}$  and  $\int d\ell_- T_{c,++}$  each carry no  $\ell_\perp$  dependence. So, to ensure the validity of Eq. (5.24), the sum of the three diagrams must be

$$\int d\ell_- T_{++} = 4eg^2q_+ \int \frac{d^4k}{(2\pi)^3} z(1-z)\mathcal{N} \frac{i\lambda}{k^2(q' - k)^2}, \quad (5.26)$$

where

$$\mathcal{N} = \left[ \frac{1}{N^2 + k_\perp^2} - \frac{1}{N^2 + (k_\perp + \ell_\perp)^2} \right] \sim \frac{\ell_\perp^2}{(N^2 + k_\perp^2)^2}. \quad (5.27)$$

Note the  $1/Q^4$  behaviour obtained after a cancellation of  $1/Q^2$  contributions from the individual diagrams. This cancellation, which is closely related to the well-known effect of colour transparency [129], has been discussed in [51] in the framework of vector meson electroproduction.

Introduce the  $k_\perp$  dependent light-cone wave function of the meson

$$\phi(z, k_\perp^2) = -\frac{iq'_+}{2} \int dk_- dk_+ \frac{i\lambda}{(2\pi)^4 k^2 (q' - k)^2} \delta(k_+ - zq'_+). \quad (5.28)$$

The final result following from Eqs. (5.19) and (5.26) is a convolution of the production amplitude of two on-shell quarks and the light-cone wave function:

$$M = ieg^2s \left( \int \frac{d^2\ell_\perp}{2(2\pi)^3} \ell_\perp^2 F(\ell_\perp^2) \right) \int dz \int d^2k_\perp \frac{z(1-z)}{(N^2 + k_\perp^2)^2} \phi(z, k_\perp^2). \quad (5.29)$$

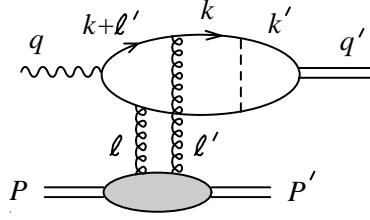


**Figure 5.7:** Diagram for meson production with the vertex modelled by scalar particle exchange.

This corresponds to the  $O(\ell_{\perp}^2)$  term in the Taylor expansion of the contribution from Fig. 5.6a, given in Eq. (5.25).

At leading order, factorization of the meson wave function was trivial since the point-like quark-quark-meson vertex  $V(k^2, (q' - k)^2) = i\lambda$  was necessarily located to the right of the all other interactions. To see how factorization comes about in the simplest non-trivial situation, consider the vector meson vertex

$$V(k^2, (q' - k)^2) = \int \frac{d^4 k'}{(2\pi)^4} \frac{i\lambda\lambda'^2}{k'^2(q' - k')^2(k - k')^2}, \quad (5.30)$$

which corresponds to the triangle on the r.h. side of Fig. 5.7. Here, the dashed line denotes a colourless scalar coupled to the scalar quarks with coupling strength  $\lambda'$ .

The diagram of Fig. 5.7 by itself gives no consistent description of meson production since it lacks gauge invariance. This problem is not cured by just adding the two diagrams 5.6b) and c) with the blob replaced by the vertex  $V$ . It is necessary to include all the diagrams shown in Fig. 5.8.

The same gauge invariance arguments that lead to Eq. (5.24) apply to the sum of all the diagrams in Figs. 5.7 and 5.8. Therefore, the complete result for  $T_{++}$ , which is now defined by the sum of the upper parts of all these diagrams, can be obtained by extracting the  $\ell_{\perp}^2$  term at leading order in the energy and  $Q^2$ . Such a term, with a power behaviour  $\sim \ell_{\perp}^2/Q^4$ , is obtained from the diagram in Fig. 5.7 (replace  $i\lambda$  in Eq. (5.25) with the vertex  $V$  of Eq. (5.30)) by expanding around  $\ell_{\perp} = 0$ . It can be demonstrated that none of the other diagrams gives rise to such a leading-order  $\ell_{\perp}^2$  contribution (see [23] for more details).

The complete answer is given by the  $\ell_{\perp}^2$  term from the Taylor expansion of Eq. (5.25). The amplitude  $M$  is precisely the one of Eqs. (5.29) and (5.28), with  $i\lambda$  substituted by  $V$  of Eq. (5.30). The correctness of this simple factorizing result has also been checked by explicitly calculating all diagrams of Fig. 5.8.

The above simple model calculation can be summarized as follows. The complete result contains leading contributions from diagrams that cannot be factorized into quark-pair production and meson formation. However, the answer to the calculation can be anticipated by looking only at one particular factorizing diagram. The reason for this simplification is gauge invariance. In the dominant region, where the transverse momentum  $\ell_{\perp}$  of the two  $t$ -channel gluons is small, gauge invariance requires the complete quark

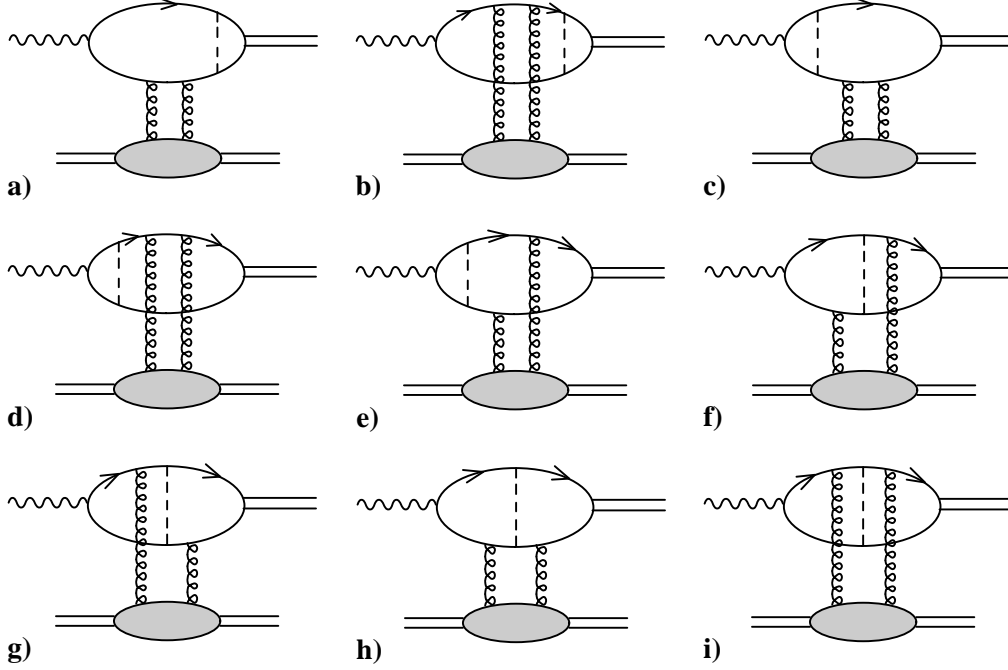


**Figure 5.8:** The remaining diagrams contributing to meson production within the above simple model for the meson wave function.

part of the amplitude to be proportional to  $\ell_{\perp}^2$ . The leading  $\ell_{\perp}^2$  dependence comes exclusively from one diagram. Thus, the complete answer can be obtained from this particular diagram, which has the property of factorizing explicitly if the two quark lines are cut. The resulting amplitude can be written in a factorized form.

### 5.3 Charm and high- $p_{\perp}$ jets

In the two previous sections, the exclusive production of vector mesons was described as an example of a diffractive process with hard colour singlet exchange. As a different possibility of keeping the colour singlet exchange in diffraction hard, the diffractive production of heavy quarks [24–27] and of high- $p_{\perp}$  jets [28–31] was considered by many authors. However, as will become clear from the discussion below, both processes can be associated with either soft or hard colour singlet exchange, and it is necessary to distinguish the two mechanisms carefully [47, 48]. The semiclassical approach provides a very convenient framework for this analysis.

One might expect the hard scale, provided by the transverse momentum of the jets, to ensure the applicability of perturbation theory. Indeed, the production of final states containing only two high- $p_{\perp}$  jets can be described by perturbative two-gluon exchange [130, 131]. This process has been studied in detail by several groups and higher-order corrections have already partially been considered [28–31].

Below, the two simplest configurations,  $q\bar{q}$  and  $q\bar{q}g$ , are discussed following [48].

In both cases, diffractive processes are obtained by projecting onto the colour singlet configuration of the final state partons. Although the discussion focusses on high- $p_\perp$  jets, all qualitative results carry over to the case of diffractive charm production [47]. Technically, it is not important whether the hard scale in the diffractive final state is  $p_\perp^2$  or  $m_c^2$ . One has simply to replace the high- $p_\perp$   $q\bar{q}$  jets with  $c\bar{c}$  jets, whose transverse momentum will automatically be  $\sim m_c$ . However, there is a clear phenomenological difference. On the one hand,  $m_c$  is fixed and not very large, while the hard scale  $p_\perp$  can, at least in principle, be arbitrarily high. On the other hand, charm production is simpler to analyse since it does not require the identification of jets.

Consider the production of a diffractive  $q\bar{q}$  final state. Using the results of Sect. 3.2, for the transversely polarized photon one easily finds

$$\left. \frac{d\sigma_T}{dt d\alpha dp_\perp^2} \right|_{t=0} = \frac{\sum_q e_q^2 \alpha_{\text{em}}}{2N_c (2\pi)^6} (\alpha^2 + (1-\alpha)^2) \left| \int_{x_\perp} \int d^2 p_\perp \frac{p_\perp \text{tr} \tilde{W}(p'_\perp - p_\perp)}{N^2 + p_\perp^2} \right|^2. \quad (5.31)$$

There are two essential differences compared to Eq. (3.20): firstly, the colour trace is taken at the amplitude level to ensure colour neutrality of the  $q\bar{q}$  state; secondly, two independent  $x_\perp$  integrations are applied to the two factors  $W$  and  $W^\dagger$ . This is the result of Eq. (5.31) being differential in  $t$  at  $t = 0$ , in contrast to Eq. (3.20), where the  $t$  integration has been performed.

The cross section for large transverse momenta is calculated by expanding the integrand around  $p_\perp = p'_\perp$ , as exercised in Sect. 3.2 for inclusive electroproduction in the longitudinal case. Note however that, due to the colour singlet condition, the first two terms (cf. Eqs. (3.22) and (3.23)) do not contribute, so that the leading contribution comes from the third term, which is proportional to the second derivative of  $W$  at the origin (compare the discussion of diffraction in Sect. 3.2). Even higher terms of the Taylor series give rise to contributions suppressed by powers of  $p_\perp^2$ , thus demonstrating the dominance of the short distance behaviour of  $\text{tr}W_{x_\perp}(y_\perp)$ . The leading order result reads

$$\left. \frac{d\sigma_T}{dt d\alpha dp_\perp^2} \right|_{t=0} = \frac{\sum_q e_q^2 \alpha_{\text{em}}}{384\pi^2} (\alpha^2 + (1-\alpha)^2) \left| \left( \frac{\partial}{\partial p'_\perp} \right)^2 \frac{p'_\perp}{N^2 + p_\perp^2} \right| \left| \partial_{y_\perp}^2 \int_{x_\perp} \text{tr}W_{x_\perp}(0) \right|^2. \quad (5.32)$$

As the derivation illustrates, this cross section describes the interaction of a small  $q\bar{q}$  pair with the proton. Hence, it is perturbative or hard. According to Eq. (5.6), the cross section Eq. (5.32) is proportional to the square of the gluon distribution. In order to obtain the  $t$  integrated cross section, one has to multiply Eq. (5.32) by the constant

$$C = \left( \int \frac{d\sigma}{dt} dt \right) / \left( \left. \frac{d\sigma}{dt} \right|_{t \simeq 0} \right) \sim \Lambda^2, \quad (5.33)$$

where  $\Lambda$  is a typical hadronic scale. The resulting cross section integrated down to the transverse momentum  $p_{\perp,\text{cut}}^2$  yields a contribution to the diffractive structure function  $F_2^D$  which is suppressed by  $\Lambda^2/p_{\perp,\text{cut}}^2$ .

As discussed in Sect. 3.3, a leading twist diffractive cross section for jets with  $p_\perp \sim Q$  requires at least three partons in the final state, one of which has to have low transverse

momentum. It can be written as a convolution of ordinary partonic cross sections with diffractive parton distributions. In the case of high- $p_\perp$  quark jets there is an additional wee gluon. The partonic process is then boson-gluon fusion, and the cross section

$$\frac{d\sigma_T}{d\xi dp_\perp'^2} = \int_x^\xi dy \frac{d\hat{\sigma}_T^{\gamma^* g \rightarrow q\bar{q}}(y, p'_\perp)}{dp_\perp'^2} \frac{dg(y, \xi)}{d\xi} \quad (5.34)$$

involves the diffractive gluon distribution of Eq. (4.54).

In addition to boson-gluon fusion, the QCD Compton process can also produce high- $p_\perp$  jets. In this case either the quark or the antiquark is the wee parton. The corresponding cross section

$$\frac{d\sigma_T}{d\xi dp_\perp'^2} = \int_x^\xi dy \frac{d\hat{\sigma}_T(y, p'_\perp)^{\gamma^* q \rightarrow gq}}{dp_\perp'^2} \frac{dq(y, \xi)}{d\xi}, \quad (5.35)$$

involves the diffractive quark distribution of Eq. (4.53). An analogous relation holds in the antiquark case.

The cross sections of Eqs. (5.34), (5.35) for diffractive boson-gluon fusion and diffractive Compton scattering can be evaluated along the lines described in [47]. In the leading- $\ln(1/x)$  approximation, one obtains for the longitudinal and transverse boson-gluon fusion cross sections

$$\frac{d\sigma_L}{d\alpha dp_\perp'^2} = \frac{\Sigma_q e_q^2 \alpha_{\text{em}} \alpha_s}{2\pi^3} \frac{[\alpha(1-\alpha)]^2 Q^2 p_\perp'^2}{(N^2 + p_\perp'^2)^4} \ln(1/x) h_{\mathcal{A}}, \quad (5.36)$$

$$\frac{d\sigma_T}{d\alpha dp_\perp'^2} = \frac{\Sigma_q e_q^2 \alpha_{\text{em}} \alpha_s}{16\pi^3} \frac{(\alpha^2 + (1-\alpha)^2) (p_\perp'^4 + N^4)}{(N^2 + p_\perp'^2)^4} \ln(1/x) h_{\mathcal{A}}, \quad (5.37)$$

$$h_{\mathcal{A}} = \int_{y_\perp} \int_{x_\perp} \frac{|\text{tr} W_{x_\perp}^{\mathcal{A}}(y_\perp)|^2}{y_\perp^4}. \quad (5.38)$$

Similarly, one finds for the QCD-Compton cross sections

$$\frac{d\sigma_L}{d\alpha dp_\perp'^2} = \frac{16\Sigma_q e_q^2 \alpha_{\text{em}} \alpha_s}{27\pi^3} \frac{Q^2}{[\alpha(1-\alpha)] \hat{Q}^6} h_{\mathcal{F}}, \quad (5.39)$$

$$\frac{d\sigma_T}{d\alpha dp_\perp'^2} = \frac{4\Sigma_q e_q^2 \alpha_{\text{em}} \alpha_s}{27\pi^3 \hat{Q}^6 p_\perp'^2} \left[ \hat{Q}^4 - 2Q^2(\hat{Q}^2 + Q^2) + \frac{\hat{Q}^4 + Q^4}{\alpha(1-\alpha)} \right] h_{\mathcal{F}}, \quad (5.40)$$

$$\hat{Q}^2 = Q^2 + \frac{p_\perp'^2}{\alpha(1-\alpha)}, \quad (5.41)$$

where the constant  $h_{\mathcal{F}}$  is defined analogously to Eq. (5.38) but with the  $U$  matrices in the fundamental representation.

Comparing Eqs. (5.36), (5.37) with Eqs. (5.39), (5.40), it is apparent that the configurations with a wee gluon are enhanced by  $\ln(1/x)$  at small  $x$  relative to those with a wee quark or antiquark. The origin of this enhancement can be understood as follows. Eqs. (5.34) and (5.35) provide cross sections differential in  $\xi$ ,  $p_\perp'^2$  and  $y$  or, equivalently, in  $\xi$ ,  $p_\perp'^2$  and  $\alpha$ , since  $y = x [Q^2 + p_\perp'^2/\alpha(1-\alpha)]/Q^2$ . The above  $p_\perp$ -spectra are obtained

after performing the  $\xi$ -integration from  $y$  to some fixed  $\xi_0 \ll 1$ . The integral is dominated by  $\xi \gg y$ , i.e.,  $\beta \ll 1$ , where one has  $ydg/d\xi \sim 1/\xi$ . The  $\xi$ -integration then yields a factor  $\ln(1/x) + \text{constant}$ . In contrast, the diffractive quark distribution behaves as  $ydq/d\xi \sim y/\xi^2$ , and consequently the  $\xi$ -integration only yields a constant.

Simple arguments concerning colour, outlined in [47], suggest an additional large suppression of the wee fermion contributions due to colour factors ( $h_A \gg h_F$ ). This is in qualitative agreement with model calculations of Sects. 6.1 and 6.2, which predict the diffractive gluon distribution to be much larger than the quark distribution. As a result, it can be claimed that configurations with a wee gluon dominate over those with a wee fermion in the small- $x$  region relevant to diffraction. The latter shall be ignored from now on.

The differential cross section for the leading order  $q\bar{q}$  fluctuation can be calculated as described above (cf. Eq. (5.32)). The longitudinal and transverse cross sections are

$$\frac{d\sigma_L}{d\alpha dp_\perp^2} = \frac{2\Sigma_q e_q^2 \alpha_{\text{em}} \alpha_s^2 \pi^2 [\xi G(\xi)]^2 C}{3} \frac{[\alpha(1-\alpha)]^2 Q^2 (a^2 - p_\perp'^2)^2}{(N^2 + p_\perp'^2)^6}, \quad (5.42)$$

$$\frac{d\sigma_T}{d\alpha dp_\perp'^2} = \frac{2\Sigma_q e_q^2 \alpha_{\text{em}} \alpha_s^2 \pi^2 [\xi G(\xi)]^2 C}{3} \frac{(\alpha^2 + (1-\alpha)^2) p_\perp'^2 N^4}{(N^2 + p_\perp'^2)^6}. \quad (5.43)$$

Identical differential distributions have been found for two-gluon exchange in leading order [28]. One can easily see that the region of  $\alpha$  close to 0 or 1 dominates, and that high- $p_\perp$  configurations are unlikely. This statement will now be quantified.

The quantitative differences between the  $q\bar{q}$  and  $q\bar{q}g$  configurations are particularly pronounced in the integrated cross section with a lower cut on the transverse momentum of the quarks. Since the overall normalization of the contributions is uncertain (it is inherently non-perturbative), the shape in  $p_\perp'^2$  of each configuration is compared. Consider the quantity

$$\sigma(p_{\perp,\text{cut}}'^2) = \int_{p_{\perp,\text{cut}}'^2}^{\infty} dp_\perp'^2 \int_0^1 d\alpha \frac{d\sigma}{dp_\perp'^2 d\alpha}, \quad (5.44)$$

which is the fraction of events remaining above a certain minimum  $p_\perp'^2$ . The integrand here is obtained by adding the contributions from longitudinal and transverse photons. Figure 5.9 shows the dependence of the corresponding event fraction on the lower limit,  $p_{\perp,\text{cut}}'^2$ . Each curve is normalized to its value at  $p_{\perp,\text{cut}}'^2 = 5 \text{ GeV}^2$ . One can see that the spectrum for the  $q\bar{q}g$  configuration is much harder than that for the  $q\bar{q}$  configuration. This is expected since in boson-gluon fusion  $p_\perp$  is distributed logarithmically between the soft scale and  $Q$  thus resulting in a significant high- $p_\perp$  tail above  $p_{\perp,\text{cut}}'$ .

Let  $M_j$  be the invariant mass of the two-jet system in diffractive events containing two high- $p_\perp$  jets in the diffractive final state. The measurement of this observable provides, in principle, a clean distinction between  $q\bar{q}$  final states, where  $M_j^2 = M^2$ , and  $q\bar{q}g$  final states, where  $M_j^2 < M^2$ . In practice, however, this requires the contribution of the wee gluon to the diffractive mass, which is responsible for the difference between  $M^2$  and  $M_j^2$ , to be sufficiently large. To quantify the expectation within the semiclassical approach, consider the transverse photon contribution to the differential diffractive cross section  $d\sigma/dM^2 dM_j^2$ .



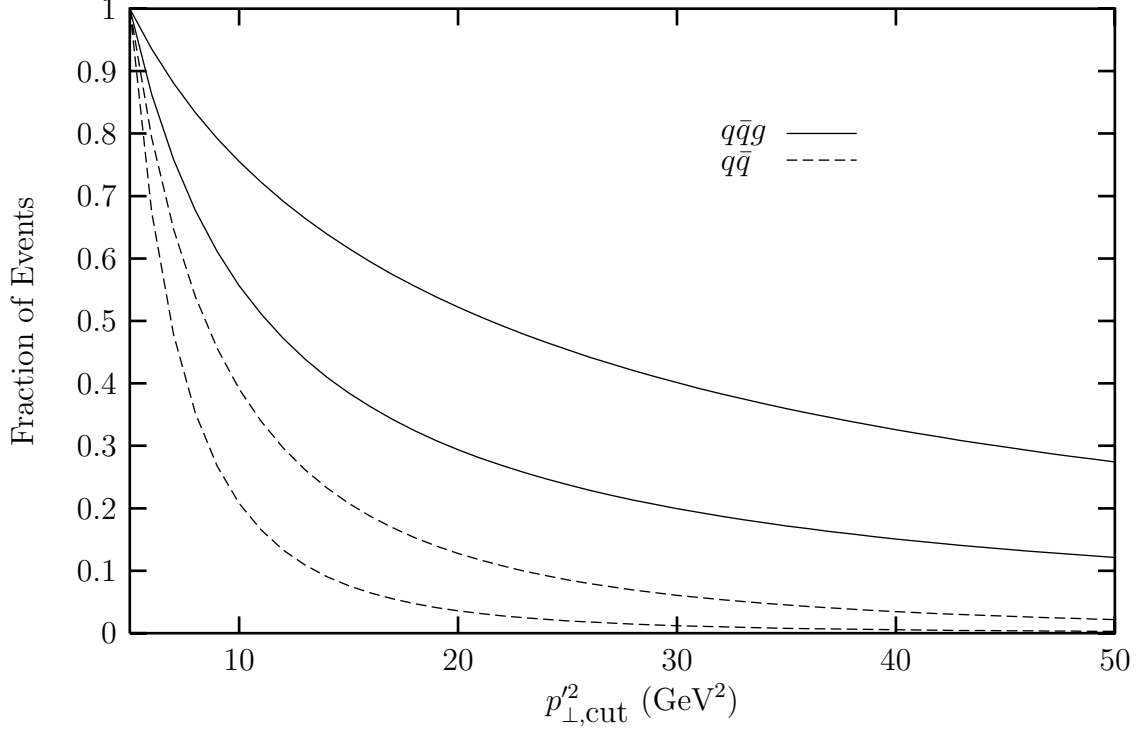


**Figure 5.9:** The fraction of diffractive events with  $p_{\perp}^2$  above  $p_{\perp,\text{cut}}^2$  for  $Q^2$  of 10 GeV<sup>2</sup> and 100 GeV<sup>2</sup> (lower and upper curve in each pair).

In the case of a  $q\bar{q}$  final state this cross section can be obtained directly from Eq. (5.43),

$$\frac{d\sigma_T}{dM^2 dM_j^2} = \Sigma_q e_q^2 \alpha_{\text{em}} \alpha_s^2 \pi^2 [\xi G(\xi)]^2 C \delta(M^2 - M_j^2) \frac{16M^2 Q^4 \sqrt{1-\kappa}}{3(M^2 + Q^2)^{6\kappa}}. \quad (5.45)$$

Here the  $\delta$ -function setting  $M^2 = M_j^2$  is only precise up to hadronization effects, which are expected to be of the order of the hadronic scale. The dependence on the transverse momentum cutoff enters via the variable  $\kappa = 4p_{\perp,\text{cut}}^2/M_j^2$ .

By contrast, the mass distribution for diffractive processes with three-particle final states is not peaked at  $M_j^2 = M^2$ . Concentrating, as before, on the transverse photon polarization and on the contribution from the diffractive gluon distribution, the following formula can be derived from Eq. (5.34)

$$\frac{d\sigma_T}{dM^2 dM_j^2} = 2\pi \Sigma_q e_q^2 \alpha_{\text{em}} \alpha_s y^2 \frac{dg(y, \xi)}{d\xi} \frac{Q^4 + M_j^4}{(Q^2 + M_j^2)^5} \left[ 2 \text{Arctanh} \sqrt{1-\kappa} - \sqrt{1-\kappa} \right]. \quad (5.46)$$

Explicit results can be obtained by using model calculations for the diffractive gluon distribution (cf. Chapter 6) or utilizing a simple parametrization (cf. the numerical predictions of [47, 48].)

Note that the  $\ln(1/x)$ -enhancement present in Eq. (5.37) can be recovered if the  $M^2$  integration is performed in Eq. (5.46). The origin of this enhancement is the integration measure  $dM^2/M^2$ , which appears since  $y^2(dg(y, \xi)/d\xi) \sim 1/M^2$  for  $M^2$  sufficiently large.

The main contribution to the total cross section comes from the region where  $M^2$  is significantly larger than  $M_j^2$ . Thus it is clear, even without detailed calculations, that the distribution of Eq. (5.46) differs qualitatively from Eq. (5.45). With sufficient statistics, a determination of the relative weight of soft colour singlet exchange, relevant in the  $q\bar{q}g$  case, and hard colour singlet exchange, relevant in the  $q\bar{q}$  case, should be feasible.

The above calculations can be summarized as follows. The diffractive production of a  $q\bar{q}$  final state with high  $p_\perp$  or with charm quarks proceeds via hard colour singlet exchange. The description in the semiclassical framework reproduces the two-gluon exchange calculations. By contrast, high- $p_\perp$  jets or charm in  $q\bar{q}g$  final states are predominantly produced via boson-gluon fusion. The colour neutralization mechanism is soft, and the cross section is proportional to the diffractive gluon distribution. The boson-gluon fusion mechanism is distinguished by a much harder  $p_\perp$  spectrum and a diffractive mass that is, on average, much larger than the invariant mass of the two-jet system.

The energy dependence of the process could be very different for the above two mechanisms. For hard colour singlet exchange, a steep rise is expected from the known small- $x$  behaviour of the gluon distribution. For soft colour singlet exchange, the  $\xi$  dependence is expected to be less steep.

In Ref. [25], the importance of higher order  $\alpha_s$  corrections to diffractive charm production was estimated in the framework of two-gluon exchange. A sizeable enhancement of the cross section was found. Clearly, the  $c\bar{c}g$  final state is part of these corrections. However, the above discussion shows that this final state is dominated by the region where the gluon is soft. In this case, the  $c\bar{c}g$  contribution is not perturbatively calculable and can not be considered an  $\alpha_s$  correction to the hard  $c\bar{c}$  process. Thus, the systematic calculability of corrections to hard  $c\bar{c}$  or jet production is an interesting open problem, which may be related to the problem of defining ‘exclusive’ jet production at higher orders.

## 5.4 Inclusive diffraction

There are a number of attempts by several authors to approach the bulk of the diffractive DIS data, as described by the structure function  $F_2^D$ , from the perspective of two gluon exchange in the  $t$  channel. The degree to which perturbation theory is taken seriously varies significantly in the different investigations discussed below.

In what can be possibly called the most modest approach, two gluons with an appropriate form-factor-like coupling to the proton are used as a simple model for colour singlet exchange, even if this exchange is believed to be non-perturbative. In the context of the diffractive electroproduction cross section at HERA, two gluon exchange calculations were performed in [7], where the importance of the soft region was pointed out, and the result was parametrized in terms of an effective two gluon form factor of the proton.

Furthermore, the two gluon calculation was used to describe both diffractive and inclusive cross sections in terms of the  $q\bar{q}$  component of the light-cone wave function of the virtual photon and of  $\sigma(\rho)$ , the cross section for a  $q\bar{q}$  pair to interact with the hadronic

target [7]. If the  $q\bar{q}$  component dominates, which is, however, a non-trivial assumption, this approach allows one to link the diffractive cross section at  $t = 0$  to the inclusive DIS cross section via the optical theorem.

In Ref. [29], the diffractive structure function was discussed on the basis of the exchange of two gluons with non-perturbative propagators in the sense of the Landshoff-Nachtmann model [50]. Further analyses extend the two gluon exchange calculations to include the  $q\bar{q}g$  component of the incoming photon [31, 101, 131].

Going one step further in the direction of perturbation theory, the known relation between the  $q\bar{q}$  cross section  $\sigma(\rho)$  and the inclusive gluon distribution [132],

$$\sigma(\rho) = \frac{\pi^2}{3}\alpha_s[xg(x)]\rho^2 + \mathcal{O}(\rho^4), \quad (5.47)$$

may be employed for the calculation of diffractive cross sections. This is similar to what was discussed in Sects. 5.1 and 5.3 in the case of meson production and high- $p_\perp$  jet or charm production respectively. However, such a relation to the gluon distribution, employed, e.g., in [28, 133], is problematic since the diffractive structure function is dominated by large transverse sizes of the  $q\bar{q}$  fluctuation of the photon, where Eq. (5.47) is not valid. It was emphasized in [134] that small, perturbative values of  $\rho$  become more important if the analysis is restricted to small diffractive masses.

In spite of the evident problems with the applicability of perturbation theory to the diffractive structure function, it is still interesting to take the perturbative approach even further, calculating the BFKL leading-log corrections [135] to the two gluon exchange amplitude. A possible formal justification of such a treatment can be obtained by considering diffractive DIS off a heavy quark-antiquark state, a so-called onium, which provides a perturbative scale in addition to the  $Q^2$  of the virtual photon. The focus is clearly on the energy dependence of the cross section, which so far can not be quantitatively described by non-perturbative QCD based methods.

A detailed discussion of the BFKL technique of summing leading logarithms in the high-energy limit of perturbative QCD amplitudes is beyond the scope of the present review. The essential qualitative result, relevant for the following brief overview, concerns the scattering of two small colour dipoles at very high centre-of-mass energy  $\sqrt{s}$ . It states that all corrections of the form  $\alpha_s \ln s$  to the above process, which proceeds via two gluon exchange at leading order, can be summed. This results in a power-like growth of the amplitude with  $s$ . One may think of the energy logarithms as being associated with gluonic ladders, although the ladder topology does not exhaust all relevant diagrams.

More recently, a colour dipole picture of the BFKL amplitude has been developed [28, 136–138]. In this picture, each of the colliding colour dipoles radiates gluons, thus creating new colour dipoles with smaller energy, which are the source of further gluon radiation. Eventually, two dipoles, one from each of the two colliding cascades, interact via simple two gluon exchange. The equivalence with the original BFKL technique has been established for the most fundamental, but not for all relevant applications. In particular, the role of the large  $N_c$  limit, which is used in addition to the leading logarithmic approximation [136, 137], is not yet fully understood.

For illustration, the particularly simple formula for the total cross section of two onia with radius  $R$  and mass  $m$  is given (see, e.g., [137]). It reads

$$\sigma(s) = 16\pi^2 R^2 \alpha_s^2 \frac{(s/m^2)^{(\alpha_P-1)}}{\sqrt{(7/2)\alpha_s N_c \zeta(3) \ln(s/m)}}, \quad (5.48)$$

where  $\alpha_P = 1 + (4N_c\alpha_s/\pi) \ln 2$  is the intercept of the BFKL pomeron. The reader is referred to the original papers [135] and to the modern introductory text [17] for further details.

The most straightforward application of the above perturbative techniques to diffraction at HERA relies on postulating the exchange of a BFKL pomeron between target proton and partonic photon fluctuation. For forward diffraction, the conventional BFKL amplitude has to be introduced between, say, the  $q\bar{q}$  fluctuation of the photon and a quark of the proton. More generally, the BFKL amplitude at non-zero  $t$  is needed. Corresponding formulae appear as a by-product in the more general investigations of [35, 36]. In the framework of the colour dipole approach, they are discussed in [139, 140]. Clearly, the method provides the desired rise of the cross section with energy or, equivalently, of  $F_2^D$  with  $1/\xi$ . However, with the simple asymptotic BFKL result, the rise appears to be far too strong (cf. Sect. 7.1 more details).

It is a further, even more challenging theoretical problem to consider the double limit  $W^2 \gg M^2 \gg Q^2$ , which corresponds to the simultaneous small- $\xi$  and small- $\beta$  limit of  $F_2^D$ . The relevant process, illustrated in Fig. 5.10, is similar to large-mass soft diffraction, discussed in Sect. 4.2. Several authors proposed to use perturbative BFKL techniques for the calculation of this process of large-mass electroproduction. The obvious idea is to use the knowledge of the perturbative BFKL amplitude and to interpret the three pomerons in Fig. 5.10 as BFKL pomerons. In particular, the cut pomeron in the upper part of the diagram corresponds to gluonic radiation being responsible for the large diffractive mass created in the process. The dominance of gluons in the large mass region is well-known from fixed order perturbative calculations.

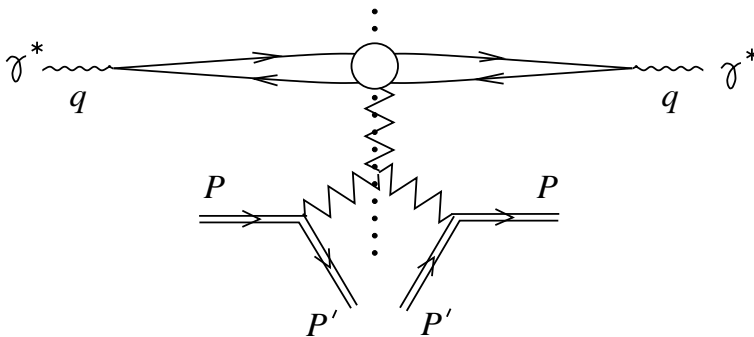


**Figure 5.10:** Triple pomeron vertex in diffractive electroproduction of large masses.

In the framework of conventional BFKL summation, the triple pomeron vertex in diffractive electroproduction was considered in [35, 36]. It was found that the cut pomeron in Fig. 5.10 is more complicated than the usual gluonic ladder. Four-gluon states were found to contribute to the leading amplitude.

The triple pomeron vertex was derived in the colour dipole approach and used for the calculation of large-mass diffractive electroproduction in [37, 141]. As expected, an enhancement of the cross section both in the limit of large  $W^2$  and large  $M^2$  is obtained. More details of the phenomenological analysis will be given in Sect. 7.1.

In spite of the impressive theoretical work discussed above, the perturbative calculability of the triple pomeron vertex appearing in large-mass hard diffraction remains questionable. On the one hand, it is not clear how far down the gluon ladder the influence of the hard scale  $Q^2$ , introduced by the  $\gamma^*$ , extends. On the other hand, it is difficult to justify the ad-hoc introduction of a hard scale at the bottom of the diagram, as advocated in [37], since the proton is a soft hadronic object.

Note finally that next-to-leading order results in the BFKL framework have recently become available (see [142] and refs. therein). For realistic values of  $\alpha_s$ , the obtained corrections are larger than the leading order contributions and of opposite sign, thus complicating the theoretical status of the perturbative energy dependence even further. However, according to the very recent result of [143], the use of BLM scale setting improves the situation dramatically.

# 6 Models for the Colour Field of the Proton

In this chapter, three different models for the procedure of averaging over the target colour field configurations are described. Using the formulae of Sect. 4.4, these models give rise to predictions for the diffractive quark and gluon distribution of the target hadron and thus for diffractive electroproduction cross sections.

## 6.1 Small colour dipole

A particularly simple model based entirely on perturbation theory has recently been suggested by Hautmann, Kunszt and Soper [144]. The authors study diffraction as quasi-elastic scattering off a special target photon that couples to only one flavour of very massive ( $M \gg \Lambda$ ) quarks. The large quark mass justifies a completely perturbative treatment of the target and the diffractive system. In this situation, the required  $t$  channel colour singlet exchange is realized by two gluons coupling to the massive quark loop of the target. The analysis of [144] is based on the operator definitions of diffractive parton distributions (Eqs. (4.29)–(4.31)), evaluated in an explicit two gluon exchange calculation.

Here, the results of [144] will be derived in the semiclassical framework, following Appendix B of [62]. In the semiclassical approach, the two  $t$  channel gluons are understood to be radiated by the massive quark loop and are treated as the colour field generating  $\text{tr}W\text{tr}W^\dagger$ . The semiclassical calculation proceeds as follows.

Equations (4.53) and (4.54) have the structure

$$\frac{df_i^D}{d\xi} = F_i \left[ \int_{x_\perp} \text{tr}W_{x_\perp} \text{tr}W_{x_\perp}^\dagger \right], \quad (6.1)$$

where  $F_i$  (with  $i = q, g$ ) is a linear functional depending on  $\int \text{tr}W_{x_\perp}(y_\perp) \text{tr}W_{x_\perp}^\dagger(y'_\perp)$ , interpreted as a function of  $y_\perp$  and  $y'_\perp$ . To be differential in  $t$ , one simply writes

$$\frac{df_i^D}{d\xi dt} = \frac{1}{4\pi} F_i \left[ \int_{x_\perp} \int_{x'_\perp} \text{tr}W_{x_\perp} \text{tr}W_{x'_\perp}^\dagger e^{iq_\perp(x'_\perp - x_\perp)} \right], \quad (6.2)$$

with  $q_\perp^2 = -t$ .

The field responsible for  $\text{tr}W$  is created by a small colour dipole which, in turn, is created by the special photon that models the target. At leading order in perturbation

theory, the colour field of a static quark is analogous to its electrostatic Coulomb field. The field of a quark travelling on the light cone in  $x_-$  direction at transverse position  $0_\perp$  has therefore the following line integral along the  $x_+$  direction,

$$-\frac{ig}{2} \int A_- dx_+ = -ig^2 \int \frac{d^2 k_\perp}{(2\pi)^2} \cdot \frac{e^{ik_\perp x_\perp}}{k_\perp^2} . \quad (6.3)$$

It is exactly this type of line integral that appears in the exponents of the non-Abelian phase factors  $U$  and  $U^\dagger$  that form  $W$  (cf. Eq. (3.4)). A straightforward calculation shows that the function  $\text{tr}W$  produced by a dipole consisting of a quark at  $\rho_\perp$  and an antiquark at  $0_\perp$  reads

$$\begin{aligned} \text{tr}W_{x_\perp}(y_\perp) &= -\frac{g^4(N_c^2 - 1)T_R}{2} \left[ \int_{k_\perp, k'_\perp} \frac{(1 - e^{-ik_\perp \rho_\perp})(1 - e^{-ik'_\perp \rho_\perp})}{(2\pi)^4 k_\perp^2 k'^2_\perp} \right] \\ &\times (1 - e^{ik_\perp y_\perp})(1 - e^{ik'_\perp y_\perp}) e^{i(k_\perp + k'_\perp)x_\perp} , \end{aligned} \quad (6.4)$$

where  $T_F = 1/2$  and  $T_A = N_c$  have to be used for the fundamental and adjoint representation respectively.

The final formulae for the diffractive parton distributions of the target are obtained after integrating over the transverse sizes of the colour dipoles with a weight given by the  $q\bar{q}$  wave functions of the incoming and outgoing target photon. They read

$$\begin{aligned} \frac{df_i^D}{d\xi dt} &= \int dz d^2 \rho_\perp \int dz' d^2 \rho'_\perp \frac{1}{4\pi} F_i \left[ \int_{x_\perp} \int_{x'_\perp} \text{tr}W_{x_\perp} \text{tr}W_{x'_\perp}^\dagger e^{iq_\perp(x'_\perp - x_\perp)} \right] \\ &\times \frac{1}{2} \sum_{\epsilon, \epsilon'} \left[ \psi_\gamma^*(z, \rho_\perp, p'_\perp, \epsilon'_\perp) \psi_\gamma(z, \rho_\perp, 0_\perp, \epsilon_\perp) \right] \left[ \psi_\gamma^*(z', \rho'_\perp, p'_\perp, \epsilon'_\perp) \psi_\gamma(z', \rho'_\perp, 0_\perp, \epsilon_\perp) \right] , \end{aligned} \quad (6.5)$$

where  $\text{tr}W_{x_\perp}(y_\perp)$  is produced by the field of a quark at  $\rho_\perp$  and an antiquark at  $0_\perp$ , and  $\text{tr}W_{x'_\perp}(y'_\perp)$  is produced by the field of a quark at  $\rho'_\perp$  and an antiquark at  $0_\perp$ , as detailed in Eq. (6.4).

The wave function  $\psi_\gamma(z, \rho_\perp, 0_\perp, \epsilon_\perp)$  characterizes the amplitude for the fluctuation of the incoming target photon with polarization  $\epsilon$  and transverse momentum  $0_\perp$  into a  $q\bar{q}$  pair with momentum fractions  $z$  and  $1 - z$  and transverse separation  $\rho_\perp$ . Similarly, the wave function  $\psi_\gamma^*(z, \rho_\perp, p'_\perp, \epsilon'_\perp)$  characterizes the amplitude for the recombination of this  $q\bar{q}$  pair into a photon with polarization  $\epsilon'$  and transverse momentum  $p'_\perp = -q_\perp$ . The summation over the helicities of the intermediate quark states, which are conserved by the high-energy gluonic interaction, is implicit.

The required product of photon wave functions can be calculated following the lines of [45] and using the matrix elements of Appendix B. It reads explicitly

$$\begin{aligned} &\psi_\gamma^*(z, \rho_\perp, p'_\perp, \epsilon'_\perp) \psi_\gamma(z, \rho_\perp, 0_\perp, \epsilon_\perp) \\ &= \frac{N_c e^2 e_q^2}{2(2\pi)^5} \int_{k_\perp, k'_\perp} \text{tr} \Phi^\dagger(z, k'_\perp, M, \epsilon'_\perp) \Phi(z, k_\perp, M, \epsilon_\perp) e^{i\rho_\perp(k'_\perp - k_\perp + zp'_\perp)} , \end{aligned} \quad (6.6)$$

where the notation of [144],

$$\Phi(z, k_{\perp}, M, \epsilon_{\perp}) = \frac{1}{(k_{\perp}^2 + M^2)} [(1-z) \epsilon_{\perp} \cdot \sigma k_{\perp} \cdot \sigma - z k_{\perp} \cdot \sigma \epsilon_{\perp} \cdot \sigma + iM \epsilon_{\perp} \cdot \sigma], \quad (6.7)$$

has been used,  $M$  is the quark mass, and  $\sigma_{1,2}$  are the first two Pauli matrices. Note that for  $p'_{\perp} = 0$ , the average of the diagonal elements ( $\epsilon_{\perp} = \epsilon'_{\perp}$ ) in Eq. (6.6) reproduces the well-known formula for the square of the photon wave function [7].

Inserting Eq. (6.6) into Eq. (6.5) and introducing explicitly the required functionals  $F_i$  specified by Eqs. (4.53) and (4.54), the formulae of [144] for diffractive quark and gluon distribution are exactly reproduced. For the lengthy final expressions the reader is referred to the original paper, where a number of plots, based on the numerical evaluation of these formulae, is also given. Qualitatively, the behaviour can be summarized as follows. The quark distribution  $\beta(df_q^D/d\xi dt)$  falls off like  $\beta$  as  $\beta \rightarrow 0$  and approaches a constant value, which is small compared to intermediate  $\beta$  points, as  $\beta \rightarrow 1$ . The gluon distribution  $\beta(df_g^D/d\xi dt)$  approaches a sizeable constant as  $\beta \rightarrow 0$  and a small constant as  $\beta \rightarrow 1$ . For  $t = 0$ , the behaviour at  $\beta \rightarrow 1$  changes – quark and gluon distributions vanish approximately as  $(1 - \beta)$  and  $(1 - \beta)^2$ . The overall normalization of the gluon distribution is found to be much larger than that of the quark distribution.

Even though a real proton is very different from a small colour dipole, it would certainly be interesting to perform a phenomenological analysis on the basis of the above model.

## 6.2 Large hadron

In this section, the colour field averaging procedure is described for the case of a very large hadronic target, where a quantitative treatment becomes possible under minimal additional assumptions. The following discussion is based on [61, 62], where the large hadron model was developed and applied to a combined analysis of both diffractive and inclusive structure functions (see also Sect. 4.4 and Appendix D of this review).

McLerran and Venugopalan observed that the large size of a hadronic target, realized, e.g., in an extremely heavy nucleus, introduces a new hard scale into the process of DIS [60]. From the target rest frame point of view, this means that the typical transverse size of partonic fluctuations of the virtual photon remains small [61], thus justifying the perturbative treatment of the photon wave function in the semiclassical calculation.

The basic arguments underlying this important result are best explained in the simple case of a longitudinally polarized photon coupled to scalar quarks with one unit of electric charge. As far as the  $Q^2$ -behaviour of the total  $\gamma^*p$  cross section is concerned, this is analogous to the standard partonic process where a transverse photon couples to spinor quarks [145].

In analogy to [7], the longitudinal cross section can be written as

$$\sigma_L = \int d^2\rho_{\perp} \sigma(\rho) W_L(\rho), \quad (6.8)$$



with the square of the wave function of the virtual photon given by

$$W_L(\rho) = \frac{3\alpha_{\text{em}}}{4\pi^2} \int d\alpha N^2 K_0^2(N\rho). \quad (6.9)$$

Here  $\rho = |\rho_\perp|$  is the transverse size of the  $q\bar{q}$  pair,  $\alpha$  is the longitudinal momentum fraction of the photon carried by the quark,  $N^2 = \alpha(1-\alpha)Q^2$ , and  $K_0$  is a modified Bessel function. Note that, in contrast to [7],  $W_L$  is defined to include the integration over  $\alpha$ .

Within the semiclassical approach, the dipole cross section  $\sigma(\rho)$  is given by

$$\sigma(\rho) = \frac{2}{3} \int d^2x_\perp \text{tr} \left[ \mathbf{1} - U(x_\perp)U^\dagger(x_\perp + \rho_\perp) \right], \quad (6.10)$$

but it is convenient to formulate the following arguments in terms of the more general quantity  $\sigma(\rho)$ .

The functional form of  $\sigma(\rho)$  is shown qualitatively in Fig. 6.1. For conventional hadrons of size  $\sim 1/\Lambda$  (where  $\Lambda \sim \Lambda_{\text{QCD}}$ ), its typical features are the quadratic rise at small  $\rho$  ( $\sigma(\rho) \sim \rho^2$  with a proportionality constant  $\mathcal{O}(1)$ ) and the saturation at  $\sigma(\rho) \sim 1/\Lambda^2$ , which occurs at  $\rho \sim 1/\Lambda$ . Consider now the idealized case of a very large target of size  $\eta/\Lambda$  with  $\eta \gg 1$  ( $\eta \sim A^{1/3}$  for a nucleus). It is easy to see that at small  $\rho$  the functional behaviour is given by  $\sigma(\rho) \sim \eta^3 \rho^2$  while saturation has to occur at  $\sigma(\rho) \sim \eta^2/\Lambda^2$  for geometrical reasons. It follows that the change from quadratic rise to constant behaviour takes place at  $\rho \sim 1/\sqrt{\eta}\Lambda$ , i.e., at smaller  $\rho$  than for conventional targets.

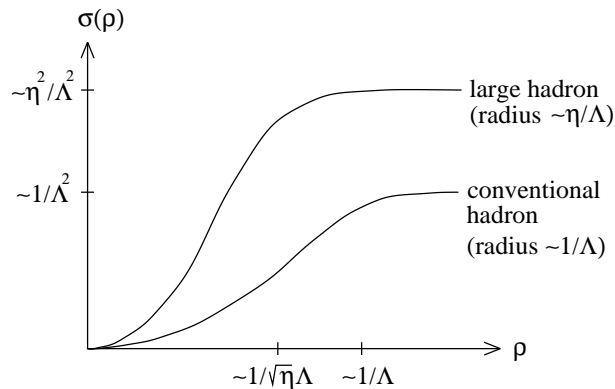


**Figure 6.1:** Qualitative behaviour of the function  $\sigma(\rho)$ .

From the above behaviour of  $\sigma(\rho)$ , the dominance of small transverse distances in the convolution integral of Eq. (6.8) will now be derived. For this purpose, a better understanding of the function  $W_L(\rho)$  is necessary. Recalling that  $K_0(x) \sim \ln(1/x)$  for  $x \ll 1$  while being exponentially suppressed for  $x \gg 1$ , it is easy to see that  $W_L(\rho) \sim Q^2 \ln^2(1/\rho^2 Q^2)$  for  $\rho \ll 1/Q$  and  $W_L(\rho) \sim 1/\rho^4 Q^2$  for  $\rho \gg 1/Q$ . Here numerical constants and non-leading terms have been suppressed.

Under the assumption  $\Lambda^2 \ll \eta\Lambda^2 \ll Q^2$ , the integral in Eq. (6.8) can now be estimated by decomposing it into three regions with qualitatively different behaviour of the

functions  $W_L(\rho)$  and  $\sigma(\rho)$ ,

$$\sigma_L = \sigma_L^{\text{I}} + \sigma_L^{\text{II}} + \sigma_L^{\text{III}} = \left( \int_0^{1/Q^2} + \int_{1/Q^2}^{1/\eta\Lambda^2} + \int_{1/\eta\Lambda^2}^{\infty} \right) \pi d\rho^2 \sigma(\rho) W_L(\rho). \quad (6.11)$$

Of the three contributions

$$\begin{aligned} \sigma_L^{\text{I}} &\sim \int_0^{1/Q^2} d\rho^2 \eta^3 \rho^2 Q^2 \ln^2(1/\rho^2 Q^2) \sim \frac{\eta^3}{Q^2} \\ \sigma_L^{\text{II}} &\sim \int_{1/Q^2}^{1/\eta\Lambda^2} d\rho^2 \eta^3 \rho^2 \frac{1}{\rho^4 Q^2} \sim \frac{\eta^3}{Q^2} \ln(Q^2/\eta\Lambda^2) \\ \sigma_L^{\text{III}} &\sim \int_{1/\eta\Lambda^2}^{\infty} d\rho^2 \frac{\eta^2}{\Lambda^2} \frac{1}{\rho^4 Q^2} \sim \frac{\eta^3}{Q^2} \end{aligned} \quad (6.12)$$

the second one dominates, giving the total cross section

$$\sigma_L \sim \frac{\eta^3}{Q^2} \ln(Q^2/\eta\Lambda^2). \quad (6.13)$$

It is crucial that the third integral is dominated by contributions from its lower limit. Therefore, the overall result is not sensitive to values of  $\rho$  that are larger than  $1/\sqrt{\eta}\Lambda$ . Phrased differently, for sufficiently large targets the transverse size of the  $q\bar{q}$  component of the photon wave function stays perturbative.

This result can be carried over to the realistic case of a transverse photon and spinor quarks, which is obtained simply by substituting  $K_0^2(\rho N)$  with  $2[\alpha^2 + (1-\alpha)^2]K_1^2(\rho N)$  in Eq. (6.9). From the above derivation, one can also expect the result to hold for the transverse size of the  $q\bar{q}g$  component of the photon wave function, both in the case of inclusive and diffractive scattering.

Note that this does not imply a complete reduction to perturbation theory since the long distance which the partonic fluctuation travels in the target compensates for its small transverse size, thus requiring the eikonalization of gluon exchange.

Within this framework, it is natural to introduce the additional assumption that the gluonic fields encountered by the partonic probe in distant regions of the target are not correlated (cf. [78] and the somewhat simplified discussion in [61]). Thus, one arrives at the situation depicted in Fig. 6.2, where a colour dipole passes a large number of regions, each one of size  $\sim 1/\Lambda$ , with mutually uncorrelated colour fields  $A_1 \dots A_n$ .

Consider the fundamental quantity  $W_{x_\perp}(y_\perp)_{ij}[A] W_{x'_\perp}(y'_\perp)_{kl}[A]$  which, after specifying the required representation and appropriately contracting the colour indices  $ijkl$ , enters the formulae for inclusive and diffractive parton distributions (cf. Sect. 4.4 and Appendix D). According to Eq. (3.17), this quantity is the sum of four terms, the most complicated of which involves four  $U$  matrices,

$$\begin{aligned} &\left\{ U_{x_\perp}[A] U_{x_\perp+y_\perp}^\dagger[A] \right\}_{ij} \left\{ U_{x_\perp+y'_\perp}[A] U_{x'_\perp}^\dagger[A] \right\}_{kl} \\ &= \left\{ U_{x_\perp}[A_n] \cdots U_{x_\perp}[A_1] U_{x_\perp+y_\perp}^\dagger[A_1] \cdots U_{x_\perp+y_\perp}^\dagger[A_n] \right\}_{ij} \\ &\times \left\{ U_{x_\perp+y'_\perp}[A_n] \cdots U_{x_\perp+y'_\perp}[A_1] U_{x'_\perp}^\dagger[A_1] \cdots U_{x'_\perp}^\dagger[A_n] \right\}_{kl}. \end{aligned} \quad (6.14)$$

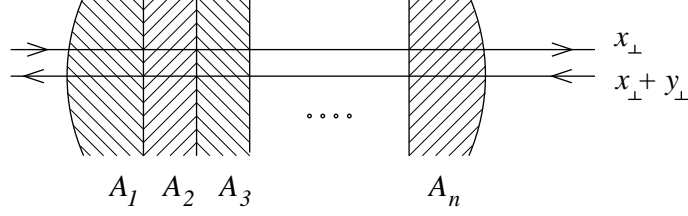


**Figure 6.2:** Colour dipole travelling through a large hadronic target.

The crucial assumption that the fields in regions 1 ...  $n$  are uncorrelated is implemented by writing the integral over all field configurations as

$$\int_A = \int_{A_1} \cdots \int_{A_n}, \quad (6.15)$$

i.e., as a product of independent integrals. Here the appropriate weighting provided by the target wave functional is implicit in the symbol  $\int_A$ .

Under the integration specified by Eq. (6.15), the  $U$  matrices on the r.h. side of Eq. (6.14) can be rearranged to give the result

$$\begin{aligned} \int_A \left\{ U_{x_\perp}[A] U_{x_\perp+y_\perp}^\dagger[A] \right\}_{ij} \left\{ U_{x_\perp+y'_\perp}[A] U_{x_\perp}^\dagger[A] \right\}_{kl} \\ = \int_{A_1} \cdots \int_{A_n} \left\{ U_{x_\perp}[A_1] U_{x_\perp+y_\perp}^\dagger[A_1] \cdots U_{x_\perp}[A_n] U_{x_\perp+y_\perp}^\dagger[A_n] \right\}_{ij} \\ \times \left\{ U_{x_\perp+y'_\perp}[A_n] U_{x_\perp}^\dagger[A_n] \cdots U_{x_\perp+y'_\perp}[A_1] U_{x_\perp}^\dagger[A_1] \right\}_{kl}. \end{aligned} \quad (6.16)$$

To see this, observe that the  $A_1$  integration acts on the integrand  $\{U_{x_\perp}[A_1] U_{x_\perp+y_\perp}^\dagger[A_1]\}_{i'j'}$   $\{U_{x_\perp+y'_\perp}[A_1] U_{x_\perp}^\dagger[A_1]\}_{k'l'}$  transforming it into an invariant colour tensor with the indices  $i'j'k'l'$ . The neighbouring matrices  $U_{x_\perp}[A_2]$  and  $U_{x_\perp}^\dagger[A_2]$  can now be commuted through this tensor structure in such a way that the expression  $\{U_{x_\perp}[A_2] U_{x_\perp+y_\perp}^\dagger[A_2]\}_{i''j''}$   $\{U_{x_\perp+y'_\perp}[A_2] U_{x_\perp}^\dagger[A_2]\}_{k''l''}$  emerges. Subsequently, the  $A_2$  integration transforms this expression into an invariant tensor with indices  $i''j''k''l''$ . Repeating this argument, one eventually arrives at the structure displayed on the r.h. side of Eq. (6.16).

To evaluate Eq. (6.16) further, observe that it represents a contraction of  $n$  identical tensors

$$F_{ijkl} = \int_{A_m} \left\{ U_{x_\perp}[A_m] U_{x_\perp+y_\perp}^\dagger[A_m] \right\}_{ij} \left\{ U_{x_\perp+y'_\perp}[A_m] U_{x_\perp}^\dagger[A_m] \right\}_{kl}, \quad (6.17)$$

where the index  $m$  refers to any one of the regions 1 ...  $n$  into which the target is subdivided. At this point, the smallness of the transverse separations  $y_\perp$  and  $y'_\perp$ , enforced by the large size of the target, is used. In fact, for a target of geometrical size  $\sim n/\Lambda$  (where  $n \gg 1$ ), the relevant transverse distances are bounded by  $y^2 \sim y'^2 \sim 1/n\Lambda^2$ .

Assuming that size and  $x_\perp$  dependence of typical field configurations  $A_m$  are characterized by the scale  $\Lambda$ , it follows that the products  $U_{x_\perp} U_{x_\perp+y_\perp}^\dagger$  and  $U_{x_\perp+y'_\perp} U_{x_\perp}^\dagger$  are close to unit matrices for all relevant  $y_\perp$  and  $y'_\perp$ . Therefore, it is justified to write

$$U_{x_\perp}[A_m] U_{x_\perp+y_\perp}^\dagger[A_m] = \exp \{ iT^a f^a(x_\perp, y_\perp)[A_m] \}, \quad (6.18)$$

where  $T^a$  are the conventional group generators and  $f^a$  are functions of  $x_\perp$  and  $y_\perp$  and functionals of  $A_m$ . Equation (6.18) and its  $y'_\perp$  analogue are expanded around  $y_\perp = y'_\perp = 0$  (which corresponds to  $f^a(x_\perp, 0) = 0$ ) and inserted into Eq. (6.17). At leading non-trivial order, the result reads

$$F_{ijkl} = \delta_{ij}\delta_{kl} \left( 1 - \frac{1}{2}\gamma C_R(y^2 + y'^2) \right) + \gamma(y_\perp y'_\perp) T_{ij}^a T_{kl}^a, \quad (6.19)$$

where  $C_R$  is the Casimir number of the relevant representation ( $C_R = C_{F,A}$ ) and the constant  $\gamma$  is defined by

$$\int_A f^a(x_\perp, y_\perp) f^b(x_\perp, y'_\perp) = \gamma \delta^{ab}(y_\perp y'_\perp) + \mathcal{O}(y^2 y'^2). \quad (6.20)$$

Note that the absence of terms linear in  $f^a$  and the simple structure on the r.h. side of Eq. (6.20) are enforced by colour covariance and transverse space covariance. The absence of an explicit  $x_\perp$  dependence is a consequence of the homogeneity that is assumed to hold over the large transverse size of the target. Neglecting boundary effects, the  $x_\perp$  integration is accounted for by multiplying the final result with a parameter  $\Omega \sim n^2/\Lambda^2$  that characterizes the geometrical cross section of the target.

Substituting the  $n$  tensors  $F_{ijkl}$  on the r.h. side of Eq. (6.16) by the expression given in Eq. (6.19) and contracting the colour indices as appropriate for the inclusive and diffractive case respectively, one obtains, in the large- $N_c$  limit,

$$\int_A \left\{ U_{x_\perp} U_{x_\perp + y_\perp}^\dagger \right\}_{ij} \left\{ U_{x_\perp + y'_\perp} U_{x_\perp}^\dagger \right\}_{ji} = d_R \left[ 1 - \frac{1}{2}\gamma C_R(y_\perp - y'_\perp)^2 \right]^n, \quad (6.21)$$

$$\int_A \left\{ U_{x_\perp} U_{x_\perp + y_\perp}^\dagger \right\}_{ii} \left\{ U_{x_\perp + y'_\perp} U_{x_\perp}^\dagger \right\}_{jj} = d_R^2 \left[ 1 - \frac{1}{2}\gamma C_R(y_\perp^2 + y'^2) \right]^n, \quad (6.22)$$

where  $d_R$  is the dimension of the representation.

Since  $n$  is assumed to be large and the typical values of  $y^2$  and  $y'^2$  do not exceed  $1/n\Lambda^2$ , the formula  $(1-x/n)^n \simeq \exp[-x]$  can be applied to the r.h. sides of Eqs. (6.21) and (6.22). Furthermore, contributions proportional to  $\{U_{x_\perp} U_{x_\perp + y_\perp}^\dagger\}_{ij} \delta_{kl}$ ,  $\delta_{ij} \{U_{x_\perp + y'_\perp} U_{x_\perp}^\dagger\}_{kl}$  and  $\delta_{ij} \delta_{kl}$  have to be added to obtain the complete expression for  $W_{x_\perp}(y_\perp)_{ij} W_{x_\perp}^\dagger(y'_\perp)_{kl}$ . The corresponding calculations are straightforward and the result reads

$$\int_{x_\perp} \int_A \text{tr} \left( W_{x_\perp}(y_\perp) W_{x_\perp}^\dagger(y'_\perp) \right) = \Omega d_R \left[ 1 - e^{-a_R y^2} - e^{-a_R y'^2} + e^{-a_R (y_\perp - y'_\perp)^2} \right], \quad (6.23)$$

$$\int_{x_\perp} \int_A \text{tr} W_{x_\perp}(y_\perp) \text{tr} W_{x_\perp}^\dagger(y'_\perp) = \Omega d_R^2 \left[ 1 - e^{-a_R y^2} \right] \left[ 1 - e^{-a_R y'^2} \right], \quad (6.24)$$

where  $a_R = n\gamma C_R/2$  plays the role of a saturation scale.

The above calculation, performed at large  $N_c$  and for the case of a large target subdivided into many uncorrelated regions, has no immediate application to realistic experiments. However, it provides a set of non-perturbative inclusive and diffractive parton distributions which are highly constrained with respect to each other. For the purpose of a phenomenological analysis, it is convenient to consider  $\Omega$  and  $a \equiv n\gamma N_c/4$  as

new fundamental parameters, giving rise to the following formulae for the basic hadronic quantities required in Sect. 4.4 and Appendix D,

$$\int_{x_\perp} \int_A \text{tr} \left( W_{x_\perp}^{\mathcal{F}}(y_\perp) W_{x_\perp}^{\mathcal{F}\dagger}(y'_\perp) \right) = \Omega N_c \left[ 1 - e^{-ay^2} - e^{-ay'^2} + e^{-a(y_\perp - y'_\perp)^2} \right], \quad (6.25)$$

$$\frac{1}{N_c} \int_{x_\perp} \int_A \text{tr} W_{x_\perp}^{\mathcal{F}}(y_\perp) \text{tr} W_{x_\perp}^{\mathcal{F}\dagger}(y'_\perp) = \Omega N_c \left[ 1 - e^{-ay^2} \right] \left[ 1 - e^{-ay'^2} \right], \quad (6.26)$$

$$\frac{1}{N_c^2} \int_{x_\perp} \int_A \text{tr} W_{x_\perp}^{\mathcal{A}}(y_\perp) \text{tr} W_{x_\perp}^{\mathcal{A}\dagger}(y'_\perp) = \Omega N_c^2 \left[ 1 - e^{-2ay^2} \right] \left[ 1 - e^{-2ay'^2} \right]. \quad (6.27)$$

Here the indices  $\mathcal{F}$  and  $\mathcal{A}$  stand for the fundamental and adjoint representation. A similar, Glauber type  $y^2$  dependence has been recently used in the analyses of [146, 147]. Note that according to Eqs. (6.25)–(6.27) the diffractive structure function is not suppressed by a colour factor relative to the inclusive structure function, as originally suggested in [39].

Using Eq. (6.26) in the generic semiclassical formula Eq. (4.53) for the diffractive quark distribution, the explicit result

$$\frac{dq(\beta, \xi)}{d\xi} = \frac{a\Omega N_c(1-\beta)}{2\pi^3\xi^2} h_q(\beta), \quad (6.28)$$

is obtained. Here  $h_q(\beta)$  is an integral over two Feynman-type parameters,

$$h_q(\beta) = 4 \int_0^\infty dx dx' \frac{\left( \frac{\sqrt{\beta} + x}{(1-\beta + (\sqrt{\beta} + x)^2)^2} \right) \left( \frac{\sqrt{\beta} + x'}{(1-\beta + (\sqrt{\beta} + x')^2)^2} \right)}{(x+x')\sqrt{\beta} + (1-\beta) \left( \frac{x}{\sqrt{\beta} + x} + \frac{x'}{\sqrt{\beta} + x'} \right)}, \quad (6.29)$$

which can be evaluated analytically at  $\beta = 0$  and  $\beta = 1$  yielding  $h_q(0) = 1/2$  and  $h_q(1) = 3\pi^2/8 - 2$ .

Analogously, Eqs. (6.27) and (4.54) give rise to an explicit formula for the diffractive gluon distribution. It reads

$$\frac{dg(\beta, \xi)}{d\xi} = \frac{a\Omega N_c^2(1-\beta)^2}{2\pi^3\xi^2\beta} h_g(\beta), \quad (6.30)$$

where  $h_g(\beta)$  is given by the two-dimensional integral

$$h_g(\beta) = 2 \int_0^\infty dx dx' \frac{\left( \frac{1-\beta + 3(1+x)^2\beta}{(1+x)^2(1-\beta + (1+x)^2\beta)^2} \right) \left( \frac{1-\beta + 3(1+x')^2\beta}{(1+x')^2(1-\beta + (1+x')^2\beta)^2} \right)}{(x+x')\beta + (1-\beta) \left( \frac{x}{1+x} + \frac{x'}{1+x'} \right)}. \quad (6.31)$$

This integral is easily evaluated for  $\beta = 0$  and  $\beta = 1$  yielding  $h_g(0) = 4 \ln 2$  and  $h_g(1) = 45\pi^2/32 - 17/2$ . For general  $\beta$ ,  $h_q(\beta)$  and  $h_g(\beta)$  can be evaluated numerically. The results can be inferred from the solid curves in Fig. 6.3, where the distribution  $d\Sigma/d\xi = 6dq/d\xi$  is displayed to account for the 3 generations of light quarks and antiquarks. The total

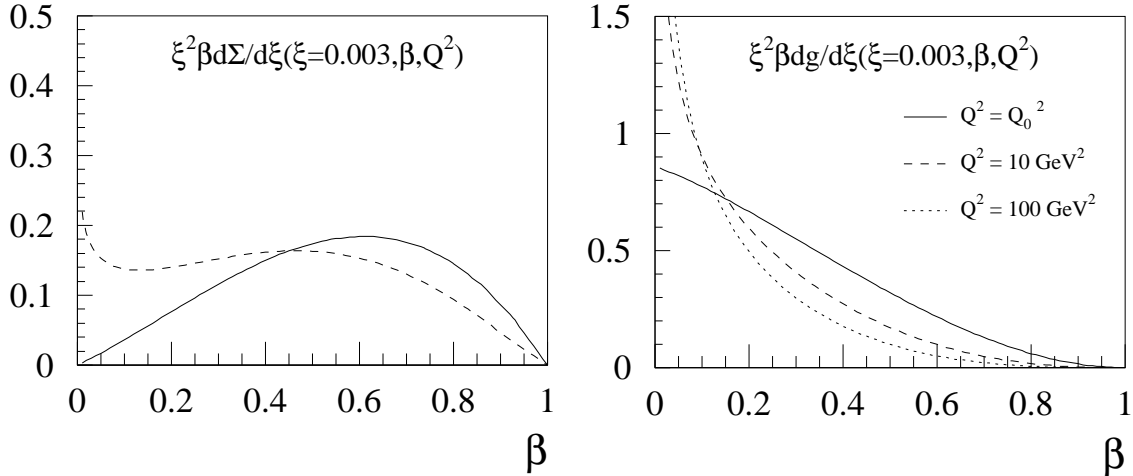


**Figure 6.3:** Diffractive quark and gluon distributions in the large hadron model at the initial scale  $Q_0^2$  and after  $Q^2$  evolution.

normalization, the value of  $\xi$ , and the  $Q^2$  evolution given in Fig. 6.3 are not relevant for the present section and will be discussed in the context of the phenomenological analysis of Sect. 7.1.

The diffractive distributions displayed in Fig. 6.3 are multiplied by  $\beta$  and thus reflect the distribution of momentum carried by the partons. The quark distribution is peaked around  $\beta \simeq 0.65$ , thus being harder than the distribution  $\beta(1 - \beta)$  suggested in [10]. It vanishes like  $\beta$  for  $\beta \rightarrow 0$  and like  $(1 - \beta)$  at large  $\beta$ ; the gluon distribution  $\beta dg/d\xi$ , on the other hand, approaches a constant for  $\beta \rightarrow 0$  and falls off like  $(1 - \beta)^2$  at large  $\beta$ . This asymptotic behaviour in the small- and large- $\beta$  region is in agreement with the results obtained in the perturbative approach of [144] at  $t = 0$ . In spite of the  $(1 - \beta)^2$  behaviour, gluons remain important even at large  $\beta$ , simply due to the large total normalization of this distribution.

Very recently, a closely related discussion of diffractive and inclusive structure functions has been given in [148]. The authors focus on the process where the target hadron remains intact, discussed in the first part of Sect. 3.4, and its relation to inclusive DIS. Technically, the results obtained are very similar to those of the large hadron model as described above [62]. It is also emphasized in [148] that the results can be generalized to the case of conventional hadrons if the assumption of a Gaussian distribution of colour sources of [60] is correct.

### 6.3 Stochastic vacuum

A further fundamentally non-perturbative approach to high-energy hadronic processes, which has recently been applied to diffractive structure functions by Ramirez [59], is based on the model of the stochastic vacuum. The model was originally developed by Dosch and Simonov in Euclidean field theory [52]. A detailed description of the stochas-

tic vacuum approach to high-energy scattering, introduced originally in [53] and closely related to the eikonal approach of [43], can be found in [149] (see also [150] for a comprehensive review). The method was first applied to diffractive DIS in [56], where vector meson production processes were considered. Here, only a brief description of the main underlying ideas will be given.

The fundamental assumption underlying the model of the stochastic vacuum of [52] is that of a convergent cumulant expansion for the vacuum expectation value of path ordered products of field operators. To calculate the average  $\langle \dots \rangle$  of the path ordered exponential

$$P \exp \left( \int_0^t \hat{O}(s) ds \right) = \sum_{n=0}^{\infty} \int_0^t ds_1 \int_0^{s_1} ds_2 \dots \int_0^{s_{n-1}} ds_n \hat{O}(s_1) \dots \hat{O}(s_n), \quad (6.32)$$

the so-called path ordered cumulants  $((\dots))$ , defined by

$$\begin{aligned} \langle 1 \rangle &= ((1)) \\ \langle 1, 2 \rangle &= ((1, 2)) + ((1))((2)) \\ \langle 1, 2, 3 \rangle &= ((1, 2, 3)) + ((1))((2, 3)) + ((1, 2))((3)) + ((1))((2))((3)) \\ \langle 1, 2, 3, 4 \rangle &= ((1, 2, 3, 4)) + \dots + ((1))((2))((3))((4)), \end{aligned} \quad (6.33)$$

are introduced. An expansion in the above cumulants can be applied to the Wegner-Wilson loop in a non-Abelian gauge theory. The supposition that the cumulants are decreasing sufficiently fast with increasing distance between the operators leads to the area law in the purely gluonic case. Neglecting all cumulants higher than quadratic in the fields amounts to the assumption of a Gaussian process, where all higher correlators can be obtained from the two-point Green's function. All of the above is naturally formulated in Euclidean space. The two-point correlator or, more precisely, its analytic continuation to Minkowski space, is the fundamental object in applications to high-energy scattering.

In the treatment of diffractive DIS, the stochastic vacuum approach describes the hadron as well as the virtual photon in terms of fast partons moving in opposite directions. The colour field facilitating the interaction is soft in the centre-of-mass frame of the  $\gamma^* p$  collision (cf. the general discussion of soft hadronic processes in [43]). In this situation, the partons from both sides interact with the field in an eikonized way, and the actual model of the stochastic vacuum is used to evaluate the correlation function of the resulting oppositely directed light-like Wegner-Wilson lines.

In the simplest case, where the photon fluctuates into a  $q\bar{q}$  pair and the hadron is modelled as a quark-diquark system, the interaction amplitude of two Wegner-Wilson loops has to be calculated (see Fig. 6.4). Introducing the notation

$$W = P \exp \left[ -ig \int_{\partial S} A_\mu(z) dz^\mu \right] \quad (6.34)$$

for the path ordered integral around the loop  $\partial S$ , which is extended to light-like infinity in both directions, this amplitude can be written as

$$J(\vec{b}, \vec{R}_1, \vec{R}_2) = \left\langle \frac{1}{N_c} \text{tr}(W_1(\vec{b}/2, \vec{R}_1) - 1) \frac{1}{N_c} \text{tr}(W_2(-\vec{b}/2, \vec{R}_2) - 1) \right\rangle_A. \quad (6.35)$$

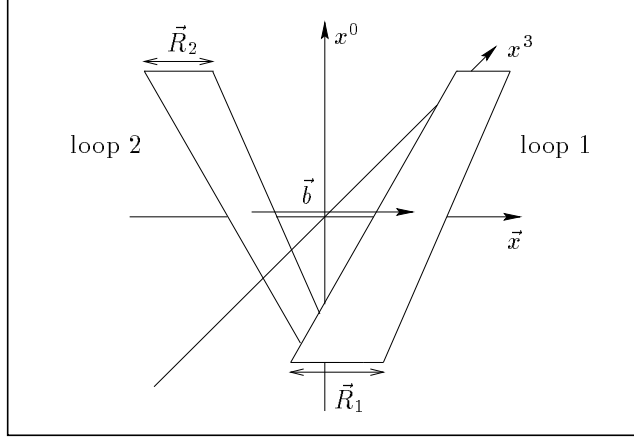


**Figure 6.4:** Wegner-Wilson loops formed by the paths of quarks and antiquarks inside two dipoles. The impact parameter  $\vec{b}$  connects the centres of the two loops, while  $\vec{R}_1$  and  $\vec{R}_2$  point from the quark to the antiquark line of each dipole. All three are vectors in the transverse plane of the collision (figure from [54]).

The notation of this section follows the original papers reviewed (see, e.g., [56, 149]), which means that the function defined in Eq. (6.34) differs by a unit matrix from the closely related function  $W$  used previously in the context of the semiclassical approach. The brackets  $\langle \dots \rangle_A$  denote the vacuum expectation value or, in the functional language, the integration over all colour field configurations.

The line integrals in Eq. (6.35) are transformed into surface integrals with the help of the non-Abelian Stokes theorem

$$P \exp \left[ \int_{\partial S} -ig A_\mu(z) dz_\mu \right] = P_S \exp \left[ \int_S -ig F_{\mu\nu}(z, \omega) d\Sigma^{\mu\nu}(z) \right]. \quad (6.36)$$

Here  $F_{\mu\nu}(z, \omega)$  are the field strength tensors  $F_{\mu\nu}(z)$ , parallel-transported to a common reference point  $\omega$ . The operator  $P_S$  denotes an appropriate surface ordering of these matrix valued tensors (see [149] and refs. therein for further details). The surface  $S$  that is chosen for each of the two Wegner-Wilson loops is the upper side of the pyramid with the loop as base and the origin of the co-ordinate system as apex (see Fig. 6.4). The reference point  $\omega$  is also chosen to be at the origin.

The interaction amplitude for two Wegner-Wilson loops, in its explicit form of Eq. (6.35) or expressed through surface integrals according to Eq. (6.36), can not be evaluated by direct application of the cumulant expansion methods discussed above. The problem is that those methods are adopted for one path ordered integral, in contrast to the two path (or surface) ordered integrals required for  $J(\vec{b}, \vec{R}_1, \vec{R}_2)$ . In Ref. [53] it was suggested to apply the Gaussian factorization hypothesis directly to products of the fields  $F_{\mu\nu}^a(z, \omega)$ ,

$$\langle F(1) \dots F(2n) \rangle = \sum_{\text{all pairings}} \langle F(i_1) F(j_1) \rangle \dots \langle F(i_n) F(j_n) \rangle, \quad (6.37)$$



where the single argument of  $F$  stands for Lorentz and colour indices and space-time co-ordinates. Note, however, that this factorization assumption is not equivalent to the original approach of [52] (cf. the discussion in [150, 151]).

Equation (6.35) can now be evaluated if the fundamental correlator

$$\langle g^2 F_{\mu\nu}^c(x, \omega) F_{\sigma\rho}^d(y, \omega) \rangle_A \quad (6.38)$$

is known. Under the further assumption that this correlator depends neither on the path used for transporting the field to  $\omega$  nor on the position of the reference point  $\omega$  itself, the most general form reads

$$\begin{aligned} \langle g^2 F_{\mu\nu}^c(x, \omega) F_{\sigma\rho}^d(y, \omega) \rangle_A &= \frac{\delta^{cd} \langle g^2 FF \rangle}{12(N_c^2 - 1)} \left\{ \kappa (g_{\mu\rho} g_{\nu\sigma} - g_{\mu\sigma} g_{\nu\rho}) D(z^2/a^2) \right. \\ &\quad \left. + (1 - \kappa) \frac{1}{2} [\partial_\mu (z_\rho g_{\nu\sigma} - z_\sigma g_{\nu\rho}) + \partial_\nu (z_\sigma g_{\mu\rho} - z_\rho g_{\mu\sigma})] D_1(z^2/a^2) \right\}, \end{aligned} \quad (6.39)$$

where  $D$  and  $D_1$  are, a priori, two independent functions, and  $\langle g^2 FF \rangle$  is the gluon condensate. Note that the model of the stochastic vacuum is formulated in Euclidean field theory and the analytic continuation to Minkowski space is non-trivial. The intricacies of this process and, in particular, the constraints it imposes on the shape of the functions  $D$  and  $D_1$  will not be discussed here. For completeness, the correlation functions used, e.g., in [56] are given:

$$D_1(z^2/a^2) = D(z^2/a^2) = \frac{27\pi^4}{4} i \int \frac{d^4 k}{(2\pi)^4} \frac{k^2}{(k^2 - (3\pi/8)^2)^4} e^{-ik \cdot z/a}. \quad (6.40)$$

Detailed information about the parameters entering Eq. (6.39) and the functional form of  $D$  and  $D_1$  is available from low energy hadronic physics as well as from lattice calculations (see, e.g., the recent results of [152]). Given these low-energy parameters, a large number of soft hadronic high-energy scattering processes is successfully described by the model of the stochastic vacuum. For the present review, it is sufficient to state that, within the present model, the behaviour of the correlator in Eq. (6.39) is quantitatively known.

Thus, the method for evaluating the fundamental dipole amplitude of Eq. (6.35) is now established. The amplitude vanishes for small dipoles, as expected from colour transparency, and grows linearly for large dipoles, as suggested by the geometric picture of string-string scattering.

The calculation of diffractive processes is straightforward as soon as a specific quark-diquark wave function of the hadronic target is chosen. The procedure of folding the dipole amplitude with the virtual photon and the hadron wave functions introduces a certain model dependence on the hadronic side.

An essential difference between the present framework and the semiclassical approach discussed above is the frame of reference where the model for the hadronic target is formulated. From the perspective of the virtual photon, the situations are similar: the  $q\bar{q}$  fluctuation scatters off a soft colour field. However, in the semiclassical approach (cf., e.g., Sect. 6.2), this field is modelled on the basis of ideas about hadron colour fields in the

rest frame of the hadron. By contrast, the stochastic vacuum model uses an intermediate frame, where both projectile and target are fast (e.g., the centre-of-mass frame), as the natural frame for the colour field. The target hadron is described in terms of quarks interacting with this field in an eikonized way, and the field, as seen by the projectile, is a result of the distribution of these partons and of the gluon dynamics in the stochastic vacuum model.

As an interesting consequence of the above discussion, the conditions required for the eikonal approximation to work are different in the two approaches. While, in the semiclassical model, the partons from the photon wave function have to be fast in the target rest frame, the stochastic vacuum approach requires them to be fast in, say, the centre-of-mass frame. The latter is a far more stringent condition, which can be numerically important in phenomenological applications [58, 59].

The reader is referred to Sections 7.1 and 7.3 for a brief discussion of recent applications of the presented model to diffractive electroproduction data.

# 7 Recent Experimental Results

In this chapter, a brief discussion of experimental results in diffractive electroproduction, focussing in particular on the diffractive structure function, on specific features of the diffractively produced final state, and on exclusive meson production is given. The discussion is aimed at the demonstration of interesting features of different theoretical models and calculational approaches in the light of the available data (see also [153] for recent reviews). From an experimentalist's perspective, what follows can only be considered a very brief and incomplete overview.

## 7.1 Diffractive structure function

As already explained in Chapter 2, the observation that diffractive DIS is of leading twist and the ensuing measurement of diffractive structure functions lie at the heart of increased recent interest in the field. While the basic experimental facts were stated at the beginning of this review, the present section supplies some additional details concerning  $F_2^D$  and compares observations with theoretical ideas.

To begin with, a brief discussion of the most recent and most precise data on  $F_2^D$ , produced by the H1 and ZEUS collaborations [73,74], is given. As mentioned previously, the most precise analyses have to be based on measurements where the scattered proton is not tagged. In Ref. [73], this problem is handled by starting from a cross section

$$\frac{d^5\sigma_{ep\rightarrow eXY}}{dx dQ^2 d\xi dt dM_Y^2}, \quad (7.1)$$

where, by definition, the two clusters  $X$  and  $Y$  are separated by the largest rapidity gap in the hadronic final state of the event. This definition allows for the possibility that the proton breaks up into a final state  $Y$  with mass square  $P'^2 = M_Y^2$  (cf. Fig. 2.1). A structure function  $F_2^{D(3)}$  is then defined, as in Sect. 2.3, after integration over  $t$  and  $M_Y^2$ . The event selection of [73] is based on the requirement that  $X$  is fully contained in the main detector while  $Y$  passes unobserved into the beam pipe. This implies that  $M_Y \lesssim 1.6$  GeV and  $|t| \lesssim 1$  GeV<sup>2</sup>, thus approximately specifying the relevant integration region for  $M_Y^2$  and  $t$ . A rapidity cut ensures that  $X$  is well separated from  $Y$ .

The most recent ZEUS analysis [74] is based on the so-called  $M_X$  method, introduced in [71]. Similarly to what was discussed above, it is assumed that  $X$  is contained in the detector while  $Y$  escapes down the beam pipe. Thus,  $M_X$  is simply defined to be the full hadronic mass contained in the main detector components. In contrast to the H1 analysis, the diffractive cross section, integrated over all  $t$  and  $M_Y$ , is defined by subtracting from

this full cross section the non-diffractive contribution. The subtraction is based on the ansatz

$$\frac{d\mathcal{N}}{d \ln M_X^2} = D + c \exp(b \ln M_X^2) \quad (7.2)$$

for the event distribution in the region of not too large masses. Here  $D$  is the diffractive contribution and the second term is the non-diffractive contribution. The exponential  $\ln M_X^2$  dependence is expected as a result of the Poisson distribution of particles emitted between current and target jet regions in non-diffractive DIS. This leads to an exponential distribution of rapidity gaps between the detector limit and the most forward detected particles and therefore to the above  $M_X$  dependence. The diffractive contribution is not taken from the fit result for  $D$  but is determined by subtracting from the observed number of events the non-diffractive contribution that corresponds to the fit values of  $b$  and  $c$ .

For more details concerning the data analysis and the experimental results themselves the reader is referred to the original papers [73, 74] and to the figures in the remainder of this section, where theoretical models are compared with measured values of  $F_2^D$ . It can be seen from the direct comparison of H1 and ZEUS data found in [74] that the two methods give similar results, although the H1 values for  $F_2^{D(3)}$  have a tendency towards a faster  $Q^2$  rise for any given  $\beta$ .

The  $M_X$  method of ZEUS has the advantage of subtracting events which happen to have a rapidity gap in spite of non-singlet colour exchange. It also allows for diffractive events with relatively forward particles, which are excluded by the rapidity cut of H1 [154]. However, the subtraction of the non-diffractive background also introduces new uncertainties, in particular the dependence on the region in  $M_X$  where the fit according to Eq. (7.2) is performed.

Note also that a measurement of  $F_2^{D(4)}$ , based on the use of the leading proton spectrometer of ZEUS, was reported in [72]. The results for  $F_2^{D(3)}$ , obtained by explicit  $t$  integration, are probably the cleanest ones from both the theoretical and experimental perspectives. They agree with the latest  $F_2^{D(3)}$  measurements discussed above, but at the moment they are, unfortunately, less precise because of limited statistics. The observed  $t$  dependence of  $F_2^{D(4)}$  can be parametrized as  $e^{bt}$ , with  $b = 7.2 \pm 1.1(\text{stat.})_{-0.9}^{+0.7}(\text{syst.}) \text{ GeV}^{-2}$ .

## Leading twist analysis

As mentioned previously, the leading twist behaviour of small- $x$  diffraction is one of its most striking features. For this reason, and in keeping with the general perspective of this review, it is convenient to start the discussion with calculations, such as the semiclassical approach, that focus on the leading twist nature of the process.

Detailed numerical predictions exhibiting this behaviour were first made in [7] based on simple aligned jet model calculations with soft two gluon exchange. Further theoretical and numerical developments by these and other authors [28, 131, 139], focussing, in particular, on high-mass diffraction and higher twist effects, are discussed below.

Data analyses based on the idea of parton distributions of the pomeron [9] and their

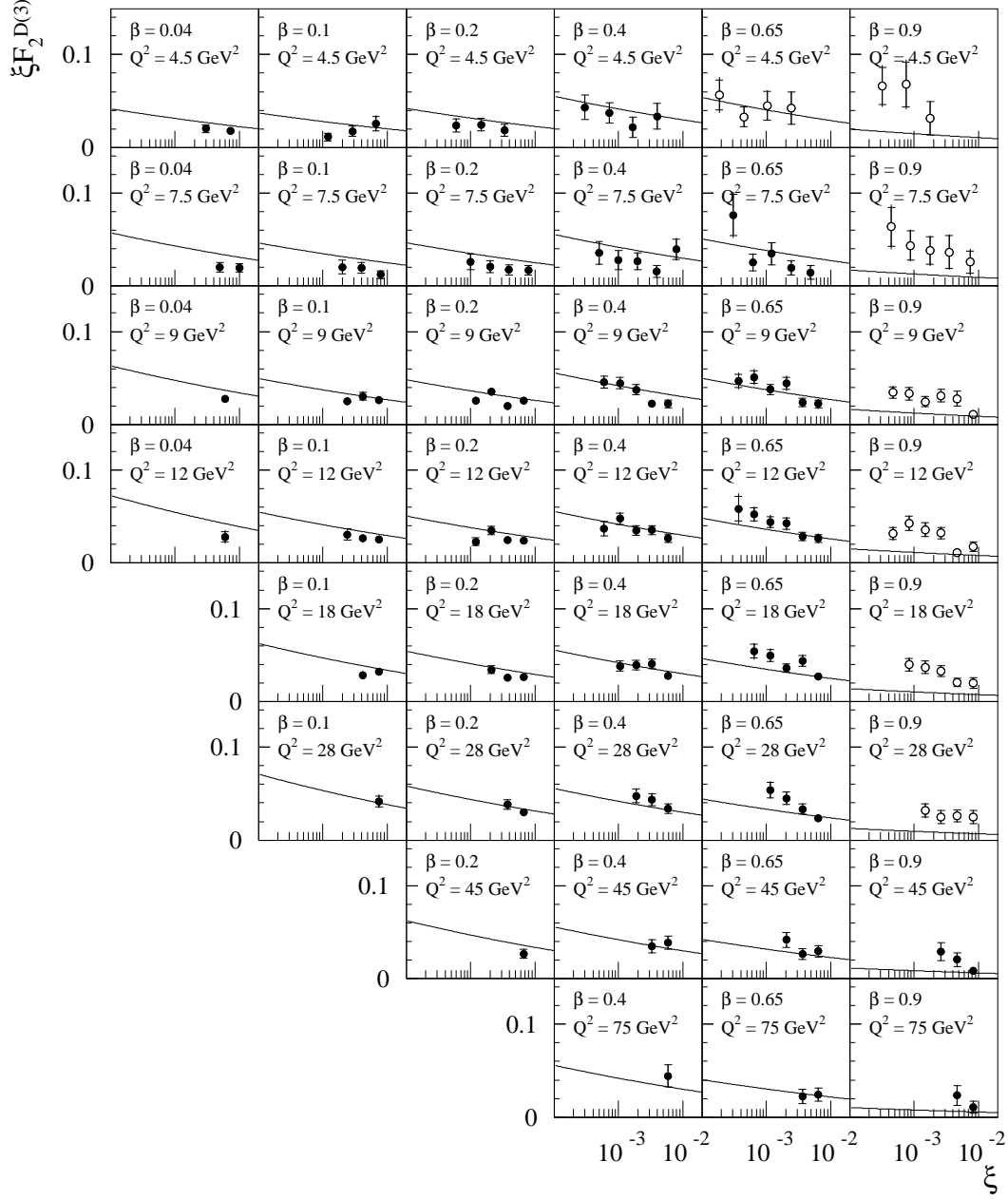


**Figure 7.1:** The structure function  $F_2^{D(3)}(\xi, \beta, Q^2)$  computed in the semiclassical approach with H1 data from [73]. The open data points correspond to  $M^2 \leq 4 \text{ GeV}^2$  and are not included in the fit.

$Q^2$  evolution were performed early on by many authors [155, 156]. The most recent H1 publication [73] includes such a partonic analysis as well.

Here, a detailed description of the approach of [62] will be given, which is based on diffractive parton distributions in the sense of Berera and Soper [13], calculated in the semiclassical approach with a specific model for the averaging over all target colour fields (cf. Sect. 6.2). As can be seen from Figs. 7.1 to 7.3, a satisfactory description of  $F_2^{D(3)}$  is achieved in this framework.

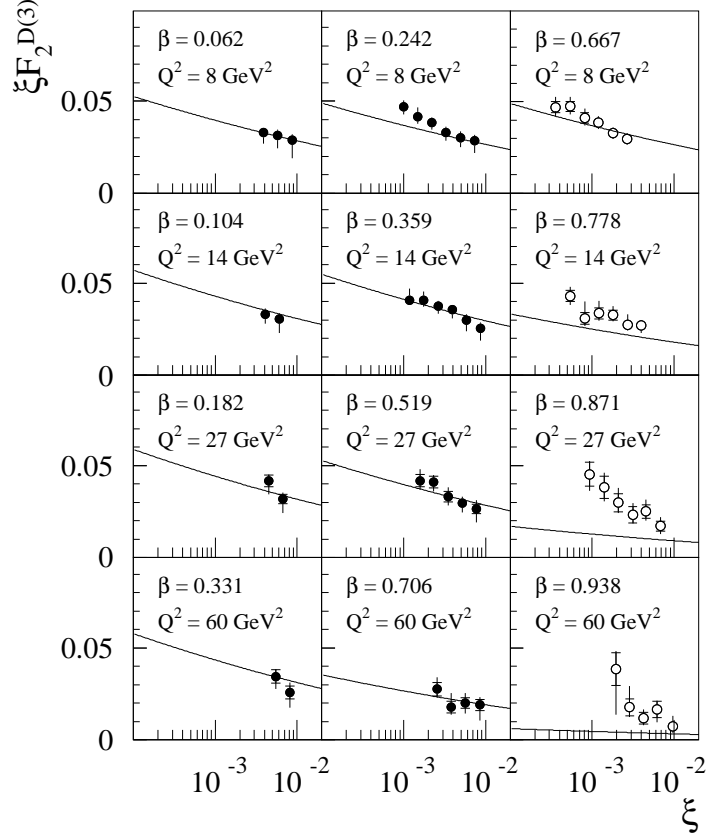


**Figure 7.2:** The structure function  $F_2^{D(3)}(\xi, \beta, Q^2)$  computed in the semiclassical approach with ZEUS data from [74]. The open data points correspond to  $M^2 \leq 4 \text{ GeV}^2$  and are not included in the fit.

In the presented approach, the diffractive distributions of Sect. 6.2 and the inclusive distributions of Appendix D are used as non-perturbative input at some small scale  $Q_0^2$ . They are evolved to higher  $Q^2$  using the leading-order DGLAP equations [157]. The non-perturbative parameters of the model as well as the scale  $Q_0^2$  are then determined from a combined analysis of experimental data on inclusive and diffractive structure functions.

At first sight, the semiclassical description of parton distribution functions always predicts an energy dependence corresponding to a classical bremsstrahlung spectrum:  $q(x), g(x) \sim 1/x$ . However, one expects, in a more complete treatment, a non-trivial energy dependence to be induced since the field averaging procedure encompasses more and more modes of the proton field with increasing energy of the probe (cf. the discussion at the end of Sect. 3.4). This energy dependence is parametrized in the form of a soft, logarithmic growth of the normalization of diffractive and inclusive parton distributions with the collision energy  $\sim 1/x$ , consistent with the unitarity bound. As a result, the additional parameter  $L$  is introduced into the formulae of both Sect. 6.2 and Appendix D, where the overall normalization factor  $\Omega$  has to be replaced according to

$$\Omega \rightarrow \Omega (L - \ln x)^2. \quad (7.3)$$

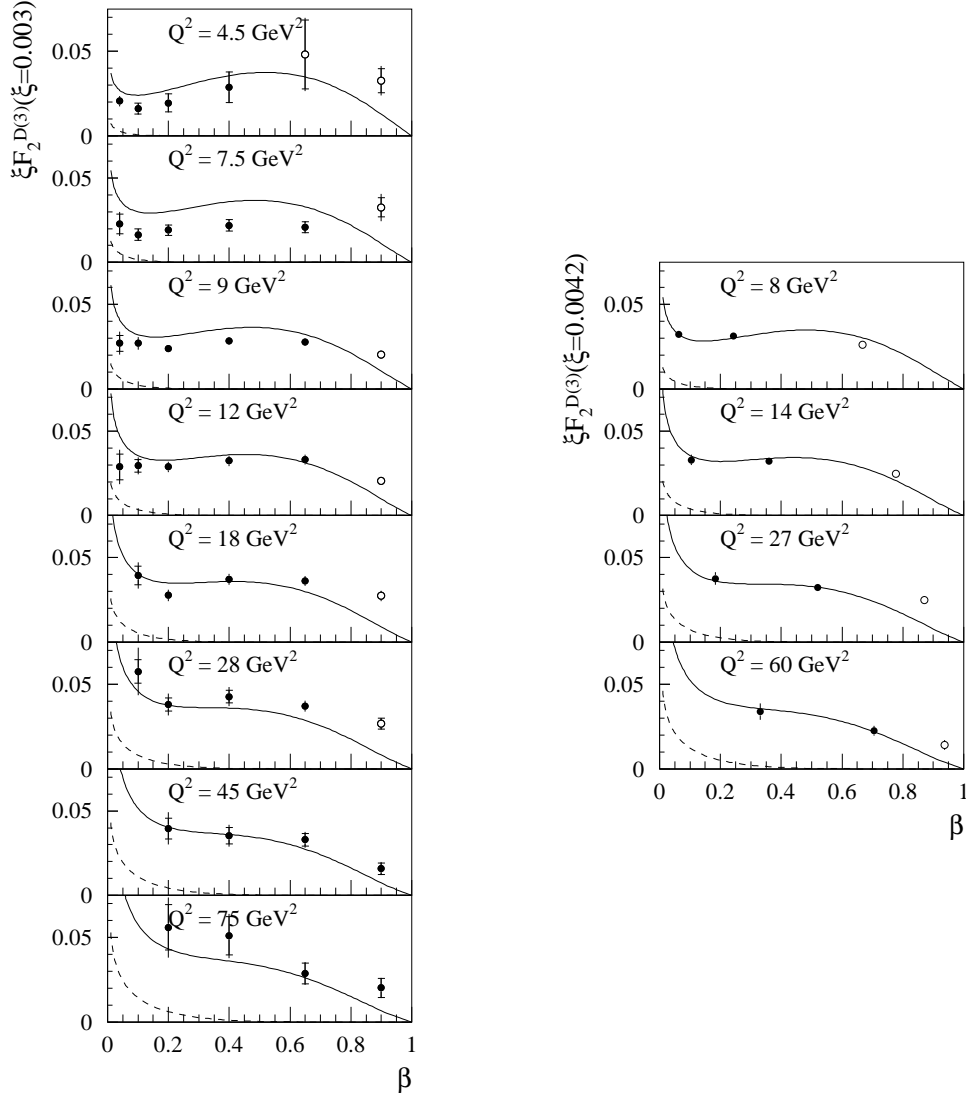


**Figure 7.3:** Dependence of the diffractive structure function  $F_2^{D(3)}$  on  $\beta$  and  $Q^2$ , compared to data from H1 (left) and ZEUS (right) [73, 74]. Open data points correspond to  $M^2 \leq 4 \text{ GeV}^2$ . The charm content of the structure function is indicated as a dashed line.

The following expressions for the diffractive parton distributions are obtained,

$$\frac{dq(\beta, \xi, Q_0^2)}{d\xi} = \frac{a\Omega N_c (1-\beta) (L - \ln \xi)^2}{2\pi^3 \xi^2} h_q(\beta), \quad (7.4)$$

$$\frac{dg(\beta, \xi, Q_0^2)}{d\xi} = \frac{a\Omega N_c^2 (1-\beta)^2 (L - \ln \xi)^2}{2\pi^3 \beta \xi^2} h_g(\beta), \quad (7.5)$$

where the functions  $h_{q,g}(\beta)$  are defined in Sect. 6.2. Corresponding expressions for the inclusive input distributions of quarks and gluons are given in Appendix D.

Thus, the input distributions depend on  $a$ ,  $\Omega$ ,  $L$ , and on the scale  $Q_0^2$  at which these distributions are used as a boundary condition for the leading-order DGLAP evolution<sup>1</sup>.

<sup>1</sup>Note that the two variables  $a$  and  $\Omega$  can not be combined into one since the inclusive quark distribution depends on them in a more complicated way.

At this order, the measured structure function  $F_2$  coincides with the transverse structure function. In defining structure functions and parton distributions, all three light quark flavours are assumed to yield the same contribution, such that the singlet quark distribution is simply six times the quark distribution defined above. Valence quarks are absent in the semiclassical approach. Charm quarks are treated entirely as massive quarks in the fixed flavour number scheme [158]. Thus,  $n_f = 3$  in the DGLAP splitting functions, and only gluon and singlet quark distributions are evolved.

The structure functions  $F_2$  and  $F_2^{D(3)}$  are then given by the singlet quark distribution and a massive charm quark contribution due to boson-gluon fusion. Explicit formulae can, for example, be found in [156]. For the numerical studies, the values  $\Lambda_{\text{LO},n_f=3} = 144 \text{ MeV}$  ( $\alpha_s(M_Z) = 0.118$ ),  $m_c = 1.5 \text{ GeV}$ ,  $m_b = 4.5 \text{ GeV}$  are used, and the massive charm quark contribution is evaluated for a renormalization and factorization scale  $\mu_c = 2m_c$ .

The resulting structure functions can be compared with HERA data on the inclusive structure function  $F_2(x, Q^2)$  [159] and on the diffractive structure function  $F_2^{D(3)}(\xi, \beta, Q^2)$  [73, 74]. These data sets from the H1 and ZEUS experiments are used to determine the unknown parameters of the model. The following selection criteria are applied to the data:  $x \leq 0.01$  and  $\xi \leq 0.01$  are needed to justify the semiclassical description of the proton; with  $Q_0^2$  being a fit parameter, a sufficiently large minimum  $Q^2 = 2 \text{ GeV}^2$  is required to avoid that the data selection is influenced by the current value of  $Q_0^2$ ; finally  $M^2 > 4 \text{ GeV}^2$  is required in the diffractive case to justify the leading-twist analysis.

The optimum set of model parameters is determined from a minimization of the total  $\chi^2$  (based on statistical errors only) of the selected data. As a result,

$$\begin{aligned}
Q_0^2 &= 1.23 \text{ GeV}^2, \\
L &= 8.16, \\
\Omega &= (712 \text{ MeV})^{-2}, \\
a &= (74.5 \text{ MeV})^2.
\end{aligned}
\tag{7.6}$$

All parameters are given with a precision which allows reproduction of the plots, but which is inappropriate with respect to the crudeness of the model. The distributions obtained with these fitted parameters yield a good qualitative description of all data on inclusive and diffractive DIS at small  $x$ , as illustrated in Figs. D.1, 7.1 and 7.2. The starting scale  $Q_0^2$  is in the region where one would expect the transition between perturbative and non-perturbative dynamics to take place; the two other dimensionful parameters  $\Omega L^2$  and  $a$  are both of the order of typical hadronic scales.

The approach fails to reproduce the data on  $F_2^{D(3)}$  for low  $M^2$ . This might indicate the importance of higher twist contributions in this region (see, e.g., [34]). It is interesting to note that a breakdown of the leading twist description is also observed for inclusive structure functions [160], where it occurs for similar invariant hadronic masses, namely  $W^2 \lesssim 4 \text{ GeV}^2$ .

The perturbative evolution of inclusive and diffractive structure functions is driven by the gluon distribution, which is considerably larger than the singlet quark distribution



in both cases. With the parameters obtained above, it turns out that the inclusive gluon distribution is about twice as large as the singlet quark distribution. By contrast, the relative magnitude and the  $\beta$  dependence of the diffractive distributions are completely independent of the model parameters. Moreover, their absolute normalization is, up to the slowly varying factor  $1/\alpha_s(Q_0^2)$ , closely tied to the normalization of the inclusive gluon distribution.

In spite of the  $(1-\beta)^2$  behaviour, gluons remain important even at large  $\beta$ , simply due to the large total normalization of this distribution. As a result, the quark distribution does not change with increasing  $Q^2$  for  $\beta \simeq 0.5$  and is only slowly decreasing for larger values of  $\beta$ .

The dependence of the diffractive structure function on  $\beta$  and  $Q^2$  is illustrated in Fig. 7.3, where the predictions are compared with experimental data [73, 74] at fixed  $\xi = 0.003$  (H1) and  $\xi = 0.0042$  (ZEUS). The underlying diffractive parton distributions  $dg/d\xi$  and  $d\Sigma/d\xi = 6dq/d\xi$  at input scale  $Q_0^2$  and their  $Q^2$  evolution are shown in Fig. 6.3.

It is an essential feature of the above semiclassical analysis that the rise of  $F_2(x, Q^2)$  and of  $F_2^{D(3)}(\xi, \beta, Q^2)$  at small  $x$  and  $\xi$  has the same, *non-perturbative* origin in the energy dependence of the average over soft field configurations in the proton. With increasing  $Q^2$ , the  $x$  dependence is enhanced by perturbative evolution in the case of the inclusive structure function while, in the diffractive case, the  $\xi$  dependence remains unchanged.

## Importance of higher twist

To illustrate the importance of higher twist contributions, consider the parametrization of Bartels et al. [34] (cf. Figs. 7.4 and 7.5). In this analysis, four different contributions to the diffractive structure function  $F_2^{D(3)}$  are considered. These are  $F_{q\bar{q}}^T$  and  $F_{q\bar{q}g}^T$  – the leading twist contributions of  $q\bar{q}$  and  $q\bar{q}g$  components of the transverse photon wave function – supplemented by  $\Delta F_{q\bar{q}}^L$  and  $\Delta F_{q\bar{q}}^T$  – the higher twist contributions of the  $q\bar{q}$  component of longitudinal and transverse photon wave function.

As has already been explained in Sect. 3.2, there is no leading twist contribution to diffraction from the  $q\bar{q}$  component of the longitudinal photon. Nevertheless, this component is important because of its dominance in the region  $\beta \rightarrow 1$ .

The approach of [34] is to write down generic expressions for the above four contributions to the structure function. These expressions incorporate the qualitative knowledge about  $\beta$ ,  $\xi$  and  $Q^2$  dependence of each contribution. This knowledge is based on the two gluon exchange calculations of [31, 101] and is largely in agreement with what can be learned from the semiclassical treatment presented in this review. For example, the leading twist contributions are expected to have a softer  $1/\xi$  behaviour than the higher twist contributions, which are expected to behave as  $(\xi g(\xi))^2$  (cf. Sect. 5.3). Furthermore, the longitudinal  $q\bar{q}$  component is the only one known not to vanish at  $t = 0$  and  $\beta \rightarrow 1$ .

The relative weights of the four contributions, which are, in principle, determined by photon wave function and structure of the target, are allowed to vary in the fit of [34]. The results of the two independent fits to ZEUS and H1 data (cf. Figs. 7.4 and 7.5) are

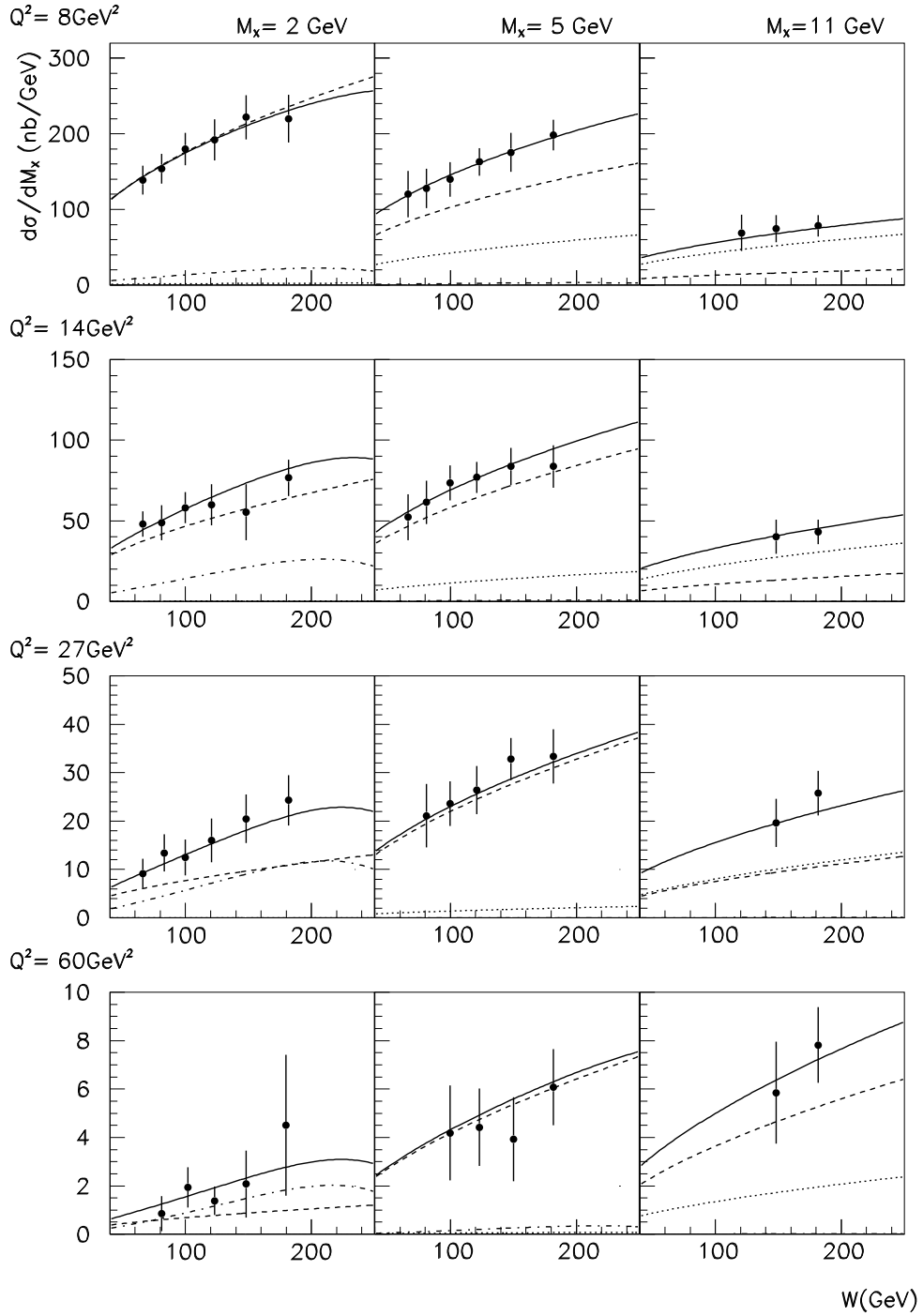


**Figure 7.4:** Fit to ZEUS data for  $F_2^{D(3)}(\xi, \beta, Q^2)$  by Bartels et al. [34]. Solid line: total result; dashed line:  $F_{q\bar{q}}^T$ ; dotted line:  $F_{q\bar{q}g}^T$ ; dashed-dotted line:  $\Delta F_{q\bar{q}}^L$  (data from [161], see also [74]).

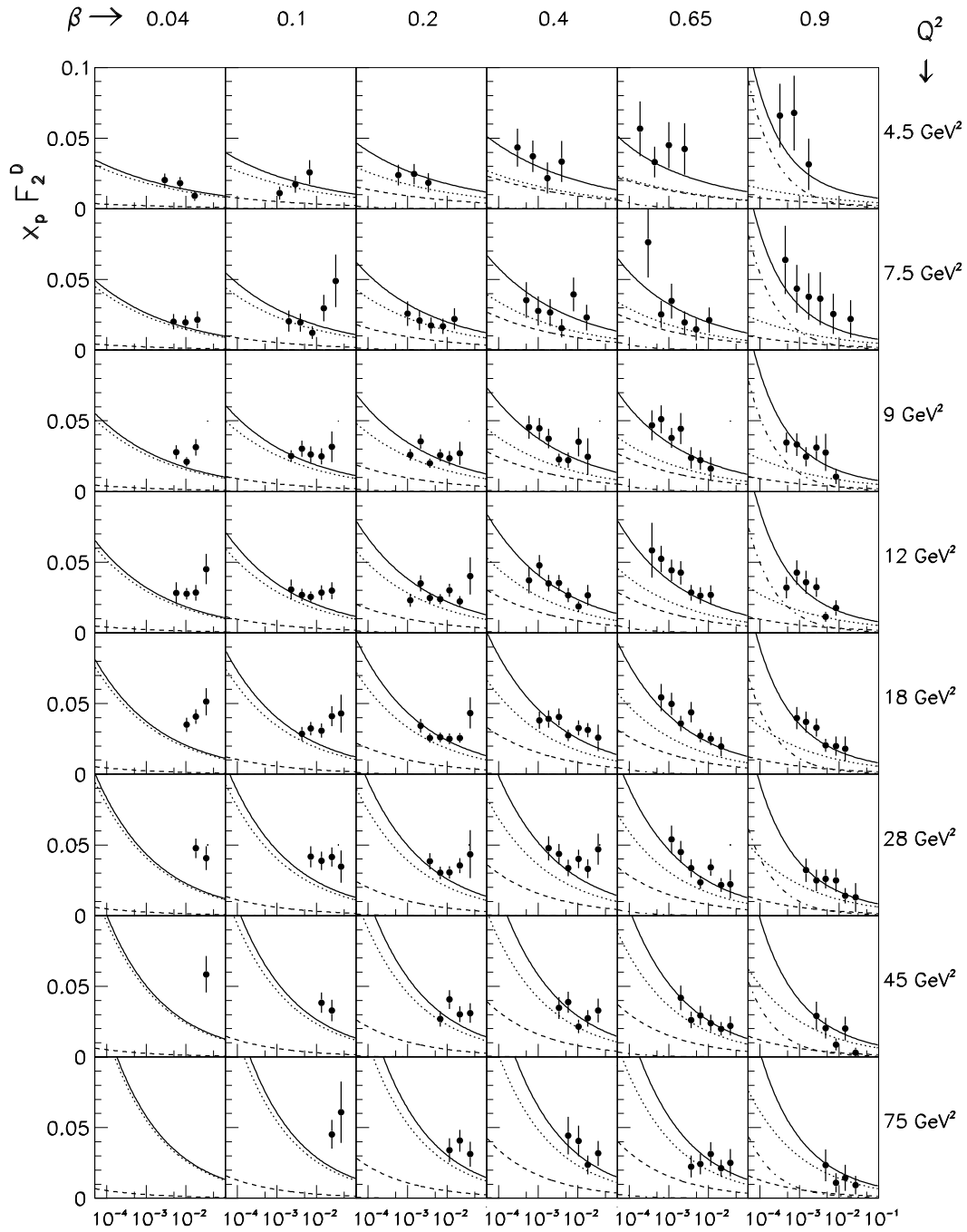


**Figure 7.5:** Fit to H1 data for  $F_2^{D(3)}(\xi, \beta, Q^2)$  by Bartels et al. [34]. Solid line: total result; dashed line:  $F_{q\bar{q}}^T$ ; dotted line:  $F_{q\bar{q}g}^T$ ; dashed-dotted line:  $\Delta F_{q\bar{q}}^L$  (data from [73]).

in good agreement with physical expectations. Note especially the dominance of  $\Delta F_{q\bar{q}}^L$  at  $\beta \rightarrow 1$  and of  $F_{q\bar{q}g}^T$  at  $\beta \rightarrow 0$ . Note also the steep  $\xi$  dependence of  $\Delta F_{q\bar{q}}^L$ , the need of which is visible, in particular, in the top right-hand bins of Fig. 7.5. Thus, the data clearly has room for the higher twist contributions introduced in [34]. It would certainly be desirable to include such contributions in the leading twist analysis of [62], with its consistent treatment of the  $Q^2$  evolution. An obvious problem to be solved before such a development can be realized is the  $\xi$  dependence of leading and higher twist terms.

As an interesting feature of the data, the authors of [34] notice that the H1 results can be described by two different sets of parameters: one in which  $F_{q\bar{q}g}^T$  is enhanced at large  $\beta$  (corresponding to Fig. 7.5) and a second one which is more similar to the ZEUS fit. The solution with enhanced  $q\bar{q}g$  contribution can be interpreted as the analogue, within the framework of this parametrization, of the singular gluon proposal of H1 [73].

As can be seen from the QCD analysis in [73], the H1 data exhibit some preference for a gluon distribution that is large for high  $\beta$ , such that for low values of  $Q^2$  most of the pomeron's momentum is carried by a single gluon. This singular gluon proposal, which has some similarity with the naïve boson-gluon fusion model of [39], is hard to justify theoretically. In particular, the validity of the partonic leading twist picture at  $\beta \sim 1$  and not too large  $Q^2$  is questionable. Given the successful analysis of [62] and the alternative, less singular parametrizations in [34, 73], a singular diffractive gluon distribution is not unavoidable with the present data.

Note that the QCD analysis of [73] has the important advantage of explicitly dealing with the Reggeon contribution, which, although suppressed in the high-energy limit, represents an important correction in the upper region of the  $\xi$  range. A Reggeon contribution is also included in the recent, more detailed analysis of H1 data [162] in the framework of the parametrization of [34]. For a discussion of Reggeon exchange in diffractive DIS the reader is referred, e.g., to [163].

A further interesting analysis, based on the model of the stochastic vacuum (cf. Sect. 6.3) and including both leading and higher twist contributions, was reported by Ramirez [59]. As an example, results for  $F_2^{D(3)}$  and for the transverse contribution  $F_T^{D(3)}$  at  $Q^2 = 12 \text{ GeV}^2$  and  $x = 0.0075$  are shown in Fig. 7.6.

The presented calculation is limited to the  $q\bar{q}$  fluctuation of the photon and does not include Altarelli-Parisi evolution. Therefore, the author limits the discussion of data to the high- $\beta$  region, where gluon radiation effects are not yet dominant. The model as used in previous analyses tends to overshoot the data. Modifications proposed by Rueter (see [58, 164]) subtract integration regions where one of the quarks is too slow for the eikonal approach to work, and where the transverse size of the pair is too small for the non-perturbative model to be applicable. The modified model gives a good description of the data (cf. Fig. 7.6).

It is particularly interesting to see the absolute magnitude of the longitudinal structure function at large  $\beta$  as a prediction of an explicit calculation. Furthermore, the model shows a non-vanishing contribution from the  $q\bar{q}$  component at  $\beta \rightarrow 1$ . This is an improvement compared to the treatment of [62] which is related to the better description of the dynamics of the outgoing proton at non-zero  $t$  in the calculation of [59].

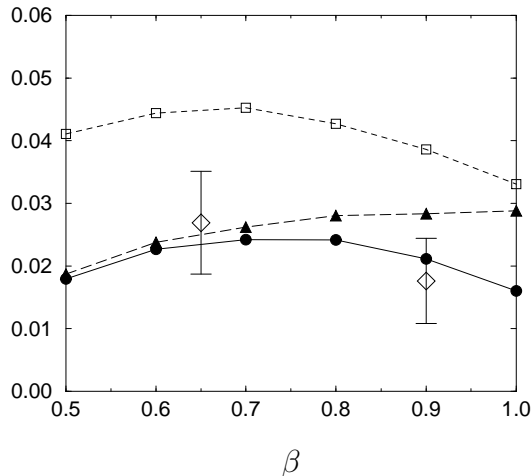


**Figure 7.6:** Diffractive structure functions at  $Q^2 = 12 \text{ GeV}^2$  and  $x = 0.0075$  in the model of the stochastic vacuum, calculated by Ramirez [59], compared to H1 data from [73]:  $\xi F_2^{D(3)}(\xi, \beta, Q^2)$  and  $\xi F_T^{D(3)}(\xi, \beta, Q^2)$  in the modified model (long-dashed and solid lines respectively);  $\xi F_2^{D(3)}(\xi, \beta, Q^2)$  in the model without modifications (short-dashed line); figure from [59].

Note that the above approach allows, in principle, for the inclusion of explicit  $q\bar{q}g$  contributions of the photon wave function as well as for the all orders resummation of  $\ln Q^2$  terms, in a way similar to [62]. It would be very interesting to see the results of such an extended analysis.

The analysis of Bertini et al. [33] is devoted to the influence of higher twist terms on the  $Q^2$  dependence of diffractive DIS. It is found that, similar to what is known about the longitudinal  $q\bar{q}$  contribution, the higher twist terms in the transverse cross section are short distance dominated and are therefore perturbatively calculable. These contributions affect the  $Q^2$  dependence at  $\beta \rightarrow 1$  and should be subtracted from the cross section before a conventional DGLAP analysis of the large  $\beta$  region is performed.

The data analyses of [165,166] are based on the dipole picture of the BFKL pomeron discussed briefly in Sect. 5.4. The diffractive structure function is described as a sum of two components: the elastic component, where the  $q\bar{q}$  fluctuation of the virtual photon scatters off the proton [140], and the inelastic component, where, based on the original  $q\bar{q}$  fluctuation, a multi-gluon state develops, giving rise to high-mass diffraction [37]. While the first contribution is modelled by BFKL pomeron exchange in the  $t$  channel, the second one involves the triple-pomeron coupling and a cut gluon ladder representing the final state.

In Ref. [165], a combined analysis of both inclusive and diffractive structure functions was performed. The inclusive structure function was fitted on the basis of a colour dipole BFKL calculation, which, however, contains a number of free parameters and a smaller pomeron intercept than naïve perturbation theory would suggest. Introducing further parameters for the normalization of the elastic and inelastic components discussed above, qualitative agreement with both the diffractive and inclusive DIS data was achieved.

A further phenomenological investigation of diffraction on the basis of colour dipole BFKL was performed in [166], where a good 7 parameter fit to the diffractive structure function was presented. It is certainly a challenging problem to gain a better understanding of the dynamics, thus reducing the number of required parameters. In particular, the applicability of perturbative methods needs further investigation.

Very recently, an analysis of diffraction has appeared [147] that is based on the previous inclusive DIS fit with a Glauber type model for the dipole cross section  $\sigma(\rho)$  [146]. Motivated by the idea of saturation (compare the discussion in [167]), an energy or  $x$  dependence of  $\sigma(\rho)$  is introduced according to the formula

$$\sigma(x, \rho) = \sigma_0 \left\{ 1 - \exp \left( -\frac{\rho^2}{4R_0^2(x)} \right) \right\}, \quad (7.7)$$

where the function  $R_0(x)$  vanishes as  $x \rightarrow 0$ . The authors find a similar energy dependence of the diffractive and inclusive cross section. Two new parameters required for the analysis of diffraction are the diffractive slope and the fixed coupling constant  $\alpha_s$ . The very successful description of  $F_2^D$  is based on the  $q\bar{q}$  and  $q\bar{q}g$  fluctuations of the virtual photon. It includes higher twist terms but no Altarelli-Parisi evolution.

In the different approaches discussed above, separate predictions for transverse and longitudinal photon cross sections can be derived. Corresponding measurements, which are, however, very difficult, would be immensely important in gaining a better understanding of the underlying colour singlet exchange. An interesting possibility of obtaining the required polarization information is the measurement and analysis of the distribution in the azimuthal angle, which, at non-zero  $t$ , characterizes the relative position of the leptonic and hadronic plane of a diffractive event [168].

## 7.2 Final states

A further tool for studying the mechanism of diffraction is provided by the details of the hadronic final states. In this section, the focus is on events with a diffractive mass of the order of  $Q^2$  or larger. Diffractive production of single particles forms the subject of the next section.

The first topic is the production of jets with high transverse momentum relative to the  $\gamma^*p$  collision axis within the diffractively produced final state. Such diffractive dijet events were reported soon after the beginning of the investigation of diffraction at HERA [169]. Given the kinematic constraints and the available number of events, a direct analysis of jet cross sections in diffractive DIS proved difficult. Therefore, event shape observables such as thrust were first considered by both collaborations [170]. One of the main results was the alignment of the diffractive state along the  $\gamma^*p$  axis and, furthermore, the presence of significant transverse momentum components. If this is to be interpreted in terms of diffractive parton distributions, a large gluonic component seems to be required.

A direct analysis of diffractive dijet events has recently been reported by the H1 collaboration [171]. In the following, this analysis is discussed in more detail since, for

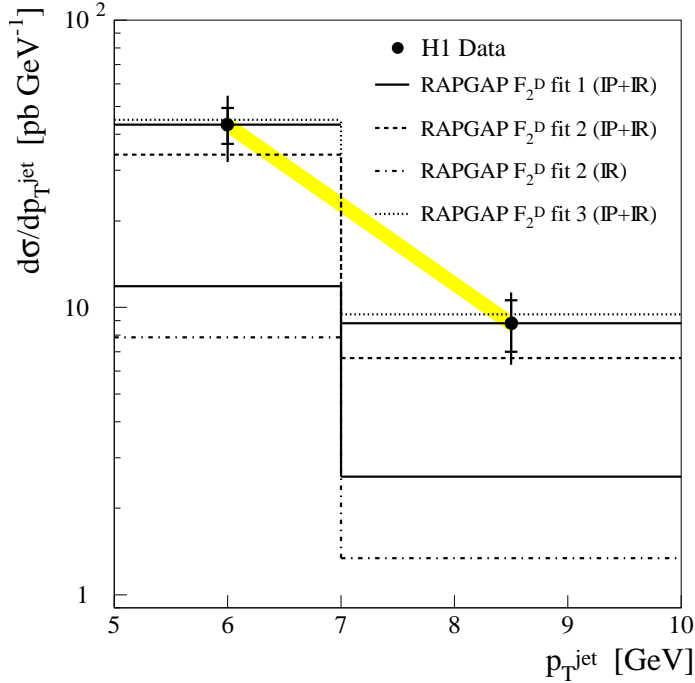


**Figure 7.7:** Differential cross section in transverse jet momentum for events where the diffractively produced hadronic state contains two jets. Photon virtualities vary in the range  $7.5 < Q^2 < 80 \text{ GeV}^2$ . The data are compared to predictions of RAPGAP Monte Carlo models with leading order pomeron and reggeon parton distributions: quarks only (fit 1), ‘flat’ gluon dominated (fit 2) and ‘peaked’ gluon dominated (fit 3). The figure is from [171], where further details can be found.

such measurements, a qualitative comparison with different theoretical models is simpler and less affected by hadronization effects. As an illustration, one of the distributions published in [171] is reproduced in Fig. 7.7.

As explained in Sect. 5.3, jets in the diffractive final state can be the result of either boson-gluon fusion, with the gluon coming from the diffractive gluon distribution of the proton, or of so-called exclusive dijet production, where the jets are associated with the pure  $q\bar{q}$  component of the photon wave function. The former case, viewed in the target rest frame, is associated with the  $q\bar{q}g$  component of the photon wave function, where the gluon has small  $p_\perp$  and the colour singlet exchange in the  $t$  channel is soft.

In Fig. 7.7, the data points are compared to predictions based on the boson-gluon fusion scenario. They are well described if the diffractive parton distributions are dominated by the gluon, a situation realized, e.g., in the semiclassical calculation based on the colour field model of Sect. 6.2. It would certainly be interesting to substitute the diffractive parton distributions underlying the Monte Carlo results of Fig. 7.7 (see, e.g., [172] for a recent review of Monte Carlo generators used for HERA diffraction) with the model distributions of Chapter 6. However, given the precision of the data, which is at present

consistent with the two very different gluon distributions of fit 2 and fit 3, it appears unlikely that any gluon dominated model can be ruled out.

The most important qualitative conclusion to be drawn is that the data favours boson-gluon fusion rather than exclusive dijet production. As discussed in Sect. 5.3, the exclusive process has a much steeper  $p_{\perp}$  distribution, which would be reflected in the quality of the fit in Fig. 7.7. This conclusion is made even clearer by the distribution of the variable  $z_{\mathcal{P}}^{\text{jets}}$ , which characterizes the fraction of the proton's momentum loss absorbed by the jets. In exclusive jet production,  $z_{\mathcal{P}}^{\text{jets}} = 1$ , which, even taking into account the smearing caused by hadronization, is in sharp contrast to the data. Thus, the observations suggest that only a small fraction of the observed dijet events are related to exclusive jet production with hard colour singlet exchange. It would be important to try to quantify this statement.

A further interesting aspect of the diffractive final state is the presence of open charm. So far, no published results by either the H1 or ZEUS collaboration are available on this subject. However, preliminary data have recently been presented by both collaborations [173, 174]. Cross section measurements for the production of  $D^{*\pm}$  mesons in diffractive events are reported. It is found in [174] that both  $W^2$  and  $Q^2$  dependences of diffractively produced open charm as well as the fraction of charmed events are consistent with the observations made in inclusive DIS. This is in agreement with the semiclassical scenario of [47] or, equivalently, with a boson-gluon fusion scenario based on gluon dominated diffractive parton distributions.

It should finally be mentioned that a number of more inclusive diffractive final state analyses focussing, in particular, on charged particle distributions [175], transverse energy flow [176] and the multiplicity structure [177] were reported by both collaborations. Although a detailed discussion of the obtained results can not be given here, it is important to note that all observations seem to be consistent with the physical picture of a partonic pomeron. Clearly, this is also in accord with the more general concept of diffractive parton distributions. As expected, particle distributions and energy flow support the by now well-established picture of colour singlet exchange with the target. In agreement with the jet oriented analyses, a significant gluonic component is required by the data. It was emphasized by H1 (see [175, 177]) that a relatively hard diffractive gluon distribution is favoured.

As already mentioned in the Introduction, an approach describing diffractive DIS by the assumption of soft colour interactions in the final state was proposed by Edin, Ingelman and Rathsman in [40]. The idea of soft colour exchange is similar to the naïve boson-gluon fusion model of [39], but the Monte-Carlo based implementation is quite different. After the hard scattering, the physical state is given by a number of quarks and gluons – those created in the scattering process and those from the proton remnant. It is assumed that, at this point, colour exchange can take place between each pair of colour charges, the probability of which is described by a certain phenomenological parameter  $R$ . This changes the colour topology and leads, in certain cases, to colour singlet subsystems, giving rise to rapidity gaps in the final state. The number of gap events initially increases with  $R$ , but saturates or even decreases at larger values of this parameter since further colour exchanges can destroy neutral clusters previously created.



A more detailed description of the soft colour interaction model can be found in [178], where the consistency of the approach with the large transverse energy flow in the proton hemisphere, a feature of HERA data that appears to be ‘orthogonal’ to the rapidity gaps, is demonstrated. In a more recent development [179], the colour exchange is described on the level of colour strings rather than on the partonic level discussed above. Furthermore,  $e^+e^-$  data is included in the analysis. In conclusion it can be said that an impressive agreement with many features of hadronic final states in small- $x$  DIS has been achieved within the framework of soft colour interactions. It is an interesting question in how far the perturbatively known suppression of interactions with small colour-singlet objects, i.e., colour transparency, is consistent with this approach.

### 7.3 Meson production

Exclusive meson production in DIS is, both theoretically and experimentally, a very interesting and active area that certainly deserves more space than is devoted to it in the present review. The main theme of the previous chapters was the semiclassical approach, the applicability of which to meson production processes is limited by the lack of a genuine prediction for the energy dependence of the amplitude. Although, as discussed in Sect. 5.1, Ryskin’s double-leading-log result is reproduced, two essential problems in going beyond it, the dynamics of the energy growth and details of the meson wave function, have not been addressed. Nevertheless, this review would be incomplete without at least a brief discussion of the most important new experimental results and their implications for theory.

Recent analyses of exclusive vector meson electroproduction have been published by ZEUS for  $\rho$  and  $J/\psi$  mesons [180] and by H1 for  $\rho$  mesons [181]. New preliminary results on exclusive  $J/\psi$  production were also reported by H1 [182], with previous measurements published in [183]. Agreement is observed between the most recent results of the two experiments [181].

For illustration, the ZEUS results for a particularly interesting quantity, the forward longitudinal  $\rho$  meson cross section, are shown in Fig. 7.8. As discussed in Sects. 5.1 and 5.2, this quantity can, at least in principle, be calculated in perturbation theory. If the asymptotic form of the meson wave function  $\phi_\rho(z) \sim z(1-z)$  is used, the amplitude of Eq. (5.13) gives rise to the cross section formula [16, 107]

$$\left. \frac{d\sigma}{dt} \right|_{t=0} = \frac{12\pi^3 \Gamma_{ee}^\rho m_\rho \alpha_s^2(Q^2) [xg(x, Q^2)]^2}{\alpha_{\text{em}} Q^6}. \quad (7.8)$$

The main qualitative predictions of this formula are in good agreement with experimental results. Taking into account the anomalous dimension of the gluon distribution, the observed  $Q^2$  dependence of roughly  $Q^{-5}$  is consistent with Eq. (7.8). The data indicate that the energy dependence becomes more pronounced with growing  $Q^2$ , as expected from the square of the gluon distribution. However, taking the above formula at face value and using, e.g., the MRS(A’) gluon distribution [184], the absolute normalization of the cross section comes out too high.

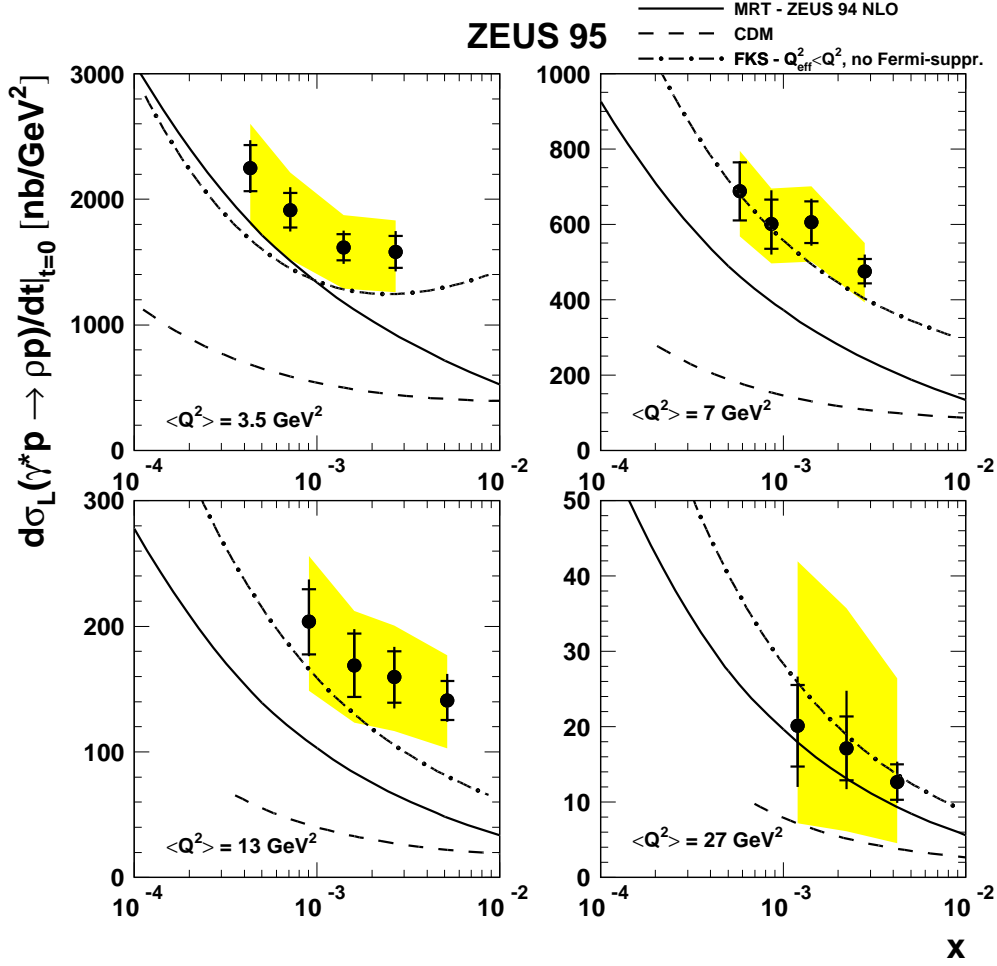


**Figure 7.8:** Forward longitudinal  $\rho$  electroproduction cross section  $d\sigma/dt|_{t=0}$  as measured by the ZEUS collaboration [180]. Shaded areas indicate normalization uncertainties in addition to the error bars shown. The curves are based on calculations by Martin, Ryskin and Teubner [126] (solid line), by Frankfurt, Koepf and Strikman [116] (dashed-dotted line) and on colour dipole model calculations of Nemchik et al. [117] (dashed line). The figure is from [180], where further details can be found.

Several improvements on the result of [16] were discussed in [116]. In particular, it was found that the Fermi motion of the quarks in the vector meson leads to a suppression factor in the cross section. Furthermore, in comparing the recent ZEUS data with the perturbative calculation, the gluon distribution is evaluated at a scale  $Q_{\text{eff}}^2 < Q^2$ . The new scale is determined from the average transverse size of the  $q\bar{q}$  pair, which turns out to be larger in the  $\rho$  production process than, say, in longitudinal electroproduction. Such a rescaling is certainly legitimate in view of the leading logarithmic nature of the approach. It leads to a further reduction of the cross section. While both suppression effects together produce results that are too small, either one of them gives a reasonable fit (see Fig. 7.8 and [180]). Note also the claim [185] that, at least in the  $J/\psi$  case, Fermi motion effects might be considerably smaller than expected.

The approach of [126], briefly mentioned in Sect. 5.1, also gives a reasonable fit to the  $\rho$  production data. Both the results of FKS [116] and MRT [126] shown in Fig. 7.8 are based on the ZEUS 94 NLO gluon distribution, which, in the relevant parameter region, is not too different from, e.g., MRS(A') [184]. Note that all calculations which derive their total normalization from the identification of the two gluon exchange amplitude with the gluon distribution are affected by the large experimental uncertainties of the latter.

The results of [117], also displayed in Fig. 7.8, are based on calculations that emphasize the non-perturbative aspects of the process. The interaction of the  $q\bar{q}$  pair with the target is described in terms of the colour dipole cross section  $\sigma(\rho, \nu)$ , where  $\nu$  is the photon energy. The amplitude for the production of a  $q\bar{q}$  pair of transverse size  $\rho$  is convoluted with a meson wave function with non-trivial  $\rho$  dependence. In the relevant region, where  $Q^2$  is not yet very large, these non-perturbative effects and the contributions from  $\sigma(\rho, \nu)$  at relatively large  $\rho$  are important. It is proposed that the energy and  $Q^2$  dependence of the measured cross section will allow for the ‘scanning’ of the dipole cross section  $\sigma(\rho, \nu)$  as a function of  $\rho$  (cf. [186]) and provide evidence for BFKL dynamics.

The violation of  $s$  channel helicity conservation is found to be small. However, evidence for a helicity flip amplitude on the level of  $8 \pm 3\%$  of the non-flip amplitude was reported in [181]. A particularly interesting feature of the data is the relatively small ratio  $R = \sigma_L/\sigma_T$  of longitudinal and transverse cross sections, which reaches the value  $R \simeq 3$  at  $Q^2 \simeq 20 \text{ GeV}^2$  [181]. This is in sharp contrast to a naïve extrapolation of the perturbative result of Eq. (5.8), leading one to expect  $R \sim Q^2/m_\rho^2$ . Even though the transverse cross section is not perturbatively calculable in the case of light vector mesons, one would still expect a linear growth of  $R$  with  $Q^2$ , which is not favoured by the data [180, 181].

In the stochastic vacuum approach of [56–58], the supposition that, at presently accessible values of  $Q^2$ , the perturbative regime is not yet reached is taken even more seriously. The analysis is based on a fundamentally nonperturbative model of the interaction with the target hadron (cf. Sect. 6.3) and is thus ideally suited for studying the transition region to photoproduction, as well as the transverse cross section, where QCD factorization theorems fail. Clearly, the approach depends on the model for the  $\rho$  meson wave function, but certain observables, such as the ratio of longitudinal and transverse cross sections or elastic slopes, represent relatively robust predictions. In particular, the ratio of longitudinal and transverse  $\rho$  meson production cross sections is well described [57].

In its original form, the model of the stochastic vacuum predicts constant high-energy cross sections. This limits the applicability of the model in the HERA regime, where the energy growth of meson electroproduction cross sections can not be neglected. Recently, the model has been extended [58] by introducing a phenomenological energy dependence based on two different pomerons coupled to small and large dipoles, very much in the spirit of [187]. Furthermore, for small dipole configurations, a perturbative two gluon exchange contribution was added. This allowed for a good description of both photo- and electroproduction of vector mesons and of  $F_2(x, Q^2)$  in the HERA regime.

The presently available data can also be described in the generalized vector dominance approach of [188]. In contrast to the calculations discussed so far, this approach predicts both longitudinal and transverse vector meson production cross sections to fall like  $\sim 1/Q^4$  at asymptotically large virtualities.

Note also the recent perturbative model calculation of [118], which finds an asymptotic behaviour of  $R = \sigma_L/\sigma_T$  that is qualitatively different from the expected linear  $Q^2$  growth. The calculations of [118, 126, 188] reproduce the experimentally observed flat behaviour of  $R$  at high  $Q^2$ .

The most striking feature of the measured  $J/\psi$  production cross sections is the strong energy growth  $\sim (W^2)^{0.4}$ . Its approximate  $Q^2$  independence up to  $Q^2 \sim 13 \text{ GeV}^2$  suggests that, in the present data, the charm quark mass rather than the photon virtuality play the dominant role in making the colour singlet exchange hard. The flavour-symmetric ratio  $\sigma(J/\psi)/\sigma(\rho) = 8/9$  is not yet reached at  $Q^2 = 13 \text{ GeV}^2$ .

Fitting the  $t$  dependence of  $\rho$  and  $J/\psi$  electroproduction cross sections with the function  $e^{bt}$ , values of  $b \sim 8 \text{ GeV}^{-2}$  and  $b \sim 5 \text{ GeV}^{-2}$  respectively were obtained [180].

The exclusive electroproduction of excitations of both the  $\rho$  and the  $J/\psi$  meson have also received much theoretical interest. However, experimental data on this subject is only beginning to emerge [189].

## 8 Conclusions

In the above review, different methods employed in the treatment of diffractive electroproduction processes were put into context.

The semiclassical approach, which was chosen as the starting point of the discussion, is well suited to develop a basic understanding of the underlying physical effects. In this approach, non-diffractive and diffractive DIS are treated along parallel lines. Diffraction occurs if, after scattering off the target, the partonic fluctuation of the virtual photon emerges in a colour singlet state. Altarelli-Parisi evolution of both the diffractive and inclusive structure function is related to the presence of higher Fock states of the photon. These fluctuations have a small transverse size and do not affect the soft colour exchange with the target. The application of the semiclassical approach to experimental results is particularly simple if the approach is used to derive both diffractive and inclusive parton distributions at some small input scale. In this case, the analysis of all higher- $Q^2$  data proceeds with standard perturbative methods. Different models for the underlying colour fields can be compared to diffractive and inclusive structure function data in a very direct way.

If the scattering amplitude of the partonic fluctuation of the photon and the target grows with energy, then, in the semiclassical framework, this growth enters both the diffractive and inclusive input distributions in precisely the same way. Such an energy growth is expected to be generated by the process of averaging over all relevant colour field configurations. However, no explicit non-perturbative calculation exists so that, at present, the energy dependence remains one of the most challenging aspects of the method.

The idea of the pomeron structure function combines methods of Regge theory with the partonic description of hard scattering processes in QCD. In the treatment of diffractive electroproduction, both the semiclassical approach and the pomeron structure function are equivalent as far as the hard part of the process, i.e., the  $Q^2$  evolution, is concerned. In this respect, they represent different realizations of the more general and less predictive concept of diffractive parton distributions. However, as far as the colour singlet exchange mechanism is concerned, the pomeron structure function idea is very different in that it assumes the existence of a ‘pre-formed’ pomeron state, off which the virtual photon scatters. By contrast, in the semiclassical approach the diffractive character of an event is only determined after the photon fluctuation has passed the target. No pre-formed colour singlet object is required. From this point of view, the semiclassical description of diffraction shows similarity to the idea of probabilistic soft colour exchange added on top of standard Monte Carlo models. However, in contrast to this method, the semiclassical calculation keeps track of the relevant transverse distances in the parton

cascade, ascribing soft colour exchange only to large size configurations.

In an apparently quite different approach, the  $t$  channel colour singlet exchange, characteristic of diffractive processes, is realized by the exchange of two  $t$  channel gluons. This is justified for certain specific final states, like longitudinally polarized vector mesons or two-jet systems, where the colour singlet exchange is governed by a hard scale. From the semiclassical perspective, this effect manifests itself in the small transverse size of the photon fluctuation at the moment of passing the external colour field. Thus, only the small distance structure of the field is tested, which corresponds to the two gluon exchange amplitude discussed above.

The fundamental advantage of two gluon exchange calculations is the understanding of the energy dependence which, one may hope, can be achieved in this framework by the resummation of large logarithms. However, leading order resummation predicts a far too steep energy growth, and the recently obtained next-to-leading correction is very large, thus calling the whole method into question. It is also possible that the mechanism responsible for the energy dependence in soft processes is fundamentally different from the above perturbative ideas.

Nevertheless, leading logarithmic two gluon calculations were successful in relating certain diffractive cross sections to the conventional gluon distribution, the energy growth of which is measured. Going beyond leading logarithmic accuracy, the non-forward gluon distribution was introduced. This is a promising tool for the further study of diffractive processes with hard colour singlet exchange.

On the experimental side, much attention has been devoted to the diffractive structure function, which represents one of the most interesting new observables in small- $x$  DIS. Leading twist analyses, based on the concept of diffractive parton distributions, are successful in describing the bulk of the data. It has been demonstrated that a simple large hadron model for the target colour fields allows for the derivation of a consistent set of diffractive and inclusive parton distributions in the semiclassical framework. Other colour field models, such as a perturbative dipole field and the model of the stochastic vacuum, promise a successful data analysis as well. It can be hoped that future work with the data will expose the qualitative differences among the available models, thus advancing our understanding of the proton bound state and non-perturbative QCD dynamics.

The available data shows the importance of higher twist contributions in the small-mass region of diffractive structure functions. A consistent theoretical description of both leading and higher twist effects has yet to be developed. Furthermore, the energy dependence of the diffractive structure function and, even more importantly, its relation to the energy dependence of the inclusive structure function are interesting unsolved problems. While the naïve summation of logarithms appears to be disfavoured, no new standard framework has emerged. The proposal of an identical, non-perturbative energy dependence of both diffractive and inclusive cross sections at some small virtuality  $Q_0^2$  is phenomenologically successful. This energy growth is reflected in the  $\xi$  dependence of the diffractive structure function, which is not altered by the perturbative  $Q^2$  evolution.

The detailed investigation of diffractive final states provides a further broad field where different approaches can be tested. Here, considerable improvements on present

data are expected in the near future. So far, the analyses performed emphasize the dominance of the soft colour exchange mechanism and the importance of the diffractive gluon distribution. Diffractive meson production is, on a qualitative level, well described by perturbative QCD wherever the dominance of the hard scale is established. However, large uncertainties remain, and non-perturbative contributions are important even at relatively high values of  $Q^2$ . In particular, the ratio of longitudinal and transverse  $\rho$  meson production cross sections is far smaller than suggested by simple perturbative estimates. A better understanding of the dynamics of meson formation appears to be required.

In summary, it is certainly fair to say that diffractive electroproduction at small  $x$  proved a very rich and interesting field. Its investigation over the recent years has led, in many different ways, to the improvement of our understanding of QCD dynamics on the interface of perturbative and non-perturbative physics. However, many important problems, such as the energy dependence and the systematic treatment of higher twist contributions, remain at present unsolved.

## Acknowledgements

I am deeply indebted to W. Buchmüller, who introduced me to the subject of diffraction at HERA, for our very interesting and fruitful collaboration and for his continuing support of my work over the recent years. I am also very grateful to S.J. Brodsky, T. Gehrmann, P.V. Landshoff, M.F. McDermott and H. Weigert, with whom I had the privilege to work on several of the topics described in this review and from whose knowledge I have greatly benefited. Furthermore, I would like to thank J. Bartels, M. Beneke, E.R. Berger, J.C. Collins, M. Diehl, J.R. Forshaw, L. Frankfurt, G. Ingelman, B. Kopeliovich, L. McLerran, A.H. Mueller, D.E. Soper, M. Strikman, T. Teubner, B.R. Webber and M. Wüsthoff for their many valuable comments and discussions. Finally, I am especially grateful to H.G. Dosch and O. Nachtmann for their encouragement, for numerous interesting discussions, and for their comments on the final version of the manuscript.

# Appendix

## A Derivation of Eikonal Formulae

A particularly simple way to derive the eikonal formulae of Sect. 3.1 is based on the direct summation of all Feynman diagrams of the type shown in Fig. 3.2 in the high-energy limit. In the case of scalar quarks, the one gluon exchange contribution to the  $S$ -matrix element reads

$$S_1(p', p) = -ig(p_\mu + p'_\mu) \int d^4x A^\mu(x) e^{ix(p'-p)}. \quad (\text{A.1})$$

Working in a covariant gauge and in the target rest frame, all components of  $A$  are expected to be of the same order of magnitude. If, in the high-energy limit,  $p_+$  and  $p'_+$  are the large momentum components, the approximation  $(p_\mu + p'_\mu)A^\mu \simeq (p_+ + p'_+)A_-/2$  can be made. Assuming that the  $x$  dependence of  $A$  is soft, one can write

$$\int dx_- e^{ix_-(p'_+-p_+)/2} A_-(x_+, x_-, x_\perp) \simeq 4\pi \delta(p'_+ - p_+) A_-(x_+, x_\perp), \quad (\text{A.2})$$

where the  $x_-$  dependence of  $A$  has been suppressed on the r.h. side since it is irrelevant for the process. More precisely, one has to think of the incoming and outgoing particles as wave packets, localized, say, at  $x_- \simeq 0$ , which is the  $x_-$  position where  $A$  has to be evaluated. Equation (A.1) takes the form

$$S_1(p', p) = 2\pi \delta(p'_+ - p_+) 2p_+ \int d^2x_\perp e^{-ix_\perp(p'_\perp - p_\perp)} \left( -\frac{ig}{2} \int dx_+ A_-(x_+, x_\perp) \right), \quad (\text{A.3})$$

which, within the approximation  $k_+ \delta(k_+) \simeq k_0 \delta(k_0)$ , is precisely the first term of the expansion of Eq. (3.3) in powers of  $A$ .

The  $n$  gluon exchange contribution to the  $S$ -matrix element can be written as

$$\begin{aligned} S_n(p', p) &= \prod_{i=2}^n \left\{ -\frac{ig}{2} \int d^4x^{(i)} \int \frac{d^4p^{(i-1)}}{(2\pi)^4} (p_+^{(i)} + p_+^{(i-1)}) A_-(x^{(i)}) \frac{i e^{ix^{(i)}(p^{(i)} - p^{(i-1)})}}{(p^{(i-1)})^2 + i\epsilon} \right\} \\ &\times \left\{ -\frac{ig}{2} \int d^4x^{(1)} (p_+^{(1)} + p_+^{(0)}) A_-(x^{(1)}) e^{ix^{(1)}(p^{(1)} - p^{(0)})} \right\}, \end{aligned} \quad (\text{A.4})$$

where  $x^{(i)}$  is the space-time variable at vertex  $i$ , the momentum of the quark line between vertex  $i$  and vertex  $i+1$  is denoted by  $p^{(i)}$ , and the initial and final momenta are  $p = p^{(0)}$  and  $p' = p^{(n)}$ . With Eq. (A.2), all  $p_+$  integrations in Eq. (A.4) become trivial, and all momentum plus components become identical with  $p_+^{(0)}$ . Integrations over the momentum minus components are performed using the identity

$$\int dp_- \frac{e^{-ip_-(y_+ - z_+)/2}}{p_+ p_- - p_\perp^2 + i\epsilon} = -\theta(y_+ - z_+) \frac{2\pi i}{p_+}. \quad (\text{A.5})$$



The resulting step functions translate into path ordering of the matrix valued fields  $A$  along the plus direction,

$$\int dx_+^{(1)} \dots dx_+^{(n)} \theta(x_+^{(2)} - x_+^{(1)}) \dots \theta(x_+^{(n)} - x_+^{(n-1)}) \{\dots\} = \frac{1}{n!} \int dx_+^{(1)} \dots dx_+^{(n)} P\{\dots\}. \quad (\text{A.6})$$

Now that all dependence on the intermediate transverse momenta  $p_\perp^{(1)} \dots p_\perp^{(n-1)}$  originating in the propagators has disappeared, the corresponding integrations are straightforward. They produce  $\delta$ -functions in transverse co-ordinate space,

$$\int d^2 p_\perp e^{ip_\perp(y_\perp - z_\perp)} = (2\pi)^2 \delta^2(y_\perp - z_\perp). \quad (\text{A.7})$$

Making use of Eqs. (A.5) – (A.7), the expression for the  $n$ th order contribution to the  $S$ -matrix element finally takes the form

$$S_n(p', p) = 2\pi \delta(p'_+ - p_+) 2p_+ \left\{ \int d^2 x_\perp e^{-ix_\perp(p'_\perp - p_\perp)} \right\} \frac{1}{n!} P \left( -\frac{ig}{2} \int dx_+ A_-(x_+, x_\perp) \right)^n. \quad (\text{A.8})$$

Since this is precisely the  $n$ th term of the expansion of Eq. (3.3) in powers of  $A$ , the derivation of the eikonal formula in the scalar case is now complete.

To obtain the eikonal formula for spinor quarks, Eq. (3.5), write down the analogue of Eq. (A.4) using the appropriate expressions for quark propagator and quark-quark-gluon vertex. Applying the identity of Eq. (3.11) to each of the quark propagators, neglecting the  $\gamma_+$  term, which is suppressed in the high-energy limit, and making use of the relation

$$\bar{u}_{s'}(k')(-ig\not{A})u_s(k) \simeq -igk_+ A_- \delta_{ss'}, \quad (\text{A.9})$$

valid if  $k_+ \simeq k'_+$  are the big components, the exact structure of Eq. (A.4) is recovered. The only difference is an additional overall factor  $\delta_{ss'}$ , corresponding to the conservation of the quark helicity. The further calculation, leading to the analogue of Eq. (A.8), is unchanged, and the eikonal formula follows.

The further generalization to the gluon case, Eq. (3.6), proceeds along the same lines. Begin by writing down the analogue of Eq. (A.4), i.e., the  $S$ -matrix element for Fig. 3.2 with a gluon line instead of the quark line. The expression contains conventional three-gluon vertices and gluon propagators in Feynman gauge. Contributions with four-gluon vertices are suppressed in the high-energy limit. The colour structure is best treated by introducing matrices

$$A_{\mathcal{A}} = A^a (T_{\mathcal{A}}^a)^{bc} = -iA^a f^{abc}, \quad (\text{A.10})$$

where  $f^{abc}$  are the usual structure constants appearing in the three-gluon vertex. Now, the product of matrices  $A$  in Eq. (A.4) is, in the gluonic case, simply replaced by an identical product of adjoint representation matrices  $A_{\mathcal{A}}$ .

Next, the  $g^{\mu\nu}$  tensor of each gluon propagator  $-ig^{\mu\nu}/k^2$  is decomposed according to the identity

$$g^{\mu\nu} = \left( \sum_{i=1}^2 e_{(i)}^\mu e_{(i)}^\nu + \frac{m^\mu k^\nu}{(mk)} + \frac{k^\mu m^\nu}{(mk)} - \frac{m^\mu m^\nu}{(mk)^2} k^2 \right), \quad (\text{A.11})$$

where  $m$  is a light-like vector with a non-zero minus component,  $m = (0, 2, 0_\perp)$ , and the polarization vectors are defined by  $ek = em = 0$  and  $e^2 = -1$ . An explicit choice is given by

$$e_{(i)} = \left( 0, \frac{2(k_\perp \epsilon_{(i)\perp})}{k_+}, \epsilon_{(i)\perp} \right), \quad (\text{A.12})$$

where the transverse basis  $\epsilon_{(1)\perp} = (1, 0)$  and  $\epsilon_{(2)\perp} = (0, 1)$  has been used. If, in the high-energy limit,  $g^{\mu\nu}$  appears between two three-gluon vertices, the last three terms of Eq. (A.11) can be neglected. Note that, for the second and third term, this is a non-trivial statement since the vector  $k$  in the numerator could, in principle, compensate for the suppression by the  $k_+$  in the denominator. However, this is prevented by the gauge invariance of the three gluon vertex.

Thus, the analogue of Eq. (A.4) is written down with three-gluon vertices and propagators proportional to

$$g^{\mu\nu} \simeq \sum_{i=1}^2 e_{(i)}^\mu e_{(i)}^\nu. \quad (\text{A.13})$$

Now, each of the three-gluon vertices  $V_{\mu\nu\sigma}(-k', k, k'-k)$  (where all momenta are incoming and colour indices are suppressed) appears between two transverse polarization vectors and simplifies according to

$$e_{(i')}^\mu(k') V_{\mu\nu\sigma}(-k', k, k'-k) A_{\mathcal{A}}^\sigma e_{(i)}^\nu(k) \simeq -igk_+ A_{\mathcal{A}} \delta_{ii'}, \quad (\text{A.14})$$

where  $A_{\mathcal{A}}$  is the external field. This is similar to what was found in the quark case in Eq. (A.9), with the difference that helicity conservation is replaced by polarization conservation. Therefore, as before, the structure of Eq. (A.4) is recovered, but with the external field in the adjoint representation and with an additional polarization conserving  $\delta$ -function. The further calculation, leading to the analogue of Eq. (A.8), is unchanged, and the eikonal formula in the gluonic case follows.

# B Spinor Matrix Elements

In this appendix, the spinor matrix elements of the type  $\bar{u}_{s'}(k')\not{\epsilon}(q)u_s(k)$ , required, e.g., for the calculation the transition from virtual photon to  $q\bar{q}$  pair, are listed.

Using light-cone components for vectors,  $a = (a_+, a_-, a_\perp)$ , and orienting the photon momentum along the positive  $z$ -axis,  $q = (q_+, -Q^2/q_+, 0_\perp)$ , the longitudinal and transverse polarization vectors can be defined as

$$\epsilon_L = (q_+/Q, Q/q_+, 0_\perp) \quad , \quad \epsilon_{\pm 1} = (0, 0, \epsilon_\perp(\pm)) \quad , \quad (\text{B.1})$$

where  $\epsilon_\perp(\pm) = (1, \pm i)/\sqrt{2}$ .

The Dirac representation of  $\gamma$  matrices and the conventions of [75] for Dirac spinors are used. Introducing the matrix

$$\varepsilon = \begin{pmatrix} 0 & 1 \\ -1 & 0 \end{pmatrix} \quad . \quad (\text{B.2})$$

and the two-component spinors

$$\chi_{\frac{1}{2}} = \begin{pmatrix} 1 \\ 0 \end{pmatrix} \quad , \quad \chi_{-\frac{1}{2}} = \begin{pmatrix} 0 \\ 1 \end{pmatrix} \quad , \quad (\text{B.3})$$

the two independent Dirac spinors, with  $s = \pm 1/2$ , for negative and positive frequency solutions can be explicitly written as

$$u_s(k) = \sqrt{k_0 + m} \begin{pmatrix} \chi_s \\ \frac{\vec{\sigma}\vec{k}}{k_0 + m}\chi_s \end{pmatrix} \quad , \quad v_s(k) = -\sqrt{k_0 + m} \begin{pmatrix} \frac{\vec{\sigma}\vec{k}}{k_0 + m}\varepsilon\chi_s \\ \varepsilon\chi_s \end{pmatrix} \quad , \quad (\text{B.4})$$

where  $\vec{\sigma}$  is the vector formed by the three Pauli matrices.

The result for longitudinal photon polarization can be obtained from the relation

$$\bar{u}_{s'}(k')\gamma_0 u_s(k) = \delta_{s's} 2\sqrt{k_0 k'_0} \quad , \quad (\text{B.5})$$

which holds at leading order in the high-energy expansion. From this, the matrix element  $\bar{u}_{s'}(k')\not{\epsilon}_L(q)u_s(k)$  is obtained using the gauge invariance of the  $q\bar{q}$ -photon vertex,  $\bar{u}_{s'}(k')\not{q}u_s(k) = 0$ . Since the quark mass and transverse momentum do not enter the leading order relation, Eq. (B.5), they may be neglected so that the relation  $v_s(k) = -u_{-s}(k)$  holds. Thus, the complete result takes the form

$$\bar{u}_{s'}(k')\epsilon_L u_s(k) = \bar{v}_{s'}(k')\epsilon_L v_s(k) = -\bar{v}_{-s'}(k')\epsilon_L u_s(k) = -\bar{u}_{-s'}(k')\epsilon_L u_s(k) = \delta_{s's} 2Q\sqrt{\alpha(1-\alpha)} \quad ,$$

(B.6)

where  $\alpha = k_0/q_0$  and  $\epsilon_L = \epsilon_L(q)$ .

Neglecting terms suppressed in the high-energy limit, the relevant matrix elements for transverse photon polarization read

$$\bar{u}_{s'}(k') \not{\epsilon}_{+1/-1}(q) u_s(k) = -\sqrt{\frac{2}{k_0 k'_0}} \left( \begin{array}{cc|cc} k_{\perp+} k'_0 & / & k'_{\perp-} k_0 & | & m(k'_0 - k_0) & / & 0 \\ 0 & / & m(k_0 - k'_0) & | & k'_{\perp+} k_0 & / & k_{\perp-} k'_0 \end{array} \right)_{s's} \quad (\text{B.7})$$

$$\bar{v}_{s'}(k') \not{\epsilon}_{+1/-1}(q) v_s(k) = -\sqrt{\frac{2}{k_0 k'_0}} \left( \begin{array}{cc|cc} k'_{\perp+} k_0 & / & k_{\perp-} k'_0 & | & 0 & / & m(k'_0 - k_0) \\ m(k_0 - k'_0) & / & 0 & | & k_{\perp+} k'_0 & / & k'_{\perp-} k_0 \end{array} \right)_{s's} \quad (\text{B.8})$$

$$\bar{u}_{s'}(k') \not{\epsilon}_{+1/-1}(q) v_s(k) = +\sqrt{\frac{2}{k_0 k'_0}} \left( \begin{array}{cc|cc} -m(k_0 + k'_0) & / & 0 & | & k_{\perp+} k'_0 & / & k'_{\perp-} k_0 \\ k'_{\perp+} k_0 & / & k_{\perp-} k'_0 & | & 0 & / & m(k'_0 + k_0) \end{array} \right)_{s's} \quad (\text{B.9})$$

$$\bar{v}_{s'}(k') \not{\epsilon}_{+1/-1}(q) u_s(k) = +\sqrt{\frac{2}{k_0 k'_0}} \left( \begin{array}{cc|cc} 0 & / & -m(k_0 + k'_0) & | & k'_{\perp+} k_0 & / & k_{\perp-} k'_0 \\ k_{\perp+} k'_0 & / & k'_{\perp-} k_0 & | & m(k'_0 + k_0) & / & 0 \end{array} \right)_{s's} \quad (\text{B.10})$$

Here the notation  $k_{\perp\pm} = k_1 \pm ik_2$  is used, and the four entries (11), (12), (21) and (22) of the two-by-two matrices on the r.h. sides of the above equations correspond to the combinations  $(s's) = (+\frac{1}{2} + \frac{1}{2})$ ,  $(+\frac{1}{2} - \frac{1}{2})$ ,  $(-\frac{1}{2} + \frac{1}{2})$  and  $(-\frac{1}{2} - \frac{1}{2})$ . For each of these four entries, the expression before and after the oblique stroke ‘/’ corresponds to positive and negative photon polarization respectively. For example,

$$\bar{u}_{+\frac{1}{2}}(k') \not{\epsilon}_{+1}(q) u_{-\frac{1}{2}}(k) = -\sqrt{\frac{2}{k_0 k'_0}} m(k'_0 - k_0). \quad (\text{B.11})$$

The calculation of the transition from virtual photon to  $q\bar{q}$ -gluon configuration requires, in addition to the  $q\bar{q}$ -photon vertex, the knowledge of the  $q\bar{q}$ -gluon vertex (see Sect. 3.3). The corresponding spinor matrix elements are easily obtained from Eqs. (B.7)–(B.10) if the configuration is rotated in such a way that the gluon momentum is parallel to the  $z$ -axis. In the high-energy limit, such a rotation corresponds to the substitutions

$$k_{\perp} \rightarrow k_{\perp} - q_{\perp}(k_+/q_+) \quad , \quad k'_{\perp} \rightarrow k'_{\perp} - q_{\perp}(k'_+/q_+), \quad (\text{B.12})$$

where  $q$  is now interpreted as the gluon momentum.

Note that similar matrix elements are commonly used in light-cone perturbation theory (see, e.g., Tables II and III of [190]).

# C Derivation of Diffractive Quark and Gluon Distribution

The explicit formulae for diffractive quark and gluon distributions, Eqs. (4.53) and (4.54), can be derived by appropriately adapting the scalar calculation of Sect. 4.4 to the case of spinor or vector particles. The most economic procedure is to first identify the piece of the old squared amplitude  $|T|^2$  that depends explicitly on the spin of the soft parton. This piece, which is essentially just the squared scattering amplitude of the soft parton and the external field, is symbolically separated in Fig. C.1. The two independent integration variables for the intermediate momentum of the soft parton are denoted by  $k$  and  $\tilde{k}$  in the amplitude  $T$  and its complex conjugate  $T^*$  respectively. Note also that  $k_+ = \tilde{k}_+$  and  $k_- = \tilde{k}_-$  at leading order.

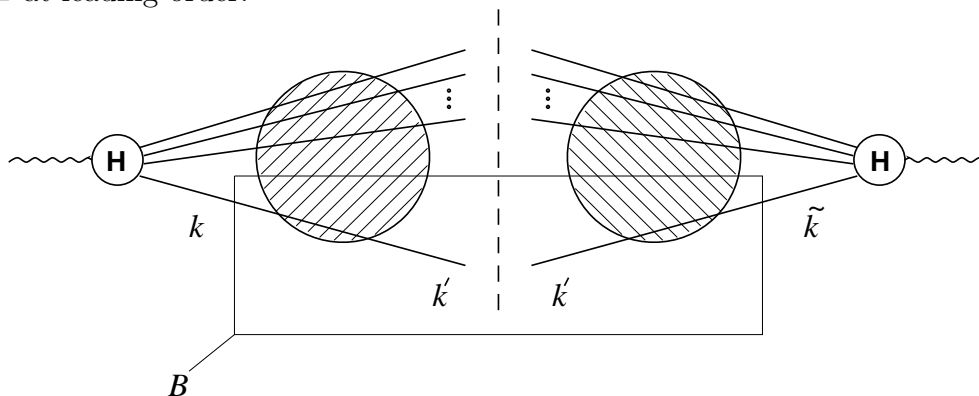


**Figure C.1:** Symbolic representation of the square of the amplitude for a hard diffractive process. The box separates the contributions associated with the soft parton and responsible for the differences between diffractive distributions for scalars, spinors and vector particles.

It is straightforward to write down the factor  $B_s$  that corresponds to the box in Fig. C.1 for the scalar case. Since the off-shell denominators  $k^2$  and  $\tilde{k}^2$  as well as the two eikonal factors and energy  $\delta$ -functions are present for all spins of the soft parton, they are not included into the definition of  $B$ . All that remains are the explicit factors  $2k_0 \simeq k_+$  from the effective vertex, Eq. (4.35). Therefore, the result for the scalar case reads simply

$$B_s = k_+^2. \quad (\text{C.1})$$

The next step is the calculation of the corresponding expressions  $B_q$  and  $B_g$ , given by the box in Fig. C.1, in the case where the produced soft parton is a quark or a gluon.

Introducing factors  $B_q/B_s$  and  $B_g/B_s$  into Eq. (4.52) will give the required diffractive parton distributions  $(df_q^D/d\xi)$  and  $(df_g^D/d\xi)$ .

### Diffractive quark distribution

Observe first, that the analogue of Eq. (4.35) for spinors is simply

$$V_q(p', p) = 2\pi\delta(p'_0 - p_0) \frac{\gamma_+}{2} \left[ \tilde{U}(p'_\perp - p_\perp) - (2\pi)^2 \delta^2(p'_\perp - p_\perp) \right]. \quad (\text{C.2})$$

The Dirac structure of  $V_q$  follows from the fact that, in the high-energy limit, only the light-cone component  $A_-$  of the gluon field contributes. The normalization is consistent with Eqs. (3.12) and (3.13).

Consider now the Dirac propagator with momentum  $k$ . The hard part  $T_H$  requires the interpretation of the quark line as an incoming parton, which collides head on with the photon. Therefore, it is convenient to switch to the Breit frame and to define a corresponding on-shell momentum  $l$ , given by  $l_- = -k_-$ ,  $l_\perp = -k_\perp$  and  $l_+ = l_\perp^2/l_-$ . The propagator can now be written as

$$\frac{1}{\not{k}} = -\frac{\sum_s u_s(l)\bar{u}_s(l)}{k^2} - \frac{\gamma_-}{2l_-}. \quad (\text{C.3})$$

This is technically similar to Sect. 3.2, where an on-shell momentum was defined by adjusting the minus component of  $k$ . In the present treatment, however, the plus component of  $l = -k$  is adjusted, so that a partonic interpretation in the Breit frame becomes possible. It has now to be shown that the second term on the r.h. side of Eq. (C.3) can be neglected, since it is suppressed in the Breit frame by the hard momentum  $l_- = yP_-$ . This can be intuitively understood by observing that this term represents a correction for the small off-shellness of the quark, which is neither important for  $T_H$ , nor for the soft high-energy scattering off the external field.

To see this more explicitly, write the relevant part of the amplitude in the form

$$\bar{u}(k')\gamma_+\frac{1}{\not{k}}T_H = -\bar{u}(k')\gamma_+\left(\frac{\sum_s u_s(l)\bar{u}_s(l)}{k^2} + \frac{\gamma_-}{2l_-}\right)T_H \equiv -(C_1 + C_2). \quad (\text{C.4})$$

It will now be shown that the  $\gamma_-$  term  $C_2$  is suppressed with respect to  $C_1$ .

The spinor matrix element in  $C_1$  can be estimated using the relation

$$\sum_s \bar{u}_s(p')\gamma_+u_s(p) = \frac{4(p'_\perp p_\perp)}{\sqrt{p'_-p_-}}, \quad (\text{C.5})$$

valid in the limit where the minus components of  $p$  and  $p'$  become large (cf. Table II of [190]). In the soft region,  $k^2 \sim k_\perp^2 \sim k'_\perp^2 \sim \Lambda^2$ , and  $-k_- \sim k'_- \sim Q$  are the large components in the Breit frame. Thus,  $[\bar{u}(k')\gamma_+u(l)] \sim \Lambda^2/Q$ , and the first term on the r.h. side of Eq. (C.4) is estimated to be

$$C_1 \sim \frac{1}{Q} [\bar{u}(l)T_H], \quad (\text{C.6})$$

where factors  $\mathcal{O}(1)$  have been suppressed.

Introducing a vector  $a = (1, 0, 0_\perp)$ , so that  $\gamma_-/2 = \not{a}$ , the  $\gamma_-$  term can be written as

$$C_2 = \sum_s [\bar{u}(k')\gamma_+u_s(a)] \frac{1}{l_-} [\bar{u}_s(a)T_H]. \quad (\text{C.7})$$

Since  $[\bar{u}(k')\gamma_+u(a)]$  vanishes for  $k'_+ = k'^2_\perp/k'_- \rightarrow 0$ , in the Breit frame, where  $k'_-$  is large, the estimate  $[\bar{u}(k')\gamma_+u(a)] \sim |k'_\perp|/\sqrt{k'_-} \sim \Lambda/\sqrt{Q}$  can be made. With  $l_- \sim Q$ , one obtains

$$\frac{C_2}{C_1} \sim \frac{\Lambda}{\sqrt{Q}} \frac{[\bar{u}(a)T_H]}{[\bar{u}(l)T_H]} \sim \frac{\Lambda}{Q}, \quad (\text{C.8})$$

where it has been assumed that no specific cancellation makes  $\bar{u}(l)T_H$  small, i.e.,  $[\bar{u}(l)T_H]/[\bar{u}(a)T_H] \sim \sqrt{Q}$ . Equation (C.8) establishes the required suppression of the  $\gamma_-$  term in Eq. (C.3).

To proceed with the evaluation of  $B_s$  note that, when the soft part is separated in Fig. C.1, the spinor  $\bar{u}_s(l) \simeq \bar{v}_{-s}(l)$  from Eq. (C.3) has to be considered a part of the hard amplitude  $T_H$ . Therefore the analogue of Eq. (C.1) reads

$$B_s = \sum_{s,s'} \bar{u}_{s'}(k') \frac{\gamma_+}{2} u_s(l) \bar{u}_s(\tilde{l}) \frac{\gamma_+}{2} u_{s'}(k'), \quad (\text{C.9})$$

where  $\tilde{l}$  is defined analogously to  $l$ , but using the momentum  $\tilde{k}$  instead of  $k$ . The spin summation decouples from the hard part if the measurement is sufficiently inclusive.

The above expression can be evaluated further to give

$$B_s = \frac{1}{2} k_+ \sum_s \bar{u}_s(\tilde{l}) \gamma_+ u_s(l) = k_+ \frac{2(l_\perp \tilde{l}_\perp)}{\sqrt{l_- \tilde{l}_-}}, \quad (\text{C.10})$$

where the last equality again uses Eq. (C.5). Simple kinematics leads to the result

$$B_s = k_+^2 \frac{2(k_\perp \tilde{k}_\perp)}{k'^2_\perp} \left( \frac{\xi - y}{y} \right). \quad (\text{C.11})$$

Comparing this with Eq. (C.1), the diffractive quark distribution, Eq. (4.53), is straightforwardly obtained from the scalar case, Eq. (4.52).

Note that the virtual fermion line corresponds to a right-moving quark with momentum  $k$  in the proton rest frame and to a left-moving antiquark with momentum  $l$  in the Breit frame. Therefore, the above result has, in fact, to be interpreted as a diffractive antiquark distribution. The diffractive quark distribution is identical.

## Diffractive gluon distribution

To obtain the diffractive gluon distribution, the procedure of the last section has to be repeated for the case of an outgoing soft gluon with momentum  $k'$  in Fig. C.1. Calculating

the contribution separated by the box will give the required quantity  $B_g$ , in analogy to Eqs. (C.1) and (C.11).

It will prove convenient to introduce two light-like vectors  $m$  and  $n$ , such that the only non-zero component of  $m$  is  $m_- = 2$  in the proton rest frame, and the only non-zero component of  $n$  is  $n_+ = 2$  in the Breit frame. Since Breit frame and proton rest frame are connected by a boost along the  $z$ -axis with boost factor  $\gamma = Q/(m_p x)$ , the product of these vectors is  $(mn) = 2\gamma$ .

Furthermore, two sets of physical polarization vectors,  $e_{(i)}$  and  $\epsilon_{(i)}$  (with  $i = 1, 2$ ) are defined by the conditions  $ek = \epsilon k = 0$ ,  $e^2 = \epsilon^2 = -1$ , and  $em = \epsilon n = 0$ . An explicit choice, written in light-cone co-ordinates, is

$$e_{(i)} = \left( 0, \frac{2(k_\perp \epsilon_{(i)\perp})}{k_+}, \epsilon_{(i)\perp} \right) \quad \text{and} \quad \epsilon_{(i)} = \left( \frac{2(k_\perp \epsilon_{(i)\perp})}{k_-}, 0, \epsilon_{(i)\perp} \right), \quad (\text{C.12})$$

where the transverse basis  $\epsilon_{(1)\perp} = (1, 0)$  and  $\epsilon_{(2)\perp} = (0, 1)$  has been used. Note that the above equations hold in the proton rest frame, in the Breit frame, and in any other frame derived by a boost along the  $z$ -axis.

These definitions give rise to the two following representations for the metric tensor:

$$g^{\mu\nu} = \left( \sum_i e_{(i)}^\mu e_{(i)}^\nu + \frac{m^\mu k^\nu}{(mk)} + \frac{k^\mu m^\nu}{(mk)} - \frac{m^\mu m^\nu}{(mk)^2} k^2 \right) \quad (\text{C.13})$$

$$= \left( \sum_i \epsilon_{(i)}^\mu \epsilon_{(i)}^\nu + \frac{n^\mu k^\nu}{(nk)} + \frac{k^\mu n^\nu}{(nk)} - \frac{n^\mu n^\nu}{(nk)^2} k^2 \right). \quad (\text{C.14})$$

The amplitude for the process in Fig. C.1, with the lowest parton being a gluon in Feynman gauge, is proportional to

$$A = \epsilon^\mu(k') V_g(k', k)_{\mu\nu} T_H^\nu = \epsilon^\mu(k') V_g(k', k)_{\mu\nu} g^{\nu\rho} g_{\rho\sigma} T_H^\sigma, \quad (\text{C.15})$$

where  $V_g^{\mu\nu}$  is the effective vertex for the scattering of the gluon off the external field. Next, the first and second metric tensor appearing in this expression for  $A$  are rewritten according to Eq. (C.13) and Eq. (C.14) respectively. In this situation, only the first terms from Eqs. (C.13) and (C.14) contribute at leading order in  $x$  and  $\Lambda/Q$ . The intuitive reason for this is the relatively small virtuality of  $k$ , which ensures that for both the hard amplitude  $T_H$  and the soft scattering vertex  $V$  only the appropriately defined transverse polarizations are important.

To see this explicitly, consider the expression

$$A = \epsilon V_g \left[ \sum e e + \frac{m k}{(mk)} + \frac{k m}{(mk)} - \frac{m m}{(mk)^2} (k^2) \right] \left[ \sum \epsilon \epsilon + \frac{n k}{(nk)} + \frac{k n}{(nk)} - \frac{n n}{(nk)^2} (k^2) \right] T_H, \quad (\text{C.16})$$

where the appropriate contractions of vector indices are understood. Several estimates involving products of  $V_g$  and  $T_H$  with specific polarization vectors will be required.



Note that both  $\epsilon$  and  $n$  are  $\mathcal{O}(1)$  in the Breit frame. For appropriate polarization, the amplitude  $(\epsilon T_H)$  involves no particular cancellation, i.e., it has its leading (formal) power behaviour in the dominant scale  $Q$ . Therefore,  $(n T_H)$  is not enhanced with respect to  $(\epsilon T_H)$ ,

$$\frac{(n T_H)}{(\epsilon T_H)} \sim \mathcal{O}(1). \quad (\text{C.17})$$

By analogy, it can be argued that  $(\epsilon V_g m)$  is not enhanced with respect to  $(\epsilon V_g e)$ : since both  $e$  and  $m$  are  $\mathcal{O}(1)$  in the proton rest frame and  $(\epsilon V_g e)$  has the leading power behaviour for appropriate polarizations  $\epsilon$  and  $e$ , the following estimate holds,

$$\frac{(\epsilon V_g m)}{(\epsilon V_g e)} \sim \mathcal{O}(1). \quad (\text{C.18})$$

Gauge invariance requires  $(k T_H)$  to vanish if  $k^2 = 0$ . Since the amplitude  $T_H$  is dominated by hard momenta  $\mathcal{O}(Q)$ , and  $k^2 \sim \Lambda^2 \ll Q^2$ , this leads to the estimate

$$\frac{(k T_H)}{(\epsilon T_H)} \sim \frac{k^2}{Q}. \quad (\text{C.19})$$

Analogously, from  $(\epsilon V_g k) = 0$  at  $k^2 = 0$ , the suppression of this quantity at small virtualities  $k^2$  can be derived,

$$\frac{(\epsilon V_g k)}{(\epsilon V_g e)} \sim \frac{k^2}{k_+}. \quad (\text{C.20})$$

For this estimate it is also important that none of the soft scales involved in  $V_g$ , like  $k_\perp^2$  or the gauge field  $A_\mu$ , can appear in the denominator to compensate for the dimension of  $k^2$ .

All the vector products  $nk$ ,  $mk$ ,  $ne$ ,  $m\epsilon$ ,  $mn$ , and  $e\epsilon$  can be calculated explicitly. Using the relations in Eqs. (C.17) – (C.20), it is now straightforward to show that  $(\epsilon V_g e)(e\epsilon)(\epsilon T_H)$  is indeed the leading term in Eq. (C.16). The other terms are suppressed by powers of  $Q$  or  $k_+$ .

Thus, the leading contribution to  $|A|^2$ , with appropriate polarization summation understood, reads

$$|A|^2 = \sum_{i,j,i',j',l} \left[ (\epsilon_{(l)}(k') V_g e_{(i)}) (e_{(i)} \epsilon_{(j)}) (\epsilon_{(j)} T_H) \right] \left[ (\epsilon_{(l)}(k') V_g e_{(i')}) (e_{(i')} \epsilon_{(j')}) (\epsilon_{(j')} T_H) \right]^*, \quad (\text{C.21})$$

where the arguments  $k$  and  $\tilde{k}$  of the polarization vectors in the first and second square bracket respectively have been suppressed.

In the high-energy limit, the scattering of a transverse gluon off an external field is completely analogous to the scattering of a scalar or a spinor,

$$\epsilon_{l'}(p') V_g(p', p) \epsilon_l(p) = 2\pi \delta(p'_0 - p_0) 2p_0 \delta_{l'l} \tilde{U}^A(p'_\perp - p_\perp), \quad (\text{C.22})$$

the only difference being the non-Abelian eikonal factor, which is now in the adjoint representation.

In analogy to the spinor case, the polarization sum decouples from the hard part for sufficiently inclusive measurements, so that the squared amplitude is proportional to

$$|A|^2 = |T_H|^2 \left( \epsilon_{(l)}(k') V_g e_{(l)}(k) \right) \left( \epsilon_{(l)}(k') V_g e_{(l)}(\tilde{k}) \right)^* \sum_{i,j} \left( e_{(i)}(k) \epsilon_{(j)}(k) \right) \left( e_{(i)}(\tilde{k}) \epsilon_{(j)}(\tilde{k}) \right). \quad (\text{C.23})$$

Note that there is no summation over the index  $l$ . Recall the definition of  $B$ , the soft part of the amplitude square, given at the beginning of the last section and illustrated in Fig. C.1. The corresponding expression in the case of a soft gluon can now be read off from Eqs. (C.22) and (C.23):

$$B_g = k_+^2 \sum_{i,j} \left( e_{(i)}(k) \epsilon_{(j)}(k) \right) \left( e_{(i)}(\tilde{k}) \epsilon_{(j)}(\tilde{k}) \right). \quad (\text{C.24})$$

This is further evaluated using the explicit formulae in Eq. (C.12) and the identity

$$\sum_i \epsilon_{(i)\perp}^a \epsilon_{(i)\perp}^b = \delta^{ab} \quad (a, b \in \{1, 2\}). \quad (\text{C.25})$$

Comparing the resulting expression,

$$B_g = k_+^2 \left( \delta^{ij} + \frac{2k_\perp^i k_\perp^j}{k_\perp'^2} \left( \frac{1-\beta}{\beta} \right) \right) \left( \delta^{ij} + \frac{2\tilde{k}_\perp^i \tilde{k}_\perp^j}{k_\perp'^2} \left( \frac{1-\beta}{\beta} \right) \right), \quad (\text{C.26})$$

to Eq. (C.1), the diffractive gluon distribution of Eq. (4.54) is obtained.

Note that the factor  $N_c$  appearing in the denominator of Eq. (4.52) has been replaced by the dimension of the adjoint representation,  $N_c^2 - 1$ .

# D Inclusive Parton Distributions

This appendix is devoted to the calculation of inclusive parton distributions and inclusive structure functions in the semiclassical framework. Inclusive DIS was discussed in Sect. 3.2, where the cross section for  $q\bar{q}$  production off a colour field was derived, at the end of Sect. 4.4, where the parton model interpretation of this cross section was outlined, and in Sect. 7.1, where it was part of the semiclassical analysis of diffractive and inclusive structure function data. Here, the above scattered information is collected, and a more coherent account, including further technical details, is given (cf. [62]).

Recall the leading twist cross section  $\sigma_T$  for  $q\bar{q}$  pair production by a transversely polarized photon obtained in Sect. 3.2 (cf. Eq.(3.27)). The corresponding transverse structure function reads

$$F_T(x, Q^2) = \frac{4}{3(2\pi)^3} \left( \ln \frac{Q^2}{\mu^2} - 1 \right) \int_{x_\perp} \text{tr} \left( \partial_{y_\perp} W_{x_\perp}(0) \partial_{y_\perp} W_{x_\perp}^\dagger(0) \right) + \frac{2}{(2\pi)^7} \int_0^{\mu^2} dN^2 \int dk_\perp'^2 \int_{x_\perp} \left| \int d^2 k_\perp \frac{k_\perp \tilde{W}_{x_\perp}(k'_\perp - k_\perp)}{N^2 + k_\perp^2} \right|^2. \quad (\text{D.1})$$

To map this calculation onto the conventional parton model framework, identify the result as  $F_T(x, Q^2) = 2xq(x, Q^2)$ . The corresponding quark distribution reads

$$xq(x, Q^2) = \frac{2}{3(2\pi)^3} \left( \ln \frac{Q^2}{\mu^2} - 1 \right) \int_{x_\perp} \text{tr} \left( \partial_{y_\perp} W_{x_\perp}(0) \partial_{y_\perp} W_{x_\perp}^\dagger(0) \right) + \frac{2}{(2\pi)^4} \int_0^{\mu^2} N^2 dN^2 \int_{y_\perp} K_1(yN)^2 \int_{x_\perp} \text{tr} \left( W_{x_\perp}(y_\perp) W_{x_\perp}^\dagger(y_\perp) \right). \quad (\text{D.2})$$

Here the modified Bessel function  $K_1$  has been introduced so that, in both terms, the functions  $W$  appear in co-ordinate space. This makes it particularly clear that the first term is only sensitive to the short distance behaviour, while the second term depends on the non-perturbative long-distance structure of the colour field. Note that the sum of both terms is independent of  $\mu^2$ .

The corresponding gluon distribution at small  $x$  is most easily calculated as

$$xg(x, Q^2) = \frac{3\pi}{\alpha_s} \cdot \frac{\partial F_T(x, Q^2)}{\partial \ln Q^2} = \frac{1}{2\pi^2 \alpha_s} \int_{x_\perp} \text{tr} \left( \partial_{y_\perp} W_{x_\perp}(0) \partial_{y_\perp} W_{x_\perp}^\dagger(0) \right). \quad (\text{D.3})$$

Equations (D.2) and (D.3) can serve as the starting point for a conventional partonic analysis of inclusive DIS.

To gain more physical insight into the correspondence of the semiclassical and the parton model approach, return to the starting point, Eq. (D.1). It is instructive to view  $F_T$  as a sum of two terms:  $F_T^{\text{asym}}$ , the contribution of asymmetric configurations where quark or antiquark are slow,  $\alpha < \mu^2/Q^2$  or  $1 - \alpha < \mu^2/Q^2$  (Fig. 4.11a), and  $F_T^{\text{sym}}$ , the contribution of symmetric configurations where both quark and antiquark are fast,  $\alpha, 1 - \alpha > \mu^2/Q^2$  (Fig. 4.11b). In a frame where the proton is fast, say, the Breit frame, the asymmetric and symmetric contribution to  $F_T$  correspond to photon-quark scattering and photon-gluon fusion respectively.

The symmetric part is dominated by small  $q\bar{q}$  pairs, i.e., by the short distance contribution to the Wilson-loop trace,

$$\int_{x_\perp} \text{tr} \left( W_{x_\perp}(y_\perp) W_{x_\perp}^\dagger(y_\perp) \right) = \frac{1}{2} y^2 \int_{x_\perp} \text{tr} \left( \partial_{y_\perp} W_{x_\perp}(0) \partial_{y_\perp} W_{x_\perp}^\dagger(0) \right) + \mathcal{O}(y^4). \quad (\text{D.4})$$

The corresponding contribution to the structure function is related to the first term on the r.h. side of Eq. (D.2), which generates the gluon distribution, Eq. (D.3). It can also be written as

$$F_T^{\text{sym}}(0, Q^2) = \frac{e_q^2}{2\pi^3} \int_0^1 dz P_{qg}(z) \left( \ln \frac{Q^2}{\mu^2} - 1 \right) \int_{x_\perp} \text{tr} \left( \partial_{y_\perp} W_{x_\perp}^{\mathcal{F}}(0) \partial_{y_\perp} W_{x_\perp}^{\mathcal{F}\dagger}(0) \right), \quad (\text{D.5})$$

where  $P_{qg}(z)$  is the conventional gluon-quark splitting function.

The other splitting functions appear if  $\alpha_s$  corrections to  $F_T$  and  $F_L$ , associated with higher Fock states of the virtual photon, are considered in the semiclassical approach. For example, the  $q\bar{q}g$  parton configuration involves, in the case where one of the quarks carries a small fraction of the photon momentum, a  $\ln Q^2$  term associated with  $P_{qq}(z)$ .

The splitting function  $P_{gg}(z)$  is most easily derived by considering an incoming virtual scalar which couples directly to the gluonic action term  $F_{\mu\nu} F^{\mu\nu}$ . Such a current was used previously in [191] to study small- $x$  saturation effects. The relevant lowest order Fock state consists of two gluons. As reported in [62], it can be checked explicitly that the semiclassical calculation of the corresponding high-energy scattering process yields the usual gluon-gluon splitting function.

Since the semiclassical approach exactly reproduces the well-known DGLAP splitting functions, the large logarithms  $\ln(Q^2/\mu^2)$  can be resummed in the conventional way, by means of the renormalization group. To this end, the parton distributions  $q(x, Q^2)$  and  $g(x, Q^2)$  are evaluated using DGLAP evolution equations, with the input distributions  $q(x, Q_0^2)$  and  $g(x, Q_0^2)$  given by Eqs. (D.2) and (D.3). Here  $Q_0^2$  is some small scale where logarithmic corrections are not yet important. The parton model description of the structure function at leading order includes only photon-quark scattering. The leading logarithmic term from the photon-gluon fusion process appears now as part of the resummed quark distribution.

The large hadron model of Sect. 6.2 provides an expression for the basic function  $\int_{x_\perp} \text{tr} \left( W_{x_\perp}(y_\perp) W_{x_\perp}^\dagger(y_\perp) \right)$ . Inserting the explicit formula of Eq. (6.25) into Eqs. (D.2) and (D.3), the following compact expressions for the inclusive parton distributions at a low scale  $Q_0^2$  are obtained

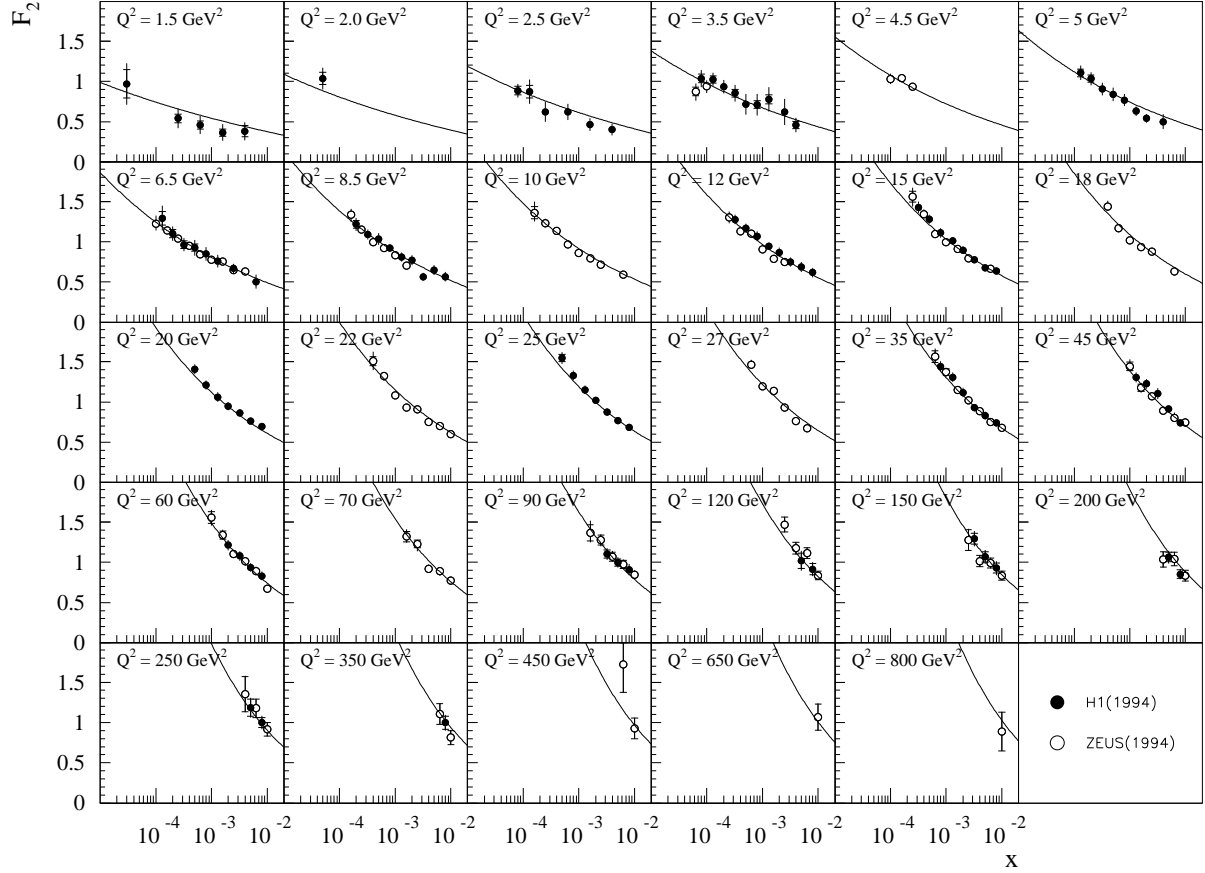


**Figure D.1:** The inclusive structure function  $F_2(x, Q^2)$  at small  $x$  computed in the semiclassical approach with data from [159]. The data with  $Q^2 = 1.5 \text{ GeV}^2$  are not included in the fit.

$$xq(x, Q_0^2) = \frac{a\Omega N_c}{3\pi^3} \left( \ln \frac{Q_0^2}{a} - 0.6424 \right), \quad (\text{D.6})$$

$$xg(x, Q_0^2) = \frac{2a\Omega N_c}{\pi^2 \alpha_s(Q_0^2)}. \quad (\text{D.7})$$

As discussed in Sect. 7.1, the analysis of [62] introduces a soft energy dependence into these input distributions by ascribing a logarithmic growth to the total normalization,

$$\Omega \rightarrow \Omega (L - \ln x)^2. \quad (\text{D.8})$$

Note also the observation of [192] that the small- $x$  structure function is well described by a simple  $\ln(1/x)$  with an additional  $\ln Q^2$  enhancement, similar to the effects of Altarelli-Parisi evolution.

The DGLAP evolution of the above inclusive parton distributions and corresponding diffractive distributions given in Sect. 7.1 provides predictions for both the inclusive and diffractive structure functions. In the numerical analysis, the inclusive distributions are multiplied with  $(1-x)$  to ensure vanishing of the distributions in the limit  $x \rightarrow 1$ , which is required for the numerical stability of the DGLAP evolution.

A combined fit to small- $x$  HERA data gives a good description of the experimental results. While plots of  $F_2^{D(3)}$  are given Figs. 7.1 and 7.2, here, corresponding results for the inclusive structure function are presented (see Fig. D.1). Since the underlying model is only valid in the small- $x$  region, data points above  $x = 0.01$  are not considered. To appreciate the quality of the fits, recall that, within the large hadron model, the diffractive (Eqs. (7.4) and (7.5)) and inclusive (Eqs. (D.6) and (D.7)) parton distributions are highly constrained with respect to each other.

# Bibliography

- [1] M.L. Good and W.D. Walker, Phys. Rev. 120 (1960) 1857
- [2] UA8 collab., A. Brandt et al., Phys. Lett. B297 (1992) 417
- [3] ZEUS collab., M. Derrick et al., Phys. Lett. B315 (1993) 481
- [4] H1 collab., T. Ahmed et al., Nucl. Phys. B429 (1994) 477
- [5] J.D. Bjorken and J.B. Kogut, Phys. Rev. D8 (1973) 1341
- [6] J. D. Bjorken, J. Kogut and D. E. Soper, Phys. Rev. D3 (1971) 1382
- [7] N.N. Nikolaev and B.G. Zakharov, Z. Phys. C49 (1991) 607
- [8] A. Donnachie and P.V. Landshoff, Nucl. Phys. B244 (1984) 322 and Phys. Lett. B296 (1992) 227
- [9] G. Ingelman and P. Schlein, Phys. Lett. B152 (1985) 256
- [10] A. Donnachie and P.V. Landshoff, Phys. Lett. B191 (1987) 309
- [11] A. Donnachie and P.V. Landshoff, Nucl. Phys. B303 (1988) 634
- [12] L. Trentadue and G. Veneziano, Phys. Lett. B323 (1994) 201
- [13] A. Berera and D.E. Soper, Phys. Rev. D50 (1994) 4328
- [14] F.E. Low, Phys. Rev. D12 (1975) 163;  
S. Nussinov, Phys. Rev. Lett. (1975) 1286
- [15] M.G. Ryskin, Z. Phys. C57 (1993) 89
- [16] S.J. Brodsky et al., Phys. Rev. D50 (1994) 3134
- [17] J.R. Forshaw, M.G. Ryskin, Z. Phys. C68 (1995) 137
- [18] D. Müller et al., Fortsch. Phys. 42 (1994) 101
- [19] X. Ji, Phys. Rev. Lett. 78 (1997) 610
- [20] A.V. Radyushkin, Phys. Lett. B380 (1996) 417

- [21] F.-M. Dittes et al., Phys. Lett. B209 (1988) 325
- [22] J.C. Collins, L. Frankfurt and M. Strikman, Phys. Rev. D56 (1997) 2982
- [23] A. Hebecker and P.V. Landshoff, Phys. Lett. B419 (1998) 393
- [24] M. Genovese, N.N. Nikolaev and B.G. Zakharov, Phys. Lett. B378 (1996) 347
- [25] E.M. Levin et al., Z. Phys. C74 (1997) 671
- [26] H. Lotter, Phys. Lett. B406 (1997) 171
- [27] M. Diehl, Eur. Phys. J. C1 (1998) 293
- [28] N.N. Nikolaev and B.G. Zakharov, Z. Phys. C64 (1994) 631 and JETP 78 (1994) 598
- [29] M. Diehl, Z. Phys. C66 (1995) 181
- [30] J. Bartels, H. Lotter and M. Wüsthoff, Phys. Lett. B379 (1996) 239
- [31] J. Bartels and M. Wüsthoff, J. Phys. G22 (1996) 929
- [32] J. Bartels and M. Wüsthoff, preprint ANL-HEP-CP-97-51 (1997) and Proc. of *DIS 97*, Ed. J. Repond and D. Krakauer, AIP Conf. Proc. No. 407, Woodbury, New York, 1997, p. 472
- [33] M. Bertini et al., Phys. Lett. B422 (1998) 238
- [34] J. Bartels et al., Eur. Phys. J. C7 (1999) 443
- [35] J. Bartels and M. Wüsthoff, Z. Phys. C66 (1995) 157
- [36] J. Bartels, H. Lotter and M. Wüsthoff, Z. Phys. C68 (1995) 121
- [37] A. Bialas and R. Peschanski, Phys. Lett. B378 (1996) 302
- [38] W. Buchmüller, Phys. Lett. B353 (1995) 335
- [39] W. Buchmüller and A. Hebecker, Phys. Lett. B355 (1995) 573
- [40] A. Edin, G. Ingelman and J. Rathsman, Phys. Lett. B366 (1996) 371
- [41] O. Nachtmann and A. Reiter, Z. Phys. C24 (1984) 283
- [42] J.C. Collins, D.E. Soper and G. Sterman, Nucl. Phys. B263 (1986) 37
- [43] O. Nachtmann, Ann. Phys. 209 (1991) 436
- [44] W. Buchmüller and A. Hebecker, Nucl. Phys. B476 (1996) 203
- [45] W. Buchmüller, M.F. McDermott and A. Hebecker, Nucl. Phys. B487 (1997) 283; B500 (1997) 621 (E)



- [46] H. Abramowicz, L. Frankfurt and M. Strikman, Proc. of the *SLAC Summer Institute 1994* p. 539
- [47] W. Buchmüller, M.F. McDermott and A. Hebecker, Phys. Lett. B404 (1997) 353
- [48] W. Buchmüller, M.F. McDermott and A. Hebecker, Phys. Lett. B410 (1997) 304
- [49] A. Hebecker, Nucl. Phys. B505 (1997) 349
- [50] P.V. Landshoff and O. Nachtmann, Z. Phys. C35 (1987) 405
- [51] A. Donnachie and P.V. Landshoff, Nucl. Phys. B311 (1988) 509
- [52] H.G. Dosch, Phys. Lett. B190 (1987) 177;  
H.G. Dosch and Yu.A. Simonov, Phys. Lett. B205 (1988) 339
- [53] H.G. Dosch, A. Krämer, Phys. Lett. B252 (1990) 669
- [54] H.G. Dosch and M. Rueter, Phys. Rev. D57 (1998) 4097
- [55] H.G. Dosch, O. Nachtmann and M. Rueter, Phys. Rev. D59 (1999) 014018;  
E.R. Berger et al., preprint HD-THEP-99-3 and TAUP-2548-99 (hep-ph/9901376)
- [56] H.G. Dosch et al., Phys. Rev. D55 (1997) 2602
- [57] H.G. Dosch, G. Kulzinger and H.J. Pirner, Eur. Phys. J. C7 (1999) 73
- [58] M. Rueter, Eur. Phys. J. C7 (1999) 233
- [59] O.E. Ramirez del Prado, talk at the *Int. Euroconf. on QCD*, Montpellier, 1998 (hep-ph/9808450)
- [60] L. McLerran and R. Venugopalan, Phys. Rev. D49 (1994) 2233
- [61] A. Hebecker and H. Weigert, Phys. Lett. B432 (1998) 215
- [62] W. Buchmüller, T. Gehrmann and A. Hebecker, Nucl. Phys. B537 (1999) 477
- [63] S.J. Brodsky, A. Hebecker and E. Quack, Phys. Rev. D55 (1997) 2584
- [64] A.R. White, preprint ANL-HEP-PR-95-57 (hep-ph/9509309);  
A.R. White, Proc. of the *Int. Conf. On Elastic and Diffractive Scattering*, Seoul 1997, Ed. K. Kang, S.K. Kim and C. Lee, World Scientific, 1998, p. 60
- [65] C. Boros, Z. Liang and T. Meng, Phys. Rev. D54 (1996) 6658
- [66] J.C. Collins, hep-ph/9705393
- [67] B. Andersson et al., Phys. Rep. 97 (1983) 31
- [68] G. Ingelman and K. Janson-Prytz, Proc. of the Workshop *Physics at HERA*, Hamburg 1991, Ed. W. Buchmüller and G. Ingelman;  
G. Ingelman and K. Prytz, Z. Phys. C58 (1993) 285

- [69] H1 collab., T. Ahmed et al., Phys. Lett. B348 (1995) 681
- [70] R.K. Ellis, W.J. Stirling and B.R. Webber, *QCD and Collider Physics*, Cambridge University Press, 1996
- [71] ZEUS collab., M. Derrick et al., Z. Phys. C70 (1996) 391
- [72] ZEUS collab., J. Breitweg et al., Eur. Phys. J. C1 (1998) 81
- [73] H1 collab., C. Adloff et al., Z. Phys. C76 (1997) 613
- [74] ZEUS collab., J. Breitweg et al., Eur. Phys. J. C6 (1999) 43
- [75] O. Nachtmann, *Phänomene und Konzepte der Elementarteilchenphysik*, Vieweg, Braunschweig/Wiesbaden, 1986
- [76] M. Lüscher, Nucl. Phys. B254 (1985) 52
- [77] E. Verlinde and H. Verlinde, preprint PUPT-1319 (hep-th/9302104);  
I.Ya. Aref'eva, Phys. Lett. B325 (1994) 171 and B328 (1994) 411;  
I.A. Korchemskaya and G.P. Korchemsky, Nucl. Phys. B437 (1995) 127;  
L.N. Lipatov, Nucl. Phys. B452 (1995) 369;  
I. Balitsky, Nucl. Phys. B463 (1996) 99 and Phys. Rev. Lett. 81 (1998) 2024;  
E. Meggiolaro, Z. Phys. C76 (1997) 523 and Eur. Phys. J. C4 (1998) 101;  
J. Jalilian-Marian, A. Kovner and H. Weigert, Phys. Rev. D59 (1999) 014015
- [78] J. Jalilian-Marian et al., Phys. Rev. D55 (1997) 5414
- [79] E. Predazzi, lectures at the *6th Workshop on Hadron Physics*, Florianopolis, Santa Catarina, Brazil, 1998 (hep-ph/9809454)
- [80] J.D. Bjorken, talk at the *Conf. on Fundamental Interactions of Element. Particles*, Moscow, 1995 (hep-ph/9601363)
- [81] V.N. Gribov, Sov. Phys. JETP 30 (1970) 709
- [82] P.D.B. Collins, *An Introduction to Regge Theory and High Energy Physics*, Cambridge University Press, 1977
- [83] J.R. Forshaw and D.A. Ross, *Quantum Chromodynamics and the Pomeron*, Cambridge University Press, 1997
- [84] M. Froissart, Phys. Rev. 123 (1961) 1053;  
L. Lukaszuk and A. Martin, Nuovo Cim. A52 (1967) 122
- [85] P.D.B. Collins, F.D. Gault and A. Martin, Nucl. Phys. B80 (1974) 135
- [86] G.F. Chew and S.C. Frautschi, Phys. Rev. Lett. 7 (1961) 394
- [87] I.Ya. Pomeranchuk, Sov. Phys. JETP 7 (1958) 499
- [88] A.H. Mueller, Phys. Rev. D2 (1970) 2963

- [89] C.E. DeTar et al., Phys. Rev. Lett. 26 (1970) 675
- [90] A.B. Kaidalov and K.A. Ter-Martirosyan, Nucl. Phys. B75 (1974) 471
- [91] E.L. Berger et al., Nucl. Phys. B286 (1987) 704
- [92] D.E. Soper, Proc. of *DIS 97*, Ed. J. Repond and D. Krakauer, AIP Conf. Proc. No. 407, Woodbury, New York, 1997, p. 147
- [93] A. Berera and D.E. Soper, Phys. Rev. D53 (1996) 6162
- [94] J.C. Collins, D.E. Soper and G. Sterman, Nucl. Phys. B261 (1985) 104 and B308 (1988) 833;  
G.T. Bodwin, Phys. Rev. D31 (1985) 2616 and D34 (1986) 3932
- [95] J.C. Collins, D.E. Soper and G. Sterman, in *Perturbative QCD*, Ed. A.H. Mueller, World Scientific, Singapore, 1989, p. 1
- [96] A.H. Mueller, Phys. Rev. D18 (1978) 3705 and Phys. Rep. 73 (1981) 237
- [97] M. Grazzini, L. Trentadue and G. Veneziano, Nucl. Phys. B519 (1998) 394
- [98] J.C. Collins, Phys. Rev. D57 (1998) 3051
- [99] J.C. Collins, L. Frankfurt and M. Strikman, Phys. Lett. B307 (1993) 161
- [100] D.E. Soper, talk at the *3rd Workshop on Small-x and Diffractive Physics*, Argonne National Laboratory, 1996
- [101] M. Wüsthoff, Phys. Rev. D56 (1997) 4311
- [102] S.J. Brodsky, P. Hoyer and L. Magnea, Phys. Rev. D55 (1997) 5585
- [103] E.L. Berger and D. Jones, Phys. Rev. D23 (1981) 1521
- [104] V.L. Chernyak and A.R. Zhitnitsky, Phys. Rep. 112 (1984) 173
- [105] B. Pire, Lectures at *Les Houches Summer School 1996: Trends in Nuclear Physics* (nucl-th/9612009)
- [106] P. Ball and V.M. Braun, Phys. Rev. D54 (1996) 2182
- [107] L. Frankfurt and M. Strikman, talk at *DIS 95*, Paris, 1995 (hep-ph/9510291)
- [108] M.G. Ryskin et al., Z. Phys. C76 (1997) 231
- [109] A.V. Radyushkin, Phys. Rev. D56 (1997) 5524;  
X. Ji, J. Phys. G24 (1998) 1181;  
K.J. Golec-Biernat and A.D. Martin, Phys. Rev. D59 (1999) 014029
- [110] M. Diehl and T. Gousset, Phys. Lett. B428 (1998) 359
- [111] R.L. Jaffe, Nucl. Phys. B229 (1983) 205

- [112] X. Ji, W. Melnitchouk and X. Song, Phys. Rev. D56 (1997) 5511;  
V.Yu. Petrov et al., Phys. Rev. D57 (1998) 4325;  
L. Mankiewicz, G. Piller and T. Weigl, Eur. Phys. J. C5 (1998) 119;  
A. Freund and V. Guzey (hep-ph/9806267)
- [113] P. Hoodbhoy and X. Ji, Phys. Rev. D58 (1998) 054006
- [114] A.V. Belitsky et al., Phys. Lett. B421 (1998) 312;  
Z. Chen, Nucl. Phys. B525 (1998) 369
- [115] A.G. Shuvaev et al., preprint DTP-99-18 (hep-ph/9902410);  
K.J. Golec-Biernat, A.D. Martin and M.G. Ryskin, preprint DTP-99-24  
(hep-ph/9903327)
- [116] L. Frankfurt, W. Koepf and M. Strikman, Phys. Rev. D54 (1996) 3194
- [117] J. Nemchik, N.N. Nikolaev and B.G. Zakharov, Phys. Lett. B341 (1994) 228;  
J. Nemchik et al., Phys. Lett. B374 (1996) 199, Z. Phys. C75 (1997) 71 and JETP  
86 (1998) 1054
- [118] J.R. Cudell and I. Royen, preprint ULG-PNT-98-2-JRC (hep-ph/9807294)
- [119] A. Donnachie and P.V. Landshoff, Phys. Lett. B348 (1995) 213;  
L.P.A. Haakman, A. Kaidalov and J.H. Koch, Phys. Lett. B365 (1996) 411;  
E. Gotsman, E. Levin and U. Maor, Nucl. Phys. B464 (1996) 251;  
I.F. Ginzburg and D.Yu. Ivanov, Phys. Rev. D54 (1996) 5523
- [120] E. Gotsman, E. Levin and U. Maor, Phys. Lett. B403 (1997) 120
- [121] I.M. Dremin, Mod. Phys. Lett. A12 (1997) 2717
- [122] M. Vanttinen and L. Mankiewicz, Phys. Lett. B434 (1998) 141 and B440 (1998)  
157;  
D.Yu. Ivanov and R. Kirschner, Phys. Rev. D58 (1998) 114026
- [123] J.R. Cudell and I. Royen, Phys. Lett. B397 (1997) 317
- [124] I. Halperin and A. Zhitnitsky, Phys. Rev. D56 (1997) 184
- [125] D.Yu. Ivanov, Phys. Rev. D53 (1996) 3564
- [126] A.D. Martin, M.G. Ryskin and T. Teubner, Phys. Rev. D55 (1997) 4329
- [127] X. Ji and J. Osborne, Phys. Rev. D58 (1998) 094018;  
J.C. Collins and A. Freund, Phys. Rev. D59 (1999) 074009
- [128] H. Cheng and T.T. Wu, *Expanding Protons: Scattering at High Energy*, MIT Press,  
Cambridge, Massachusetts, 1987, Sect. 3.4
- [129] B.Z. Kopeliovich, L.I. Lapidus and A.B. Zamolodchikov, JETP Lett. 33 (1981)  
595;  
G. Bertsch et al., Phys. Rev. Lett. 47 (1981) 297

- [130] M.G. Ryskin, *Sov. J. Nucl. Phys.* 52 (1990) 529
- [131] N.N. Nikolaev and B.G. Zakharov, *Z. Phys.* C53 (1992) 331
- [132] L. Frankfurt, G.A. Miller and M. Strikman, *Phys. Lett.* B304 (1993) 1
- [133] N.N. Nikolaev and B.G. Zakharov, *Proc. of DIS 97*, Ed. J. Repond and D. Krakauer, AIP Conf. Proc. No. 407, Woodbury, New York, 1997, p. 445
- [134] E. Gotsman, E. Levin and U. Maor, *Nucl. Phys.* B493 (1997) 354
- [135] E.A. Kuraev, L.N. Lipatov and V.S. Fadin, *Sov. Phys. JETP* 44 (1976) 443 and 45 (1977) 199;  
Y.Y. Balitsky and L.N. Lipatov, *Sov. J. Nucl. Phys.* 28 (1978) 822
- [136] A.H. Mueller, *Nucl. Phys.* B415 (1994) 373;  
A.H. Mueller and B. Patel, *Nucl. Phys.* B425 (1994) 471
- [137] A.H. Mueller, *Nucl. Phys.* B437 (1995) 107
- [138] N.N. Nikolaev, B.G. Zakharov and V.R. Zoller, *JETP Lett.* 59 (1994) 6
- [139] M. Genovese, N.N. Nikolaev and B.G. Zakharov, *JETP* 81 (1995) 625
- [140] A. Bialas and R. Peschanski, *Phys. Lett.* B387 (1996) 405
- [141] M. Genovese, N.N. Nikolaev and B.G. Zakharov, *JETP* 81 (1995) 633
- [142] V.S. Fadin and L.N. Lipatov, *Phys. Lett.* B429 (1998) 127;  
M. Ciafaloni and G. Camici, *Phys. Lett.* B430 (1998) 349
- [143] S.J. Brodsky et al., preprint SLAC-PUB-8037 and IITAP-98-010 (hep-ph/9901229)
- [144] F. Hautmann, Z. Kunszt and D.E. Soper, *Phys. Rev. Lett.* 81 (1998) 3333
- [145] S.J. Brodsky, V. Del Duca and P. Hoyer, *Phys. Rev.* D46 (1992) 931
- [146] K. Golec-Biernat and M. Wüsthoff, *Phys. Rev.* D59 (1999) 014017
- [147] K. Golec-Biernat and M. Wüsthoff, preprint DTP/99/20 (hep-ph/9903358)
- [148] Yu.V. Kovchegov and L. McLerran, preprint NUC-MN-99-2-T (hep-ph/9903246)
- [149] H.G. Dosch, E. Ferreira and A. Krämer, *Phys. Rev.* D50 (1994) 1992
- [150] O. Nachtmann, *Lectures at Workshop on Topics in Field Theory*, Kloster Banz, 1993 and at *35th Int. Univ. School of Nucl. and Part. Phys.*, Schladming, 1996 (hep-ph/9609365)
- [151] A. Krämer, *Ph.D. Thesis*, Heidelberg, 1991
- [152] E. Meggiolaro, preprint HD-THEP-98-34 (hep-ph/9807567)

- [153] P. Marage, talk at *LISHEP 98*, Rio de Janeiro, 1998 (hep-ph/9810551);  
H1 and ZEUS collab. (P. Newman for the collaborations), talk at the *Int. Conf. on Hadron Structure*, Stara Lesna, Slovakia, 1998 (hep-ex/9901026)
- [154] J. Ellis and G.G. Ross, *Phys. Lett.* B384 (1996) 293;  
J. Ellis, G.G. Ross and J. Williams, preprint CERN-TH/98-396 and OUTP-98-91P (hep-ph/9812385)
- [155] A. Capella et al., *Phys. Lett.* B343 (1995) 403;  
B.A. Kniehl, H.-G. Kohrs and G. Kramer, *Z. Phys.* C65 (1995) 657;  
K. Golec-Biernat and J. Kwieciński, *Phys. Lett.* B353 (1995) 329
- [156] T. Gehrmann and W.J. Stirling, *Z. Phys.* C70 (1996) 89
- [157] V.N. Gribov and L.N. Lipatov, *Sov. J. Nucl. Phys.* 15 (1972) 438, 675;  
G. Altarelli and G. Parisi, *Nucl. Phys.* B126 (1977) 298;  
Yu.L. Dokshitzer, *Sov. Phys. JETP* 46 (1977) 641
- [158] M. Glück, E. Reya and M. Stratmann, *Nucl. Phys.* B422 (1994) 37
- [159] H1 collab., S. Aid et al., *Nucl. Phys.* B470 (1996) 3;  
ZEUS collab., M. Derrick et al., *Z. Phys.* C72 (1996) 399
- [160] A. Milsztajn and M. Virchaux, *Phys. Lett.* B274 (1992) 221;  
A.D. Martin et al., *Phys. Lett.* B443 (1998) 301
- [161] ZEUS collab., H. Kowalski, talk at *LISHEP 98*, Rio de Janeiro, 1998
- [162] J. Bartels and C. Royon, preprint DESY-98-152 (hep-ph/9809344)
- [163] K. Golec-Biernat and J. Kwiecinski, *Phys. Rev.* D55 (1997) 3209;  
N.N. Nikolaev, W. Schäfer and B.G. Zakharov, preprint KFA-IKP-TH-1996-06 (hep-ph/9608338);  
K. Golec-Biernat, J. Kwiecinski and A. Szczurek, *Phys. Rev.* D56 (1997) 3955;  
W. Schäfer, talk at *DIS 98*, Brussels, 1998 (hep-ph/9806296)
- [164] M. Rueter, talk at the *Int. Euroconf. on QCD*, Montpellier, 1998 (hep-ph/9808475)
- [165] A. Bialas, R. Peschanski and C. Royon, *Phys. Rev.* D57 (1998) 6899
- [166] S. Munier, R. Peschanski and C. Royon, *Nucl. Phys.* B534 (1998) 297
- [167] A.H. Mueller, *Eur. Phys. J.* A1 (1998) 19
- [168] T. Arens et al., *Z. Phys.* C74 (1997) 651;  
M. Diehl, *Z. Phys.* C76 (1997) 499 and *Eur. Phys. J.* C4 (1998) 497;  
N.N. Nikolaev, A.V. Pronyaev and B.G. Zakharov, *Phys. Rev.* D59 (1999) 091501
- [169] ZEUS collab., M. Derrick et al., *Phys. Lett.* B332 (1994) 228
- [170] H1 collab., C. Adloff et al., *Eur. Phys. J.* C1 (1998) 495;  
ZEUS collab., J. Breitweg et al., *Phys. Lett.* B421 (1998) 368

- [171] H1 collab., C. Adloff et al., Eur. Phys. J. C6 (1999) 421
- [172] H. Jung, talk at *LISHEP 98*, Rio de Janeiro, 1998 (hep-ph/9809374)
- [173] H1 collab., talk at *ICHEP 98*, Vancouver, 1998 (abstract 558)
- [174] ZEUS collab., talk at *ICHEP 98*, Vancouver, 1998 (abstract 785)
- [175] ZEUS collab., M. Derrick et al., Z. Phys. C70 (1996) 1;  
H1 collab., C. Adloff et al., Phys. Lett. B428 (1998) 206
- [176] ZEUS collab., M. Derrick et al., Phys. Lett. B338 (1994) 483;  
H1 collab., S. Aid et al., Z. Phys. C70 (1996) 609
- [177] H1 collab., C. Adloff et al., Eur. Phys. J. C5 (1998) 439
- [178] A. Edin, G. Ingelman and J. Rathsmann, Z. Phys. C75 (1997) 57
- [179] J. Rathsmann, preprint SLAC-PUB-8034 (hep-ph/9812423)
- [180] ZEUS collab., J. Breitweg et al., Eur. Phys. J. C6 (1999) 603
- [181] H1 collab., C. Adloff et al., preprint DESY-99-010 (hep-ex/9902019)
- [182] H1 collab., talk at *ICHEP 98*, Vancouver, 1998 (abstract 572)
- [183] H1 collab., S. Aid et al., Nucl. Phys. B468 (1996) 3
- [184] A.D. Martin, W.J. Stirling and R.G. Roberts, Phys. Lett. B354 (1995) 155
- [185] P. Hoodbhoy, Phys. Rev. D56 (1997) 388
- [186] B.Z. Kopeliovich et al., Phys. Lett. B309 (1993) 179
- [187] A. Donnachie and P.V. Landshoff, Phys. Lett. B437 (1998) 408
- [188] D. Schildknecht, G.A. Schuler and B. Surrow, preprint CERN-TH-98-294  
(hep-ph/9810370)
- [189] H1 collab., talk at *ICHEP 98*, Vancouver, 1998 (abstract 572)
- [190] S.J. Brodsky and G.P. Lepage, Phys. Rev. D22 (1980) 2157
- [191] A.H. Mueller, Nucl. Phys. B335 (1990) 115
- [192] W. Buchmüller and D. Haidt, preprint DESY-96-061 (hep-ph/9605428)